

**A-kinase anchoring proteins AKAP1, -4, -10
and -11 with different subcellular localizations in
Sertoli cells and their roles in male fertility**

Inaugural Dissertation
submitted to the
Faculty of Medicine
in partial fulfillment of the requirements
for the PhD-Degree
of the Faculties of Veterinary Medicine and Medicine
of the Justus Liebig University Giessen

by
M. Sc. Wang, Wenwen
of
Qingdao, China

Gießen (2016)

From the Institute for Anatomy and Cell Biology,
Medical Cell Biology
Director: Prof. Dr. med. Eveline Baumgart-Vogt
of the Faculty of Medicine of the Justus Liebig University Giessen

First Supervisor: Prof. Dr. med. Eveline Baumgart-Vogt
Second Supervisor: Prof. Dr. habil. Christiane Herden
Committee Members: Prof. Dr. Klaus-Dieter Schlüter, Prof. Dr. med. Eveline
Baumgart-Vogt, Prof. Dr. habil. Christiane Herden

Date of Doctoral Defense: 18th May 2016

Declaration

“I declare that I have completed this dissertation single-handedly without the unauthorized help of a second party and only with the assistance acknowledged therein. I have appropriately acknowledged and referenced all text passages that are derived literally from or are based on the content of published or unpublished work of others, and all information that relates to verbal communications. I have abided by the principles of good scientific conduct laid down in the charter of the Justus Liebig University of Giessen in carrying out the investigations described in the dissertation.”

Wenwen Wang

Date: 18th May 2016

Place: Gießen, Germany

Contents

1	INTRODUCTION.....	7
1.1	THE WORLDWIDE SOCIAL PROBLEM OF INFERTILITY.....	7
1.1.1	<i>Cause of male infertility.....</i>	7
1.2	SERTOLI CELLS.....	8
1.2.1	<i>Morphology and function of Sertoli cells.....</i>	8
1.2.2	<i>Models to study Sertoli cells in vitro.....</i>	10
1.2.3	<i>Sertoli cell function regulation.....</i>	10
1.3	AKAPS: SCAFFOLDS FOR LOCAL SIGNALING.....	13
1.3.1	<i>AKAP binding features and signaling cross-talk.....</i>	14
1.3.2	<i>Structure of AKAP-PKA interaction.....</i>	15
1.3.3	<i>Diversity and evolution within the AKAP family.....</i>	17
1.4	A CLOSER LOOK TO FOUR AKAPS USED IN THIS STUDY.....	18
1.4.1	<i>AKAP11 (=AKAP220).....</i>	18
1.4.2	<i>AKAP1.....</i>	21
1.4.3	<i>AKAP4.....</i>	28
1.4.4	<i>AKAP10.....</i>	29
1.5	THE FUNCTION OF AKAP1, AKAP4, AKAP10 AND AKAP11 IN GENITAL ORGANS.....	30
1.5.1	<i>Steroid hormone biosynthesis.....</i>	30
1.5.2	<i>Sperm development.....</i>	31
1.5.3	<i>Oocyte maturation.....</i>	31
1.5.4	<i>Prostate cancer.....</i>	32
1.6	PEROXISOMES AND INFERTILITY.....	32
1.6.1	<i>Metabolic pathways in peroxisomes involved in male fertility.....</i>	32
1.6.2	<i>Peroxisomal matrix protein translocation and import machinery.....</i>	34
1.7	AIMS OF THE THESIS.....	35
2	MATERIALS.....	36
2.1	CELL LINE AND MEDIUM.....	36
2.2	ROUTINE MATERIALS.....	36
2.3	BUFFER RECIPES.....	39
2.4	AKAP PLASMIDS.....	40
2.5	PRIMERS.....	42
2.6	ANTIBODY LIST.....	47
3	METHODS.....	49
3.1	BIOINFOMATIC SCREENING FOR THE AKAPS WITH PUTATIVE PTS1 SIGNALS.....	49
3.1.1	<i>Scan of AKAP sequences for the consensus PTS1 motif.....</i>	49
3.1.2	<i>Use of ClustalX 2.0 & MEGA 4.0.2 programs to create an evolutionary tree.....</i>	49

3.1.3	<i>Use of Python 2.7.5 & R i386 3.0.1 programs to test AKAP1, AKAP4, AKAP10 through PTS1 predictor.....</i>	50
3.2	CELL CULTURE	52
3.2.1	<i>Cell culture routine</i>	52
3.2.2	<i>Cell number and viability examination.....</i>	52
3.2.3	<i>Isolation of total RNA from TM4 cells.....</i>	53
3.3	RT-PCR	53
3.4	SDS-PAGE AND WESTERN BLOTS	54
3.5	PEROXISOME PURIFICATION BY OPTIPREP™ DENSITY GRADIENT CENTRIFUGATION.....	54
3.6	RAT DISSECTION AND RNA ISOLATION.....	59
3.6.1	<i>Anaesthesia for rats and dissection of different organs.....</i>	59
3.6.2	<i>Tissue total RNA isolation</i>	59
3.6.3	<i>Ethanol precipitation to concentrate total RNA</i>	60
3.7	WORKFLOW FOR NORTHERN BLOTTING.....	60
3.7.1	<i>Plasmid construction and probe generation by in vitro RNA transcription</i>	62
3.7.2	<i>Dot blot assay for detection of DIG-labeling efficiency.....</i>	62
3.7.3	<i>RNA samples and agarose gel preparation</i>	63
3.7.4	<i>Protocol of Northern blotting.....</i>	63
3.8	CONSTRUCTION OF MYC-TAGGED AKAP PLASMIDS AND EXPRESSION IN TM4 CELLS.....	64
3.8.1	<i>Construction of myc-tagged AKAPs and GFP plasmids.....</i>	65
3.8.2	<i>Procedures for bacterial transformation.....</i>	68
3.8.3	<i>Point mutation assay.....</i>	70
3.8.4	<i>Coating cover slips with poly-L-lysine</i>	71
3.8.5	<i>Transient transfection of TM4 cells.....</i>	72
3.8.6	<i>Immunofluorescence protocol.....</i>	72
4	RESULTS	73
4.1	AKAP FAMILY MEMBERS WITH PUTATIVE PTS1 SIGNALS.....	73
4.1.1	<i>AKAP sequence retrieval and PTS1 search matrix</i>	73
4.1.2	<i>Phylogenetic analysis of AKAP proteins containing a putative PTS1 signal.....</i>	74
4.2	TM4 SERTOLI CELL CULTURE STIMULATION WITH FSH TREATMENT	76
4.2.1	<i>Cell culture condition optimization.....</i>	76
4.2.2	<i>Effect of FSH stimulation on the peroxisome gene expression.....</i>	77
4.3	ISOLATION OF PEROXISOMES FROM TM4 CELLS.....	81
4.4	ANALYSIS OF AKAKP11 (=AKAP220) cDNA WITH GENOMIC SEQUENCES	84
4.5	NORTHERN BLOTTING.....	87
4.5.1	<i>Total RNA preparation for Northern blotting.....</i>	87
4.5.2	<i>Specific RNA probe generation and validation</i>	88
4.5.3	<i>Rat tissue total RNA Northern blot test</i>	95
4.5.4	<i>Rat total RNA RT-PCR.....</i>	96

4.5.5	<i>Concentrated total RNA and PCR-generated probes.....</i>	97
4.6	BASAL ANALYSIS AND OVER EXPRESSION OF AKAP1, AKAP4, AKAP10 IN TM4 CELLS	98
4.6.1	<i>Basic analysis of AKAP1, AKAP4, AKAP10</i>	98
4.6.2	<i>Cloning and immunolocalization of myc-tagged AKAPs.....</i>	106
5	DISCUSSION.....	121
5.1	AKAP220 (-CRL) IS PROBABLY AN ARTIFACT.....	121
5.2	PTS1 PREDICTION IS USEFUL FOR SEARCHING NOVEL PEROXISOMAL PROTEINS.....	122
5.3	EXCEPTIONS TO THE RULES OF PTS1 PREDICTION: ALTERNATIVE TARGETING OF PEROXISOMAL MATRIX PROTEINS	125
5.4	AKAP1 AND MITOCHONDRIAL FRAGMENTATION.....	126
5.5	MITOCHONDRIAL FUSION AND FISSION MECHANISMS.....	127
5.6	CONNECTION BETWEEN PEROXISOMES AND MITOCHONDRIA	128
5.7	THE ROLE OF AKAP1-STAR INTERACTION IN SERTOLI CELLS.....	129
5.8	AKAP4 DETECTION AND <i>IN VITRO</i> LOCALIZATION.....	131
6	OUTLOOK (FUTURE PLAN).....	132
7	SUMMARY	133
8	ZUSAMMENFASSUNG	136
9	LIST OF ABBREVIATIONS.....	139
10	FIGURE INDEX.....	143
11	TABEL INDEX.....	147
12	SUPPLEMENTAL DATA.....	148
13	ACKNOWLEDGEMENTS.....	159
14	CURRICULUM VITAE	161
15	REFERENCE	162

1 Introduction

1.1 The worldwide social problem of infertility

According to the world health organization (WHO), a couple can be considered infertile if it is not able to conceive after having unprotected intercourse continuously for more than one year (Tvrda et al., 2015). Infertility has remained a global concern since the first demographic survey provided by the WHO in 2002. On the average, 8-12% of sexually matured couples suffer from childlessness all over the world. In several regions, including Africa, South and Central Asia, Central and Eastern Europe, the infertility rates reach as high as 30%. Correspondingly, a global growth of *in vitro* fertilization (IVF) services and assisted reproductive techniques (ARTs) are being recorded (Inhorn and Patrizio, 2015). Therefore a better understanding of the processes that lead to female and male infertility became of crucial importance. Although in more than half of these cases, the reason for the childlessness is due to the male partner, research on male infertility remains a neglected field. One of the most important university centers, where laboratory research is currently conducted to elucidate the molecular and metabolic causes that can lead to infertility in men, is the Hessian Reproduction Center in Giessen, Germany.

1.1.1 Cause of male infertility

Male infertility can result from genetic defect such as chromosome disorder or epigenetic factors e.g. incorrect gene transcription induced by DNA methylation and histone modification. Abnormal expression of genes on Y chromosome may cause oligozoospermia or azoospermia (Reijo et al., 1996). Moreover, male patients with Klinefelter syndrome (47, XXY) suffer from hypogonadism and Down syndrome (47, XX/XY, +21) patients often show poor testicular development (Hafeez et al., 2007). An example for epigenetic alterations has been found in the NANOG promoter, a germ cell tumor marker. This promoter has been observed to be hypomethylated in spermatogonia and hypermethylated in spermatozoa, and its methylation state corresponds to the differentiation of testicular tumor cells (Nettersheim et al., 2011). Additionally, many environmental factors have been suspected to cause male infertility such as chemical and physical agents from daily life activities, including heavy metals, pesticides such as cypermethrin (Jin et al., 2011), organochlorides, radiation and plastics like bisphenol A

and plasticizers (Marques-Pinto and Carvalho, 2013). Certain chemicals with hormonal properties commonly referred to as endocrine disrupting agents (EDAs) bind membrane receptors preventing the endogenous steroid hormone synthesis, secretion and metabolism. Sertoli cells known as the testicular nurse cells and key players during spermatogenesis, have been found to be severely disrupted by EDAs accumulation. Furthermore, exposure to EDAs leads to inhibition of follicle-stimulating hormone (FSH) synthesis, which causes a decline in Sertoli cell number. The Sertoli cell malfunction in turn leads to disruption of the spermatogenesis and probably induces Testicular Dysgenesis Syndrome (TDS) (Tvrda et al., 2015).

1.2 Sertoli cells

1.2.1 Morphology and function of Sertoli cells

Sertoli cells are located in the basement membrane of seminiferous tubules in the testis (Figure 1) and play a crucial role in spermatogenesis, male phenotypic development, and the hypothalamic-pituitary-gonadal axis (Sharpe et al., 2003; Skinner and Griswold, 2004). These cells are closely connected to each other via tight junctions, forming the blood-testis barrier (BTB) also termed Sertoli cell barrier (SCB). SCB controls the chemical composition of the luminal fluid and prevents cytotoxic agents from penetrating the seminiferous tubules. Sertoli cells directly interact with male germ cells and support their development by structural protection and nutrition. Therefore, Sertoli cells are considered as support- or nurse cells (Griswold et al., 1987; Guo et al., 2015; Nenicu, 2010; Nenicu et al., 2007).

Sertoli cells also play a key role in secretion of regulatory factors, e.g. growth factors, hormones and cytokines, and the FSH response (Guo et al., 2015; McGuinness et al., 1994). Besides the support to spermatogenesis, the presence of Sertoli cells is also required to maintain the normal level of germ cell and Leydig cell population as well as functional peritubular myoid cells in the adult male testis (Rebourcet et al., 2014). The total number of Sertoli cells will determine the efficiency of sperm production and testicular size. There is a positive correlation between the number of Sertoli cells and testis weight, the percentage and volume of blood vessels, the seminiferous epithelium volume and the daily number of produced germ cells (Leal et al., 2004). For these reasons any disturbance of these cells could potentially cause infertility or an androgen-related endocrine disorder.

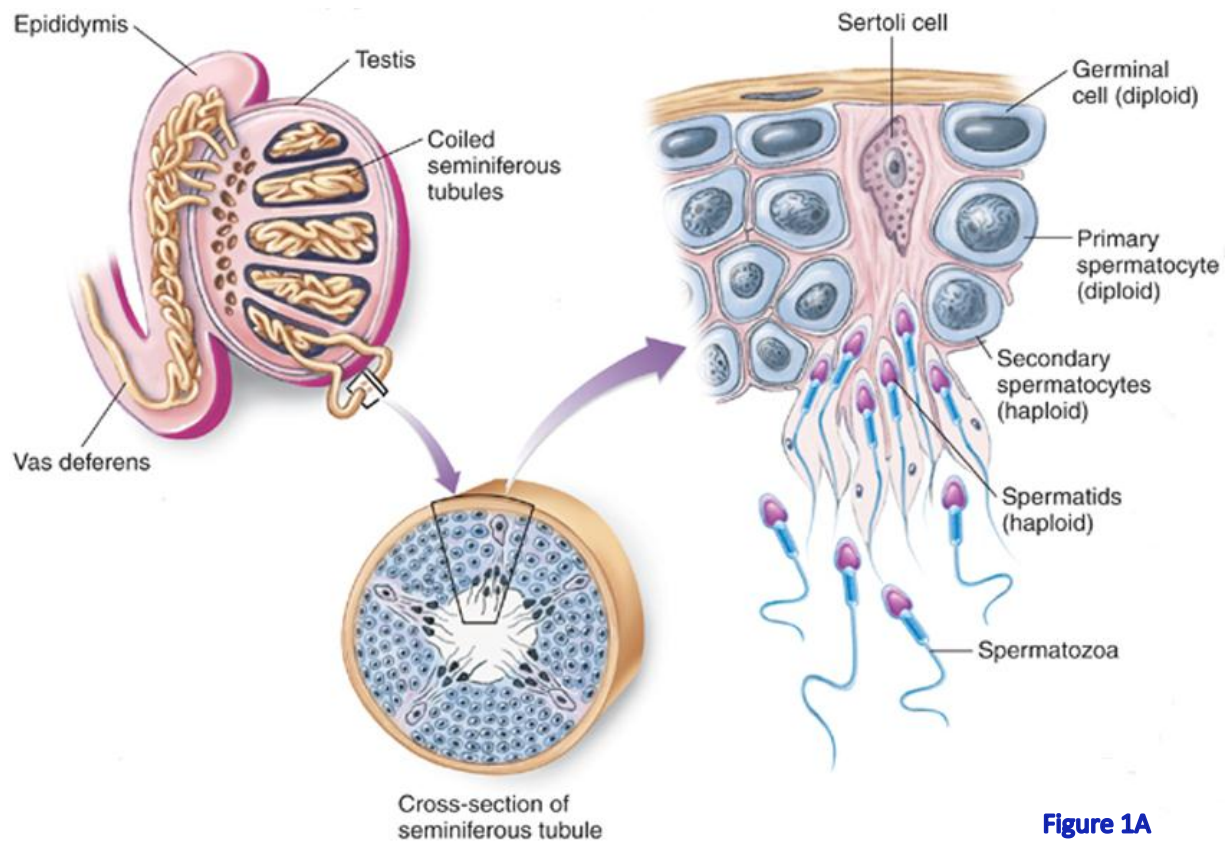


Figure 1A

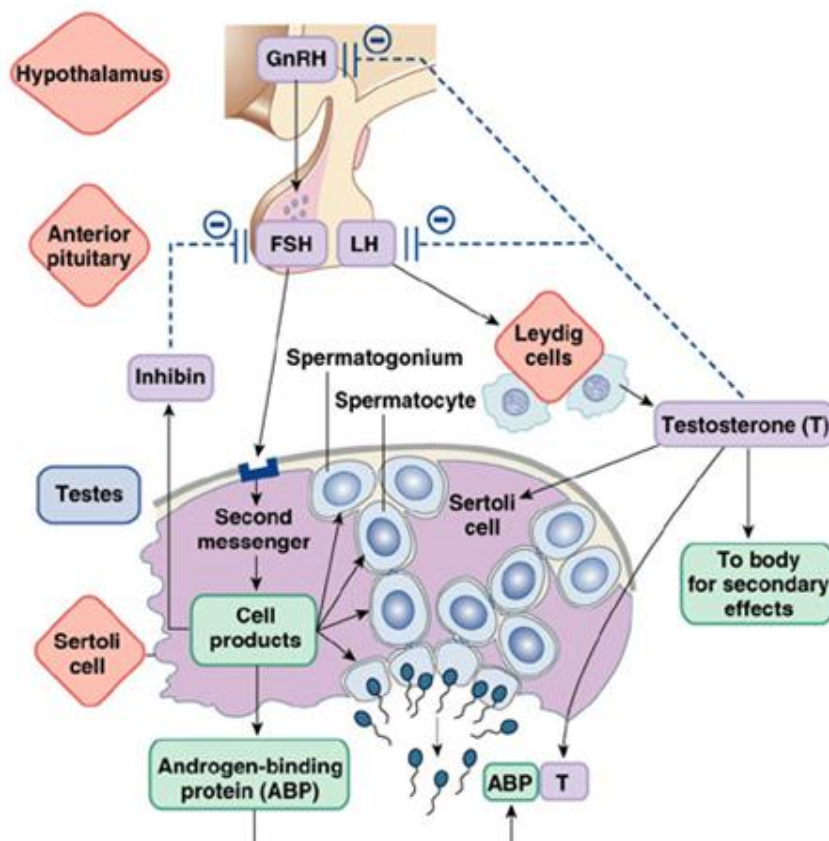


Figure 1B

Figure 1 Schematic illustration of testis structure (Figure 1A) and the hypothalamic-pituitary-testicular axis (Figure 1B). Figure 1A is taken from website of the “School of Biological Sciences at University of Texas at Austin” <http://www.zo.utexas.edu/faculty/sjasper/images/f36.12.jpg> and Figure 1B is taken from the website <https://imueos.wordpress.com/2010/05/24/spermatogenesis-x/>.

1.2.2 Models to study Sertoli cells *in vitro*

For *in vitro* studies, primary Sertoli cells are often used. These cells are usually isolated from the immature testis, and can be obtained with a relatively high purity (Neniciu et al., 2007). However, compared to aged cells, these cells have significant differences in the cell structure, transferrin expression level, and sensitivity to androgens (Anway et al., 2003). Although a method of the isolation of Sertoli cells from adult testis was recently established, these cells are often contaminated with germ cells or peritubular cells. Moreover, these primary Sertoli cells start to lose the responsiveness to hormones such as FSH within 6-10 days in culture (McGuinness et al., 1994). Therefore, in several studies the TM4 cell line was used, which provides a good model system to study Sertoli cell functions (Skinner and Griswold, 2004).

The TM4 cell line was established from immature mouse Sertoli cell cultures, which was successfully used as a feeder layer for isolated original germ cells. Compared with primary Sertoli cells, the TM4 cells are less sensitive to FSH stimulation. Additionally, TM4 cells can inhibit testosterone production in Leydig cells, which is rare *in vivo*. Nevertheless, TM4 cells still possess the major characteristics of primary immature Sertoli cells, thereby providing a good tool to study Sertoli cell line signal transduction processes (Skinner and Griswold, 2004).

1.2.3 Sertoli cell function regulation

Sertoli cell function is regulated by an interaction of endocrine and paracrine signals *in vivo*. In males, the pituitary gland gonadotropins, follicle stimulation hormone (FSH) and luteinizing hormone (LH), regulate reproductive functions, such as spermatogenesis and steroid hormone (estrogen and androgen) production (Figure 1B). FSH binds to the FSH receptor (FSHR) on the Sertoli cell surface and initiates spermatogenesis. LH binds to the luteinizing hormone receptor (LHR) on Leydig cells, where testosterone are produced and released. Testosterone diffuses into the seminiferous tubules, which in turn stimulates Sertoli cells to produce androgen-binding protein (ABP) by which the testosterone is concentrated and enriched to promote the spermatogenesis (McGuinness et al., 1994).

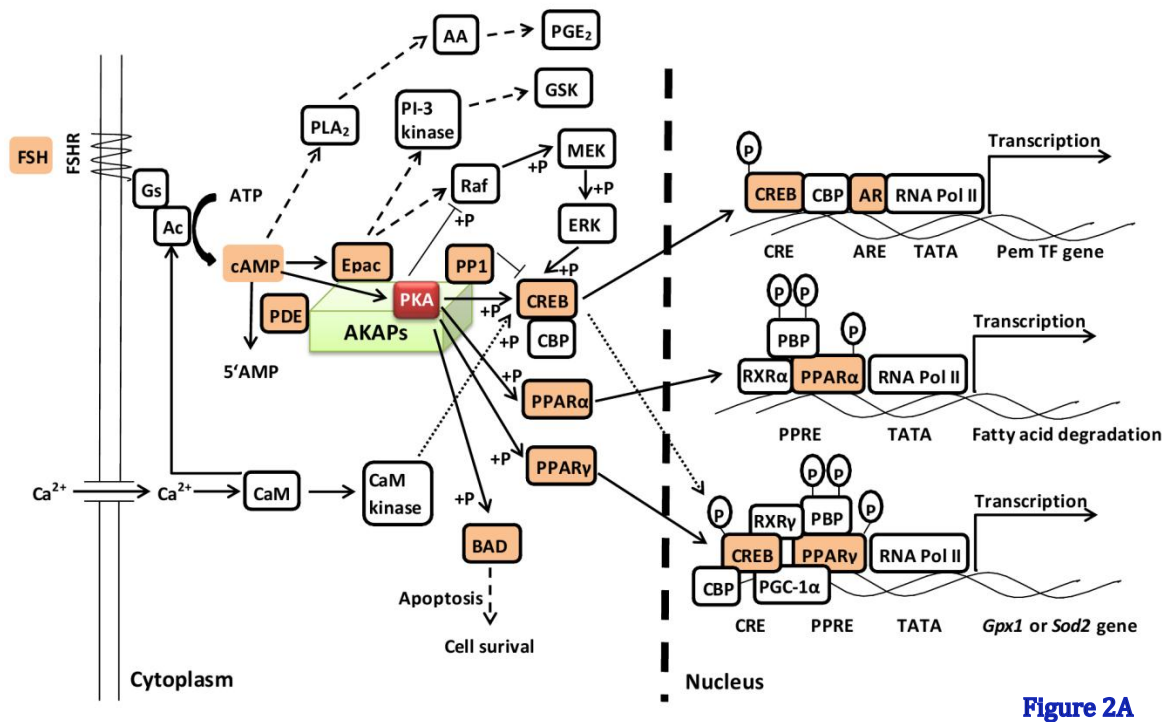


Figure 2A

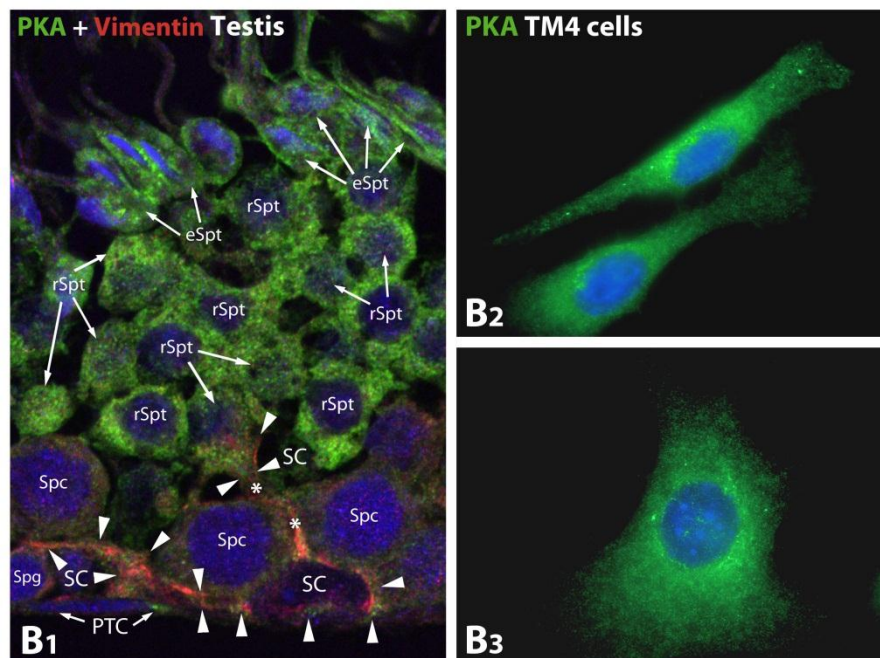


Figure 2B

Figure 2 FSH stimulated cAMP-PKA signaling pathway (Figure 2A) and localization of PKA α in different cell types of a seminiferous tubule in the testis of a 120d-old wild-type mouse (Figure 2B₁) and in TM4 Sertoli cells (Figure 2B₂-2B₃). Figure 2A contains the integrated information from the literatures (Hunzicker-Dunn and Maizels, 2006; Kim et al., 2005; Lazennec et al., 2000; Misra et al., 2002; Wahli et al., 1995; Walker and Cheng, 2005) and KEGG Pathway Database^①. In Figure 2B₁, vimentin (red) was used as Sertoli cell marker (Guo et al., 2015; Nenicu et al., 2007; Skinner and Griswold, 2004). PKA α subunit distribution exhibits strong differences between different spermatogenic stages of germ cell development. It is highest abundant in the cytoplasm of round spermatids (rSpt) and elongated spermatids (eSpt), whereas the cytoplasm of spermatocytes (Spc) contains much less PKA α . Spermatogonia (Spg) are only very weakly labelled by PKA α . Sertoli cells (SC) exhibit an intermediate PKA α staining level between spermatocytes* and round spermatids*. PKA α is abundant in the cytoplasm and is present also on a few organelle-like structures in TM4 Sertoli cells, suggesting that FSH-signalling should work properly in this cell type (Figure 2B₂-2B₃).

^①http://www.kegg.jp/kegg-bin/highlight_pathway?scale=1.0&map=map04024&keyword=FSH%20AMP%20PKA

Gonadotropin hormones modulate the Sertoli and Leydig cells via the cAMP signal-transduction pathway: FSH and LH bind to surface receptors on Sertoli or Leydig cells respectively and thereby stimulate the adenylyl cyclase (AC), causing an increase in intracellular levels of cAMP. An increase in intracellular cAMP results in the activation of the cAMP-dependent protein kinase A (PKA) (Figure 2A), leading to typical cell-specific responses in both cell types (McLean et al., 2002).

The complex cyclical interplay of FSH and testosterone maintain Sertoli cells function by providing the energy required for male germ cell maturation and testicular structure development. FSH and testosterone play a role in the regulation of the synthesis of lactate, transferrin, androgen binding protein, transforming growth factor (TGF) α and β , insulin-like growth factor-1 (IGF-1), fibroblast growth factor (FGF), epidermal growth factor (EGF), mullerian-inhibiting substance (MIS), and inhibin in Sertoli cells (Skinner and Griswold, 2004).

1.2.3.1 FSH signaling

FSH acts on Sertoli cells by binding the FSH receptor (FSHR). FSHR is a cell-surface receptor containing 7 transmembrane domains. Its structure is very similar to the LH receptor (LHR) and the thyroid-stimulating hormone receptor (TSHR). FSH-binding promotes the FSHR associated partner, the inactive heterotrimeric G proteins with α -, β -, and γ -subunits, to release the $G\alpha$ -GTP, which will bind to the adenylate cyclase (AC). The adenylate cyclase is then activated to convert ATP into cAMP, which is an ubiquitous second messenger for intracellular signal transduction. cAMP works by activating protein kinase A (PKA) to dissociate its C subunit ($C\alpha$, $C\beta$ or $C\gamma$), which will phosphorylate nearby substrates (Lazennec et al., 2000).

One PKA target is the transcription factor CREB (cAMP response element binding protein). It is rapidly activated by phosphorylation of Ser¹³³ in response to FSH. Several genes involved in spermatocyte survival are controlled by CREB, such as lactate dehydrogenase (LDH-A), stem cell factor, aromatase, and IGF-1. Mutation in CREB can cause more than 75% of spermatid loss due to apoptosis (Scobey et al., 2001; Walker and Cheng, 2005).

CREB plays also a role in ROS toxicity and mitochondrial biogenesis. These processes are under the control of the key effector- Peroxisome proliferator activated receptor gamma coactivator -1 α (PPAR γ coactivator -1 α , PGC-1 α). PGC-1 α interacts

with CREB as well as the nuclear receptor PPAR γ , driving the expression of ROS detoxifying enzymes, such as GPx1 and superoxide dismutase 2 (SOD2), to regulate oxidative stress (Figure 2A) (Lee et al., 2009). Interestingly, PPAR γ is also a key regulator of peroxisome metabolism and proliferation (Colasante et al., 2015).

In addition to the transcriptional control induced by FSH/PKA signaling, A-kinase anchoring protein (AKAP) might tether the PKA to organelle surfaces on which the PKA can directly influence metabolic processes, such as by the phosphorylation of StAR after binding to AKAP1 on the mitochondrial surface (Dyson et al., 2008; Merrill and Strack, 2014).

1.2.3.2 Testosterone signaling

The androgen testosterone is essential to maintain normal spermatogenesis. A lower intratesticular testosterone concentration would dramatically reduce the rate of spermatogenesis, for example testosterone reduction from 20 to 10ng/ml in adult rats induced an approximately 50% reduction of maintained spermatids per testis (Zirkin et al., 1989). However, compared with our knowledge on the FSH signaling pathway, little is known about testosterone-regulation on gene expression in Sertoli cells. Walker and Cheng (2005) showed that when testosterone is taken up by Sertoli cells through the plasma membrane, the Pem transcription factor is initiated via the binding of the androgen receptor (AR) to the androgen response elements (ARE) in the promoter region to support spermatogenesis (Figure 2A) (Walker and Cheng, 2005).

1.3 AKAPs: Scaffolds for local signaling

AKAP is an acronym for “A-Kinase Anchoring Protein” due to their ability to bind PKA (Carr et al., 1992). Originally AKAPs were named by their apparent molecular mass in SDS-PAGE. However, this nomenclature could be confusing when naming splice variants of the same *Akap* gene (e.g. D-AKAP1 and S-AKAP84) or homologs from different species (e.g. human AKAP149 and mouse/rat AKAP121) (Wong and Scott, 2004). Therefore, the human genome organization nomenclature committee (HGNC) renamed existing AKAPs from AKAP1 to AKAP14^① with no regard to their order of discovery or reference to their traditional name. For example, the first AKAP discovered by Carr and his colleagues in 1992 is human AKAP79 (Carr et

^① <http://www.genenames.org/genefamilies/AKAP>

al., 1992), together with its homologs bovine AKAP75 and mouse/rat AKAP150 are now known as AKAP5. Some AKAPs which were not included in this classification still maintained their original name, such as Gravin, Ezrin, Rab32 and WAVE-1 (Smith et al., 2006; Welch et al., 2010). Most AKAPs are usually high-molecular-weight proteins (e.g. AKAP450 and AKAP-Lbc, each > 300kDa) but some AKAPs exist as small molecular weight proteins (e.g. GSKIP is only 15.6kDa) (Skroblin et al., 2010).

1.3.1 AKAP binding features and signaling cross-talk

AKAPs bind PKA through the unifying motif of a 14-18 amino acid α -helix (Day et al., 2011). PKA is normally an inactive heterotetrameric holoenzyme, consisting of two catalytic and two regulatory subunit dimers (C_2R_2). Because the majority of AKAPs prefer anchoring PKA RII subunits dimers, this binding domain was also termed RII-binding domain (RIIBD). Additionally, AKAPs also contain unique protein-lipid or protein-protein targeting domains for anchoring its complex to specific subcellular locations (McConnachie et al., 2006).

Members of the AKAP protein family act as unique assemble scaffolds, tethering PKA and other enzyme components together and directing them to a particular subcellular location close to the downstream substrates. This spatial separation between effector and substrate is critical for precise regulation and facilitation of signal transduction (McConnachie et al., 2006). As shown in Figure 3, all the cAMP-dependent signal transduction pathways work with a series of similar components, such as GPCR, adenylyl cyclase, protein phosphatase, PDE, Epac and PKA. The isoform of binding partners recruited by AKAPs depend on the specific cell type. The adenylyl cyclase generates cAMP; while, PDE degrades it into 5'-AMP, not only determines the level of cAMP in cells, but also terminates the signal transduction at specific cellular sites. (Skroblin et al., 2010).

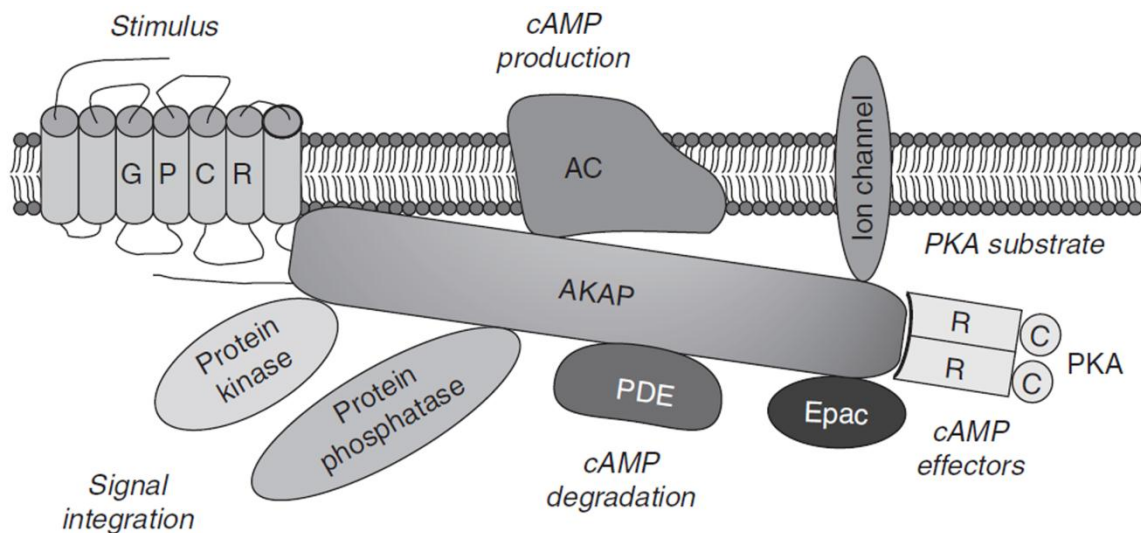


Figure 3 AKAPs assemble the key enzymes and factors, forming a complex to facilitate integration of cAMP and relative signaling pathways. This picture is taken from the book “*International review of cell and molecular biology*” (Skroblin et al., 2010). All the partners have defined functions: G-protein-coupled receptor (GPCR) initiates the signal from external stimulation; adenylyl cyclase (AC) transfers the external signal into second messenger cAMP; phosphodiesterase (PDE) is responsible for cAMP degradation, regulates cAMP concentration together with AC; exchange proteins directly activated by cAMP (Epac) acts as cAMP-effected GTP exchange factors; cyclic nucleotide gated ion channel (cNGC or CNG) is also a cAMP effector; protein kinase A and other kinases activated by cAMP phosphorylate multiple associated substrates, which are helpful for the integration and synergy of further signaling pathways; and protein phosphatase (PP) is mediating the desphosphorylation of those substrates, avoiding dysregulation of signal transduction.

AKAPs do not only coordinate cAMP signaling, but also regulate other events by forming multi-functional complexes with protein phosphatases, ion channels, PKD and other kinases, small GTP-binding proteins, ERK1/2, GSK3 β (see subsection 1.4.1.1), IQGAP1 (see subsection 1.4.1.3), StAR or mRNA (see subsection 1.4.2.3). Therefore, AKAPs play an essential role in integrating the signaling cross talk (McConnachie et al., 2006; Skroblin et al., 2010).

1.3.2 Structure of AKAP-PKA interaction

AKAP family members contain diverse amino acid sequences without any conserved region, even the unifying RIIBDs only share less than 30% amino acid identity (Figure 4). However, despite their sequences diversity, the RIIBDs of AKAP proteins display a conserved unique structural feature throughout the family, which is an amphipathic α -helix motif, interacting with D/D domain of the PKA R subunits (Figure 5).

AKAP1 (gb AAH00729.1)	EIKRAAFQIISQVISEATEQVLIATT
AKAP2 (gb AAH03735.1)	PLEYQAGLLVQNAIQQCAIAEQVDKA
AKAP3 (gb AAH47535.1)	LVIAMARKEINEKIDGSENKCVYQS
AKAP4 (emb CAI41559.1)	DLSFYVNRLSSLVIQMAHKEIKEKL
AKAP5 (gb EAW80862.1)	LLIETASSLVKNAIQLSIEQLVNEM
AKAP6 (gb AAI37233.1)	AEDCSVHNFVKEIIDMASTALKSKS
AKAP7 (emb CAI9002.1)	ELVRLSKRLVENAVLKAVQQYLEET
AKAP8 (gb EAW84474.1)	VAADVLAEVITAAVRAVDGEGAPAP
AKAP9 (gb EAL24158.1)	YQEQLIEEEVAKVIVSMSIAFAQQTE
AKAP10 (gb ABB76684.1)	AQEELAWKIAKMIVSDIMQQAQYDQ
AKAP11 (gb AAF07045.1)	KKAVLAEKIVAEAEIEKAERELSSTS
AKAP12 (dbj BAA19927.1)	ELETKSSKLVQNIIQTAVDQFV RTE
AKAP13 (gb AFH30965.1)	LIEEAASCIVDVIEQVKAARALLT
AKAP14 (gb EAW89839.1)	NYEDEL TQVALALVEDVINYAVKIV
SuperAKAP-IS	QIEYVAKQIVDYAIHQ A
AKAP-IS	QIEYLAKQIVDNAIQQAK
Ht31	LIEEAASRIVDAVIEQV
RIAD	LEQYANQLADQIIKEATE

Figure 4 Alignment of the PKA RII-binding regions of the indicated AKAPs and artificial disruptor peptides (Gold et al., 2006; Hundsrucker et al., 2010; Skroblin et al., 2010)

AKAP RIIBDs consist of hydrophobic and hydrophilic residue pairs, forming a consensus pattern [AVLISE]-X-X-[AVLIF]-[AVLI]-X-X-[AVLI]-[AVLIF]-X-X-[AVLISE] (X = any amino acid) (Hundsrucker et al., 2010; Skroblin et al., 2010). The isoelectric point (pI) of known RIIBDs is in the range of 3.43-6.23. The conserved sequence motif and the pI range could be used together to screen for unknown AKAPs with low false positive hits ratio in a database.

The PKA holoenzymes are divided into two categories: type-I with RI subunits (RI α or RI β) and type-II with RII subunits (RII α or RII β). Type-I PKA is found primarily in the cytoplasm, whereas the type-II is associated with particulate subcellular fractions (Dell'Acqua and Scott, 1997). According to the bias of binding PKA R subunits, AKAPs can be subdivided into 3 classes: RI-, RII-, or dual-specific AKAPs. For example, AKAP1, AKAP4, AKAP10 and AKAP11 are dual-specific and anchor both RI and RII subunits (Day et al., 2011; Nipper et al., 2006). In general, the specific interaction between RIIBD and RII has higher affinity and a lower release-rate than the interaction between RIIBD and RI subunits. Thus, two peptides were developed as isoform-selective R-binding peptides: RI-anchoring disruptor (RIAD) (Carlson et al., 2006) and AKAP-IS which is RII-preferring (Gold et al., 2006). The artificial disruptor peptides maintain higher affinity and specificity than natural AKAPs. These peptides bind PKA R dimer by mimicking the RIIBD amphipathic helix structure, so that they

can competitively disrupt PKA-AKAP interaction and inhibit PKA-dependent signaling by mislocalization of PKA (Carlson et al., 2006).

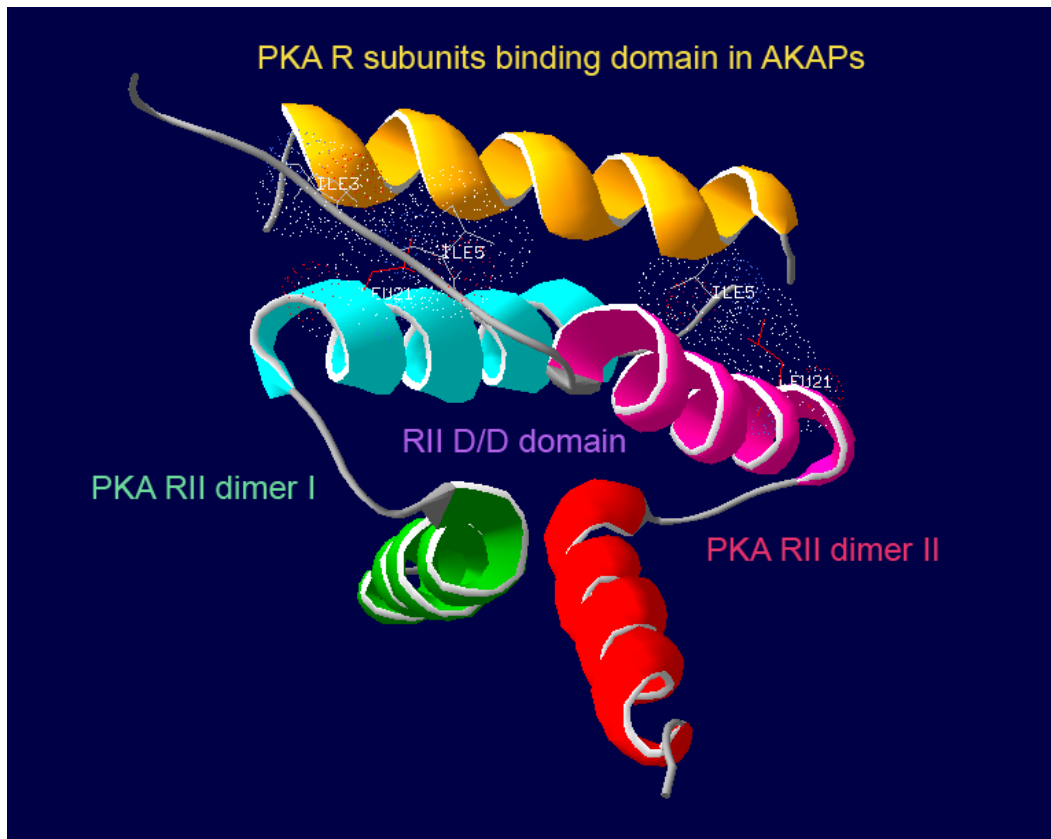


Figure 5 Crystal structure (PDB ID: 2HWN) displaying the contact point between the AKAP RIIBD and PKA RII D/D domain (dimerization and docking domain). This picture was generated by Swiss PDBViewer version 4.1.0. Residues Ile³, Lie⁵ and Leu²¹ in D/D domain are necessary for AKAPs/PKA binding. PKA RII dimer I is formed by helix I (cyan)-turn-helix II (green), and dimer II by helix I' (pink)-turn-helix II' (red). Dimer I interacts dimer II in an antiparallel manner resulting an X-form, 4-helix bundle, which is called D/D domain. The connection is stabilized by the interaction between the hydrophobic core of D/D domain and amphipathic helix from AKAPs (Kinderman et al., 2006).

1.3.3 Diversity and evolution within the AKAP family

Most AKAPs are “canonical AKAPs” and present widely in all organ and cell type, interacting with the D/D domain of PKA R subunit dimers via an amphipathic helix and anchoring PKA and other partners to target organelles, like the plasma membrane, the cytoskeleton, mitochondria, the Golgi apparatus, the nucleus, or vesicular structures (Wong and Scott, 2004).

Some AKAP-PKA binding mechanism work differently. These exceptions are called “non-canonical AKAPs”, such as pericentrin (Diviani et al., 2000) and inactive RSK1 (Gao et al., 2010). Their PKA binding sequence could even be a 100-amino acid,

non-helical, Leucine-rich region that interacts with RII. This binding is also insensitive to AKAP-PKA disruptor peptides. Therefore, the non-canonical AKAPs are often undetected during AKAP screenings and as such often classified as false positive hits, or defined as “putative AKAPs”.

Homologues of many mammalian AKAPs were found in lower vertebrates too. Such as the GSKIP homologue in the one of most basal chordate subphylum, Florida lancelet (*Branchiostoma floridae*), named DUF727, which shares more sequence similarity with human GSKIP than invertebrate GSKIP. There is a big gap between the vertebrate AKAPs and invertebrate orthologs. For example, all the vertebrate AKAP GSKIPs bind PKA RII subunit, in contrast to invertebrate or fungal GSKIP homologues that do not bind RII, suggesting that the RIIBD was formed as vertebrate evolved (Hundsruker et al., 2010).

1.4 A closer look to four AKAPs used in this study

As mentioned above in subsection 1.2.3 (Figure 2A), the hypothalamic-pituitary-testicular axis is critical for the male reproductive system development by secreting the hormone FSH and LH to maintain normal spermatogenesis. Moreover, the cAMP-PKA-dependent signaling cascades initiated by FSH and LH stimulation are assumed to be regulated by certain AKAPs. AKAP11, AKAP1, AKAP4 and AKAP10 have been identified in the testis and are assumed to contain potential organelle targeting motif. Therefore, understanding the connection between these 4 AKAPs and the FSH/LH-stimulated phosphorylation pathways are necessary to further our knowledge of male fertility.

1.4.1 AKAP11 (=AKAP220)

AKAP220, now named AKAP11, was first described as an ubiquitously expressed 220kDa PKA anchoring protein, encoded by the *Akap11* gene, which was previously shown to sequester PKA to peroxisomes (Lester et al., 1996). AKAP220 might influence peroxisomal metabolism in the testis by binding PKA to the peroxisomes. Therefore, it is of interest to define why male patients with peroxisomal dysfunction exhibit male infertility and why peroxisomes are very abundant in Sertoli and Leydig cells (Dastig et al., 2011; Nenicu et al., 2007).

1.4.1.1 Sequence structure and partner binding sites of AKAP11

The human AKAP220 [Q9UKA4.1] is the most well studied AKAP220, also a dual-specificity AKAP that can bind both PKA RI and RII subunits (Reinton et al., 2000). Other binding partners that have been identified by immunoprecipitation include protein phosphatase 1 (PP1) and glycogen synthase kinase-3 β (GSK-3 β) (Logue et al., 2011a; Tanji et al., 2002). The PKA holoenzyme recruitment could enhance protein phosphatase 1 inhibition, so that the intermolecular interactions influence the other binding partners' activity within one signaling scaffold (Schillace et al., 2001). For example GSK-3 β , another enzyme that associates with AKAP220, is phosphorylated by PKA at Ser⁹, thereby decreasing its activity. In contrast, protein phosphatase 1 dephosphorylates Ser⁹ of GSK-3 β to enhance its function (Tanji et al., 2002). GSK-3 β is a Ser/Thr kinase that regulates glycogen synthase activity (Plyte et al., 1992), and also induces apoptosis in cerebellar granule neurons (Li et al., 2000).

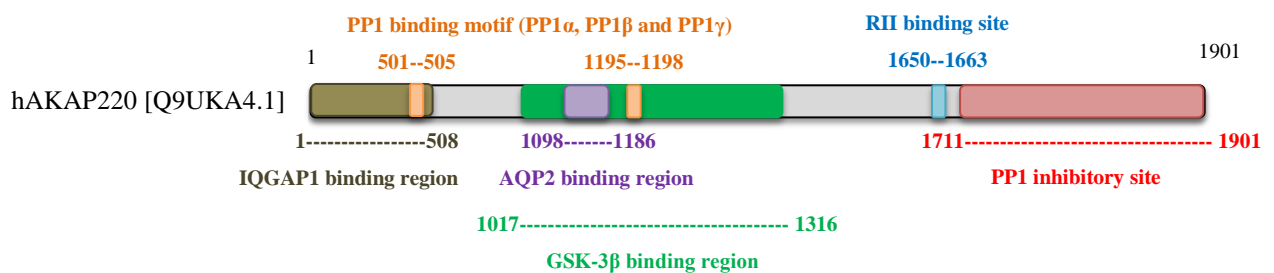


Figure 6 Schematic diagram of hAKAP220 (1901-amino acid) and its partner-binding positions examined by experiments. The color boxes indicate the binding sites or regions as described with corresponding color text (Logue et al., 2011b; Okutsu et al., 2008; Schillace and Scott, 1999; Schillace et al., 2001; Tanji et al., 2002).

1.4.1.2 Subcellular localization

In rats, the first AKAP220 [Q62924.1] was shown by immunofluorescence to be targeted to peroxisomes, which contains a putative peroxisomal targeting signal (PTS1) at its C-terminus (the last 3 amino acids “CRL”) (Lester et al., 1996). However, this peroxisomal targeting remains to be dubious since other researchers have claimed it might be the result of a “*partial overlap of a couple of puncta, possibly caused by chance, was seen in only a few cells either stained for PMP70 or stained for proteins with another peroxisomal targeting sequence –SKL*” (Day et al., 2011). PMP70 is a 70-

kDa peroxisomal membrane protein. Another AKAP220 isoform [NP_036905.2] in rats without PTS1 signal was found as the most abundant AKAP in kidney. Double immunofluorescence staining clearly colocalized AKAP220 with Aquaporin 2 (AQP2) in the subapical cytoplasmic region of inner medullary collecting ducts (Okutsu et al., 2008; Uawithya et al., 2008).

The mRNA of hAKAP220 was found to be highly transcribed in human testis, especially in isolated pachytene spermatocytes and round spermatids. Immunofluorescence labeling showed that endogenous hAKAP220 displayed different subcellular localizations during the human sperm development: cytoplasmic in premeiotic pachytene spermatocytes and centrosomal of postmeiotic male germ cells, elongating spermatocytes and mature sperm. Moreover, the hAKAP220 complex together with PKA RI, RII and protein phosphatase 1 was suggested to associate with cytoskeletal structures of the sperm tail (Reinton et al., 2000). hAKAP220 [Q9UKA4.1] also contains no peroxisomal targeting signal.

In mice, AKAP11 is located in the cytoplasm, and it recruits the type I PKA holoenzyme. Under the stimulation of increasing cAMP level, PKA C subunits are released and promote AKAP11 to target free RI α to multivesicular bodies (MVBs). No colocalization was observed with lysosomes, mitochondria, or peroxisomes, and this mAKAP220 also doesn't contain PTS1 signal (Day et al., 2011).

1.4.1.3 Metabolic functions of AKAP220

AKAP220 has been proposed to be involved in the regulation of the urine concentration. When the animal is dehydrated, the pituitary gland produces arginine vasopressin (AVP), a peptide hormone that acts on the basolateral plasma membrane of collecting ducts of the kidney. The AVP targets the vasopressin type 2 receptor (V₂R), thereby initiating a cAMP-dependent and AKAP220-mediated PKA signal cascade in the collecting ducts. Then the PKA C subunit is activated to phosphorylate a water channel Aquaporin 2 (AQP2) at Ser²⁵⁶, inducing AQP2 to translocate from cytosol to the apical membrane. With the increasing number of AQP2 inserted in the apical membrane, water permeability of the collecting ducts will be enhanced to enable water reabsorption (Okutsu et al., 2008).

Other research has proposed AKAP220 to be involved in migration of human fibrosarcoma cells. AKAP220 assembles the cytoskeletal scaffolding protein IQGAP1,

which plays a role in cytoskeletal polarization and cell motility. AKAP220 supports the spatial and temporal synchronization to regulate dynamic instability of microtubule. Therefore, AKAP220 could be essential in microtubule dynamic for cancer cells migration and invasion as shown in Figure 7 (Logue et al., 2011b).

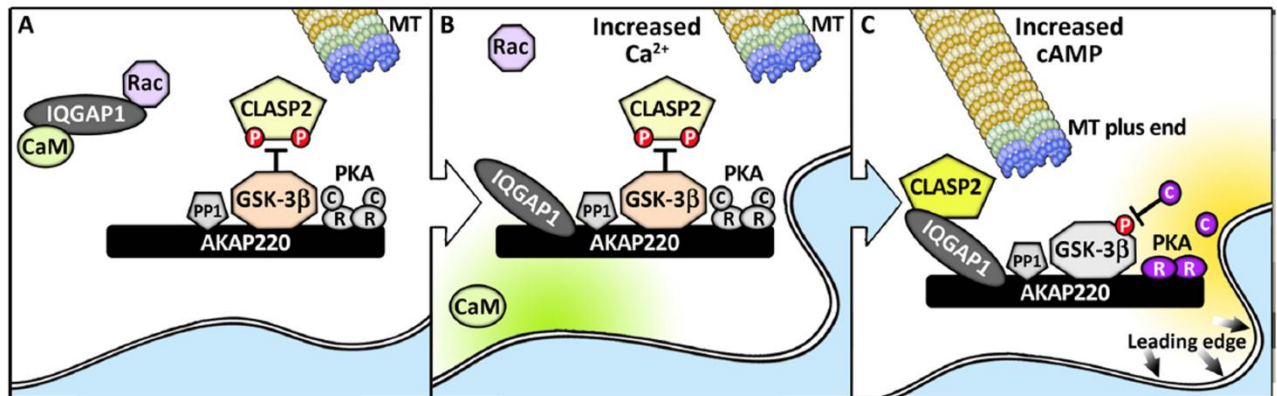


Figure 7 Schematic diagram of AKAP220 complex leading function in cell migration. This picture is taken from (Logue et al., 2011b). IQGAP1 supports Ca^{2+} /CaM-dependent association of factors that modulate microtubule dynamics. Under the integration of Ca^{2+} and cAMP signals, AKAP220 signaling platform was compartmentalized to the substrates at leading edges of migrating cells. Activated GSK-3 β , which is anchored on AKAP220 complex, phosphorylates the plus-end microtubule tracking protein CLASP2 at Ser⁵³³ and Ser⁵³⁷, and inhibits CLASP2 binding to IQGAP1. When the cellular Ca^{2+} level increases, CaM and Rac could release IQGAP1, so that IQGAP1 is then free to bind AKAP220. With an increasing cAMP concentration, PKA is activated and can phosphorylate and inhibit GSK-3 β , resulting the releasing of activated CLASP2 to anchor IQGAP1.

Research has shown a link between AKAP220 and the development of oral cancer. The retinoblastoma (RB) protein is a tumor suppressor protein, which prevents cell growth and its dysfunction can cause several different types of cancers (Murphree and Benedict, 1984). Rb pathway is known to alter the cell cycle and progression of early oral premalignant lesions (OPLs). AKAP220 takes part in the Rb pathway by regulating protein phosphatase 1 activation and RB protein dephosphorylation and the transcription switch of genes involved in cell proliferation. AKAP220 overexpressed significantly in oral tumors, suggesting a role in oral carcinogenesis (Garnis et al., 2005).

1.4.2 AKAP1

A-kinase anchoring protein 1 is also known as AKAP1, PRKA1, AKAP84, TDRD17, AKAP121 [*Mus musculus*], AKAP149 [*Homo sapiens*], D-AKAP1,

PPP1R43 or SAKAP84^①. AKAP1 binds to RI and RII of PKA and anchors them to the cytoplasmic face of the mitochondrial outer membrane^②.

1.4.2.1 Alternative splicing and subcellular locations

Akap1 transcripts are widely expressed in testis, heart, liver, kidney, skeletal muscle and brain. Diverse *Akap1* transcripts are derived from the same gene by alternative pre-mRNA splicing. A common N-terminal exon (1-572 amino acids in human) codes both the mitochondrial targeting sequence (1-30 aa) and the PKA binding helix (347-360 aa). The C-terminal exons are more conserved, coding K homology (KH) domain and a Tudor domain. The differing sequence features determine the various subcellular localizations of AKAP1. For instance, S-AKAP84, a short AKAP1 variant, is mainly expressed in male germ cells (Huang et al., 1999) and targeted selectively to the mitochondrial sheath in the sperm middle piece (Lin et al., 1995). The first 30 amino acids in the N-terminus of AKAP1 N0 form a hydrophobic helix followed by positive charges, which are necessary and sufficient to target AKAP1 to the mitochondrial outer membrane (MOM) (Huang et al., 1999; Ma and Taylor, 2008). Additionally, the AKAP1 N1 variant identified in the mouse liver was reported to target AKAP1 to the endoplasmic reticulum and its N-terminus contained additional 33 amino acids than the AKAP1 N0 variant and may be generated by either alternative splicing and/or differential initiation of translation (Merrill and Strack, 2014). The negatively charged Asp³¹ within the first 33 amino acid residues converts the mitochondrial-targeting signal into both smooth and rough ER-targeting signal consisting of the first 63 residues, without destroying the mitochondrial-targeting signal. Therefore, the availability of the Asp³¹ in AKAP1 N1 variant is responsible to determine its ER or mitochondrial specific targeting (Ma and Taylor, 2008).

^① <http://www.ncbi.nlm.nih.gov/gene/8165>

^② <http://www.phosphosite.org/proteinAction.do?id=7076&showAllSites=true>

1.4.2.2 Sequence features and domains of AKAP1

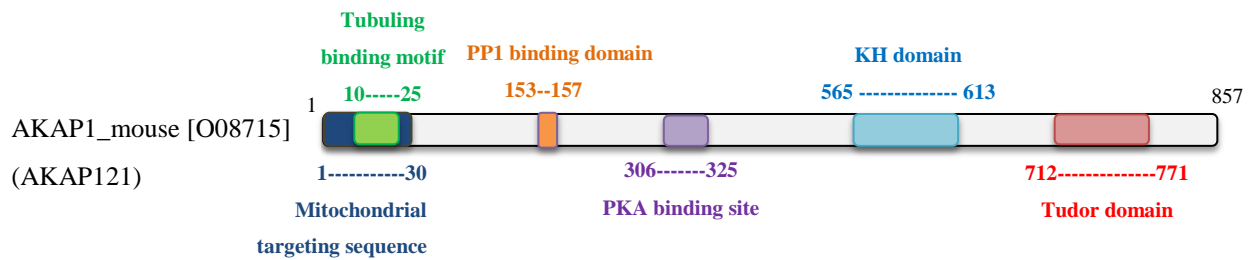


Figure 8 Schematic diagram of mouse AKAP1 (AKAP121) [O08715] (857 amino acids). The color boxes indicate the binding sites or regions as described with corresponding color text.

Within the PKA binding domain, the RII tethering domains found in the AKAP121 of rat (303-322 aa) and mouse (306-325 aa) are 80% identical (Bridges et al., 2006; Feliciello et al., 1998). Spermatid-SAKAP84 binds RII α and RII β (Lin et al., 1995), and residues 306-325 constitute the RII-binding site (Chen et al., 1997).

The K homology (KH) domain can interact independently or cooperatively with different regions of the AU-rich RNAs, and various single strand DNA/RNA-binding proteins contain such KH domain. NMR (nuclear magnetic resonance) measurement revealed its β - α - α - β - α secondary structure^① (Figure 9).

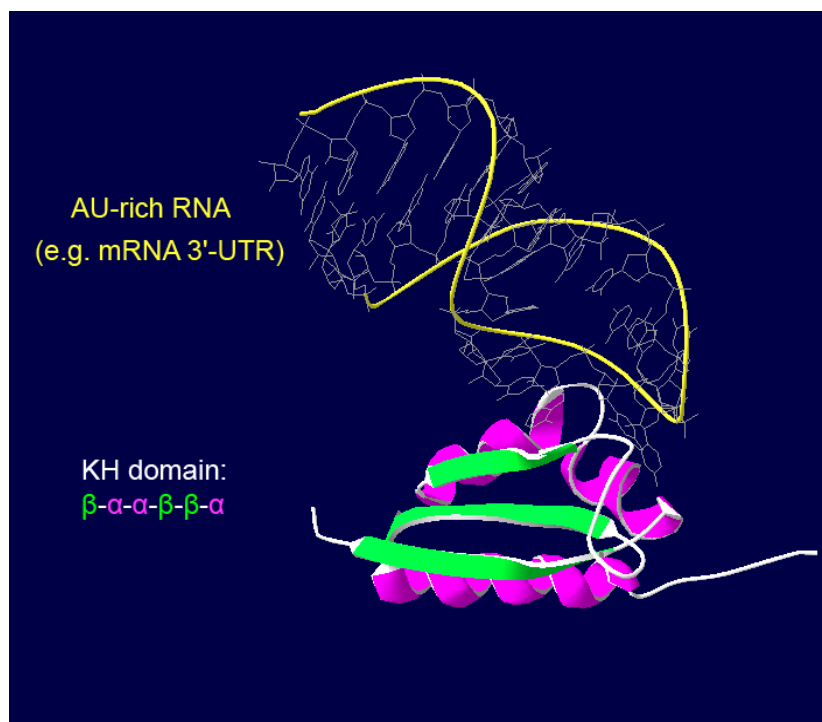


Figure 9 Structure of a KH domain (PDB ID: 2ANR). This picture was generated using the Swiss PDBViewer version 4.1.0. In the downstream of AKAP1 protein sequence, a KH domain is responsible to bind AU-rich 3'-UTR of aimed mRNA (yellow). The KH domain displays a unique secondary structure consisting of 3 α -helixes (pink) and 3 β -sheets (green): β - α - α - β - α .

^① http://pfam.xfam.org/family/KH_1

AKAP121 binds the 3' untranslated region (3'-UTR) of certain mRNAs over the KH domain and plays a role in localization, stabilization, and translational regulation of these mRNAs (Cardone et al., 2002). The KH domain, residues 565-613 in mouse and 562-610 amino acids in rat AKAP121, is highly conserved (Feliciello et al., 1998). The phosphorylation of Ser⁶³⁰ in the AKAP149 KH domain is required for its RNA binding (⁶²⁷RYVS⁶³⁰ is a conserved PKA phosphorylation site), and dephosphorylation of this residue prevents RNA association (Rogne et al., 2009).

The Tudor domain of AKAP1 consists of five anti-parallel β -sheets with a barrel-like fold^①, recognizes symmetrically dimethylated Arginines, and also possesses a weak RNase activity (Grozdanov and Stocco, 2012).

The first 30 residues in all AKAP1 isoforms constitute a mitochondrial targeting motif. High similarity between the mitochondrial anchor domain of NADH-cytochrome *b*₅ reductase and N-terminus of S-AKAP84 has been reported (Beasley et al., 1993). In 2004, a peptide was derived from the mitochondrial anchor domain of AKAP121, [Ac-¹XKKPLALPGMLALLGWWFFSRKKX²⁵-NH₂ (X= β -Ala) (AKAPwt). It displays a helical wheel conformation, which might be essential for both tubulin binding and mitochondrial targeting. This peptide exhibits a strong competing inhibitory function, preventing AKAP121 anchoring PKA to the mitochondrial outer membrane (MOM), and in consequence reduces cAMP effects and its further influence on cell survival (De Capua et al., 2004).

Furthermore, all AKAP1 isoforms (AKAP121, AKAP149, S-AKAP84) contain a conserved region to interact with cellular microtubules. The tubulin binding motif (10-25 aa) and mitochondrial targeting motif (1-30 aa) overlap each other. The tubulin monomers might promote AKAP1 scaffold to anchor mitochondria (Cardone et al., 2002).

1.4.2.3 Binding partners of AKAP1 and responding mechanism and functions

Sequence features determine secondary structures of proteins, and the three-dimensional folding of proteins supplies molecular interactions domains for protein-protein, protein-DNA or -RNA, protein-lipid, protein-ion interaction. Due to these

^① <http://pfam.xfam.org/family/TUDOR>

domain and interaction, the subcellular location and function of a specific protein can be determined and modified.

1.4.2.3.1 AKAP1 binds double-hairpin loop of „mitochondrial“ mRNAs

The KH domain of AKAP1 binds the stable stem-loop structure of pyrimidine-rich RNAs (Livigni et al., 2006). The mRNAs of the steroidogenic acute regulatory protein (*Star*), superoxide dismutase 2 (*Sod2*, *MnSOD*), ATP synthase (*F0-f*) and lipoprotein lipase (LPL) contain double-hairpin structures in their 3'UTR (Dyson et al., 2008; Rogne et al., 2009). When the KH domain is phosphorylated by PKA, the AKAP1-mRNA binding stabilizes these mRNAs, leading to more translated proteins and thereby increasing the abundance of the corresponding proteins in mitochondria after their import into the organelle (Ginsberg et al., 2003; Grozdanov and Stocco, 2012).

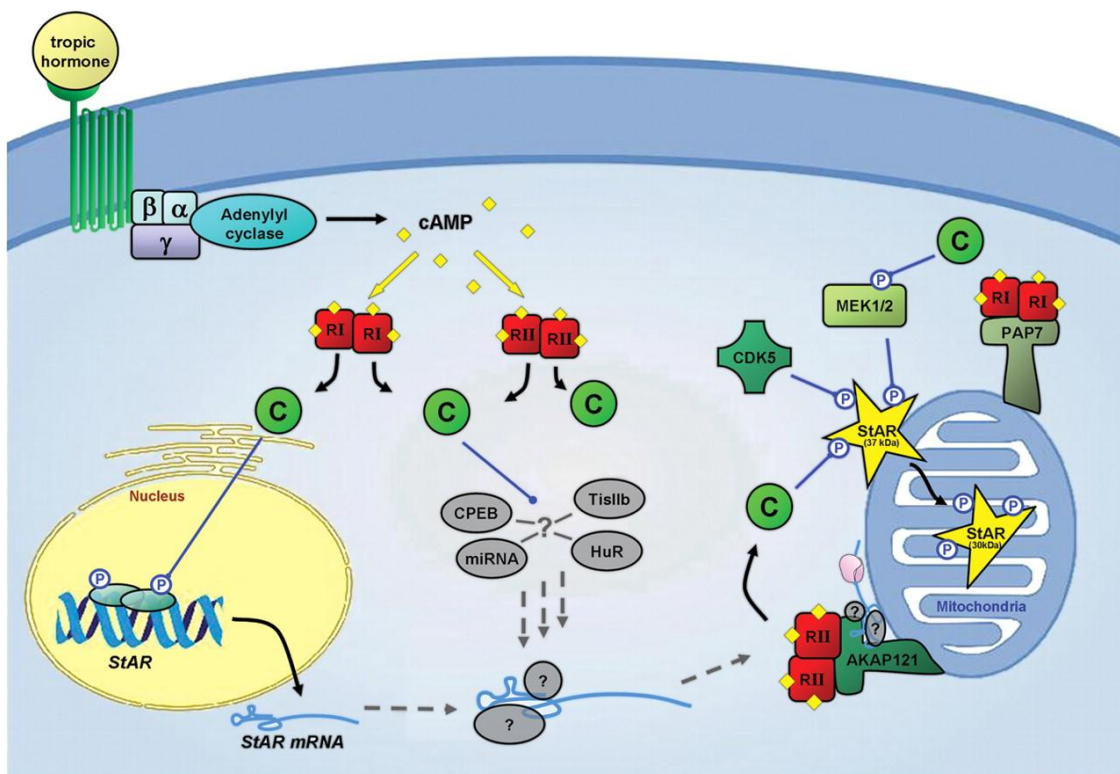


Figure 10 An illustration of cAMP-PKA pathway mediated transcriptional and translational regulation of StAR. Tropic hormone initiates cAMP-PKA depended signaling pathway to induce *Star* transcription. AKAP1 (AKAP121) recruits *Star* mRNA to the outer mitochondrial membrane, accelerating the translation and activation of StAR protein. AKAP1 also associates type II PKA to the mitochondria, which activates StAR at the mitochondrial membrane through the phosphorylation of Ser¹⁹⁵. Some other different kinases also take part in the StAR phosphorylation. And the precursor 37kDa StAR was cleaved into 30kDa mature form, translocating cholesterol from mitochondrial outer membrane to inner membrane. But this whole processing mechanism is still unclear. This picture is taken from the review on StAR regulation (Manna et al., 2009).

1.4.2.3.2 Binding through a direct protein-protein interaction

AKAP1 anchors both PKA RI and RII subunits to the outer mitochondrial membrane (Herberg et al., 2000). AKAP1/RI α interaction was suggested to influence the release of neurotransmitter (Perkins et al., 2001).

Human AKAP1 (AKAP149) was reported to bind protein phosphatase 1 via ¹⁵³KGVL¹⁵⁷ or ⁶²⁷RYVSF⁶³¹ motif (Bridges et al., 2006). Protein phosphatase 1 is a Ser/Thr phosphatases, consists of one catalytic subunit and one regulatory subunit. Most protein phosphatase 1 regulators contain an RVXF motif which interacts with the hydrophobic region of protein phosphatase 1 (Rogne et al., 2009).

AKAP1 also associated with type 4 phosphodiesterases (PDE4), which influenced T cell activation, and suppressed inflammation by hydrolyzing cAMP (Asirvatham et al., 2004).

AKAP1 has been shown to interact with a complex of protein tyrosine phosphatase D1 (PTPD1) (Møller et al., 1994) and the non-receptor tyrosine kinase Src (Dagda et al., 2011). Src was targeted to mitochondria and activated via PTPD1, increasing mitochondrial respiration (Livigni et al., 2006). Subsequently, the mitochondrial Src phosphorylates cytochrome c oxidase (COX) and stimulates COX activity, which positively regulates components of the respiratory chain (Carlucci et al., 2008).

A key-signaling event in the control of the mitochondrial morphology is the reversible phosphorylation of the fission protein dynamin-related protein 1 (Drp1). PKA phosphorylates Ser⁶³⁷ in human Drp1 (Ser⁶⁵⁶ in rat Drp1 isoform 1 (Dagda et al., 2011), results in Drp1 inhibition (Cribbs and Strack, 2007), and therefore increases the mitochondrial stability and cell survival. AKAP1 also recruits the calcium-responsive phosphatase calcineurin (CaN, PP2B). CaN dephosphorylates Ser⁶³⁷, thus activating Drp1 and promoting mitochondrial fission and fragmentation (Carlucci et al., 2008; Merrill and Strack, 2014).

c-myc binding protein (MYCBP, also called AMY-1) was found to bind to the PKA RII binding region of AKAP149 and S-AKAP84. AMY-1 and S-AKAP84 mRNAs were found to be strongly expressed in the testis after the appearance of spermatocytes (Furusawa et al., 2001).

AKAP149 binds to the RNase H region of HIV-1 reverse transcriptase (HIV-1 RT), through the association between residues 375-645 of APAK149 and residues 464-541 of HIV-1 RT p66 (Lemay et al., 2008; Warren et al., 2009).

AKAP1 also binds AKAP1 itself to form an AKAP1-dimer via their C-terminal KH and Tudor domains. Moreover, this self-association requires RNA binding to the KH domain, but the molecular mechanism and physiological role of AKAP1 self-association are not clear (Merrill and Strack, 2014; Rogne et al., 2006).

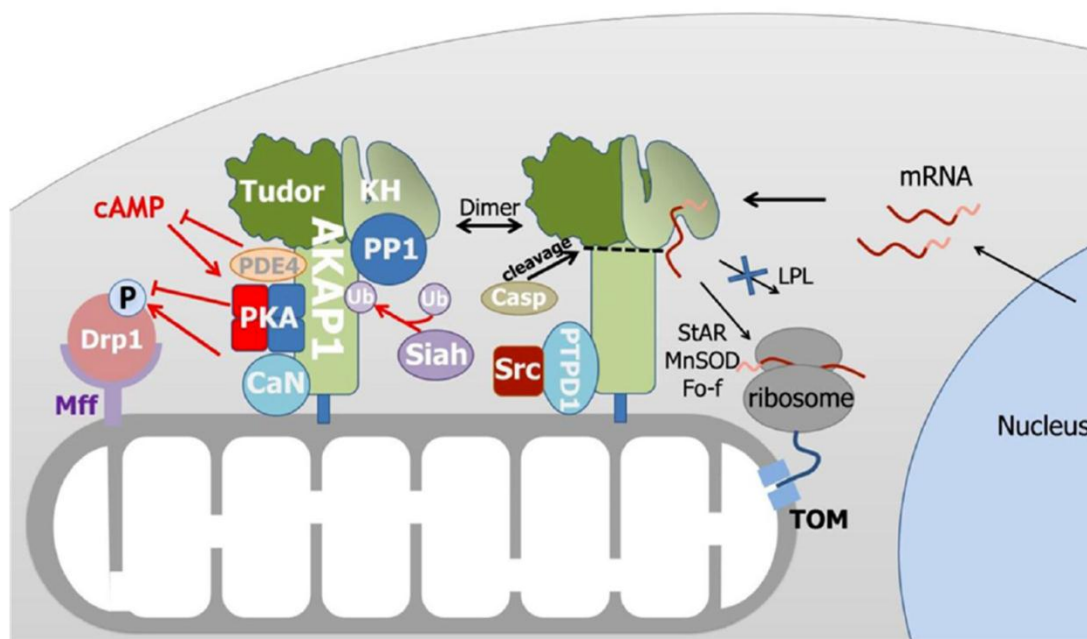


Figure 11 A model illustrating of AKAP1 scaffold complex on the mitochondrial outer membrane, assembling diverse mRNA and protein partners to facilitate and integrate signaling pathways as described above (Merrill and Strack, 2014)

1.4.2.4 *Akap1* transcript and posttranslational regulation

The translational coactivator PPAR γ (Peroxisome proliferator-activated receptor γ) was shown to be involved in the *Akap1* mRNA regulation. Knock-in mice expressing mutated PPAR γ (P465L), a mutation associated with severe dyslipidemia in humans, display reduced AKAP1 expression, whereas obese humans treated with the PPAR γ agonist rosiglitazone show increased AKAP1 mRNA levels indicating a possible involvement of AKAP1 in lipid metabolism (Rodriguez-Cuenca et al., 2012).

Caspase (Figure 11, Casp) cut the site DSVD of AKAP1 (579-582 aa in AKAP149). This cleavage results in an N-terminal fragment that contains the mitochondrial targeting sequence and the PKA binding site and a C-terminal fragment with the KH and Tudor domains. Whether this caspase cleavage of AKAP1 is functionally involved in the apoptotic program is unknown (Yoo et al., 2008).

Ischemic insults were shown to promote ubiquitination and degradation of AKAP1. This occurs through the activation of the transcription factor HIF-1 α (Hypoxia induced factor 1 α), which induces Siah2 (E3 ubiquitin-protein ligase 7 in-absentia homolog 2) for ubiquitination of AKAP1. Ubiquitination accelerates the degradation of AKAP1 and promotes apoptosis (Kim et al., 2011). Hypoxia induces transcription and accumulation of Siah2, a RING domain E3-ubiquitin ligase. Siah2 targets PHD1 and PHD3 enzymes for proteasomal degradation, enabling accumulation of HIF-1 α and downstream activation of hypoxia-induced genes. Hypoxia promotes Siah2-mediated ubiquitination and proteasomal degradation of AKAP121. This regulatory system, allows a fast adaptation of ischemic tissue to low oxygen and metabolite levels, and might be more rapid than transcriptional regulation (Carlucci et al., 2008).

1.4.3 AKAP4

A-kinase anchoring protein 4^① (AKAP4, PRKA4, AKAP-4, AKAP110, AKAP82, mAKAP82), acts as a prominent structural protein of the sperm fibrous sheath (FS), initiating sperm capacitation and influencing sperm motility^② (Hu et al., 2009).

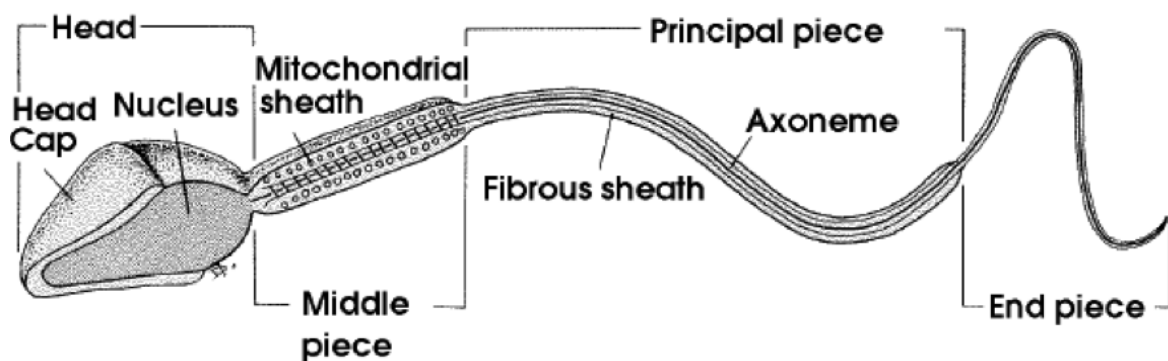


Figure 12 Normal sperm structure (this picture is taken from <https://www.studyblue.com/notes/n/male-reproductive-system/deck/4722824>)

^① <http://www.ncbi.nlm.nih.gov/gene/11643>

^② <http://www.phosphosite.org/proteinAction.do?id=9139&showAllSites=true>

Mouse AKAP4 (mAKAP82) and its homologue human AKAP4 (hAKAP82), are the most abundant proteins of the sperm fibrous sheath as shown in Figure 12 (Brown et al., 2003; Hu et al., 2009). Their precursors, pro-mAKAP82 and pro-hAKAP82 were also found in the proximal portion or entire length of the principal piece (Turner et al., 1998). The fibrous sheath is a unique and major cytoskeletal structure in the principal piece of the flagellum, together with outer dense fibers (ODFs) and the axoneme, which is required for sperm motility (Nipper et al., 2006). cAMP-dependent phosphorylation/dephosphorylation events are critical for the initiation and maintenance of sperm flagellar beating. mAKAP82 and hAKAP82 localize to the fibrous sheath, influencing sperm motility by controlling cAMP-PKA signal transduction. A high homology of sequences was shown among pro-mAKAP82, pro-hAKAP82 and a 75kDa rat fibrous sheath protein, suggesting conserved structure and function throughout AKAP4 family (Turner et al., 1998). The *Akap4* transcript is highly expressed during early spermatid development, whereas translated AKAP4 associated with fibrous sheath only in the late phase of spermatid development. The mature form of AKAP4 can bind AKAP3, which is another sperm-specific AKAP (Carr et al., 2001), as well as Fibrous Sheath Interacting Proteins 1 and 2 (FSIP1 and FSIP2) (Brown et al., 2003). AKAP4 can bind both RI α and RII α of PKA, and target them to the microtubular cytoskeleton by AKAP4-tubulin interaction (Nipper et al., 2006).

1.4.4 AKAP10

A-kinase anchoring protein 10^① (AKAP10, PRKA10, D-AKAP2, D-AKAP-2) is a dual-specific AKAP that binds type I and II PKA (Hamuro et al., 2002). AKAP10 has a C-terminal PKA binding region with conserved 27-residues (e.g. V⁵⁶⁵ to Q⁵⁹¹ in human AKAP10 [ABB76684.1]) that are sufficient for PKA binding. AKAP10 also contains one or two putative RGS domains (regulator of G protein signaling), indicating its function in signal transduction (Wang et al., 2001).

The endogenous AKAP10 protein displayed various subcellular localizations in different cell types. For example, a mitochondrial pattern was reported in mouse oocytes (Webb et al., 2008), mouse myocyte cell line, and rat cardiomyocyte primary cells (Wang et al., 2001). A cytoplasmic staining for AKAP10 was found in a human colon cancer cell line (Wang et al., 2001). AKAP10 was also detected near postsynaptic and

^① <http://www.ncbi.nlm.nih.gov/gene/56697>

presynaptic rat neuromuscular junction (NMJ) and near the actin region in rat muscle (Perkins et al., 2001). However, the targeting mechanism has not been clarified yet been clarified, while the mitochondrial targeting motif was only assumed to be in the N-terminus of AKAP10 (Wang et al., 2001).

AKAP10 plays a role in human heart rhythm control (Tingley et al., 2007). Genetic AKAP10 mutations could cause sudden cardiac death (SCD), which is one kind of unexpected rapid natural death occurring within one hour after the initial symptoms^①.

1.5 The function of AKAP1, AKAP4, AKAP10 and AKAP11 in genital organs

AKAPs in different organs execute distinct specific functions. For example, AKAP1 is highly expressed in adipocytes, and was suggested to play a role in the development of obesity (Merrill and Strack, 2014). AKAP1 in bones may promote bone growth and mineralization (Alam et al., 2010). AKAP121 (=AKAP1) down regulation has also been suggested to represent an important event in the development of cardiac dysfunction inducing heart failure (Perrino et al., 2010). Scaffold protein AKAP1 brings PKA to the mitochondria outer membrane to protect neurons from injury (Merrill et al., 2011), highlighting the importance of studying compartmentalized signaling networks in neurodegeneration and neuroprotection (Dagda et al., 2011). In the following subsections, the roles of AKAPs in the reproductive system are highlighted.

1.5.1 Steroid hormone biosynthesis

The rate-limiting step of steroidogenesis is mediated by the steroidogenic acute regulatory protein (StAR) (Dyson et al., 2008). StAR activity facilitates the transfer of cholesterol across mitochondrial membranes to provide the substrate for the cytochrome P450 side-chain cleavage enzyme (P450_{scc}; CYP11A1). Inside the mitochondria, P450_{scc} converts cholesterol to pregnenolone, which is the first steroid formed during the synthesis of all steroids (Miller and Bose, 2011). AKAP1 regulates posttranscriptional modification and degradation of StAR, especially the intracellular levels of *Star* mRNA (Grozdanov and Stocco, 2012). It is suggested that PKA in

^① <http://www.phosphosite.org/proteinAction.do?id=18193&showAllSites=true>

complex with AKAP1 directs the regulation of StAR expression in three ways: 1) PKA serves to control the *Star* promoter; 2) PKA enhances the translation of *Star* mRNA; and 3) PKA promotes StAR phosphorylation and activation (Dyson et al., 2008; Gomez-Concha et al., 2011).

1.5.2 Sperm development

S-AKAP84 (unique AKAP1 in sperm) accumulates as spermatids undergo nuclear condensation and tail elongation (Lin et al., 1995). S-AKAP84 and its splice variant AKAP121 (=AKAP1), anchor PKAII α to the cytoplasmic surface of mitochondria. This anchoring has been suggested to be involved in the translocation of mitochondria to the site of cytoskeleton assembly in male germ cells. This process ultimately may modulate the motility and/or the fertilization capacity of spermatozoa (Felicciello et al., 1998). When human AKAP220 (=AKAP11) is expressed in testis, AKAP220 switches from granular cytoplasmic pattern to the centrosome in mature sperm. Two AKAP4 isoforms, AKAP82 and AKAP110, are testis-specific and major structural proteins of the sperm tail principal piece, throughout the fibrous sheath-transverse ribs and longitudinal columns, and are important for sperm motility (Tasken and Aandahl, 2004).

1.5.3 Oocyte maturation

Homozygous female AKAP1 knockout mice are subfertile or infertile while heterozygous females and all genotype of males exhibit normal fertility. AKAPs play dual role in oocyte maturation: 1) the cAMP-PKA dependent growth arrest of oocytes at meiosis I prophase needed to be maintained by AKAPs prior to the luteinizing hormone surge. 2) after the initiation of oocyte maturation, AKAP1 is responsible for this maturation to proceed normally and irreversibly by sequestering PKA catalyzed phosphorylation from its targets (Newhall et al., 2006). The mitochondrial localization of PKA (YFP-linked catalytic subunit of PKA encoded from microinjected mRNA, YFP-PKA^{cat}) is required as the oocyte grows from 61 μ m to 68 μ m diameter. This localization is continuously detectable throughout oocyte maturation until fertilization. mRNA levels of both AKAP1 and AKAP10 are markedly reduced in growing oocytes, and increase in the germinal vesicle (GV) stage, peak during metaphase II and subsequently decrease in the 2-cell embryos stage, suggesting a pattern consistent with that observed for the exogenous PKA (YFP-PKA^{cat}) localization (Webb et al., 2008).

1.5.4 Prostate cancer

Prostate cancer (PC) remains the most common male cancer in USA. The risk to develop PC cancer is increased by male infertility (Tvrda et al., 2015). Compare to the healthy tissues (normal prostate as negative control, and normal testis as positive control), AKAP4 protein abundance in PC patients biopsies was found to be increased. The reason for this aberrant expression pattern is not yet clear. One supportive evidence is that AKAP4 mediates calcitonin-induced invasiveness in PC tumor cells (Chiriva-Internati et al., 2012).

1.6 Peroxisomes and infertility

As mentioned in subsection 1.4.1, AKAP220 in rats was suggested to be present in Sertoli cell peroxisomes. Peroxisomes are small single-membrane organelles present in all cell types, protecting cells against oxidative stress and lipid toxicity. This organelle has been associated with cAMP-responsive events, such as androgen biosynthesis and testosterone secretion (Lester et al., 1996). Peroxisomes also play an important role in spermiogenesis, spermatogenesis and lipid metabolism including β -oxidation of very long chain fatty acids (VLCFA) and cholesterol synthesis in Sertoli cells of seminiferous tubules (Lüers et al., 2006; Nenicu et al., 2007). The patients with peroxisomal biogenesis defects such as Zellweger syndrome, display degeneration in Sertoli cells and Leydig cells (Nenicu et al., 2007). Peroxisomes in germ cells were found to be functional in the synthesis of polyunsaturated fatty acids (PUFA) which are the major component of germ cell phospholipids membrane to protect them against oxidative stress. Peroxisomes were also suggested to be involved in the degradation of leukotrienes and prostaglandins from paracrine between germ cells and Sertoli cells (Dastig et al., 2011).

1.6.1 Metabolic pathways in peroxisomes involved in male fertility

Functional peroxisomes are essential for normal spermatogenesis and the lipid homeostasis of Sertoli cells. Peroxisomes protect Sertoli cells against ROS and lipid toxicity. Sertoli cell-specific *Pex5* knockout mice were infertile and exhibited a lipid accumulation in Sertoli cells (Nenicu et al., 2007). Genetic defects in the peroxisomal membrane transporter ABCD1 results in dysfunction of peroxisomal metabolic

pathways causing adrenoleukodystrophy/adrenomyeloneuropathy (ALD/AMN) disease. The patients with these defects exhibited severe testicular disorders, such as an accumulation of VLCFA, abnormal levels of LH and FSH and vacuolated Sertoli cells, resulting in poor germ cell maturation and reduced fertility (Dastig et al., 2011; Lüers et al., 2006; Nenicu, 2010). ABCD1 (also known as ALDP) is an adrenoleukodystrophy protein/lipid transporter of the peroxisomal membrane and also one of the abundant transporters in Sertoli cells, which mainly regulates cholesterol side chain oxidation by peroxisomal β -oxidation pathway 2 (Nenicu et al., 2007). ABCD1-3 transport the different types of fatty acids such as VLCFA, LCFA, 2-methyl-branched chain fatty acids, dicarboxylic acids, polyunsaturated fatty acids, leukotrienes and prostaglandins into peroxisomal matrix (Colasante et al., 2015). Recently, substrates specificities of different ABCD transporters have been analyzed in detail (Ferdinandusse et al., 2014; van Roermund et al., 2014; van Roermund et al., 2011).

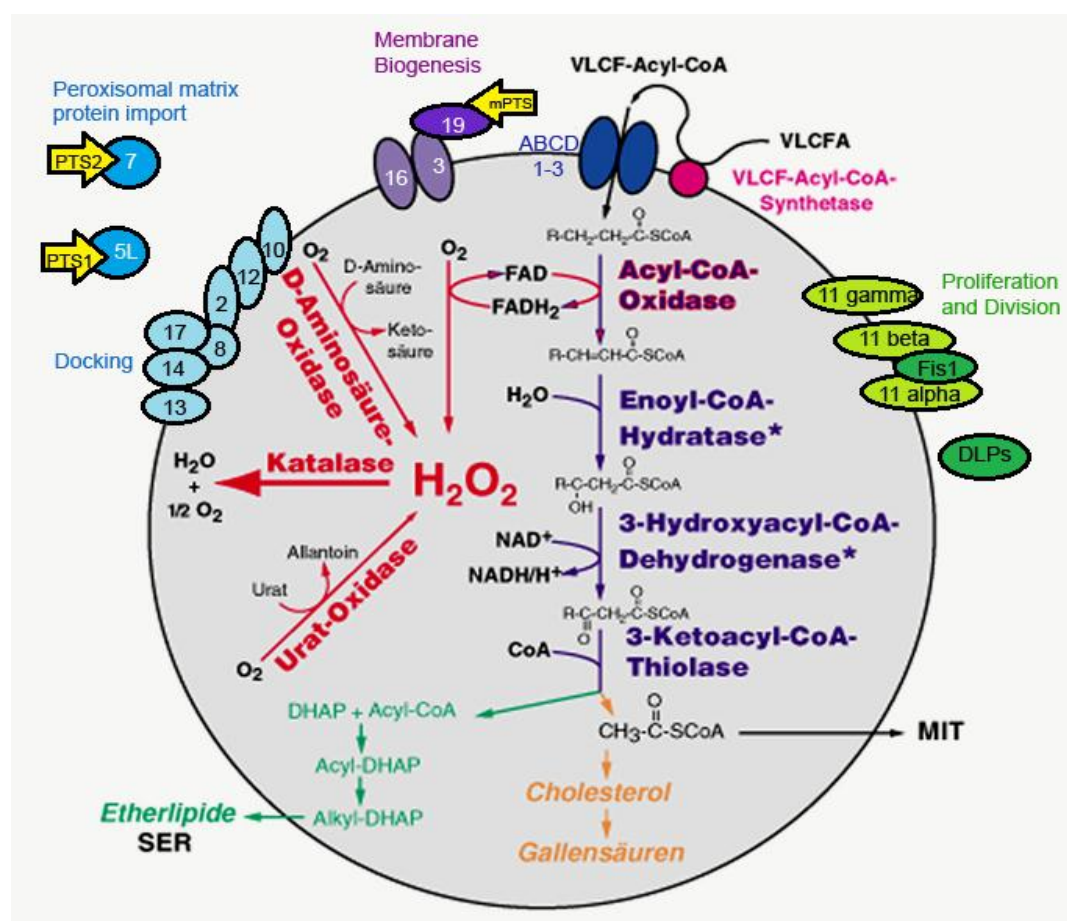


Figure 13 Brief overview of major metabolic pathways and peroxins (in number) in peroxisomes of the mammalian testis. This picture is adapted from (Colasante et al., 2015; Fahimi and Baumgart, 1999).

Deficiencies of two key enzymes, dihydroxyacetonephosphate acyltransferase (DAPAT) and alkyl dihydroxyacetonephosphate synthase (ADAPS), involved in plasmalogens (PLs) synthesis caused mice spermatogenic arrest and a Sertoli cell-only phenotype. DAPAT and ADAPS are peroxisomal proteins, which carry a PTS1 and a PTS2 respectively. Another defect in the peroxisomal protein, glyceronephosphate O-acyltransferase (GNPAT), in mice resulted in atrophic testis (Rodemer et al., 2003). Multifunctional protein-2 (MFP-2, also known as HSD17B4) is a peroxisomal protein that involved in two β -oxidation pathways to catalyse both straight chain and branched chain fatty acids in peroxisomes (Huyghe et al., 2006; Nenicu et al., 2007). *MFP-2* knockout mice developed neutral lipids accumulation in Sertoli cells and testis degeneration. This blocked peroxisomal β -oxidation in Sertoli cells might induce the seminiferous epithelium disintegration and mice infertility (Huyghe et al., 2006).

Interestingly CCDC33 protein, a cancer/testis antigen expressed exclusively in testis, is a peroxisomal protein containing a putative type 2 peroxisomal targeting signal (PTS2) (Kaczmarek et al., 2009). This again suggested the peroxisomal proteins play a role in spermatogenesis.

1.6.2 Peroxisomal matrix protein translocation and import machinery

Peroxisomal proteins are translated on free ribosomes within the cytoplasm. Protein translocation and import depend on the presence of peroxisomal targeting signal sequences (PTS) in peroxisomal matrix proteins located either at the C-terminus or at the N-terminus and interact with specific cytoplasmic receptors (Dastig et al., 2011; Lüers et al., 2006).

The two peroxisomal targeting signals are named PTS1 and PTS2. Most peroxisomal matrix proteins contain a C-terminal PTS1, which is recognized by the cytoplasmic receptor PEX5p (PEX5Lp in Figure 13 is the long isoform of PEX5p in mammals with a tetra-tricopeptide repeat domain). A few peroxisomal matrix proteins contain the PTS2 signal and are shuttled by receptor PEX7p. The PTS2 motif is mostly located at the N-terminal or less frequently at an internal region of the protein and consists of the consensus sequence pattern [RK]-[LVIQ]-X-X-[LVIHQ]-[LSGAK]-X-[HQ]-[LAF] (where X is any amino acid) (Kaczmarek et al., 2009). Both receptors bind peroxisomal matrix proteins and transfer them from the cytosol to the docking complex

(PEX13p and PEX14p) on the peroxisomal membrane. However, how the peroxisomal proteins travel across the peroxisomal membrane and are released into the peroxisomal matrix is still unclear (Islinger et al., 2012; Schrader and Fahimi, 2008).

1.7 Aims of the thesis

Although it is well known that the FSH stimulated PKA pathway affects spermatogenesis and Sertoli cell functions strongly, until now only one AKAP220 protein has been identified to be involved in targeted PKA regulation of steroid biosynthesis in Sertoli cells. This PKA-anchoring protein in the rat appeared to be restricted to the peroxisome because of its PTS1 at the C-terminus. However, it is unknown whether PKA is targeted to the peroxisomes and its role in peroxisomes has not yet been investigated. Peroxisomes function in cellular β -oxidation of fatty acids, as well as LH-responsive testosterone secretion in Leydig cells (Mendis-Handagama et al., 1992). New information on A-kinase anchoring proteins and their eventual action on peroxisomal metabolism will help to understand the role of these organelles in the normal physiology of the testis and in the molecular pathogenesis of male infertility. Furthermore, understanding the A-kinase anchoring proteins can eventually provide insights on coordination of organelles involved in steroidogenesis, such as mitochondria, the endoplasmic reticulum and peroxisomes. Finally, it is known that PPAR α , involved in regulation of many peroxisome genes, is phosphorylated by PKA. Therefore, it was hypothesized that the AKAP protein with putative PTS1 signals transported to the peroxisomes may influence peroxisome metabolic events related to the biological function of a certain cell type.

Therefore, the main aims of this project were:

- To analyze whether peroxisome gene transcription is influenced by FSH
- To analyze whether AKAP220 is really localized in Sertoli cell peroxisomes
- To characterize A-kinase anchoring proteins with putative C-terminal “PTS1”
- To clone these AKAPs and analyze their subcellular location in Sertoli cells
- To get more insights on their eventual function in Sertoli cells

2 Materials

2.1 Cell line and medium

The Sertoli cell line (TM4) and the medium used for the studies are described in details in Table 1.

Table 1 Cell line and medium (information from ATCC search and Health Protection Agency cell line data sheet 50004291)

Cell line name	TM4
ATCC® Number	CRL-1715™
Catalogue No.	88111401
Lot No.	00C013
Description	Mouse BALB/c testis Sertoli cell
Growth Mode	Adherent
Culture Medium	Ham's F12 + DMEM (1:1) + 2mM Glutamin [DMEM/F-12+GlutaMax™-L (GIBCO 31331)] + 5% Horse Serum (HS) + 2.5% Foetal Bovine Serum (FBS)
Reactivity	From primary culture of Sertoli cell enriched preparations from normal testis of a 11-13 day old BALB/c nu/+ mouse. Cells respond to FSH but not LH; Plasminogen activator secretion is FSH and also retinoic acid.
Preservation	Freeze medium: 90% culture medium + 10% DMSO Storage temperature: liquid nitrogen vapor phase

2.2 Routine Materials

Routine materials used in this thesis are summarized in Table 2.

Table 2 Routine reagents list

Reagent Name	Company / person	Cat. No.	Application
Follicle-stimulating hormone (FSH)	Sigma-Aldrich	F8174	PKA activator
Cholera toxin (CT)	Sigma-Aldrich	C8052	Gs protein activator
Forskolin (FSK)	Sigma-Aldrich	F6886	Adenylate cyclase (Ac)

			activator
8-Br-cAMP	Sigma-Aldrich	B5386	cAMP analog
3-Isobutyl-1-methylxanthine (IBMX)	Sigma-Aldrich	I5879	Phosphodiesterase (PDE) inhibitor
H89 dihydrochloride hydrate	Sigma-Aldrich	B1427	Specific inhibitor of PKA
Cell Lysis Buffer (10×)	Cell Signaling Technology®	#9803	Used for protein isolation
OptiPrep™ Density Gradient Medium	Sigma-Aldrich	D1556	Used for cell and organelle isolation
Immun-Star™ AP Substrate	Bio-Rad Laboratories, Inc.	170-5018	Western blot substrate, used for detection
Precision Plus Protein™ WesternC™ Standards	Bio-Rad Laboratories, Inc.	161-0376	Protein ladder for Western blots
Precision Plus Protein™ Standards Dual Color	Bio-Rad Laboratories, Inc.	161-0374	Protein ladder for Western blots
RNase-ZAP™	Sigma-Aldrich	R2020	Cleaning agent for removing RNase
RNA Marker	Promega	G3191	RNA ladder for gel electrophoresis
Anti-Digoxigenin	Roche Applied Science	11 333 062 910	Northern Blot
SP6 RNA Polymerase	Roche Applied Science	10 810 274 001	Northern Blot
T7 RNA Polymerase	Roche Applied Science	10 881 767 001	Northern Blot
DIG RNA Labeling Mix, 10× conc.	Roche Applied Science	11 277 073 910	Northern Blot
Nylon Membranes, positively charged	Roche Applied Science	11 209 299 001	Northern Blot
Blocking Reagent	Roche Applied Science	11 096 176 001	Northern Blot
Dispergierer IKA Ultra-Turrax® T25 basic	IKA-Werke GmbH & Co. KG	Z404578	High speed homogenizer
RNase AWAY®	MOLECULAR BIO-PRODUCTS INC	7000	For eliminating RNase and DNA from apparatus and tools surfaces
Diethyl pyrocarbonate (DEPC)	Sigma-Aldrich	D5758	Nuclease inhibitor, 0.1% DEPC water is used for RNA related work
RNAzol® RT	Sigma-Aldrich	R4533	RNA isolation
RNAlater® RNA Stabilization Reagent	Qiagen	76104	Stabilizing RNA away from risk of degradation
RNeasy Mini Kit	Qiagen	74104	Purification of high-quality RNA from tissues
RNeasy Fibrous Tissue Mini Kit	Qiagen	74704	RNA isolation kit for heart and muscle tissue
Superscript™ II Reverse Transcriptase	Invitrogen	18064-022	Reverse transcription

Oligo (dT) ₁₂₋₁₈ Primer	Invitrogen	18418-012	Hybridizes to the mRNA poly(A) tail and acts as a primer for first strand cDNA synthesis
Wasser AccuGENE®	LONZA	733-1631	Water, molecular biology grade
10× <i>Taq</i> Buffer, with 15 mM Magnesium	5PRIME	2201240	PCR
<i>Taq</i> DNA polymerase	5PRIME	2900166	PCR
Deoxynucleotide Mix, 10mM each dNTP	5PRIME	2900389	PCR
10× <i>Pfu</i> Buffer	Promega	M776A	<i>Pfu</i> -PCR
<i>Pfu</i> DNA polymerase	Promega	M774A	<i>Pfu</i> -PCR
100mM dATP solution	Invitrogen	P/N 55082	<i>Pfu</i> -PCR
<i>Dpn</i> I	Promega	R623A	A restriction enzyme which digests methylated DNA
DNase I, Amplification Grade	Invitrogen	18068-015	Digests single / double strand DNA
RNaseOUT™ Ribonuclease Inhibitor	Invitrogen	10777-019	Inhibits RNase A, RNase B, RNase C
<i>Bam</i> HI	Promega	R602A	Restrict enzyme digestion
<i>Eco</i> RI	Promega	R601A	Restrict enzyme digestion
<i>Eco</i> RV	Promega	R635A	Restrict enzyme digestion
<i>Hind</i> III	Promega	R604A	Restrict enzyme digestion
<i>Sal</i> I	Promega	R605A	Restrict enzyme digestion
<i>Sph</i> I	Promega	R626A	Restrict enzyme digestion
<i>Xho</i> I	Promega	R616A	Restrict enzyme digestion
Bovine Serum Albumin Acetylated (BSA)	Promega	R396A	Restrict enzyme digestion
Buffer B	Promega	R002A	Restrict enzyme digestion
Buffer D	Promega	R004A	Restrict enzyme digestion
Buffer K	Promega	R010A	Restrict enzyme digestion
Universal Agarose	BIOSELL	BS20.46.500	Electrophoresis for checking DNA size
Agarose LE, low electro-endosmosis	Boehringer Mannheim GmbH	1685651	Electrophoresis for DNA purification
NucleoSpin® Gel and PCR Clean-up	MACHEREY-NAGEL	REF 740609.50	Gel extraction kit
Subcloning Efficiency™ DH5α Competent Cells	Invitrogen	18265-017	Heat shock competent bacteria
ElectroTen-Blue	Agilent Technologies	200159	Electroporation Competent Cells
NucleoSpin® Plasmid	MACHEREY-NAGEL	REF 740588.250	Plasmid isolation kit

NucleoBond® Xtra Midi EF	MACHEREY-NAGEL	REF 740420.50	EF-Midi plasmid isolation kit
ViaFect™ Transfection reagent	Promega	E4981	Transfects DNA into cell lines with high efficiency and low toxicity
Poly-L-Lysine hydrobromide	Sigma-Aldrich	P2636	Poly-lysine coating cover slip

2.3 Buffer recipes

All buffers used in this thesis are summarized in Table 3.

Table 3 Buffer recipes

Buffer		Stability at °C
Buffer A (for Western blot)	1.5M Tris, 13.87mM SDS, pH 8.8	4 °C
Buffer B (for Western blot)	500mM Tris, 13.87mM SDS, pH 6.8	4 °C
Separating gel composition (12% acrylamide gel) (for Western blot)	8ml 30% acrylamide solution, 2ml ddH ₂ O, 10ml Buffer A, 130µl 10% APS, 15µl TEMED	Immediately use
Collecting gel composition (for Western blot)	1.25ml 30% acrylamide solution, 3.75ml ddH ₂ O, 5ml Buffer B, 130µl 10% APS, 15µl TEMED	Immediately use
5 × Running Buffer (for Western blot)	123.8mM Tris, 1M Glycine, 17.4mM SDS. Dilute it into 1× electrophoresis buffer before using	4 °C
SDS Laemmli Sample Buffer (for Western blot)	3.55ml ddH ₂ O, 1.25ml Tris-HCl (0.5M, pH 6.8), 2.5ml glycerol, 2ml 10% (w/v) SDS, 0.2ml 0.5% (w/v) bromophenol blue	-20 °C
10×TBS Buffer (for Western blot)	100mM Tris, 1.5M NaCl, pH 8.0	4 °C
1×TBS (0.05% Tween 20) (for Western blot)	Solve 100ml 10× TBS Buffer and 0.5ml Tween 20 into 1000ml MilliQ H ₂ O	Room temperature
Stripping Buffer (500ml, pH 6.8) (for Western blot)	10ml 10% (w/v) SDS, 62.5ml Tris-HCl (0.5M, pH 6.8), 427.5ml MilliQ H ₂ O	4 °C
Homogenizing Buffer (cell lysis buffer for peroxisome isolation)	250mM Sucrose, pH 7.4; 5mM MOPS, pH 7.4; 0.1% Ethanol, 1mM EDTA; 1mM 6-aminocaproic acid, 0.2mM DTT, Protease inhibitor mix 1:100	Prepare freshly
OptiPrep™ diluent (Solution B)	0.25M sucrose, 10mM EDTA, 1% (v/v) ethanol, 100mM MOPS-NaOH, pH 7.2	Immediately use
Working Solution (Solution C, 54% iodixanol, ρ = 1.291 g/ml)	90% OptiPrep™, 10% Solution B	Immediately use
Homogenization medium (Solution D)	0.25M sucrose, 1mM EDTA, 0.1% (v/v) ethanol, 10mM MOPS-NaOH, pH 7.2	Immediately use
Narcotic solution (rat Anaesthesia)	0.65ml Ketamin Ratiopharm (Ketamin 100mg/ml); 0.65ml Rompun (Xylazin 20mg/ml); 0.2ml	4 °C

			Sedostress (Azepromazin 10mg/ml); 8.5ml 0.9% NaCl. Each 0.1ml Narcotic solution is used for 10g bodyweight.	
Transfer gel/nylon sandwiches)	Buffer (RNA membrane		3M NaCl and 341.78mM sodium citrate in 0.1% DEPC water, pH 7.0	Room temperature
1 × Maleic acid buffer (for Northern blot)			0.1M Maleic acid, 0.15M NaCl, pH 7.5 (20 °C), sterile filtered	20 °C
Basic Buffer (for Northern blot)			40mM Tris-HCl, pH 7.4; 150mM NaCl	1 week at 4 °C
Antibody Northern blot)	Buffer (for		1% Blocking reagent (w/v) in Basic Buffer	2 months at 4 °C
Blocking solution (for Northern blot)			1g Blocking reagent powder (w/v) in 100ml 1 × Maleic acid Buffer	4 weeks at 4 °C
Washing Buffer 1 (test)			0.1% Tween 20 in Basic Buffer, pH 7.4	Not recommend
Washing Buffer 2 (test)			25mM Na ₂ HPO ₄ , 1% SDS, 1mM EDTA, pH 7.2	Not recommend
Washing Buffer 3 (test)			0.3% Tween 20 in 1 × Maleic acid buffer, pH 7.5	Not recommend
Washing Buffer 4 (test)			0.1 × SSC	Not recommend
Washing Buffer 5 (test)			0.1 × SSC, 0.1% SDS	Not recommend
Washing Buffer 6 (test)			0.5 × SSC	Not recommend
Washing Buffer 7 (test)			0.5 × SSC, 0.1% SDS	Not recommend
Washing Buffer 8 (for Northern blot)			1 × SSC: 0.75M NaCl and 0.75M sodium citrate	4 °C
Washing Buffer 9 (test)			1 × SSC, 0.1% SDS	Not recommend
Formamide Buffer (for Northern blot)	Hybridization		50% formamide (v/v) deionized, 5 × SSC, 0.1% N-lauroylsarcosine (w/v), 0.02% SDS (w/v), 2% Blocking solution (v/v)	4 °C
10 × MOPS (for Northern blot)	Running Buffer		0.2M MOPS, pH 7; 50mM sodium citrate, 0.01M EDTA	4 °C
10 × Formaldehyde Buffer (for Northern blot)	loading		1mM EDTA, pH 8; 0.25% (w/v) bromphenol blue, 0.25% (w/v) xylene cyanol, 50% (v/v) glycerol	20 °C
6 × DNA loading Dye			0.25% (w/v) bromphenol blue, 0.25% (w/v) xylene cyanol, 30% (v/v) glycerol	4 °C
Stripping Buffer (for Northern blot, but not recommend)			50% deionized formamide, 5% SDS, 50mM Tris-HCl, pH 7.5	4 °C
H ₃ BO ₃ /Na-tetraborate Buffer (for coating cover slip)			0.7mM Lysine, 100mM boric acid, 47.5mM Na-tetraborate	4 °C

2.4 AKAP plasmids

Different A-kinase anchoring plasmids were selected and a database search performed to find the appropriate IMAGE clones for purchase (Table 4). A plasmid that contains partial of *Akap11* [NM_012773.2] sequence was used as the template for Northern blot probes design. The plasmids of *Akap1* [NM_009648.2], *Akap4*

[NM_009651.4] and *Akap10* [NM_019921.3] were used for detection primers design and myc-tagged AKAPs overexpression.

Table 4 Commercial plasmids information

Gene Symbol	Company	I.M.A.G.E	Vector	Cloning Sites	Antibiotics
<i>Akap11</i>	GenomeCube	IMAGp998B0715541Q	pExpress-1	5s: <i>EcoRV</i> , 3s: <i>NotI</i>	Ampicillin (50 µg/ml)
<i>Akap1</i>	GenomeCube	IRAVp968B01135D	pYX-Asc	5s: <i>EcoRI</i> , 3s: <i>NotI</i>	Ampicillin (100 µg/ml)
<i>Akap4</i>	GenomeCube	IRCLp5011A0634D	pCR- BluntII- TOPO	5s: TOPO sites, 3s: TOPO sites	Kanamycin (100 µg/ml)
<i>Akap10</i>	GenomeCube	IRAVp968B05107D	pSPORT1	5s: <i>SalI</i> , 3s: <i>NotI</i>	Ampicillin (100 µg/ml)

2.5 Primers

All the primers used in this study are listed in Table 5, including verified ones (*) and new designed ones.

Table 5 List of primers designed and used in this study

Gene Name	Tageted tamplate	Len. (bp)	Primer Lab-ID	Primer Lab-Name	Sequence (5'- 3')	Optimized Ann. Temp. (°C)
28S rRNA	NR_003279	254	G12*	rRNA-For1	CCTTCGATGTCGGCTCTTCCTAT	65
			G14*	rRNA-Rev1	GGCGTTCAGTCATAATCCCACAG	
ABCD1	NM_007435	465	D24*	ALDP-For2	GAGGGAGGTTGGGAGGCAGT	67
			D26*	ALDP-Rev2	GGTGGGAGCTGGGGATAAGG	
ABCD2	NM_011994.2	406	K19*	ABCD2-For3	TGCAAAATTCTGGGGAAGA	58
			K20*	ABCD2-Rev2	TGACATCAGTCCTCCTGGTG	
ABCD3	NM_008991.2	523	L02*	HAbcd3for1	CTGGGCGTGAAATGACTAGATTGG	65
			L03*	HAbcd3rev1	AGCTGCACATTGTCCAAGTACTCC	
ACOX1	NM_015729.3	566	D15*	Acox1-For1	CTGAACAAGACAGAGGTCCACGAA	60
	NM_001271898.1	566	D16*	Acox1-Rev1	TGTAAGGGCCACACACTCACATCT	
ACOX2	NM_053115.2	688	D17*	Acox2-For1	CTCTTGACGATATGAGGGTGAGAA	60
	NM_001161667.1	688	D18*	Acox2-Rev1	CTGAGTATTGGCTGGGGACTTCTG	
ACOX3	NM_030721.2	813	D19*	Acox3-For1	GCCAAAGCTGATGGTGAGCTCTAT	55
			D20*	Acox3-Rev1	AGGGGTGGCATCTATGTCTTTTCAG	
Catalase	NM_009804.2	833	D49*	Catalase-For3	ATGGTCTGGGACTTCTGGAGTCTTC	64
			D53*	Catalase-Rev3	GTTTCCTCTCCTCCTCGTTCAACAC	

Gpx1	NM_008160.6	197	J64*	Gpx1-For1	GGGACTACACCGAGATGAACGA	61
			J65*	Gpx1-Rev1	ACCATTCACTTCGCACTTCTCA	
SOD1	NM_011434.1	153	G40*	SOD1-For1	TGGGTTCACGTCCATCAG	63
			G42*	SOD1-Rev1	ACACCGTCCTTTCCAGCAG	
Pex5	NM_008995.2	508	F47*	Pex5-For1	GAGTGAAGAAGCAGTGGCTGCATAC	64
	NM_175933.2	508	F48*	Pex5-Rev1	GGACAGAGACAGCTCATCCCTACAA	
Pex13	NM_023651.4	718	F27*	Pex13-For1	GACCACGTAGTTGCAAGAGCAGAGT	65
			F28*	Pex13-Rev1	CTGAGGCAGCTTGTGTGTTCTACTG	
Pex14	NM_019781.2	131	F29*	Pex14-For1	CACCTCACTCCGCAGCCATA	60
			F32*	Pex14-Rev1	AGGATGAGGGGCAGCAGGTA	
Pex11 α	NM_011068.1	420	F20*	Pex11 α -For1	TCAGCTGCTGTGTTCTCAGTCCTT	64
			F19*	Pex11 α -Rev1	GTACTTAGGAGGGTCCCGAGAGGA	
Pex11 β	NM_011069.3	590	F21*	Pex11 β -For1	ATCTGTCCCTGGCTACGACTCAAG	63
			F22*	Pex11 β -Rev1	AAACTGGAAAGTGTGGAGGCAGTC	
Pex11 γ	NM_026951.2	682	F23*	Pex11 γ -For1	GACTCTGCTTGGTGGTGGACACT	64
			F24*	Pex11 γ -Rev1	TGTCTCTCCCACTCACCTTTAGGC	
PPAR α	NM_011144.6	584	F68*	PPAR α -For2	AGACCGTCACGGAGCTCACA	68
	NM_001113418.1	584	F70*	PPAR α -Rev2	GGCCTGCCATCTCAGGAAAAG	
PPAR β	NM_011145.3	363	F71*	PPAR β -For1	CACCGAGTTCGCCAAGAACA	60
			F72*	PPAR β -Rev1	AGAGCCCGCAGAATGGTGTC	
PPAR γ	NM_001127330.1	441	F74*	PPAR γ -For2	TCCGTAGAAGCCGTGCAAGA	60
	NM_011146.3	441	F76*	PPAR γ -Rev2	CACCTTGGCGAACAGCTGAG	
FSHR	NM_013523.3	345	L70*	Fshr F1	CCAGCCTTACCTACCCCAGT	62
			L71*	Fshr R1	CTGTGGTGTTCACAGTGATG	

GAPDH	NM_001289726.1		E12*	GAPDH-For1	CACCATGGAGAAGGCCGGGG	
		417	E15*	GAPDH-Rev1	GACGGACACATTGGGGGGTAG	60
		440	BK16	T7-GAPDH-R	<u>TAATACGACTCACTATAGGGAGAG</u> T7 RNA polymerase promoter	60
β-actin	NM_007393.3		M29*	Mm beta-Actin-1146F	GGATCAGCAAGCAGGAGTACGAT	
		120	M30*	Mm beta-Actin-1266R	CTGCGCAAGTTAGGTTTTGTCAA	62
		143	BK17	T7-beta-actin-R	<u>TAATACGACTCACTATAGGGAGACT</u> T7 RNA polymerase promoter	62
StAR	NM_011485.4	292	K21*	StAR-For1	GTTCTCTGCTACGTTCAAGC	58
			K22*	StAR-Rev1	TTCCTTCTTCCAGCCTTCCT	
AKAP11-LSP	NM_012773.2		AZ47	LSP-1240F	AATGTTAGAAAGCCAACACC	
		230	AZ48	LSP-1449R	GCATAATCTTCGTAAGTGCAG	56
		253	BK18	T7-LSP-R	<u>TAATACGACTCACTATAGGGAGAGC</u> T7 RNA polymerase promoter	56
AKAP11-BSP1	NM_012773.2		AZ49	BSP-3113F	ATCTGACTAATACTGCGCTTG	
		308	AZ51	BSP-3399R	CTCAGATAAACTACCAACGGAT	56
		331	BK19	T7-BSP1-R	<u>TAATACGACTCACTATAGGGAGACT</u> T7 RNA polymerase promoter	56
AKAP11-BSP2	NM_012773.2	893	AZ50	BSP-2528F	GCCAGAATGACTTCAAACCAAC	56
			AZ51	BSP-3399R	CTCAGATAAACTACCAACGGAT	
AKAP11-BSP3	NM_012773.2	608	AZ50	BSP-2528F	GCCAGAATGACTTCAAACCAAC	57
			AZ52	BSP-3115R	CTCAAGCGCAGTATTAGTCAG	

AKAP11-rat	NM_012773.2	1147	AZ57	rAKAP11-2124F	CTTCACAGCAAAGGCAGCAG	55
			AZ58	rAKAP11-3341R	ATTCTTTGGCTAACTCCCCTT	
M13 promotor	pGEM-Teasy plasmid	266	BE61	M13FS	CCCAGTCACGACGTTGTAAAACG	60
	Express 1 plasmid	190	BE62	M13RS	AGCGGATAACAATTTACACACAGG	
AKAP1-N terminus	NM_009648.2	402	BJ25	F1N	CGGAGACAAAGCTATGACCC	54
	NM_001042541.1	295	BJ26	R1N	CTTGCCAATCAGTCGACCA	
AKAP1-C terminus	NM_009648.2	312	BJ27	F1C	TTTGTGACCCTGCCATTCCAA	54
	NM_001042541.1	312	BJ28	R1C	AACAGTGCAAAGAAGACCGAA	
AKAP1 IMAGE clone	IRAVp968B01135D	2573	BH42	AKAP1-Mm-F3B	ATAGGATCCGCAATCCAGTTGCGTTCGCTC <i>Bam</i> HI	58
			BH43	AKAP1-Mm-R3B	ATACTCGAGTCAGAGGCTGGCATAGTAGCT <i>Xho</i> I Stop codon	
	IRAVp968B01135D	2573	BH48	AKAP1-Mm-F5B	ATAGGATCCATGGCAATCCAGTTGCGTTTCG <i>Bam</i> HI Start codon	58
			BH49	AKAP1-Mm-R5B	ATACTCGAGGAGGCTGGCATAGTAGCTGTC <i>Xho</i> I	
	IRAVp968B01135D		BL03	1-5B-771F	GGACTGGAGATGCTGTGTTGG	
	IRAVp968B01135D		BL27	1-5B-1420F	ACCAAGGACCAGAAGCCAAAG	
	IRAVp968B01135D		BL30	AKAP1-Mut-F	ATGGTATCACTGTGGGAAGTCATCGTGGTCAAC	55
			BL31	AKAP1-Mut-R	GGTTGACCACGATGACTTCCACAGTGATACCATC	
AKAP4-N terminus	NM_009651.4	202	BH58	F4N	ACAACAAGATCAGGACCGAA	53
	NM_001042542.2	202	BH59	R4N	GAAAAGGCACACAGATCCCTC	
AKAP4-C terminus	NM_009651.4	224	BH60	F4C	TGGCCCTGAAGTTATTGTCAACA	53
	NM_001042542.2	224	BH61	R4C	TGGCAAACCTTCATGACCTCC	

AKAP4 IMAGE clone	IRCLp5011A0634D	2550	BH44	AKAP4-Mm-F3B	ATAGGATCCATTGCCTACTGTGGTACTACA <i>Bam</i> HI	58
			BH45	AKAP4-Mm-R3B	ATACTCGAGTTACAGGTTAGCGAGAAGCAA <i>Xho</i> I Stop codon	
	IRCLp5011A0634D	2550	BH50	AKAP4-Mm-F5B	ATAGGATCCATGATTGCCTACTGTGGTACT <i>Bam</i> HI Start codon	58
			BH51	AKAP4-Mm-R5B	ATACTCGAGCAGGTTAGCGAGAAGCAAGTC <i>Xho</i> I	
	IRCLp5011A0634D		BL05	4-3B-920F	ATTGCTTCGGAGATGGCCCAT	
IRCLp5011A0634D		BL06	4-3B-1830R	CACATGGATCTTTGCCCTTGG		
AKAP10- C terminus	NM_019921.3	335	BK20	F10C	TCCCTGGCTGCTCACGGCTCT	56
			BK21	R10C	AGCTCTTCTTGGGCCTCGTC	
AKAP10 IMAGE clone	IRAVp968B05107D	1018	BH47	AKAP10-Mm-R3B	ATACTCGAGTCATAGCTTTGTAGACTTCTC <i>Xho</i> I Stop codon	58
			BL28	10-3B-355F	GAATTCAAAAGTATAGAACAAGATGCAGTG <i>Eco</i> RI	
	IRAVp968B05107D	1018	BH53	AKAP10-Mm-R5B	ATACTCGAGTAGCTTTGTAGACTTCTCTAG <i>Xho</i> I	58
			BL29	10-5B-355F	GAATTCATGAAAAGTATAGAACAAGATGCA <i>Eco</i> RI Start codon	
myc-GFP- 3B	pGeneClip hMGFP vector	701	BL48	GFP-BamHI-NoStart	ATAGGATCCGGCGTGATCAAGCCCGAC <i>Bam</i> HI	62
			BE66*	RvGfP-XhoI	ATACTCGAGTTAGCCGGCCTGGCGGG <i>Xho</i> I Stop codon	
GFP-myc- 5B	pGeneClip hMGFP vector	701	BE65*	fvGfP-BamHI	ATAGGATCCATGGGCGTGATCAAGCC <i>Bam</i> HI Start codon	59
			BE67*	RvGfP-XhoIWoS	ATACTCGAGGCCGGCCTGGCGGG <i>Xho</i> I	

2.6 Antibody list

All antibodies used in this thesis are listed with appropriate source, catalog number and dilution used in the different experiments (Table 6).

Table 6 Antibody dilution list

Antibody Name	Host	Source (company / person)	Catalog ID	Dilution
Anti-Digoxigenin	Mouse monoclonal Ab	Roche Applied Science	11 333 062 910	3 : 5000 (NB)
AKAP220 (H-300)	Rabbit polyclonal Ab	Santa Cruz Biotechnology, Inc.	Sc-135335	1 : 200 (WB)
Oxphos III core subunit II	Mouse monoclonal Ab	Molecular Probes, Invitrogen	459220	1 : 5000 (WB)
Phospho-(Ser/Thr) PKA Substrate	Rabbit polyclonal Ab	Cell Signaling Technology®	#9621	1 : 1000 (WB)
PKA C- α (D38C6)	Rabbit monoclonal Ab	Cell Signaling Technology®	#5842	1 : 1000 (WB); 1 : 400 (IF)
Catalase	Rabbit polyclonal Ab	Gift from Denis I. Crane, School of Biomol. Biophys. Sci., Griffith Univ., Nathan, Brisbane, Australia	/	1 : 500 (IF)
Myc-Tag (9B11)	Mouse monoclonal Ab	Cell Signaling Technology®	#2276	1 : 8000 (IF)
Pex3	Rat polyclonal Ab	made by Dr. Claudia Colasante	/	1 : 200 (IF)
Pex14	Rabbit polyclonal Ab	Gift from Denis I. Crane, School of Biomol. Biophys. Sci., Griffith Univ., Nathan, Brisbane, Australia	/	1 : 100 (IF)
Superoxide dismutase 2 (SOD2, Mn-SOD)	Rabbit polyclonal Ab	Research Diagnostics, Inc., NJ, USA	RDI-RTSODMa bR	1 : 5000 (IF)
anti-mouse IgG Alkaline Phosphatase antibody	Goat	Sigma-Aldrich	A3562	1 : 30,000 (IB)
anti-rabbit IgG Alkaline Phosphatase antibody	Goat	Sigma-Aldrich	A3687	1 : 30,000 (WB)
anti-mouse IgG	Donkey	Molecular Probes	A21202	1 : 300 (IF)

Alexa Fluor 488 green				
anti-mouse IgG Alexa Fluor 555 red	Donkey	Molecular Probes	A31570	1 : 300 (IF)
anti-mouse IgG Texas Red	Horse	Vector Laboratories	TI-2000	1 : 1000 (IF)
anti-rabbit IgG Alexa Fluor 488 green	Donkey	Molecular Probes, Invitrogen	A21206	1 : 500 (IF)
anti-rat IgG Alexa Fluor 594 red	Goat	Molecular Probes	A11007	1 : 300 (IF)

3 Methods

3.1 Bioinformatic screening for the AKAPs with putative PTS1 signals

In 1980's, the Gould and Subramani group started to investigate a peptide targeting signal that necessary and sufficient to transport proteins into peroxisomes. Through a series of gene mutagenesis, they demonstrated the firefly luciferase contains minimal peroxisomal targeting signal consists of three amino acids, Ser (S)-Lys (K)-Leu (L), at the extreme carboxy terminus. They also suggested this minimal PTS tripeptide with consensus sequence was a conserved feature of peroxsomal proteins through evolution (Gould et al., 1987; Gould et al., 1989). In order to identify proteins of the AKAP family containing a peroxisomal targeting signal 1 (PTS1), a computer program was developed to scan all AKAP member sequences for an eventual PTS1 tripeptide.

3.1.1 Scan of AKAP sequences for the consensus PTS1 motif

All known AKAP amino acid sequences were downloaded from UniProt protein database, including validated and predicted AKAPs (1306 items in all), to produce a test library. Peroxisomal matrix proteins known to contain a real “PTS1 binding site” were downloaded from the PTS1 BLOCK^① at the “PeroxisomalDB Home” webpage^②. Total 98 PTS1 containing proteins from *Homo sapiens*, *Mus musculus*, *Saccharomyces cerevisiae* and *Arabidopsis thaliana* are highly conserved in evolution. The PTS1 tripeptide consensus from these 98 proteins was summarized as [A/C/H/K/N/P/Q/S/T]-[A/H/K/N/Q/R/S]-[F/I/L/M/V]. Within the 1306 AKAPs, the sequence matched by this motif were selected and saved into a *.txt file (81 items in all).

3.1.2 Use of ClustalX 2.0 & MEGA 4.0.2 programs to create an evolutionary tree

The AKAPs sequence file needed to be loaded into the ClustalX 2.0 program to accomplish a complete sequence alignment, and saved as *.dnd and *.aln files. Thereafter, the program MEGA 4.0.2 was used to convert the *.aln file into a *.meg file, which is the MEGA format. The new file of the *.meg format can be indicated as

^① http://216.92.14.62/diy_PTS1.html

^② <http://www.peroxisomedb.org/home.jsp>

“Protein Sequence” by MEGA 4.0.2 and constructed a Phylogeny tree by using the “Neighbor-Joining” (NJ) algorithm. The program will execute a self-calculation and generate a tree image, which is in a *.tiff format.

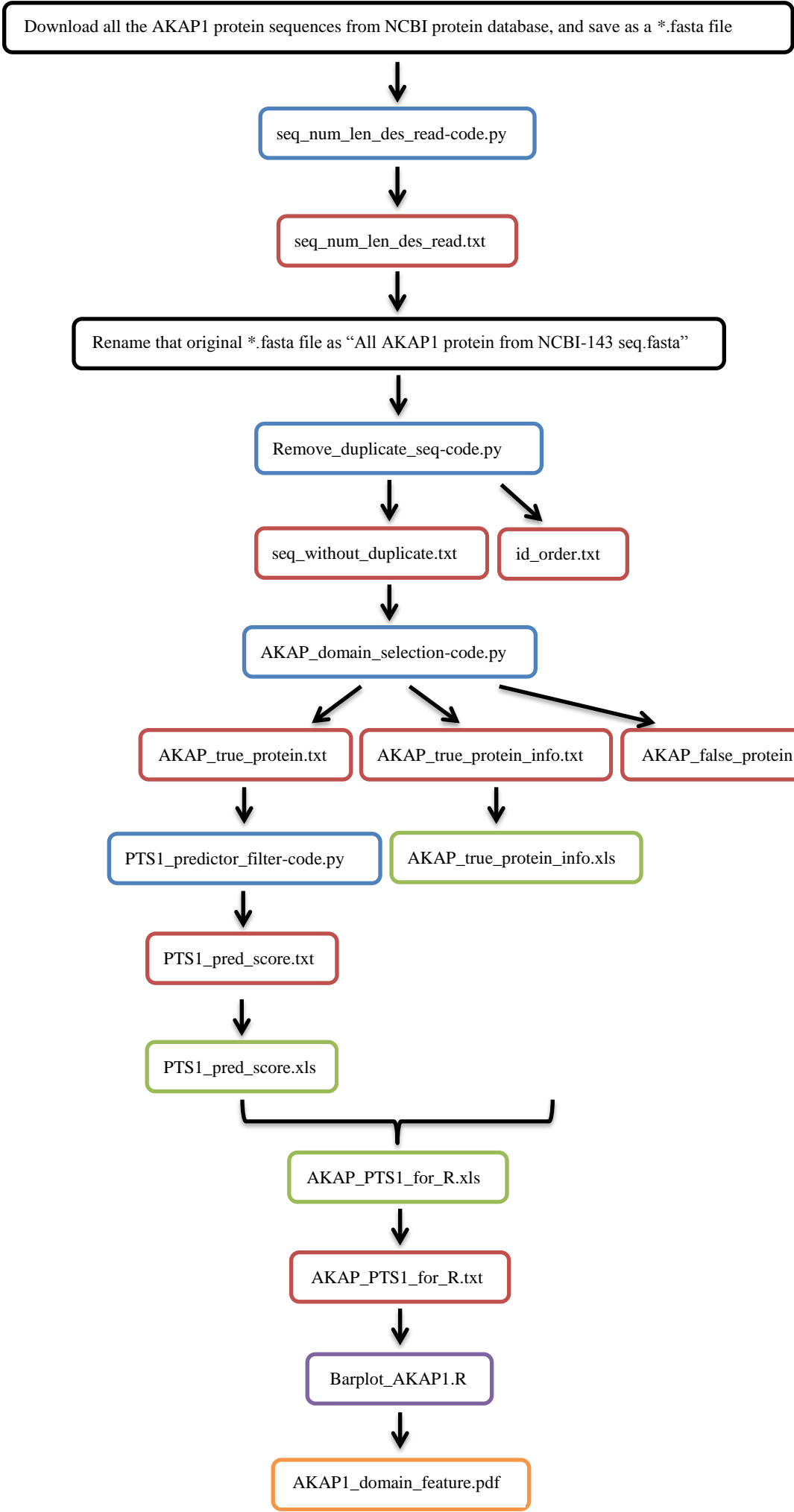
3.1.3 Use of Python 2.7.5 & R i386 3.0.1 programs to test AKAP1, AKAP4, AKAP10 through PTS1 predictor

From the rough PTS1 screening throughout 14 AKAP families, 3 families of 14 (AKAP1, AKAP4 and AKAP10) were implied to be evolutionary conserved “peroxisomal” AKAPs. Then the protein members of these 3 families were respectively further analyzed by 1) a PKA binding domain screening and 2) a comparable strict PTS1 online prediction.

PKA binding domain forms a consensus pattern: [AVLISE]-X-X-[AVLIF]-[AVLI]-X-X-[AVLI]-[AVLIF]-X-X-[AVLISE] (X = any amino acid) (Hundsruker et al., 2010; Skroblin et al., 2010).

As mentioned in Brocard’s paper, the PTS1 signal is considered to consist of 3 parts: a crucial C-terminal tripeptide, an upstream tetrapeptide, and a flexible approximately 12 amino acid long hinge (Brocard and Hartig, 2006). Their group also successfully developed an online tool to predict candidates^①. Computer programming was used for sequence scanning under the Python 2.7.5 environment, and the R i386 3.0.1 program was used to convert the statistical results generated from Python into ostensive graphs. The codes of Python (in blue frame) and R (in purple frame) are presented in the end of this thesis (see Chapter 12. Supplemental data S1), and the screening workflow was set as follows (this workflow of AKAP1 as the example):

^① <http://mendel.imp.ac.at/mendeljsp/sat/pts1/PTS1predictor.jsp>



3.2 Cell culture

3.2.1 Cell culture routine

The procedure was slightly modified from the original protocol from ATCC^①. At first passage, cells which have been resuscitated from a frozen stock were split at a ratio of 1:3. Thereafter, the culture medium was renewed every 2 to 3 days, until cells were fully confluent. For subculturing, the cell layer was briefly rinsed with 0.25% trypsin/EDTA 1ml per 200ml flask and incubated at 37 °C for 5 minutes to induce the detachment. Cells were gently removed and mixed by aspiration and pipetting. The sub-confluent cultures were split in a concentration of 1×10^4 cells/cm², and incubated at 37 °C with 5% CO₂.

3.2.2 Cell number and viability examination

The Sertoli cell number was determined with a hemocytometer. Trypan blue exclusion assays were used to determine the percent survival of the Sertoli cells. The procedure was slightly modified from the original Sigma “Protocol 6 – Cell Quantification”^②.

The adherent cells needed to be suspended as above described, thereafter, 150 µl of that cell suspension was transferred into an Eppendorf tube under sterile conditions and mixed gently with 150 µl of Trypan Blue. The needed hemocytometer and coverslip were cleaned by EtOH and ddH₂O and air-dried. The chamber was filled with 10 µl of the stained cell suspension without air bubbles. The cell number was counted under 20 × magnification with a bright field/phase contrast-equipped inverted light-microscope. Dead cells were recognised by being blue stained. Ideally, >100 viable cells were used for accurate counting. Finally the cell concentration of the Eppendorf tube, which was used in the first step before Trypan blue stain, was calculated with the following formula:

$$\text{Viable cell concentration} = \frac{(\text{total live cell numbers from 4 corner squares}) \div 4 \times 9}{3\text{mm} \times 3\text{mm} \times 0.1\text{mm}} \times 2$$

^① http://www.lgcstandards-atcc.org/products/all/CRL-1715.aspx?geo_country=de#culturemethod

^② <http://www.sigmaaldrich.com/technical-documents/protocols/biology/cell-quantification.html>

3.2.3 Isolation of total RNA from TM4 cells

According to the experiment requirement, TM4 cells were grown in flasks or 6-well plates. The whole procedure of total RNA isolation was modified from the Qiagen protocol “Purification of Total RNA from Animal Cells Using Spin Technology” in RNeasy® Mini Handbook, 4th Edition. For a 200ml flask as an example, cells were cultured upto an ideal density, the medium was discarded and 10ml PBS was added for rinsing. Then the cells were trypsinized by 0.1-0.25% trypsin at 37 °C for 10min. 8ml new medium was added to stop the digestion and the cells were resuspended for the cell number counting as described above and collected by centrifugation at 300×g for 5min. After removal of the supernatant, the cell pellet (ideally < 5×10⁶ cells) was resuspended and disrupted in 350µl Buffer RLT (including 1% β-mercaptoethanol, the volume of RLT Buffer used depends on the cell number, see page 28 in handbook of Qiagen RNeasy Mini Kit) and homogenized by spinning through a QIAshredder column, supplied by the Qiagen RNeasy Mini Kit. The mixture of 10µl DNase I (RNase-free) and 70µl RDD Buffer (Qiagen) was added onto the column to digest the contaminated genomic DNA. Thereafter, the rest procedure was done as described in the manufacturer's instruction.

3.3 RT-PCR

According to the protocol from Invitrogen “First-Strand cDNA Synthesis Using SuperScript™ II RT”^①, 2µg total RNA (in 10µl) was reverse transcribed in a 20µl reaction mixture at 42 °C for 50min using 200U of SuperScript™ II RT and 500ng of oligo-dT primers in the 1× first-strand synthesis buffer. The PCR reaction was done in a volume of 25µl reaction mixture containing 2µl of cDNA (reverse transcription reaction), 18.8µl ddH₂O, 2.5µl of 10× PCR Buffer, 0.5µl of 10mM dNTP Mix, 2µl of 10µM Forward + Reverse primer mixture, 0.2µl of 5U/µl *Taq* DNA polymerase. The PCR conditions were first a 5min denaturation period at 95 °C and subsequent 35 cycles of denaturation at 95 °C for 30 sec, annealing of individual primer pairs at optimal temperature for 45 sec, extension at 72 °C for 1 min and one final extension for 10 min at 72 °C.

^① http://tools.lifetechnologies.com/content/sfs/manuals/superscriptII_pps.pdf

3.4 SDS-PAGE and Western blots

According to the protocol in our lab, a standard curve for protein measurements was made with the Bradford method with serial BSA gradient dilutions. The adherent cells were lysed by Lysis buffer (Cell Signaling) and handled following manufacturer's instruction. Thereafter, the protein concentrations of the samples supernatant were measured triplicates by using a spectrophotometer at OD₅₉₅. 50 µg of protein samples per lane were loaded onto 12% SDS-polyacrylamide gel, together with dual color marker in the 1st lane and unstaining marker in the 2nd lane. The proteins were collected by electrophoresis at 80V until they reached the separation gel and thereafter separated at 120V. The separated proteins were transferred from the SDS-gel onto a polyvinylidene fluoride (PVDF) membrane. The membrane was incubated in 10% nonfat milk powder at 4 °C overnight for blocking of non-specific protein binding sites. The next day, the milk was removed and the membrane was incubated with first antibody overnight also at 4 °C. On the 3rd day morning, the membrane was washed with 1×TBST 3 times for 10min each at room temperature. The bound primary antibody was detected by incubation with an alkaline phosphatase-conjugated secondary antibody for 1h at RT. The membrane was washed with 1×TBST 5 times for 10min each at RT. Immune-Star™ AP was used as substrate to visualize the bands with immune complexes in the dark room. Western blots were exposed from 30s to 10min to X-ray film to visualize the appropriate bands.

3.5 Peroxisome purification by OptiPrep™ density gradient centrifugation

OptiPrep™ is a 60% (w/v) solution of Iodixanol® in water, density = 1.32 g/ml, which is used for density gradient centrifugation to purify subcellular organelles. Iodixanol is an ideal medium, since it is non-ionic and non-toxic to cells and metabolically inert. The Iodixanol solution possesses a low viscosity and can be made isosmotic at variant densities, which is helpful for a rapid separation of whole cells or isolated organelles^①. It was reported that peroxisomes can be highly purified from other organelles by this method (Van Veldhoven et al., 1996). In iodixanol, lysosomes band at

^① <http://www.axis-shield-density-gradient-media.com/Purification%20of%20subcellular%20organelles.pdf>

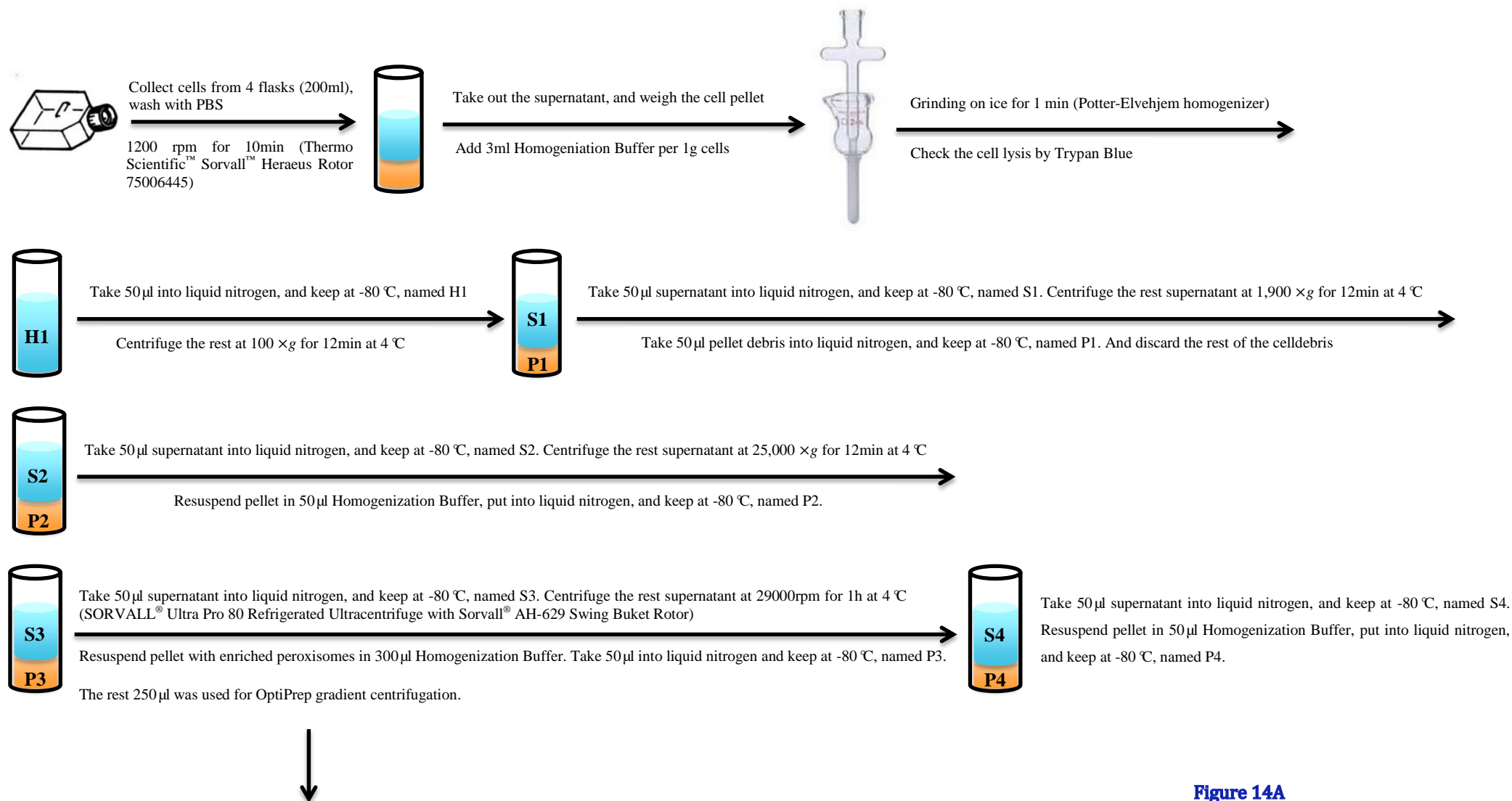
a density of 1.115 g/ml, endoplasmic reticulum band at a density of 1.13 g/ml, mitochondria band at a density of 1.13-1.15 g/ml and peroxisomes band at a density of 1.18-1.20 g/ml (Graham, 2002a; Graham, 2002b).

The isosmotic gradient should be prepared one day before and immediately frozen at -20 °C. The gradient is thawed 15min before usage.

Table 7 Properties and preparation of Iodixanol-sucrose solution

No.	% iodixanol	ρ (g/ml)	Solution C	Solution D
1	18%	1.12	2ml	3ml
2	25%	1.15	1.82ml	1.68ml
3	34%	1.19	4.08ml	1.92ml
4	40%	1.22	2.4ml	0.6ml
5	48%	1.26	3.84ml	0.16ml

In order to get pure peroxisomal fractions from the TM4 cell culture ($\sim 10^7$ cells), differential centrifugation was used after homogenization of the cells. The whole procedure is depicted in details in Figure 14 A&B.



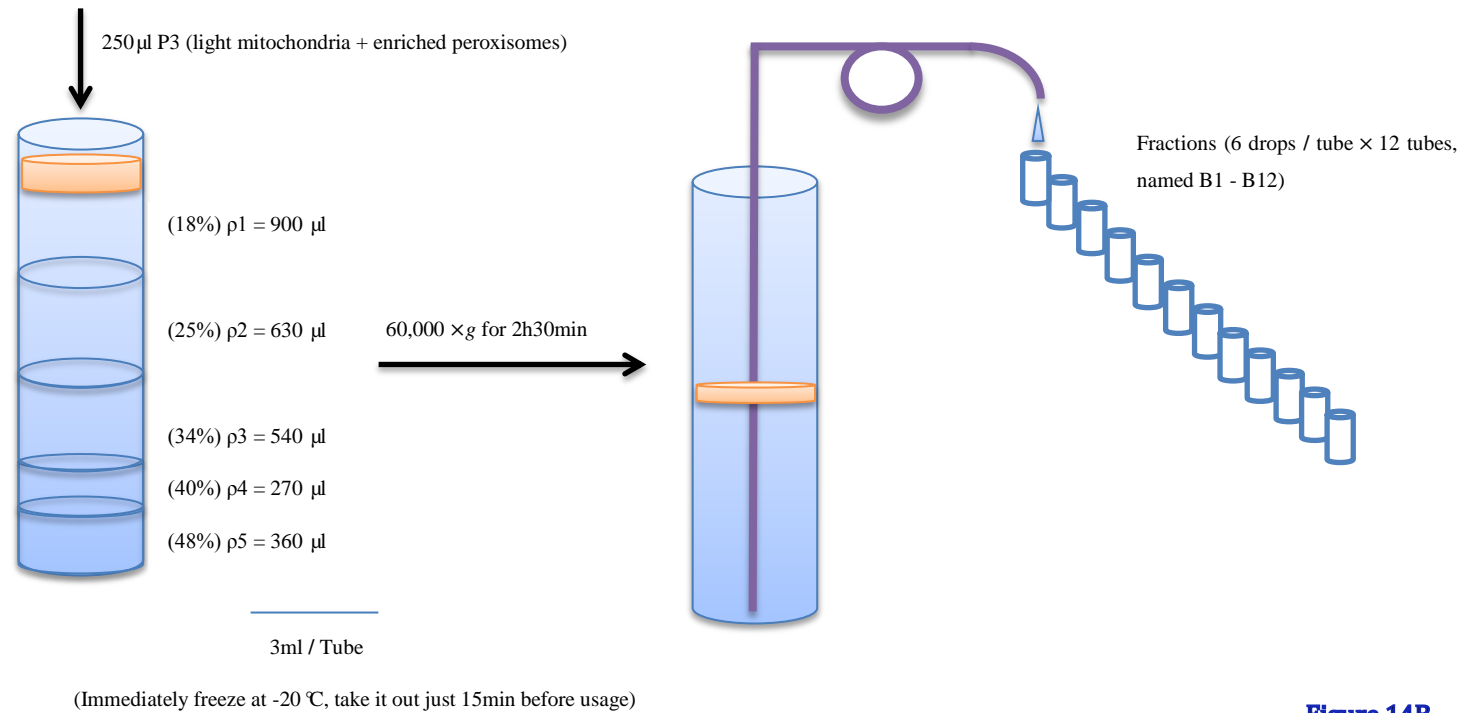


Figure 14B

Figure 14 Schematic illustration of peroxisome purification by OptiPrep™ (keep all solutions and carry out all operations at 4 °C).

The fractions were named as follows:

- H1: total homogenate;
- S1: supernatant after 1st centrifugation from H1, containing all organelles and cytosol;
- P1: pellet after 1st centrifugation from H1, mainly containing cell debris;
- S2: supernatant after 2nd centrifugation from S1, mainly containing small mitochondria, peroxisomes, lysosomes, microsomes and cytosol;
- P2: pellet after 2nd centrifugation from S1, mainly containing heavy mitochondria and nuclei, a few large peroxisomes;
- S3: supernatant after 3rd centrifugation from S2, mainly containing microsomes and cytosol;
- P3: pellet after 3rd centrifugation from S2, mainly containing enriched peroxisomes, light mitochondria, few lysosomes and microsomes, used for further OptiPrep density gradient centrifugation;
- S4: supernatant after 4th centrifugation from S3, mainly containing cytoplasmic proteins;
- P4: pellet after 4th centrifugation from S3, mainly containing microsomes and very small peroxisomes.

250 µl P3 was then added on top of a discontinuous OptiPrep gradient (3ml 18%-48% iodixanol: 900 µl 18%, 630 µl 25%, 540 µl 34%, 270 µl 40% and 360 µl 48%) in thick-walled polycarbonate tubes. The gradient was centrifuged at 60,000 × *g* for 2h30min in a superspeed centrifuge (Thermo Scientific Sorvall[®] Evolution[™] RC). During centrifugation the gradient became continuous and the peroxisomal fraction displayed a smeared white suspended layer in the tube. A needle was carefully inserted and lowered to the tube bottom. All fractions (6 drops per tube) were collected of the 3ml gradient solution by a peristaltic pump into Eppendorf tubes. A total of 12 numbers of fractions were collected (named B1-B12) in separate tubes for further protein analysis.

3.6 Rat dissection and RNA isolation

3.6.1 Anaesthesia for rats and dissection of different organs

Five male rats (7 weeks old, 240-260g for each) were used for this study. The rats were anaesthetized by intraperitoneal injection of a mixture of Narcotic solution (use 0.1ml for 10g bodyweight, Narcotic solution recipe see Table 3). Then the rats were soon dissected and organs (brain, heart, kidney, liver, lung, muscle, pituitary, spleen, testis) were kept in liquid nitrogen for further total RNA isolation.

3.6.2 Tissue total RNA isolation

Before isolation of total RNA, the bench surface, glassware and plastic were cleaned with RNase AWAY[®]. The rat samples frozen in liquid nitrogen were melted on ice. 60mg of tissue should be quickly cut into slices with less than 0.5cm thickness and submerged into 600µl RLT Buffer (containing 1% β-mercaptoethanol and 3% Proteinase K) supplied in the Qiagen RNeasy[®] Mini Kit. The dispergierer IKA Ultra-Turrax[®] T25 was used to disperse and disrupt the cells from the tissues. Whenever another tissue sample was operated, the dispergierer needed to be rinsed with SDS in DEPC water for 10 seconds and with 70% ethanol in DEPC water for 10 seconds. Thereafter, the tissues were homogenized using the clean dispergierer IKA Ultra-Turrax[®] T25, and the cell debris was spun down by centrifugation at 10,000×g for 3min. The supernatant was transferred into a new tube and 0.5 volumes of pure ethanol were added and mixed gently. The mixture from fiber-rich tissues (such as heart and muscle) was handled according to the Qiagen RNeasy[®] Fibrous Tissue Mini Kit protocol^①, and the other mixtures from easy-to-lyse tissues were handled according to the Qiagen RNeasy[®] Mini Kit protocol^②. The total RNA was stored in RNase-free water at -80 °C and the RNA quality was examined before further use. In this study, the RNA quality was checked by running a RNA-Chip with a Bioanalyzer (Figure 15 and Supplemental data S2).

^① <https://www.qiagen.com/de/resources/resourcedetail?id=8039840d-4815-4375-8933-bc09247e47c0&lang=en>

^② <https://www.qiagen.com/de/resources/resourcedetail?id=14e7cf6e-521a-4cf7-8cbc-bf9f6fa33e24&lang=en>

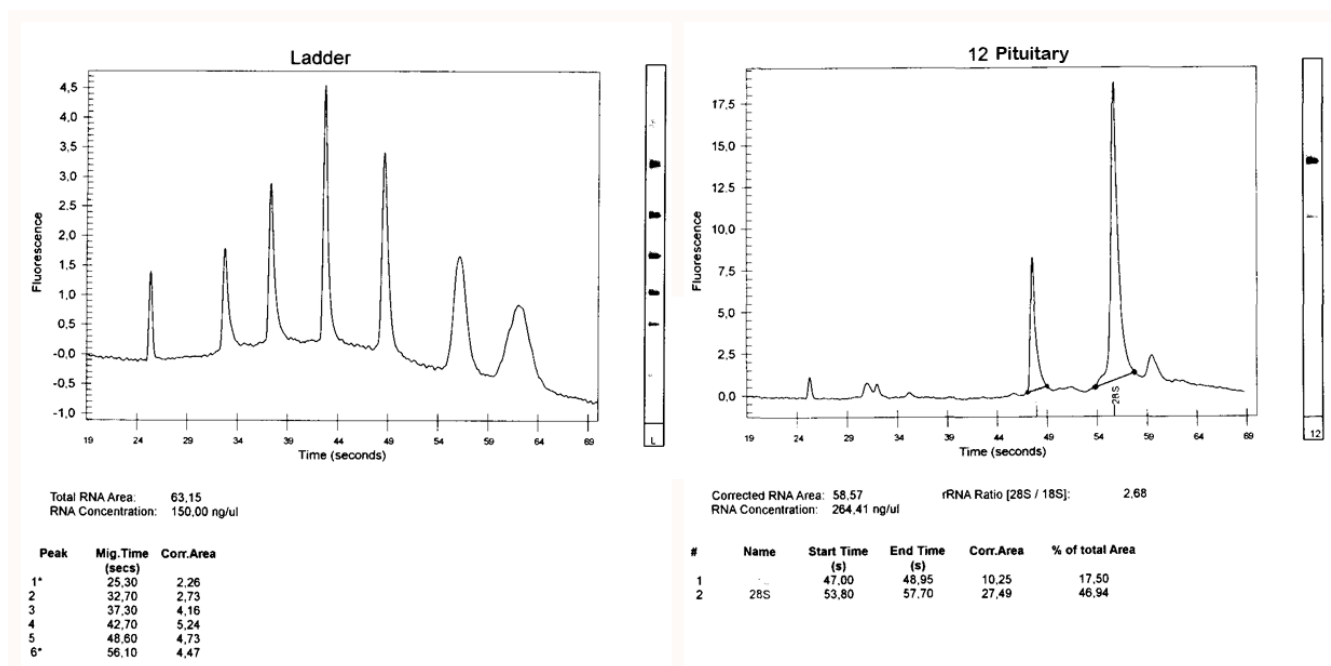


Figure 15 An example of RNA-Chip results to check the quality of isolated RNAs.

3.6.3 Ethanol precipitation to concentrate total RNA

50 µl of total RNA sample needed to be mixed with 125 µl of 100% ethanol and 5 µl sodium citrate (pH 5.2) and incubated at -20 °C for one hour. Thereafter, the mixture was centrifuged at 13,000rpm for 30 minutes at 4 °C. The supernatant was discarded and the pellet was resuspended in 500 µl of 70% ethanol for washing. Thereafter, the centrifugation was repeated under the same condition and the supernatant was discarded. The final RNA pellet was solved in RNase free water and kept in -80 °C.

3.7 Workflow for Northern blotting

Northern blotting is a method to detect target mRNA by specific RNA probes. We planed to eventually reveal distinct alternatively spliced forms of *Akap11* transcripts ([U48288.1] 9.7k bases and [NM_012773.2] 7k bases, Figure 29) by a non-radioactive method. Figure 16 depicts a work flow of the probe generation, Northern blotting hybridization and detection steps. The RNA probe generation and validation is described in details in the following subsection 3.7.1 and 3.7.2.

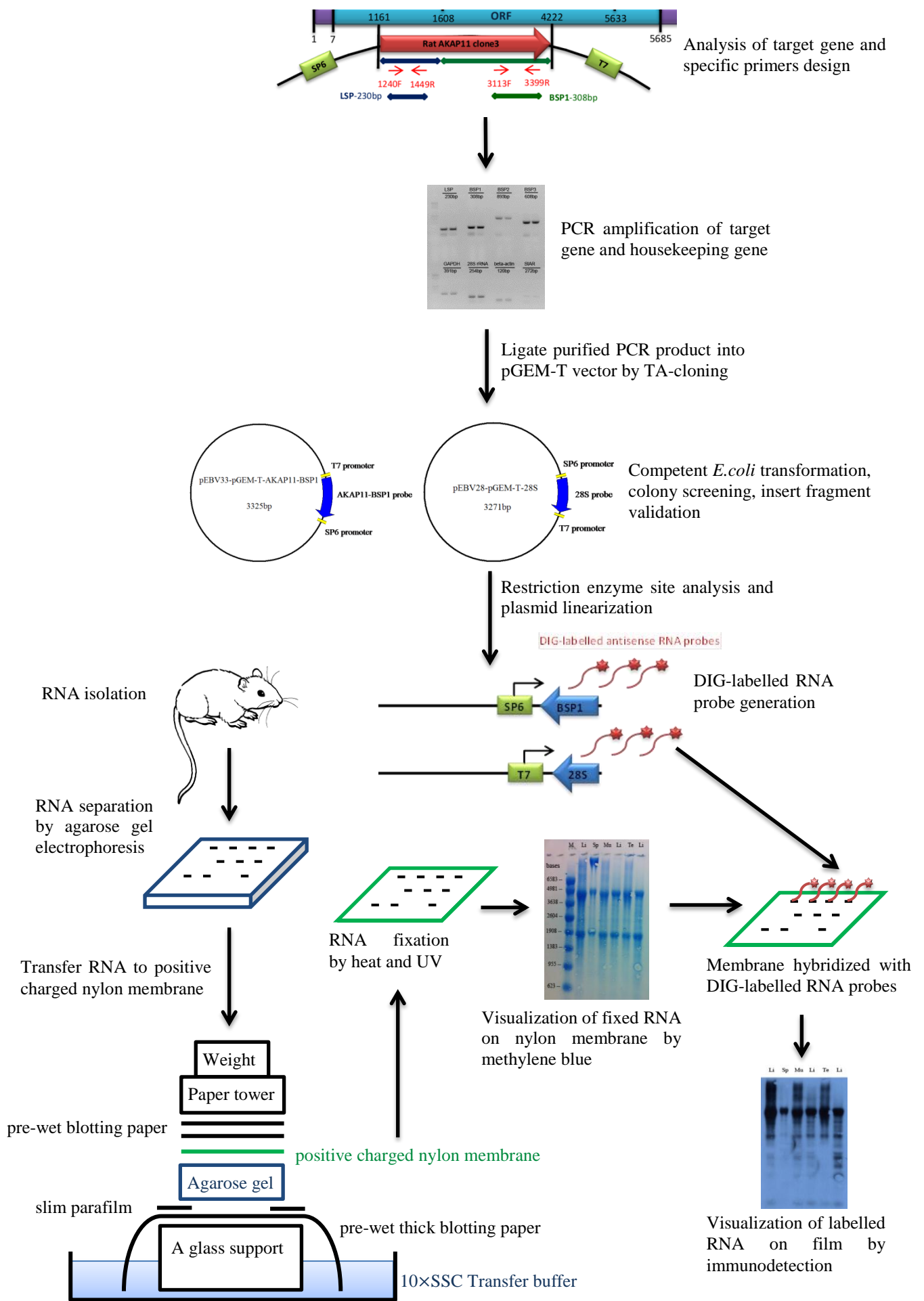


Figure 16 workflow of Northern blot

3.7.1 Plasmid construction and probe generation by *in vitro* RNA transcription

The AKAP11 clone3 plasmid was bought from GenomeCube. The plasmid was sequenced from both SP6 and T7 promoters until fully overlapping. According to the sequence feature analysis of the AKAP11 clone3 plasmid, a fragment of 448bp was suitable to design primers for a rat AKAP11 mRNA [NM_012773.2] specific probe. A fragment of 2615bp was suitable to design probes for the two rat AKAP11 mRNAs both [NM_012773.2] and [U48288.1], available in the NCBI database. As controls, sequences for 28S (Lab-ID: G12/14), GAPDH (Lab-ID: E12/15), β -actin (Lab-ID: M29/30), StAR (Lab-ID: K21/22) probes were amplified with specific primers. All specific PCR products were cloned by TA-cloning into the pGEM-Teasy vector. Positive clones were identified by colony PCR and subsequent plasmid sequencing. All plasmids were sequenced to identify the orientation and precise length of the insert sequences. Thereafter, it was decided which promoter (SP6 or T7) had to be used for antisense RNA-probe *in vitro* transcription. Linearized plasmids were used to generate RNA probes according to the instruction of the “DIG RNA Labeling Mix, Roche”^①. Quality and quantity of the transcripts were analyzed by non-denaturing agarose gel electrophoresis and ethidium bromide staining. According to the kit description, the signal from the *in vitro* transcribed RNA band should be about 10 fold stronger than that from the DNA used for amplification.

3.7.2 Dot blot assay for detection of DIG-labeling efficiency

A dot blot assay was used to determine the labeling efficiency and sensitivity of the DIG-labeling reaction. Dilutions of 100ng/ μ l, 10ng/ μ l, 2ng/ μ l, 500pg/ μ l, 100pg/ μ l, 50pg/ μ l, 25pg/ μ l, 10pg/ μ l, 5pg/ μ l, 2.5pg/ μ l, 1pg/ μ l of the DIG-labelled RNA probes in sterile RNase-free ddH₂O, were spotted in a drop of 1 μ l for each dilution onto a positive-charged nylon membrane. After RNA fixation by 30min baking at 80 °C and 30s UV-treatment at 1.5J/cm², staining of the RNA on the membrane was done in 0.03% (w/v) methylene blue in 0.3M sodium acetate (pH 5.2) for 1min, followed by destaining in DEPC water for 2min. The immunological detection of the labeled probe was performed with a chemiluminescence procedure. Ideally, DIG-probes exhibited a detectable spot in a concentration as low as 0.1pg/ μ l. Probes with a detectability of at

^① http://netdocs.roche.com/DDM/Effective/pdf_0900b2fc80acecf6.pdf

least 1pg/μl are required to obtain positive signal on Northern blots. The protocol was modified in overall steps from the Roche manufacture's instruction and Box3in Zimmerman's Nature publication (Zimmerman et al., 2013).

3.7.3 RNA samples and agarose gel preparation

The denaturing agarose gel used for RNA electrophoresis was made by 0.1% DEPC water, containing 1.8% agarose, 1×MOPS, 6% Formaldehyde and 0.4μg/ml Ethidium bromide. 1-10μg RNA was solved in DEPC water, containing 1×MOPS, 6% Formaldehyde, 42% Formamide and 1× loading buffer. RNA samples were denatured by heating at 65 °C for 15min. The electrophoresis was done in 1×MOPS running buffer at 20V overnight.

3.7.4 Protocol of Northern blotting

1-10μg total RNA sample (Table 17 and 18) in high quality (no degradation, “pure” RNA: $A_{260/280} = \sim 2.0$, $A_{260/230} = 2.0\sim 2.2$ (Scientific, 2013)) was denatured and loaded to a 1% agarose gel and separated by gel electrophoresis at 20V overnight (17h30min). The RNA was transferred by capillary blotting (blotting “sandwich”, Figure 16) from the gel to a positive-charged nylon membrane. The following Northern blotting procedure is a modified form of the instruction of the “DIG Northern Starter Kit” and Nature Protocols (Streit et al., 2008; Zimmerman et al., 2013).

The nylon membrane with the total RNA on top was rinsed with 6×SSC buffer for 5min followed by air drying. Thereafter, the membrane was baked at 80 °C in an oven for 30min (RNA-side-up). Additional RNA fixation was done by cross-linking was in a UV-trans-illuminator at 1.5J/cm² for 30s (RNA-side-up). The membrane with fixed RNA was rinsed with ddH₂O again and stained with Methylene Blue for 1min to indicate the position of the RNA marker, 18S and 28S rRNA and reveal the transferred total RNA. The blue color could be washed away by ddH₂O. To be prepared for the RNA hybridization, the membrane should be first rinsed with 6×SSC buffer and then incubated in a formamide containing prehybridization buffer (1ml/10cm² membrane) in a glass tube for 3h with rotation in a hybridization oven at a constant temperature of 42 °C. The DIG-labeled specific RNA probe was denatured at 65 °C for 15min before use and kept on ice for 10min. The membrane with total RNAs was incubated with the denatured RNA probe at the concentration of 100ng probe/ml hybridization buffer and continuously rotated at 42 °C in the hybridization oven overnight. The next morning, the

hybridization buffer was discarded and the same amount of 2×SSC was added for 5min rotation at room temperature. Thereafter, the membrane was rinsed by 1×SSC for 10min and incubated with Roche protein blocking buffer for 40min. For the 1st antibody incubation, mouse anti-DIG monoclonal unconjugated antibody was used at the working dilution of 3: 5000 in blocking buffer for 30min at RT. The membrane was washed with washing buffer 1×SSC for four times 10min each at RT. The 2nd antibody anti-mouse IgG was used at a working dilution of 1: 30,000 in washing buffer for 45min incubation. Thereafter, the membrane was washed five times with 1×SSC washing buffer for 10min each to remove the unspecific binding. Immune-Star™ AP was used as substrate to detect the hybridization signal in the dark room.

The stripping protocol from Roche suggested to rinse the membrane thoroughly in DEPC water and incubate it at 80 °C in stripping buffer for 2× 60min, followed another 5min rinse thoroughly in 2×SSC buffer. However this stripping protocol proved to be not optimal in this study, wherefore this is not recommended and a new one needed to be developed.

3.8 Construction of myc-tagged AKAP plasmids and expression in TM4 cells

By the bioinformatic screening for the AKAPs with putative PTS1 signals, we were able to find three potential conserved “peroxisomal” AKAP subfamilies (AKAP1, AKAP4 and AKAP10) in the first round rough screening (Figure 17). Eventhough the tripeptide “SKL”-variant was contained in all species analyzed, the PTS1 finder used in the second round PTS1 screening did recognize these signals as putative peroxisomal targeting signal 1, but not judged them as peroxisomal AKAPs (Figure 38-40). Subcellular localization of a protein should, however, not only rely on computer predictions, but also revealed by experimental confirmation. Since our group had already bought many commercially available antibodies against several peroxisomal proteins which showed various cross-reactions with other non-specific proteins in homogenates, we decided to clone several interesting AKAP-families members with putative “SKL”-variants. Therefore, AKAPs with different myc tags were constructed and myc-tagged GFP was used as control for the protein overexpression in Sertoli cells. For each AKAP and the GFP control, two types of recombinants were used for the

expression analysis and subcellular localization: myc tag at the amino-terminus & myc tag at the carboxyl-terminus of the fusion protein.

3.8.1 Construction of myc-tagged AKAPs and GFP plasmids

Three IMAGE clones (Table 4 pYX-Asc-AKAP1, pCR-Blunt II-TOPO-AKAP4, and pSPORT 1-AKAP10) were selected and purchased from GenomeCube as the templates for whole length amplification of AKAP1, 4 and 10. At the same time, the pGeneClip™ hMGFP vector was used as the template for the recombinant positive control. Thereafter, for two types vectors expression primers were designed (Table 5). Two *Taq*-PCRs were performed (Table 8) to amplify whole GFP cDNA (684bp) and Six *Pfu*-PCRs were performed (Table 9) to amplify accurately the AKAP complete cDNAs (*Akap1* cDNA 2589bp; *Akap4* cDNA 2565bp; *Akap10* cDNA 1131bp).

Table 8 *Taq*-PCR reaction

	Reagent	Volume
GFP_3B(BL48/BE66); GFP_5B(BE65/BE67)	<i>Taq</i> PCR 10× Buffer	2.5 µl
	dNTP mix (10mM each)	0.5 µl
	primer mix (10 µM)	2 µl
	<i>Taq</i> DNA polymerase (5U/µl)	0.5 µl
pGeneClip™ hMGFP Vector [AY744386.1]	plasmid (5ng/µl)	2 µl
	LONZA H ₂ O	18 µl
		25 µl

Taq-PCR procedure: 95 °C for 2min initiate denaturation, followed by 35 cycles of denaturation at 95 °C for 30s, annealing at 58 °C for 30s, elongation at 72 °C for 5min30sand one final extension step at 72 °C for 5min.

Table 9 *Pfu*-PCR reaction

	Reagent	Volume
	10× <i>Pfu</i> Buffer	2.5 µl
	dNTP mix (10mM each)	0.5 µl

AKAP1_3B(BH42/BH43); AKAP1_5B(BH48/BH49); AKAP4_3B(BH44/BH45); AKAP4_5B(BH50/BH51); AKAP10_3B(BL28/BH47); AKAP10_5B(BL29/BH53)	primer mix (10 μ M)	2 μ l
	<i>Pfu</i> DNA polymerase(2U/ μ l)	0.5 μ l
AKAP1_IMAGE [BC065135.1]; AKAP4_IMAGE [BC130271.1]; AKAP10_IMAGE [BC054105.1]	plasmid (5ng/ μ l)	2 μ l
	LONZA H ₂ O	18 μ l
		25 μ l

The *Pfu*-PCR procedure was as follows: initial denaturation at 95 °C for 2min, followed by 35 cycles of 95 °C for 30s denaturation, 58 °C for 30s annealing, 72 °C for 5min30s elongation and a final extension step at 72 °C for 5min.

Compared to the *Taq* DNA polymerase, at one hand, *Pfu* polymerase possesses a higher thermostability and fewer false proofreading properties, because *Pfu* is able to correct errors by its 3'-5' exonuclease activity during DNA amplification. At the other hand, DNA products made by *Pfu* are not useful in direct TA cloning, since they are lacking of "A (adenine)" 3'overhangs at their blunt ends. Therefore, blunt end PCR fragment ligation needs an extra "dATP" addition to the blunt end.

All the *Pfu*-PCR products were therefore purified by regular gel extraction method. 7 μ l of the eluted PCR fragment was mixed with 1 μ l *Taq* PCR 10 \times Buffer (25mM MgCl₂), 1 μ l 2mM dATP, 5 units of *Taq* DNA polymerase, and deionized H₂O (LONZA H₂O) to a final volume of 10 μ l. Thereafter, this 10 μ l mixture was incubated at 70 °C for 30min to add an extra "dATP" to the blunt end. This procedure for blunt end PCR fragment ligation was slightly modified from Promega protocol^①.

Following the regular TA cloning procedure, a 12 μ l ligation reaction including 5 μ l of the PCR fragment mixture, 1 μ l pGEM-T easy vector, 5 μ l 2 \times ligation buffer and 1 μ l T4 ligase was incubated at 4 °C overnight (14-16 hours).

The two types of GFP ligation were transformed into *E.coli* (see subsection 3.8.2) and sent to verify the sequences. Thereafter, the two types of GFP were subcloned into the expression vector pCMV-3B and pCMV-5B, respectively (Table 10

^① <http://www.promega.com/~media/files/resources/promega%20notes/62/cloning%20bluntend%20dna%20fragments%20into%20the%20pgem-t%20vector%20systems.pdf>

and Table 11). These two types recombinants were sequenced to make sure that GFP was in-frame with the myc-tag. The transfection of two types myc-tagged GFP were to double assess the cytoplasmic localization of GFP by its green fluorescence and the myc-tag by indirect red fluorescence with a mouse anti-myc secondary antibody (subsection 3.8.4-3.8.6). With this procedure, a perfect colocalization of GFP and the myc-tag was observed, suggesting that the used anti-myc antibody was excellent and suitable to use for the detections of the myc-tagged AKAP constructs.

The procedure for the three AKAP-recombinant plasmid constructions was following similar protocols as ones for the GFP constructs. Only AKAP1 needed an additional point mutation assay before being ligated into the expression vectors (subsection 3.8.3) because of an unexpected stop codon mutation.

Table 10 Restriction enzyme digestion of GFP and 3 AKAPs (4h incubation at 37 °C)

Reagent	Volume	Reagent	Volume	Reagent	Volume
LONZA H ₂ O	X µl	LONZA H ₂ O	X µl	LONZA H ₂ O	X µl
AKAP1-pGEM-T (total 3.75 µg)	Y µl	AKAP4-pGEM-T (total 3.75 µg)	Y µl	AKAP10-pGEM-T (total 3.75 µg)	Y µl
RE 10× Buffer B	5 µl	RE 10× Buffer B	5 µl	RE 10× Buffer D	5 µl
Acetylated BSA	0.5 µl	Acetylated BSA	0.5 µl	Acetylated BSA	0.5 µl
<i>Bam</i> HI (10U/µl)	1.25 µl	<i>Bam</i> HI (10U/µl)	1.25 µl	<i>Eco</i> RI (10U/µl)	1.25 µl
<i>Xho</i> I (10U/µl)	1.25 µl	<i>Xho</i> I (10U/µl)	1.25 µl	<i>Xho</i> I (10U/µl)	1.25 µl
	50 µl		50 µl		50 µl
Reagent	Volume	Reagent	Volume	Reagent	Volume
LONZA H ₂ O	X µl	LONZA H ₂ O	X µl	LONZA H ₂ O	X µl
GFP-pGEM-T (total 3.75 µg)	Y µl	pCMV-3B or pCMV- 5B (total 3.75 µg)	Y µl	pCMV-3B or pCMV- 5B (total 3.75 µg)	Y µl
RE 10× Buffer B	5 µl	RE 10× Buffer B	5 µl	RE 10× Buffer D	5 µl
Acetylated BSA	0.5 µl	Acetylated BSA	0.5 µl	Acetylated BSA	0.5 µl
<i>Bam</i> HI (10U/µl)	1.25 µl	<i>Bam</i> HI (10U/µl)	1.25 µl	<i>Eco</i> RI (10U/µl)	1.25 µl
<i>Xho</i> I (10U/µl)	1.25 µl	<i>Xho</i> I (10U/µl)	1.25 µl	<i>Xho</i> I (10U/µl)	1.25 µl
	50 µl		50 µl		50 µl

Table 11 Ligation reaction (overnight incubation at 4 °C)

Reagent	Volume
Digested and purified insert fragment (total 500ng)	X µl
Digested and purified vector fragment (total 200ng)	Y µl
10× ligation Buffer	2 µl
T4 ligase	1 µl
	20 µl

3.8.2 Procedures for bacterial transformation

3.8.2.1 Heat shock procedure

The LB/Ampicillin^r (100 µg/ml) plates were prepared freshly and store in the clean bench prior to use. 5 µl ligation reaction were added into 50 µl DH5α competent cells aliquot and mixed gently by pipetting. After 20 minutes incubation on ice, a 90 seconds heat-shock was performed in a water bath with a constant temperature of 42 °C. The shocked cells were immediately chilled on ice for 2 minutes. 200 µl of SOC medium were added to grow the transformed cells at 37 °C for 30 minutes incubation. During the incubation period, a mixture of 100 µl LB, 20 µl IPTG (1M) and 40 µl X-gal (2%) was spreaded onto the Amp^r plates, followed by air drying. The complete 255 µl transformation culture of the tube was spread onto the Amp^r plate. A plasmid as the positive control had been previous transformed efficiently and an Amp^r plate with DH5α alone was used as the negative control. After an overnight incubation at 37 °C, the blue white screening was used to identify successfully ligated clone. This protocol was slightly modified from the original protocol of promega^①.

3.8.2.2 Electroporation procedure

Efficient introduction of DNA into bacteria is critical for the success of many molecular biology procedures. The electroporation method for transforming *E.coli* cells

^①<https://www.promega.com/~media/files/resources/protcards/pgem%20t%20and%20pgem%20t%20easy%20vector%20systems%20quick%20protocol.pdf>

can produce efficiencies greater than those achieved with the best chemical methods^①, especially for large plasmids (4.1kb-6.9kb). Commercial available ElectroTen-Blue[®] cells needed only to be thawed and mixed with DNA prior to electroporation.

The genotype of bacteria DH5 α used for heat shock transformation is F⁻ Φ 80*lacZ* Δ *M15* Δ (*lacZYA-argF*) *U169* *recA1* *endA1* *hsdR17* (rK⁻, mK⁺) *phoA* *supE44* λ -*thi-1* *gyrA96* *relA1*^②. The DH5 α exhibits no antibiotic resistance. However, some electroporation competent cells possess resistance to antibiotics.

The electroporation competent cell used in our lab is called “EletroTen-Blue[®]”. It is a derivative of the XL1-Blue MRF⁺ strain that can withstand much higher levels of electrical current. This increases the survival of the cells during electroporation, and thus the efficiency of the ligated constructs transformation. In addition, EletroTen-Blue strain genotype is Δ (*mcrA*)183 Δ (*mcrCB-hsdSMR-mrr*)173 *endA1* *supE44* *thi-1* *recA1* *gyrA96* *relA1* *lac* Kan^r [F⁺ *proAB* *lacI*^q *Z* Δ *M15* *Tn10* (Tet^r)], which are resistant to both kanamycin and tetracycline. Thus plasmids that carry the Kanamycin-resistance or Tetracycline-resistance selection marker cannot be propagated in this strain^③.

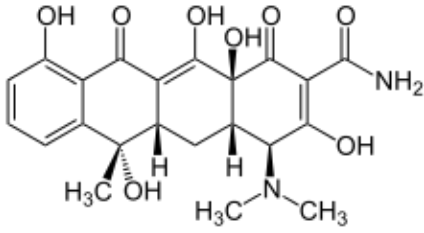
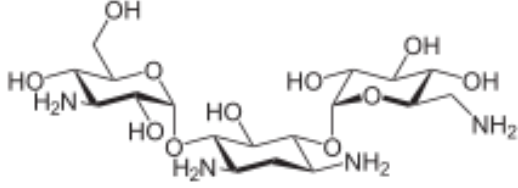
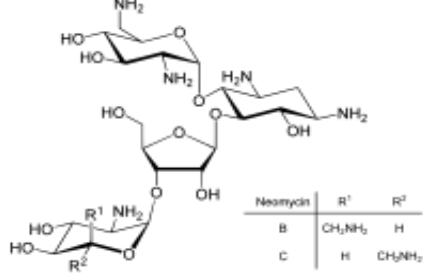
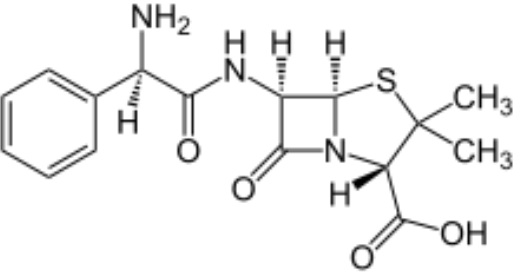
Moreover, from the structural point of view, Neomycin whose chemical structure is similar to Kanamycin (Table 12) can also not be used for selection of transformed EletroTen-Blue clones. Therefore, the expression plasmids pCMV-Tag 3B and pCMV-Tag 5B could not be used for this electroporation procedure, since they have Neo^r/Kan^r selection, while the cloning vector pGEM-T, ideal for Amp^r selection, was suitable for EletroTen-Blue cells.

^① <http://www.chem.agilent.com/library/usermanuals/Public/200159.pdf>

^② <http://www.lifetechnologies.com/de/de/home/life-science/cloning/competent-cells-for-transformation/chemically-competent/dh5alpha-genotypes.html>

^③ <http://www.chem.agilent.com/library/usermanuals/Public/200159.pdf>

Table 12 Chemical structure of common used antibiotics

Antibiotics	Tetracycline	Kanamycin									
Structure											
Antibiotics	Neomycin	Ampicillin									
Structure	 <table border="1" data-bbox="592 786 778 875"> <thead> <tr> <th>Neomycin</th> <th>R¹</th> <th>R²</th> </tr> </thead> <tbody> <tr> <td>B</td> <td>CH₂NH₂</td> <td>H</td> </tr> <tr> <td>C</td> <td>H</td> <td>CH₂NH₂</td> </tr> </tbody> </table>	Neomycin	R ¹	R ²	B	CH ₂ NH ₂	H	C	H	CH ₂ NH ₂	
Neomycin	R ¹	R ²									
B	CH ₂ NH ₂	H									
C	H	CH ₂ NH ₂									

3.8.3 Point mutation assay

Aligned with AKAP1 mRNA variant 2 [NM_001042541.1], the sequenced AKAP1_IMAGE clone cDNA [BC065135.1] contained 2 mutation points: **T**A(A)(STOP)1993**G**A(Glu) and TCT**T**(Ser)2208TCC**C**(Ser). The second point mutation (C2208T) caused no amino acid change, which could be neglected. But the first point mutation (G1993T) caused an extra STOP codon, which had to be mutated back to the original base pairs.

Table 13 AKAP1-Mutation-PCR reagent

	Reagent	Volume
	10× <i>Pfu</i> Buffer	5 µl
	dNTP mix (10mM each)	0.8 µl
AKAP1_Mut_F (10pmol/ µl) / AKAP1_Mut_R (10pmol/ µl)	primer mix (10 µM)	2 µl
pGEM-T-AKAP1_3B; pGEM-T-AKAP1_5B	plasmid (20ng/ µl)	1 µl
	<i>Pfu</i> DNA polymerase	1 µl
	DMSO	2.5 µl
	LONZA H ₂ O	38 µl
		50 µl

The Mut-PCR procedure was as follows: initial denaturation at 94 °C for 1min30s followed by 18 cycles of 94 °C for 30s denaturation, 55 °C for 1min annealing, 68 °C for 13min elongation and a final extension step at 68 °C for 13min.

1 tube of PCR reagent without Mut-Primers was set as the negative control. The DNA template was digested completely by *DpnI* and no colony were observed on Amp^r plate. Unmutated plasmids had been previous transformed efficiently to DH5α as positive control to verify the transformation procedure.

Table 14 AKAP1-Mutation-PCR *Dpn I* digestion (4h incubation at 37 °C)

	Reagent	Volume
pGEM-T-AKAP1-3B_Mut; pGEM-T-AKAP1-5B_Mut	Purified mutation plasmid	42 µl
	10× Buffer B	5 µl
	BSA (10mg/µl)	0.5 µl
	<i>DpnI</i>	2.5 µl
		50 µl

15 µl digested plasmids (samples or negative control) or 5 µl ligated plasmids (positive control) were transformed to DH5α by the heat shock procedure (see subsection 3.8.2.1). Clones with the correct mutated sequence verified by sequencing were subcloned into expression vectors pCMV-3B and pCMV-5B (Table 10 and Table 11).

3.8.4 Coating cover slips with poly-L-lysine

10mg of poly-L-lysine was dissolved in 100ml H₃BO₃/Na-tetraborat buffer (see Table 3 Buffer recipes). The solution needed to be sterilized through 0.22 µm Millipore filtration. Moreover, 12mm cover slips were sterilized by 4h baking at 180 °C. All the glassware and materials used were sterile and all operations performed in a laminar hood. The cover slips were incubated in poly-L-lysine solution in a 3.5 mm Petri dish overnight. On the next morning, the poly-L-lysine solution was removed by aspiration and the cover slips were incubated with sterile water in Petri dish for 5h at RT. Thereafter, the coated cover slips were rinsed with sterile water twice and air dried in the hood prior to storage at 4 °C.

3.8.5 Transient transfection of TM4 cells

One day before transfection, the TM4 cells need to be sown on the poly-L-lysine coated coverslips at a density of 5×10^4 cell/well with 500 μ l serum containing medium in a 24-well plate. After 24h growth (37 °C, 5%CO₂), cells were approximately 75% confluent. Transient transfection was then carried out according to the Promega protocol by using the ViaFect™ Transfection Reagent^①. For this study, all the plasmids for transfection were purified with an endotoxin-free plasmid DNA purification kit (NucleoBond® Xtra Midi EF, Macherey-Nagel Co.). 500ng plasmid DNA (myc-GFP plasmids used as positive control) and 3 μ l reagent were mixed with 500 μ l serum free medium per well. The transfection efficiency on TM4 cells was about 15% after one-day growth. On the second day of transfection, the cells were ready for immunofluorescence staining.

3.8.6 Immunofluorescence protocol

TM4 cells, grown on poly-L-lysine coated coverslips for 48h, were fixed with 4% paraformaldehyde in PBS for 30min at room temperature. After 3 times washing with warm PBS for 10min each, cells were treated with 1% glycine or/and 0.1% Triton X-100 for permeabilization. Cells were washed 3 times with PBS for 5min each, and blocked for 1h in 1% PBSA with 0.05% Tween, thereafter incubated with primary antibody (dilutions described in Table 6) overnight at room temperature. The next day, cells were washed 3 times with PBS for 5min each, followed by 1h secondary antibody incubation in the dark. Thereafter, cells were washed with PBS for 10min, followed by nuclear staining and final washing of 2×10min. The coverslips were mounted with the cell-side down onto glass slides with Mowiol 4-88 containing propylgallat mixture as anti-bleaching agent. The staining pattern was checked and pictures were taken with a fluorescence microscope (Leica DMR) or a laserscan confocal microscope (Leica TCS SP2) using 63× oil immersion objectives.

^① <https://www.promega.de/~media/files/resources/protcards/viafect%20transfection%20reagent%20quick%20protocol.pdf>

4 Results

Follicle-stimulating hormone (FSH)-mediated flux through metabolic pathways is controlled by secondary modification of proteins such as phosphorylation and dephosphorylation at specific subcellular locations. This regulation has been shown for mitochondrial cholesterol influx to occur via the AKAP1-StAR interaction. However, very limited knowledge is available to date on the direct control of these metabolic pathways in peroxisomes.

4.1 AKAP family members with putative PTS1 signals

Since a previous report showed that AKAP11 is probably localized to the peroxisome, it is interesting to determine whether other proteins of AKAP family are putative peroxisomal proteins. Therefore, I screened for AKAP isoforms with putative peroxisomal targeting signals.

4.1.1 AKAP sequence retrieval and PTS1 search matrix


All known AKAP sequences (1306 sequences) from diverse species were retrieved from “UniProt” database^① followed by the screening for a putative C-terminal PTS1. Only the C-terminal tripeptide was used to screen for the putative C-terminal PTS1, since it is the crucial portion for peroxisome import. After removing the duplicates, 531 different tripeptides were left over from all AKAP sequences (Supplemental data S3).

For classification of all variants of possible PTS1 signals, all known PTS1 binding sites from the “Peroxisomal Target Signal Predictor (PTSP)” were downloaded (Supplemental data S4) and summarized into a Combination Matrix (Table 15).

^① <http://www.uniprot.org/uniprot/>

Table 15 Summarized PTS1 tripeptides derived from the “Peroxisomal Target Signal Predictor (PTSP)”
PTS1 tripeptides in standard amino acid 1-letter code

AHL	CKL	PRL	SNL
AKF	CRL	QAL	SQL
AKI	HKL	SHL	SRI
AKL	HRL	SKI	SRL
ANL	KKL	SKL	SRM
ARL	NKL	SKM	SSL
ASL	PKL	SKV	THL



A	A	F
C	H	I
H	K	L
K	N	M
N	Q	V
P	R	
Q	S	
S		
T		

4.1.2 Phylogenetic analysis of AKAP proteins containing a putative PTS1 signal

Using the combination matrix for conserved PTS1 substitutions, 81 AKAP proteins with possible PTS1 ends were identified and used to generate a phylogenetic tree (Figure 17). The AKAPs clustered into six large groups belonging to the AKAP1, 3, 4, 10, 11, 14 and 17A families, while two sequences distributed into distinct groups as individual entities. An unexpected finding was that the short form of AKAP11 from the rat (sp|Q62924|AKAP11 Rat-CRL) clustered into a separate group. Interestingly, AKAP family members within the described groups displayed similar PTS1 signals, suggesting that the signal was conserved during evolution and that they might be real peroxisomal targeting signals.

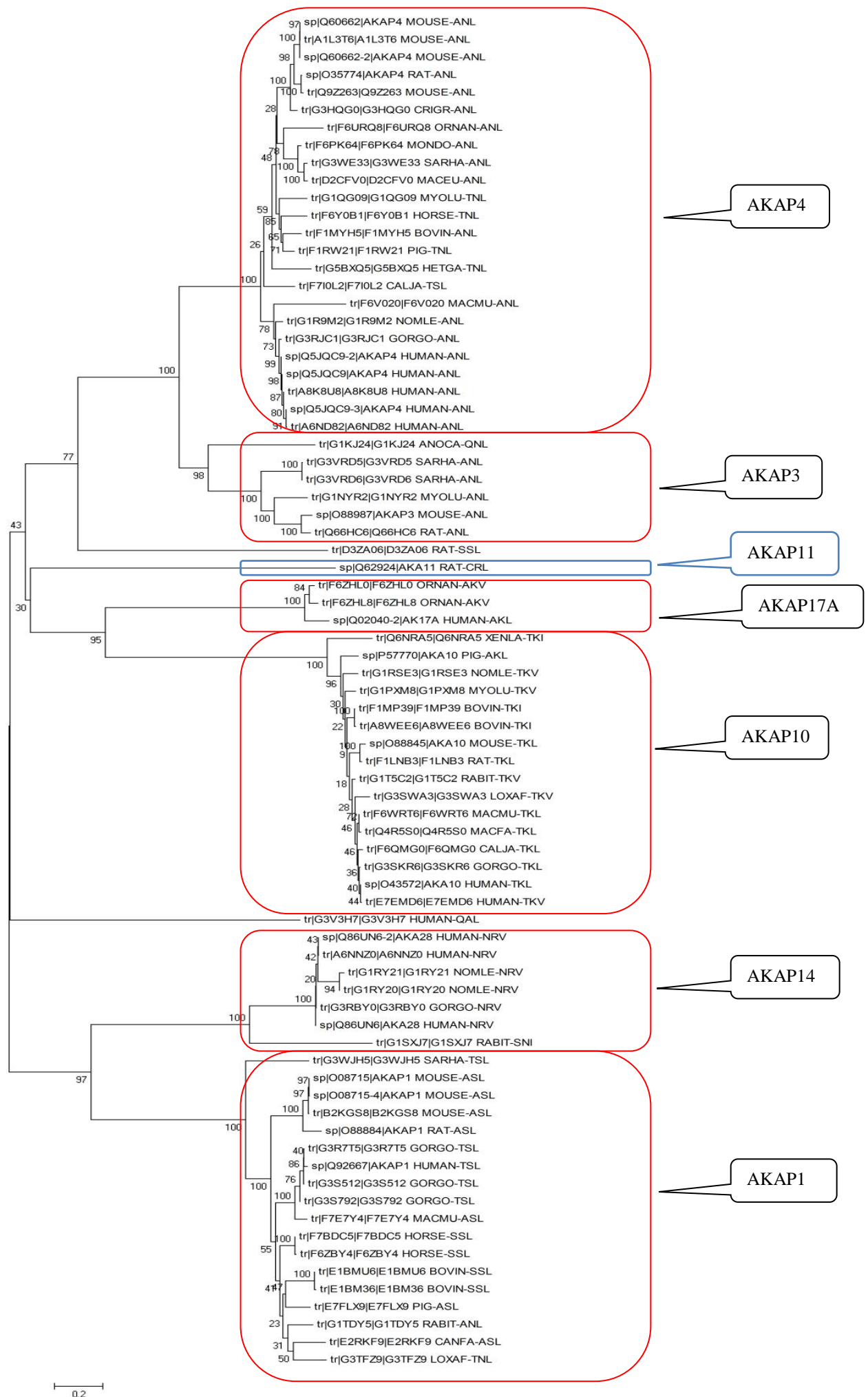


Figure 17 Phylogenetic tree of AKAPs with putative PTS1

By analysis of the EST expression profile I found that the AKAP1, 4, 10 families are highly expressed in testis (Figure 41-42). The sequence and the phylogenetic analysis of these AKAPs indicated that they might contain a putative PTS1 signal, however, these proteins were reported to be localized to the mitochondria or other subcellular sites and not the peroxisome (see subsection 1.4.2-1.4.4). However, peroxisomal localization of proteins has been overlooked quite frequently in the past and some peroxisomal protein isoforms have multiple subcellular locations (Islinger et al., 2009). Therefore, it was speculated that depending on the cellular requirements and developmental stages, AKAPs might be localized in different subcellular compartments (e.g. mitochondria and peroxisome). In section 4.6, the subcellular location of myc epitope tagged AKAP1, AKAP4 and AKAP10 in TM4 Sertoli cell line were analyzed.

4.2 TM4 Sertoli cell culture stimulation with FSH treatment

To study the regulation of the peroxisomal compartment by FSH signaling and AKAPs, a good cell culture model was established.

4.2.1 Cell culture condition optimization

Follicle-stimulating hormone (FSH) binds to its receptor on the plasma membrane of Sertoli cells of the testis and granulosa cells of the ovary, thereby initiating an intracellular signaling cascade inducing the activation of PKA to phosphorylate downstream target proteins, which are essential for the regulation of androgen and progesterone production and sperm motility (Tasken and Aandahl, 2004; Walker and Cheng, 2005). It is known that peroxisomes play an important role in spermatogenesis and oxidative stress protection in the testis (Dastig et al., 2011) and that Sertoli cells in the testis contain high levels of metabolic peroxisomal proteins (Nenicu et al., 2007). However, it was not known whether peroxisomes or peroxisomal genes are affected by activation of the FSH signaling pathway. To study potential effect of FSH on the peroxisomal compartment, the mouse Sertoli cell line-TM4 cells were purchased from the ATCC. The exact cell culture condition of the TM4 Sertoli cells was established by seeding them at different densities (Table 16)

Table 16 Optimization of cell density to obtain a monolayer of TM4 cells on Day 4-6

The 1 st set	Density of cells seeded per ml	Day 4	Day 6
A Group	2×10	No cells	Almost no cells, all cells are round
B Group	2×10^2	Very few cells	Still no connection, too many round cells
C Group	2×10^3	No cluster, no connection	Some part is monolayer, some part no connection
D Group	2×10^4	Some part is monolayer, some part is multilayer	Too full
E Group	2×10^5	Multilayer, overgrown	Too full
F Group	2×10^6	Too full	Too full
The 2 nd set	Density of cells seeded per ml	Day 4	Day 5
G Group	3×10^3	No connection, single cell	Most part no connection, some part is monolayer
H Group	6×10^3	Some part is monolayer, some part is single cell	Most part is monolayer, some part no connection
I Group	1.2×10^4	Monolayer, perfect!	Half part is monolayer, half part is multilayer

The best monolayer at Day 4 was obtained with a seeding density of 2.34×10^3 cells/cm² = 9×10^3 cells/ml. This experimental condition was used further for stimulation of TM4 Sertoli cells with FSH stimulation.

4.2.2 Effect of FSH stimulation on the peroxisome gene expression

After optimization of the culturing conditions, TM4 cells were treated with increasing FSH concentration (W0 = 0ng/ml, W1 = 10ng/ml, W2 = 100ng/ml, W3 = 1000ng/ml). From all four experimental groups (W0, W1, W2, W3), total RNA was isolated, reverse transcribed and used for semiquantitative analysis of mRNA expression of genes involved in peroxisomal biogenesis and proliferation, antioxidative enzymes and lipid metabolism (Figure 18-24).

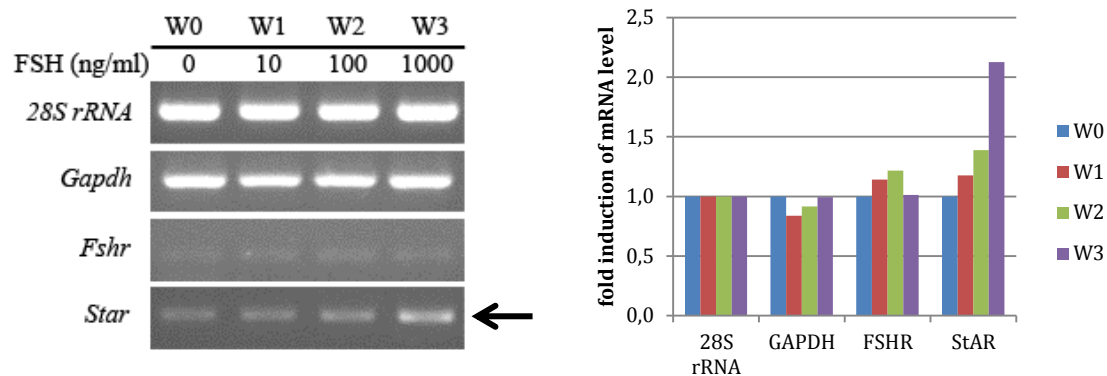


Figure 18 Measurement of the mRNA of internal control and positive controls by conventional RT-PCR

FSH receptor is present in TM4 cells. The FSH stimulation of TM4 cells worked well with 1000ng/ml, since *Star* gene was upregulated, whereas GAPDH and FSHR were not altered (Figure 18). The calculations for Figure 18-24 were made with the 28S rRNA values from Figure 18.

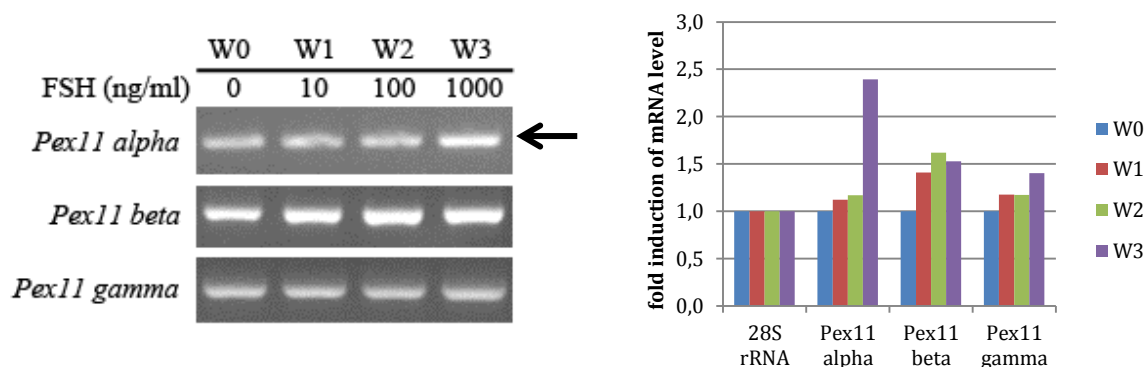


Figure 19 Alterations of mRNA levels of peroxins on peroxisome proliferation

There is a clear indication for the *Pex11a*, the inducible form of the PEX11 proteins, whereas the other family members were not changed (Figure 19).

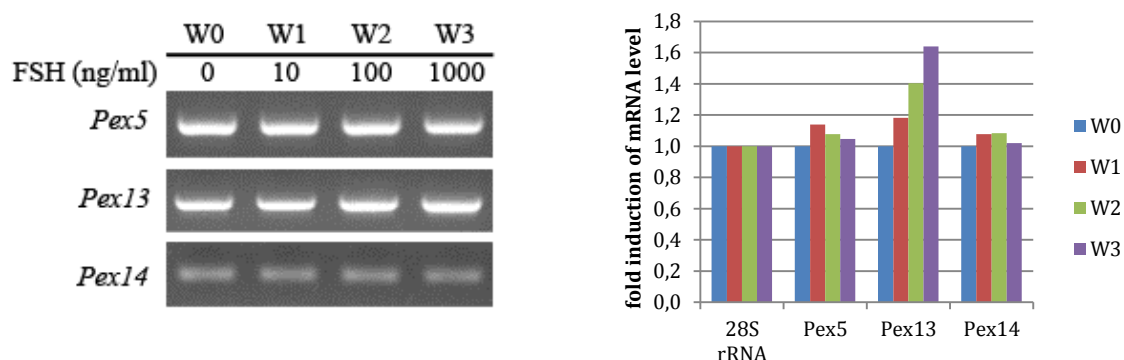


Figure 20 Alterations of mRNA levels of peroxins on peroxisomal matrix protein import

In comparison to the *Pex11a* gene, some marker genes for peroxisomal matrix protein import (*Pex5*, *Pex14*) were not altered while *Pex13* showed a slight upregulation in gel measurements (Figure 20).

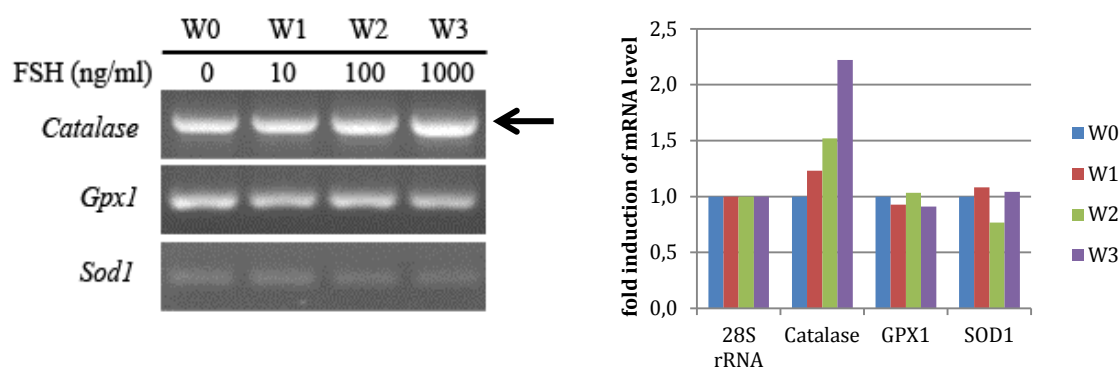


Figure 21 Quantification of alterations of mRNA levels of antioxidative enzymes by conventional RT-PCR

FSH treatment leads to the upregulation of the *catalase* expression, whereas *Gpx1* and *Sod1* were not altered. This is of interest, since *catalase* is the only one protein involved in anti-oxidation metabolism that is exclusively present in peroxisomes, whereas *Gpx1* and *Sod1* are also present in other cellular compartments (Figure 21).

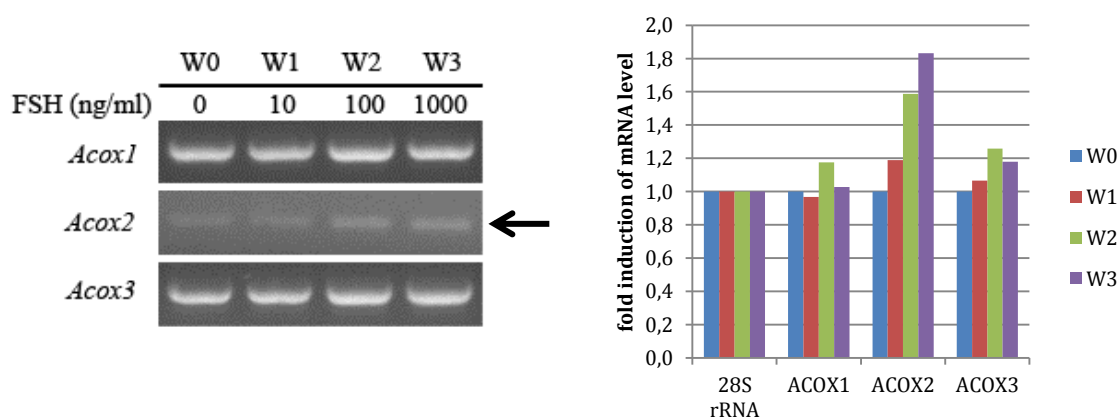


Figure 22 Alterations of mRNA levels of Acyl-CoA oxidases by FSH treatment

From the three Acyl-CoA oxidase mRNAs, only the one of *Acox2* showed a significant upregulation (Figure 22). This is of interest, since this enzyme is involved in the conversion of the cholesterol side-chain, whereas the other members of the Acox

family degrade mainly straight chain- and branched chain fatty acids (Baumgart et al., 1996b).

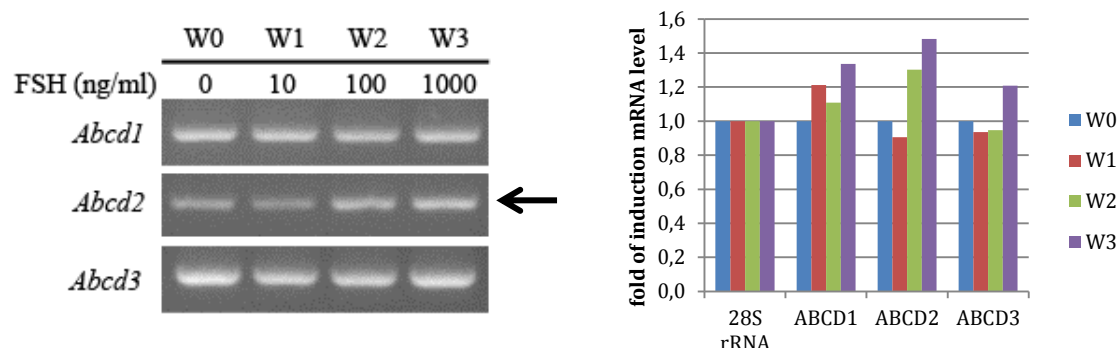


Figure 23 Conventional RT-PCR results of alterations of mRNA levels of fatty acid transporters

ABCD1-ABCD3 are the members of ATP-binding cassette (ABC) transporters superfamily in peroxisomal membrane and play a role in transporting fatty acids for the lipid metabolism into the peroxisomal matrix. From the fatty acid transporters ABCD1-ABCD3, mainly ABCD2 is upregulated by the increasing FSH stimulation. These 3 members of ABCD proteins were found to have overlapping substrates as well as distinct specificities (van Roermund et al., 2014). ABCD1 (also called ALDP) preferentially transported saturated VLCFA such as C24:0 and C26:0 as substrates for β -oxidation activity, and the X-ALD patients (X-linked adrenoleukodystrophy) with genetic defective ABCD1 exhibit the accumulation of VLCFA in plasma. The substrates of ABCD2 (also called ALDRP) were C22:0 and also unsaturated VLCFA such as C24:6 and C22:6 (van Roermund et al., 2011). ABCD3 (also called PMP70) was suggested to transport long branched chain fatty acids, long-chain unsaturated- and dicarboxylic fatty acids (C27 bile acids) across the peroxisomal membrane, which is important for bile acid biosynthesis (Ferdinandusse et al., 2014; van Roermund et al., 2014).

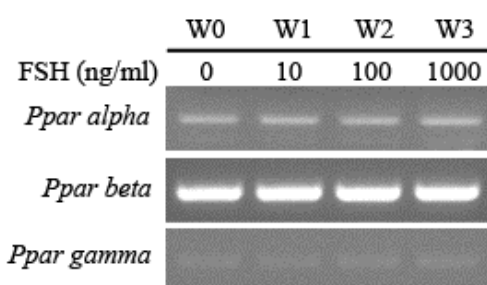


Figure 24 Measurement of PPAR transcription factors after treatment with different concentration of FSH

Since many peroxisomal genes are regulated by PPARs, PPAR α , - β , - γ expression in TM4 Sertoli cells were also analyzed. Indeed, the mRNAs of all PPAR family members were expressed in Sertoli cell line, with the PPAR β mRNA showing the strongest signal (Figure 24). PPAR α performs multiple functions in the liver, heart and blood vessel wall, and is also known to be activated by FSH to compose phospholipids in germ cells. PPAR β is present ubiquitously and plays a role in glucose homeostasis and fatty acid oxidation. PPAR γ is mainly expressed in mature Sertoli cells, adipocytes and skeletal muscles and takes part in anti-diabetic and anti-atherosclerotic mechanisms (Kota et al., 2005; Thomas et al., 2010). PPARs are also known to be involved in the regulation of fertility. However, there was no major change in their mRNA levels after FSH treatment.

4.3 Isolation of peroxisomes from TM4 cells

AKAP220, the short form of AKAP11 in the rat (a single frame in the Figure 17), was the only AKAP protein to be reported in peroxisomes. I tried to repeat and establish the peroxisomal localization in our laboratory to study effects of FSH-stimulation of this protein on the peroxisomal compartment. However, this protein clustered singly into a separate group from all other AKAP family members in the phylogenetic tree. It was speculated that there might be a problem with the peroxisomal localization of this protein reported by Scott group (Lester et al., 1996). Therefore, attempt was made to localize this protein from highly purified peroxisomal fractions by antibody-based test. To localize AKAP11 in peroxisomes, the differential centrifugation and OptiPrep density gradient centrifugation were used to isolate pure peroxisomal fractions followed by detection with a commercially available anti-AKAP220 antibody.

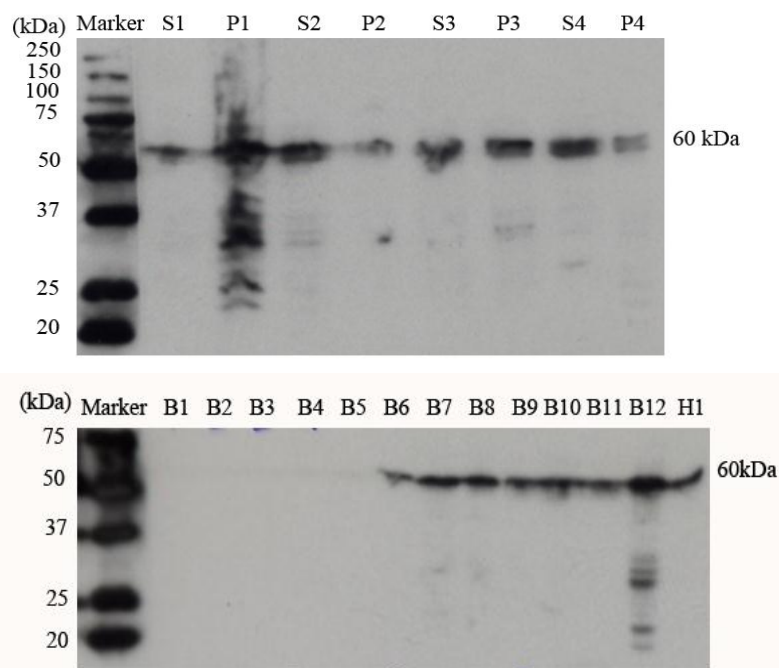


Figure 25 Peroxisome marker PEX14p (60 kDa) distribution. H1: homogenization; S1: supernatant after 1st centrifugation from H1; P1: pellet after 1st centrifugation from H1, mainly contains cell debris; S2: supernatant after 2nd centrifugation from S1; P2: pellet after 2nd centrifugation from S1, mainly contains heavy mitochondria and some peroxisomes; S3: supernatant after 3rd centrifugation from S2; P3: pellet after 3rd centrifugation from S2, mainly contains light mitochondria and enriched peroxisome, using for the further density gradient centrifugation; S4: supernatant after 4th centrifugation from S3, mainly contains cytoplasm substance; P4: pellet after 4th centrifugation from S3, mainly contains microsome and small peroxisome. Then P3 was taken for 2h30min OptiPrep density gradient centrifugation. B1 to B12 are the 12 tubes fraction of handled OptiPrep through constant speed pump.

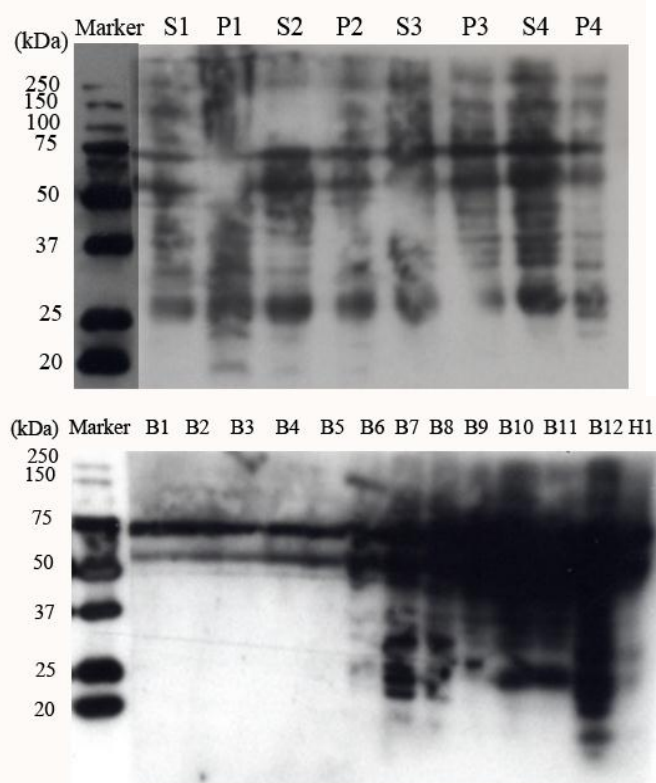


Figure 26 Western blot of AKAP220 (AKAP220 should be 220 kDa). The samples H1to P4 and B1 to B12 are the same as Figure 25.

An excellent antibody against PEX14p, a peroxisomal membrane protein of the docking complex (Figure 13), was used to analyze the distribution of peroxisomes in the different fractions obtained after differential centrifugation and density gradient centrifugation in Western blots.

PEX14p-labelling was very specific, except in the fraction P1 with the cell debris, revealing the high quality of the antibody used. The main protein band was found at the expected molecular weight of 60kDa, as expected for PEX14p (Grant et al., 2013). Peroxisomes were enriched in P3, the typical fraction where most of the organelles were found. This fraction is frequently called enriched peroxisomal fraction and corresponds to the “light mitochondrial” fraction, since it also contains the small mitochondria. In comparison, the heavy mitochondrial fraction (P2), exhibiting also large peroxisomes, is less intensively labelled as well as the microsomal fraction (P4), in which very small peroxisomes were described by electron microscopy (Baumgart, 1997). The strong labelling of the supernatant S4 suggested that during the isolation procedure of peroxisomes from TM4 cells, some peroxisomes broke. The stronger peroxisomal enrichment in the gradient is found in fraction B7 and B8. Broken organelles were also observed in the soluble fraction at the top of the gradient, indicated by some degradation bands in addition to the PEX14p signal.

Attempts to localize AKAP220 in different subcellular fractions with the anti-AKAP220 antibody (Santa Cruz Biotechnology, Inc.) did not give any satisfactory results. The antibody detected a plethora of different cross-reactive protein bands, but the expected 220kDa band was labelled very weakly. The strongest signal intensity was observed for most of the bands in S4, the final supernatant with cytoplasmic proteins.

Based on the results from the Western blot analysis and the peculiar single localization of the short rat AKAP form into a separate group in the phylogenetic tree (Figure 17), it appears that the results described by Scott and colleagues (Lester et al., 1996) with the antibody made against the C-terminal part of the rat AKAP11 protein might be incorrect. Indeed, careful analysis of the data presented in the paper revealed several discrepancies. First, they used the TM3 and TM4, which are mouse Leydig cell line and mouse Sertoli cell line, respectively (Harrison et al., 2001), as rat testis cell lines to test for rat AKAP220 subcellular distribution study. Second, the mRNA of the rat AKAP11_{short} from their study was 9748bp in length [U48288.1] containing a 5'-untranslated region (UTR) of 5406bp and an open reading frame (ORF) of 3387bp that

encodes a 1129 amino acid polypeptide. However, analysis of this mRNA [U48288.1] showed that it contains a 5'-UTR of 5411bp and the position of ORF is 5411-8800 (Figure 29). Third, for the expression of a partial AKAP220 of 368 amino acids in *E. coli*, they amplified a 1104-bp fragment by PCR, which was encompassing the coding region of the original AKAP220 cDNA flanked by artificially *NdeI* and *BamHI* sites at the 5' and 3' ends, respectively. However, alignment of this primer pair with the AKAP220 mRNA [U48288.1] showed the forward primer aligned at the position of 8483 and the reverse primer at the position of 8950, which produced an only 467bp amplicon and 150 bases out of the ORF. Therefore, this incorrect primer pair is assumed to have negative effect on their analysis.

4.4 Analysis of AKAP11 (=AKAP220) cDNA with genomic sequences

Since the commercial anti-AKAP11 rat antibody was not specific against its target protein, there was a plan to generate a self-made antibody. For this purpose, we searched for suitable fragments of this protein as the antigen epitope residues by screening the gene and protein databases for AKAP11. However, the alignment of various *AKAP11* cDNAs showed that sequences from human [NM_016248.3], mouse [NM_001164503.1] and rat long isoform [NM_012773.2] are highly conserved. It also revealed that the rat short isoform [U48288.1] does not obey the conservation rule of *AKAP11* evolution. Therefore, it was determined to further analyze the correlation of the *Akap11*'s cDNA/mRNA and genome (Figure 27).

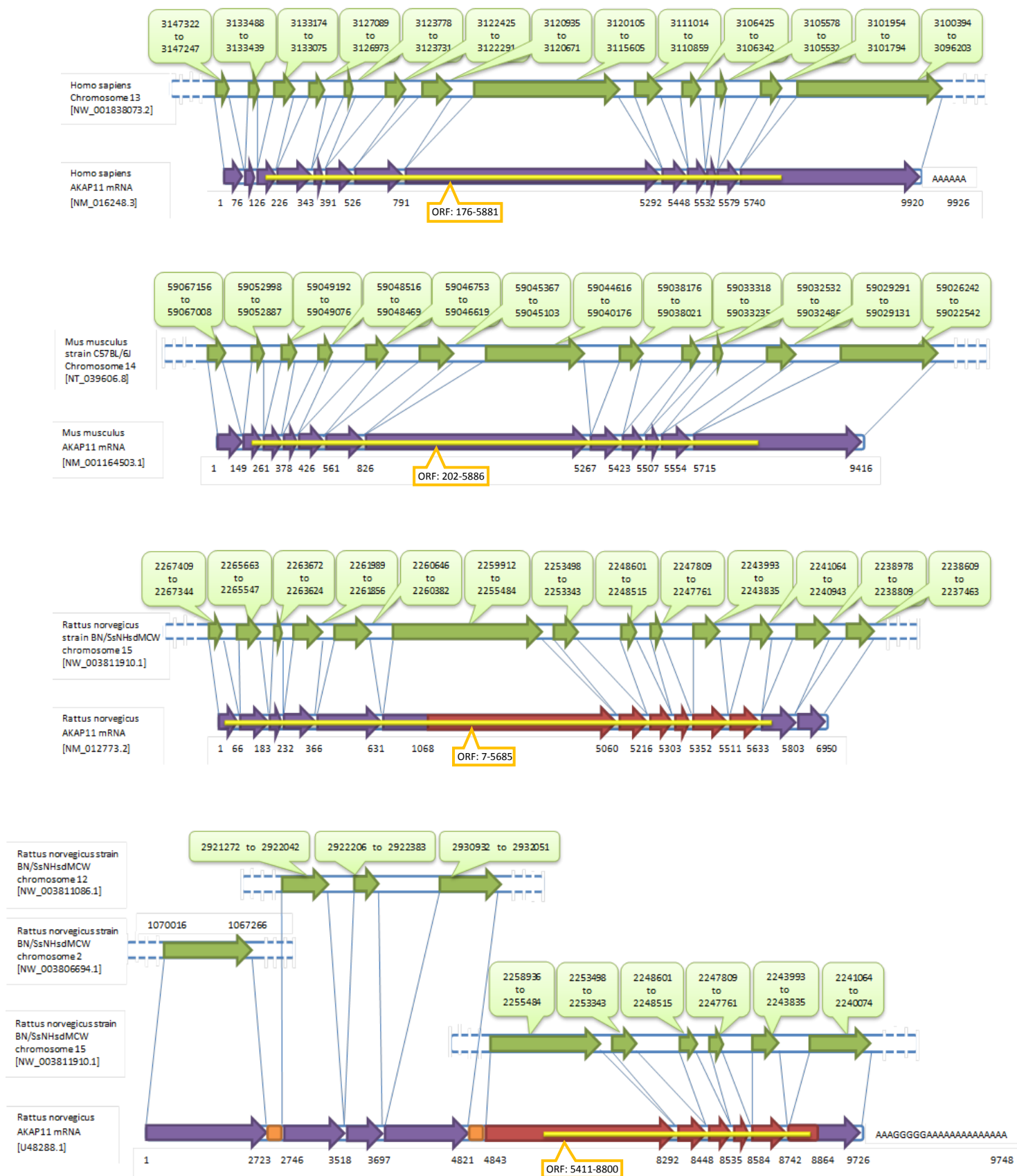


Figure 27 BLAST Results of *Akap11* mRNAs from Genome Database of human [NM_016248.3], mouse [001164503.1], rat (long [NM_012773.2] and short [U48288.1]), respectively. The exons in red are the identical sequence in both distinct rat *Akap11* mRNAs. The lower short form was published by Scott group and the protein was suggested to be localized in peroxisomes.

The first AKAP220 antibody was made by Prof. Scott's group and published in 1996 in the Journal of Biological Chemistry, where the rat AKAP220 protein short isoform was identified. But from Figure 27, the existence of AKAP11_rat-short mRNA [U48288.1] and protein isoform [Q62924.1] are questionable.

By BLAST searching the *Akap11*-human mRNA [NM_016248.3] against the Human Genome Database^①, the exons of the *Akap11*-human mRNA were localized on chromosome 13 [NW_001838073.2]. By BLAST searching the *Akap11*-mouse mRNA [NM_001164503.1] against the Mouse Genome Database^②, all exons of the *Akap11*-mouse mRNA were localized on chromosome 14 [NT_039606.8]. Similarly, by BLAST searching *Akap11*-rat-long isoform mRNA [NM_012773.2] against the Rat Genome Database^③, all the exons of *Akap11*-rat-long form mRNA were localized on chromosome 15 [NW_003811910.1]. Furthermore, [NM_012773.2] and [NP_036905.2] are mentioned as corresponding mRNA and protein on the *Akap11* tag [*Rattus norvegicus* (Norway rat)] (Gene ID: 498549, updated on 1-Feb-2015)^④ in the NCBI Gene database.

However, when a BLAST search was performed for the *Akap11*-rat-short form mRNA [U48288.1] originally published by the Scott group, against the Rat Genome Database as above, the *Akap11*-rat-short form mRNA was divided into three parts. The 1st part of the mRNA sequence [U48288.1] was identified on chromosome 2 [NW_003806694.1], the 2nd part on chromosome 12 [NW_003811086.1], and the 3rd part on chromosome 15 [NW_003811910.1]. Also, our analysis showed that the putative mRNA [U48288.1] was not only including exons from other genes, but also introns (survival motor neuron protein [NM_022509.1] and EIA-binding protein p400 [NM_001107149.1]). In addition, there were two smaller fragments (2724-2745 and 4822-4842, in orange) identified that couldn't be found on any chromosome (Figure 27). According to the definition in the book "Gene Cloning and Manipulation" (Howe, 2007), these two fragments contain *EcoRI* linkers (Figure 28)

^① http://blast.ncbi.nlm.nih.gov/Blast.cgi?PAGE_TYPE=BlastSearch&BLAST_SPEC=OG_P_9606_9558&LINK_LOC=blasthome

^② http://blast.ncbi.nlm.nih.gov/Blast.cgi?PAGE_TYPE=BlastSearch&BLAST_SPEC=OG_P_10090_9559&LINK_LOC=blasthome

^③ http://blast.ncbi.nlm.nih.gov/Blast.cgi?PAGE_TYPE=BlastSearch&BLAST_SPEC=OG_P_10116_10621&LINK_LOC=blasthome

^④ <http://www.ncbi.nlm.nih.gov/gene/498549#genomic-regions-transcripts-products>

CLUSTAL 2.1 multiple sequence alignment

```

2723-2746_U48288.1_      GTGCCTCGTGCCGAATTCGG--ACGA-- 24
4821-4843_U48288.1_      ----CTCGTGCCGAATTCGGCACGAGA 23
                        *****

```

Figure 28 The sequence in the orange frame shows two potential *EcoRI* linkers in mRNA [U48288.1]. Sequence alignment was done between the position of (2723-2746) and (4821-4843) in [U48288.1].

Taken together with the other identified mistakes, the report of Scott and colleagues (Lester et al., 1996) described an artificial recombinant clone of *Akap11* that does not exist in nature, in which clone three different genes were fused together via *EcoRI*-linkers during the cDNA library construction.

4.5 Northern blotting

To analyze alternatively spliced variants of *AKAP11* and to prove that the short form AKAP11 [Q62924.1] is indeed not existing in rat testis or pituitary gland contrary to previous report from Scott and colleagues (Lester et al., 1996), it was planned to detect the expression of all possible isoforms of *Akap11* [NM_012773.2] and [U48288.1] in different rat tissues by Northern blot hybridization.

4.5.1 Total RNA preparation for Northern blotting

Total RNA was isolated from the following rat tissues: testis, brain, lung, kidney, heart, liver, skeletal muscle, spleen, pituitary.

Table 17 Total RNA was isolated using combined methods, and the RNA quality was checked by RNA-Chip analysis

Number	Sample (date)	Tissue weight	RNA Concentration	Volume	A _{260/280}	A _{260/230}
1	Brain-V (18.04)	60mg	307.4 ng/μl	50 μl	2.08	2.18
2	Liver-V (18.04)	60mg	2148.2 ng/μl	50 μl	2.03	2.04
3	Muscle-V (18.04)	60mg	529.5 ng/μl	50 μl	2.08	2.24
4	Liver-V (17.04)	80mg	562.9 ng/μl	80 μl	2.04	1.57
5	Kidney-V (17.04)	80mg	340.9 ng/μl	80 μl	2.10	2.03
6	Spleen-V (18.04)	80mg	1276.4 ng/μl	80 μl	1.95	2.20
7	Pituitary-II (24.04)	20mg	445.9 ng/μl	50 μl	2.08	1.72

8	Testis-V (24.04)	80mg	884.9 ng/μl	50 μl	2.09	2.18
9	Heart-V (18.04)	80mg	111.5 ng/μl	80 μl	2.13	1.66
11	Brain-V (17.04)	80mg	164.3 ng/μl	80 μl	2.08	2.04
12	Pituitary-III (24.04)	20mg	190.6 ng/μl	50 μl	2.10	1.86
14	Muscle-V (26.04)	60mg	153.7 ng/μl	30 μl	1.77	2.25
15	Liver-II (05.03)	20mg	545.9 ng/μl	40 μl	2.07	2.06
16	Testis-V (17.04)	80mg	378.1 ng/μl	80 μl	2.11	2.00
17	Spleen-II (05.03)	20mg	211.1 ng/μl	40 μl	2.08	1.82
19	Testis-II (06.03)	20mg	243.5 ng/μl	40 μl	2.10	1.70
20	Brain-II (05.03)	20mg	118.9 ng/μl	40 μl	2.08	1.39
22	Liver-V (18.04)	80mg	816.4 ng/μl	80 μl	2.08	1.77
23	Testis-II (05.03)	20mg	476.6 ng/μl	40 μl	2.07	1.55
25	Kidney-V (09.05)	80mg	128.0 ng/μl	30 μl	1.77	2.52
27	Brain-V (09.05)	20mg	84.3 ng/μl	40 μl	2.08	1.37
29	Spleen-V (09.05)	20mg	211.1 ng/μl	40 μl	2.08	1.82
30	Lung-V (17.04)	80mg	281.9 ng/μl	40 μl	2.08	2.17

4.5.2 Specific RNA probe generation and validation

The mRNA of *Akap11*_{short} [U48288.1] has a length of 9748nt comprising both the 3'- and 5'-UTRs. The ORF is located between nucleotide 5411 and 8800 of the mRNA sequence. The 3'-UTR is so long that is rare in nature (>5.4kb). The mRNA of *Akap11*_{long} [NM_012773.2] has a length of 6950nt including the 3'- and 5'-UTR regions. The ORF is located between nucleotide 7 and 5685 of the mRNA sequence. The two *Akap11* mRNAs share a common region with 99% identity with 8 gaps (position 4843-8864 in *Akap11*_{short} [U48288.1], and position 1608-5633 in *Akap11*_{long} [NM_012773.2]).

After a search at the GenomeCube co., one *Akap11* EST clone was subsequenced to be 100% identical with the fragment from 1161 to 4222 in *Akap11*_{long} [NM_012773.2], also including a partial common region (1608 to 4222). This clone was used to generate the specific probes for Northern blot hybridization to identify eventual *Akap11* alternative splicing (Figure 29).

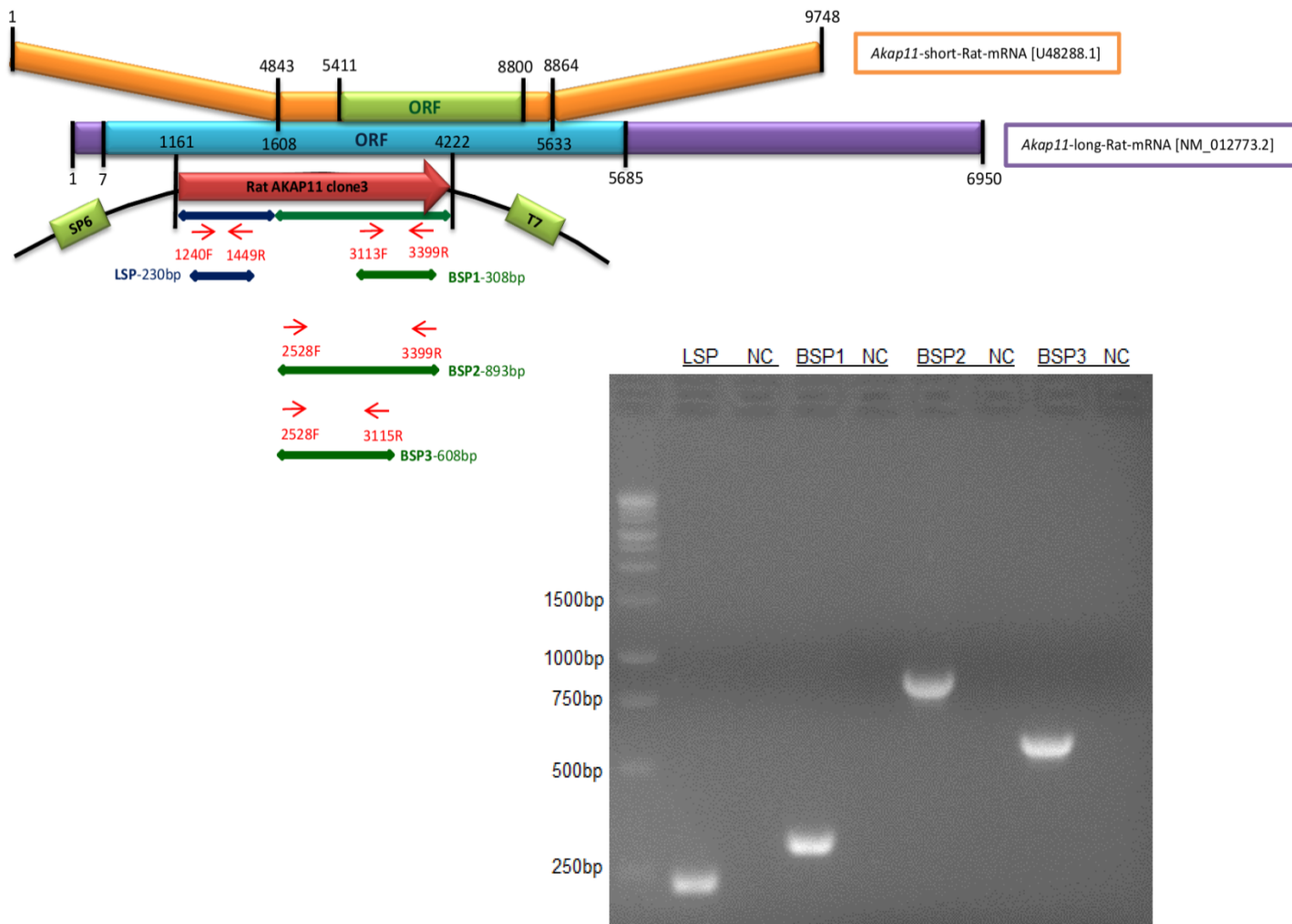


Figure 29 Schematic illustration of the alignment and position of *Akap11* rat mRNA [NM_012773.2], [U48288.1], *Akap11* EST clone3 vector and designed primers. Four fragments from the AKAP11 clone3 plasmid that could be used for hybridization probes generation are LSP (230bp), BSP1 (308bp), BSP2 (893bp) and BSP3 (608bp). LSP: Long *Akap11* specific probe; BSP: Both *Akap11* specific probe; NC: negative control.

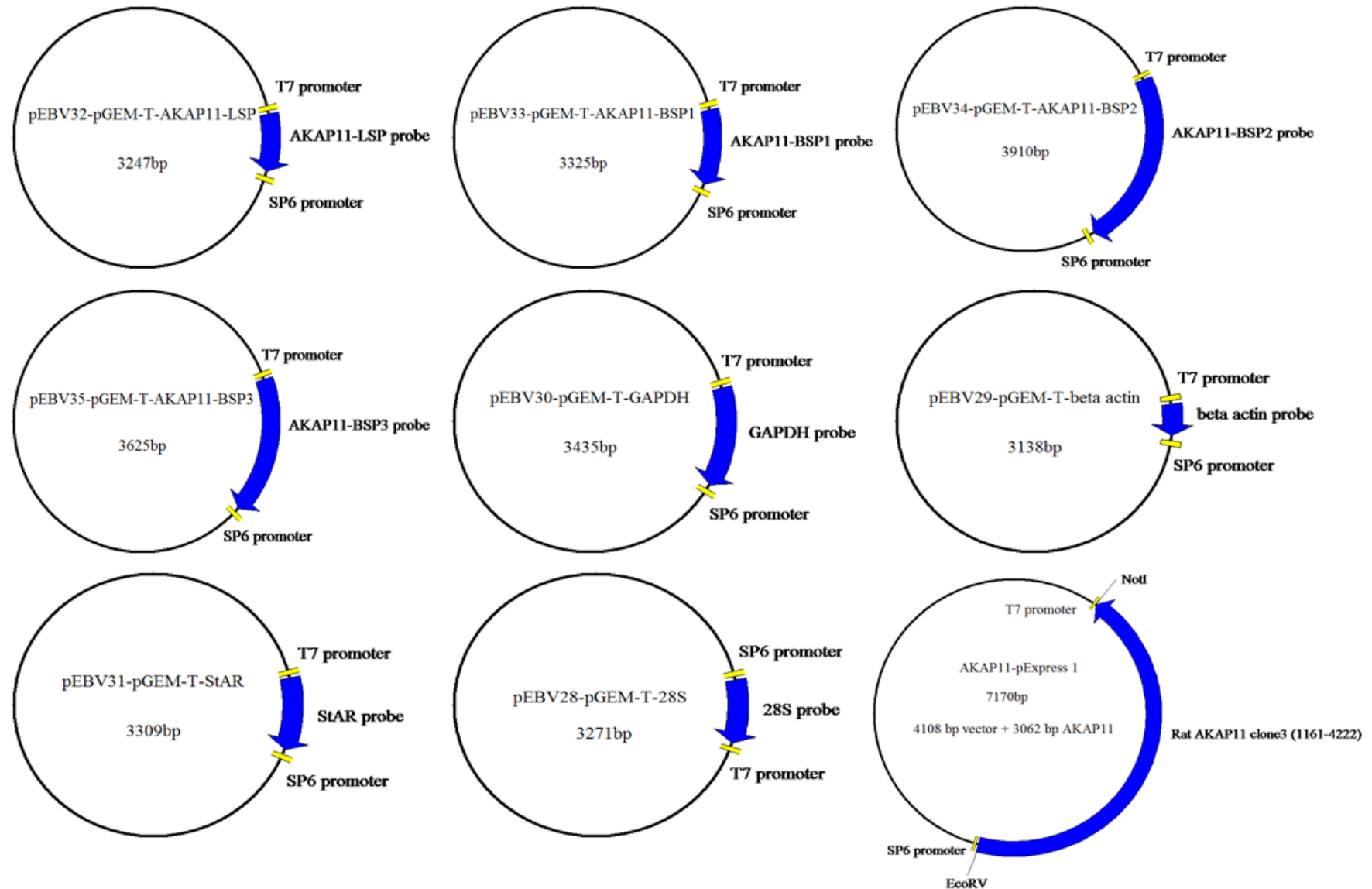


Figure 30 Constructed plasmids maps, including *Akap11* rat mRNA specific hybridization probes LSP (230bp), BSP1 (308bp), BSP2 (893bp) and BSP3 (608bp) and housekeeping gene probes, such as GAPDH (417bp), β -actin (120bp), 28S rRNA (254bp), and StAR (292bp).

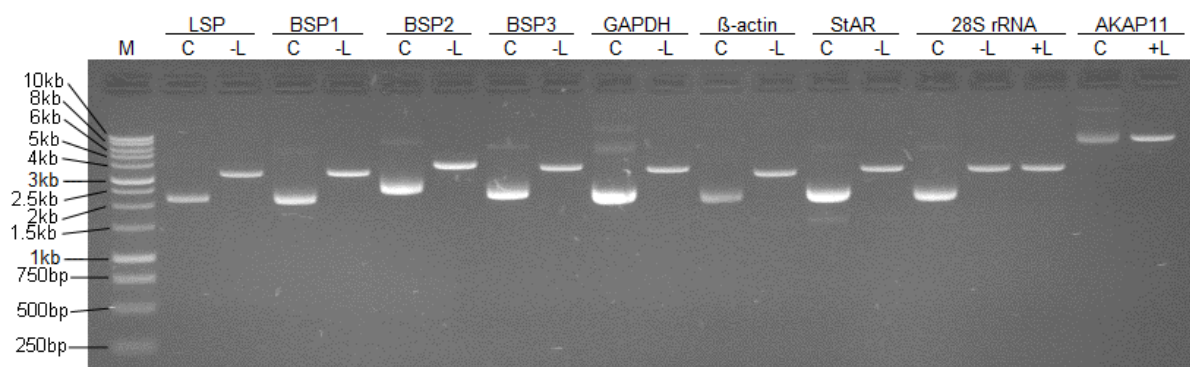


Figure 31 Plasmids linearization for *in vitro* transcription. C: supercoiled plasmid; -L: antisense linearized plasmid to generate antisense RNA probes; +L: sense linearized plasmid to generate sense RNA as positive template control. Plasmid size: LSP (3247bp), BSP1 (3325bp), BSP2 (3910bp), BSP3 (3625bp), GAPDH (3435bp), β -actin (3138bp), StAR (3309bp), 28S rRNA (3271bp), AKAP11 clone3 (7170bp). The 1kb DNA ladder (Promega) was used as the DNA marker

All vectors were linearized with appropriate restriction enzymes and digoxigenin-labelled RNA probes generated by *in vitro* transcription as described in methods (see subsection 3.7.1). The quality of the hybridization probes was verified using dot blot assay to estimate RNA-probe concentration and DIG-labeling efficiency, prior to *in situ* hybridization.

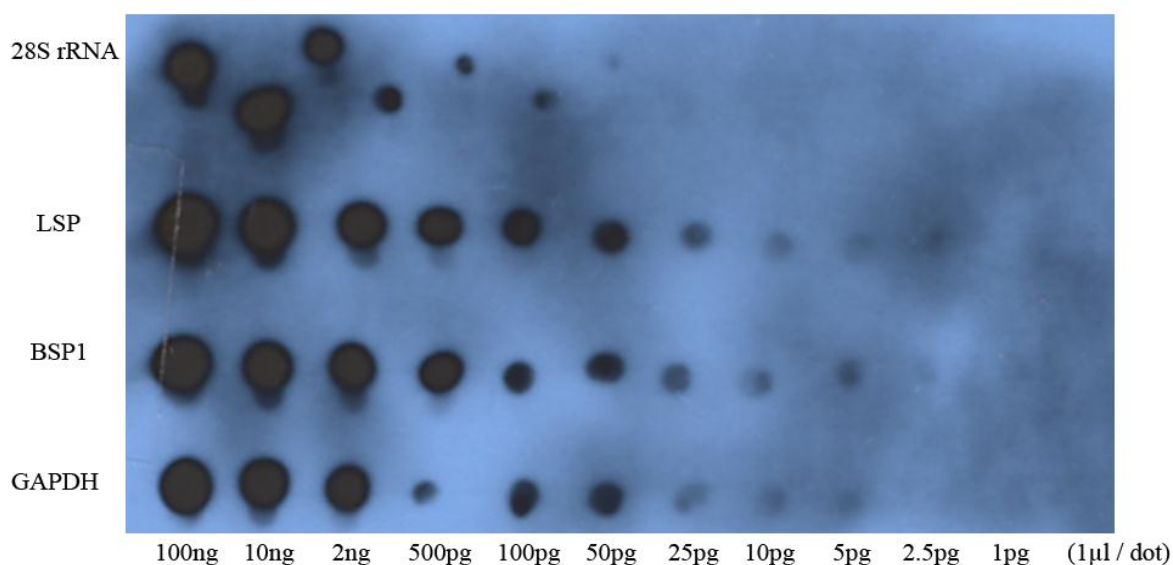


Figure 32 Sensitivity of DIG-labeled antisense RNA probes were verified by dot blot assay.

The intensity of the DIG-labeled probe spots depends on the yield of probe synthesized during the labeling reaction during *in vitro* transcription. It depends on the amount, size, and purity of the DNA template (linearized plasmids shown in Figure 31). By detecting of the DIG-labeled RNA with a dot blot, also the detection system, antibody and developing agent were tested. Gradient dilutions of DIG-labeled RNA were spotted on a positively charged nylon membrane (Figure 32). After heat- and UV crosslinking of the RNA on the membrane, immunological detection was done by using a mouse anti-DIG-antibody in combination with a goat anti-mouse IgG secondary antibody labelled with alkaline phosphatase and subsequent enzyme staining. Our probes could detect 1-2.5pg RNA, which is sufficiently sensitive for a Northern blot^①. Concerning the specificity and sensitivity of this technique, “rare mRNA can be detected in 0.1 µg of total RNA” by the DIG-labelled non-radioactive Northern blotting method (DIG Northern Starter Kit Instruction Manual, Roche)^②.

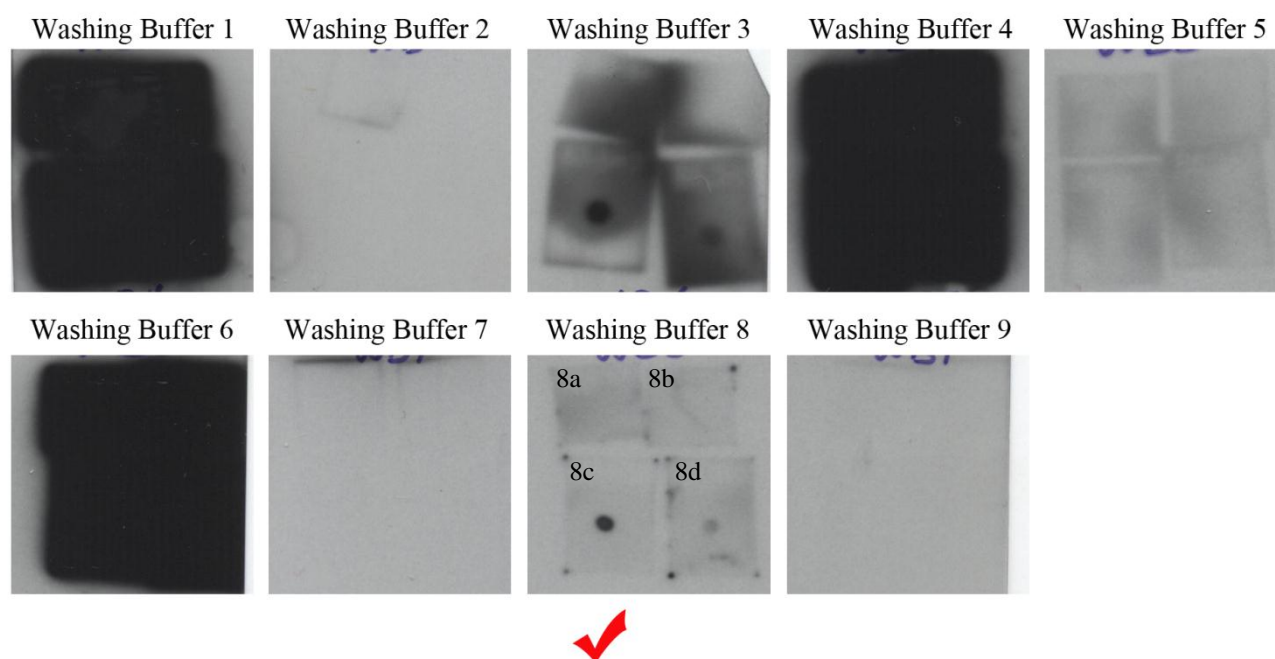


Figure 33 Test of 9 different types of washing buffer with 2 distinct dilutions of anti-DIG concentration

^① https://lifescience.roche.com/wcsstore/RASCatalogAssetStore/Articles/DIG_AN1_03.12.pdf

^② <http://post.queensu.ca/~chinsang/lab-protocols/handbooks-and-manuals/dig-northern.pdf>

The recipes of 9 types of washing buffers are shown in Table 3, and the combined 2 kinds of anti-DIG concentration are High anti-DIG (60ng anti-DIG/ml antibody buffer) and Low anti-DIG (4ng anti-DIG/ml antibody buffer), respectively. When the washing buffer 8 was used, the membrane 8a appeared as a blank membrane without the spotted RNA incubated in High anti-DIG as the negative control of membrane 8c. The membrane 8b was a blank membrane without the spotted RNA incubated in Low anti-DIG as the negative control of membrane 8d. The membrane 8c was a membrane containing 1 µl of spotted DIG-labelled RNA (4ng) incubated in High anti-DIG. The membrane 8d was a membrane with 1 µl of spotted DIG-labelled RNA (4ng) incubated in Low anti-DIG. All the membranes were run concurrently using the different 9 washing conditions and the conditions used for the membrane 8c “Washing Buffer 8 + High anti-DIG” (with ✓ mark) yielded the optimal result.

After checking the labelling efficiency in the spot assay, a rat tissue RNA dot blot was used to test the hybridization efficiency of the DIG-labeled RNA. The concentration of DIG-labeled RNA probes required was between 20ng/ml (for abundant mRNA detection, e.g. housekeeping gene) and 100ng/ml (for rare mRNA detection).

Four gradient amounts of total RNA from three different tissues were spotted on Nylon membranes to analyze the hybridization efficiency, using the probes described in Figure 32. Hybridization was carried out as described in methods (see subsection 3.7.4). 100ng DIG-labelled *Akap11* antisense RNA was used as positive signal control for all the blots. 1 µg non-labelled *Akap11* sense RNA was used as positive template control for LSP and BSP1 blots.

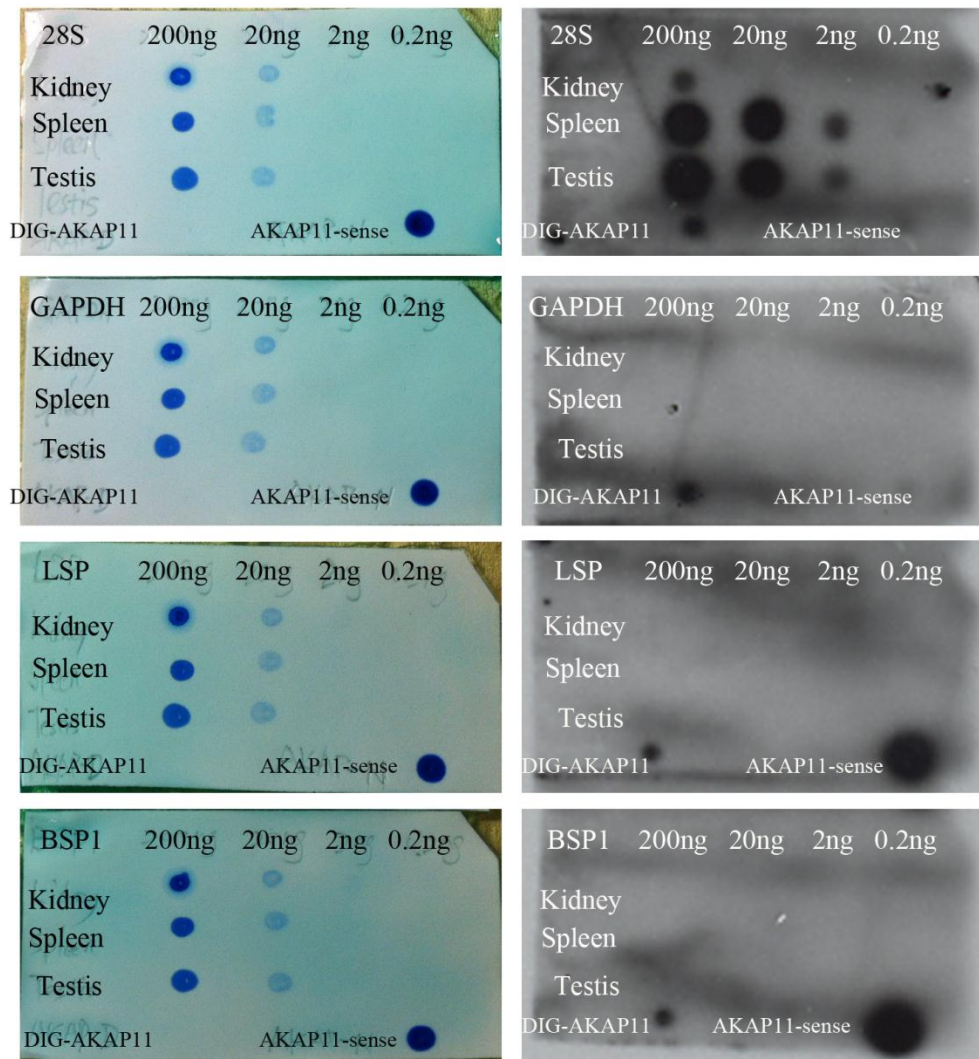


Figure 34 Rat tissue total RNA dot blot hybridization with 4 probes. Left side: methylene blue staining of the membranes; Right side: corresponding hybridizations. The total RNAs used were from rat kidney, spleen, testis. The specific RNA hybridization probes used were antisense DIG-labelled RNA of 28S, *Gapdh*, *Akap11* [NM_012773.2], *Akap11* [NM_012773.2] and [U48288.1]. 100ng DIG-labeled *Akap11* was used as positive signal control and 1 µg non-labeled *Akap11* sense RNA was used as the positive template control for LSP and BSP1.

Dots were visible on the membrane labelled with the antisense RNA probe for the detection of the 28S rRNA, indicating that the probe bound correctly to the RNAs from different tissues (Figure 34). Also, the positive signals from the membranes probed with LSP and BSP1 indicated that the antisense probes bound to the non-labelled *Akap11* sense template correctly. Thus, the absence of signal from the probed tissue RNAs suggested that the amount of the *Akap11* mRNA in the total RNAs was below the detection limit.

4.5.3 Rat tissue total RNA Northern blot test

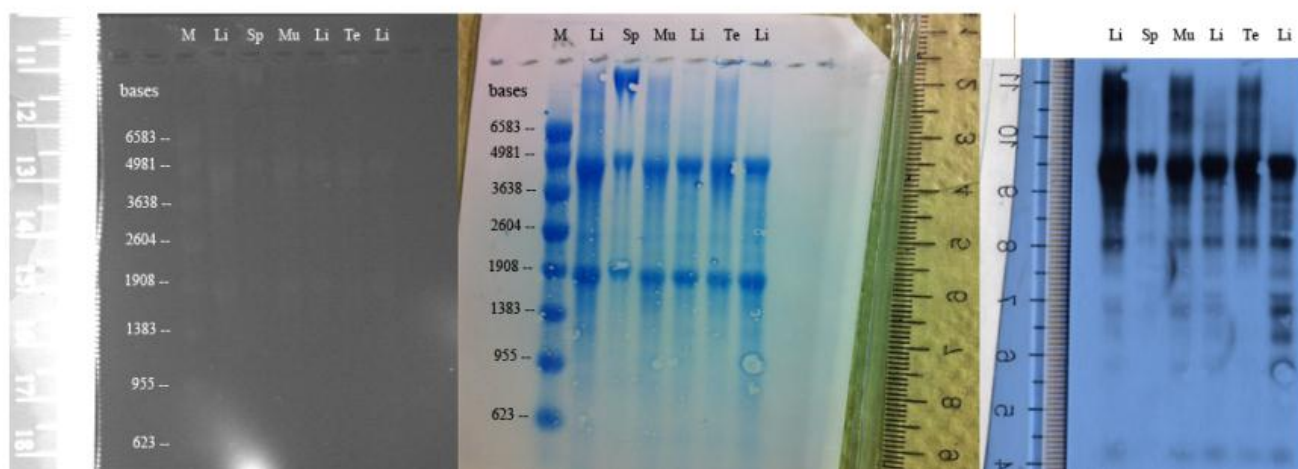


Figure 35 Total RNA separation by electrophoresis in a 1.8% formaldehyde-agarose gel using 1× MOPS running buffer at 20V for 17.5 hours. Methylene blue staining was used to check the transferred RNA on the membrane, followed by hybridization with the 28S rRNA probe. M: RNA marker (Promega) 6 µl/lane; Lane1: 2# liver 5 µg; Lane2: 6# spleen 5 µg; Lane3: 3# muscle 3 µg; Lane4: 4# liver 3 µg; Lane5: 8# testis 3 µg; Lane6: 22# liver 3 µg (# from Table 17, the RNA quality of these 6 samples see Chapter 12. Supplemental data S2)

Figure 35 showed that, the whole procedure for non-radioactive Northern blotting with DIG-labelled probes worked as expected. Different RNA probes were used to label Northern blots of total RNA isolated from different tissues. However, only the 28S rRNA control probe hybridization was working well while no positive signals were obtained from the other probes. There are 2 possible explanations for the observation. First, the target sense RNA template (e.g. *Akap11*) is below the detection limit. In contrast, the 28S rRNA is one of the highest expressed RNAs, therefore its amount is within the detection limit of the assay. Around 80% of total RNA is rRNA, 15% is tRNA, and some of the rest includes non-coding RNA, thus, protein-coding mRNA is less than 5% (Lodish et al., 2000). Second, the use of the T7 promoter for the 28S rRNA probe generation supported the efficient *in vitro* transcription compared to SP6 promoter used for the other probes (LSP, BSP1, BSP2, BSP3, GAPDH, β -actin, StAR) (Logel et al., 1992). Suggestion for next trial would be to load more total RNA (>10 µg/well) and to use higher amounts of labelled probes in the hybridization reaction.

4.5.4 Rat total RNA RT-PCR

Because the detection of different *Akap11* mRNA form with LSP and BSP1 using the Northern blot did not work as expected, and from the the report that that RT-PCR detection is more sensitive than Northern blotting hybridization (Fehr et al., 2000; Streit et al., 2008), the RT-PCR was used to identify the amount of *Akap11* mRNA in total RNA from rat tissues (Table 17).

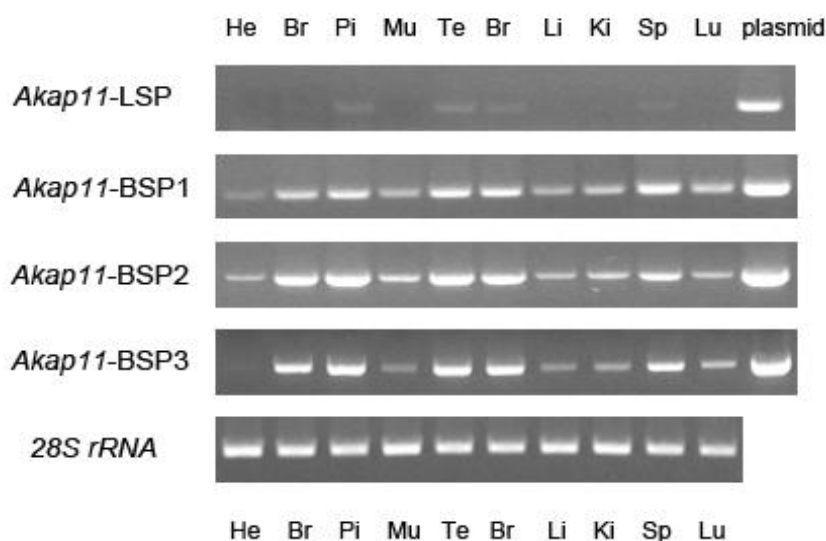


Figure 36 Distribution profile of *Akap11* mRNA in different rat organs. Lane1: 9# Heart; Lane2: 11# Brain; Lane3: 12# Pituitary; Lane4: 14# Muscle; Lane5: 16# Testis; Lane6: 20# Brain; Lane7: 22# Liver; Lane8: 25# Kidney; Lane9: 29# Spleen; Lane10: 30# Lung (# from Table 17); Lane11: 1ng AKAP11 plasmid clone3 used as positive template control for LSP, BSP1, BSP2, BSP3. As described in Figure 29, LSP probe is in position of 1240-1449, 230bp; BSP1 is 3113-3399, 308bp; BSP2 is 2528-3399, 893bp, BSP3 is 2528-3115, 608bp.

Akap11 could be detected with all primer pairs in the different tissues (Figure 36). The expression of the RNA was highest in the pituitary RNA, which is logical and interesting, since the putative false AKAP11 clone from Scott and colleagues was also isolated from a cDNA library constructed from pituitary mRNA. Additionally, brain, testis and spleen exhibited relative high amount of *Akap11* expression, whereas this mRNA was only expressed in low amount in heart muscle and in intermediate quantity in skeletal muscle, liver, kidney and lung.

The primer pair “*Akap11*-LSP” for the 5’ part of the mRNA did not amplify the *Akap11* product in the same amounts as “BSP1-3”, since an oligo-dT based RT-PCR kit

was used for the cDNA amplification. For a long mRNA as *Akap11* mRNA, it is better to use a random primer based reverse-transcription kit when it is necessary to amplify the 5' part of the mRNA. Regardless of the lower sensitivity of amplification, the pattern of the tissue distribution for the *Akap11*-LSP primer pair remained similar, depicting pituitary, testis, brain and spleen as the tissues with higher expression of *Akap11*.

4.5.5 Concentrated total RNA and PCR-generated probes

Since *Akap11* mRNA was detectable in RT-PCR, the possibility that *Akap11* primers/probes did not work was excluded. The next solution is to precipitate total RNAs to get concentrated template, or elute it by polyT columns to get pure mRNAs for Northern blotting.

Table 18 Total RNA precipitation

Sample	RNA concentration	A _{260/280}	A _{260/230}
Brain	416.8 ng/μl	2.01	2.21
Heart	369.7 ng/μl	1.91	2.38
Liver	378.4 ng/μl	2.03	2.00
Lung	360.6 ng/μl	1.90	2.38
Kidney	1024.1 ng/μl	2.08	2.21
Muscle	2648.2 ng/μl	2.08	2.20
Pituitary	3122.2 ng/μl	2.09	2.17
Spleen	3163.0 ng/μl	1.98	2.26
Testis	3340.4 ng/μl	2.11	2.21

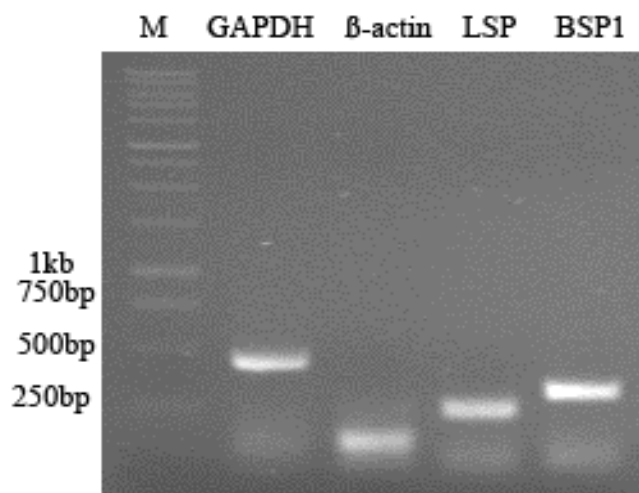


Figure 37 Alternative method of template generation for *in vitro* RNA transcription. PCR product with T7 promotor could be used as template instead of linearized plasmid to further produce RNA probes. The size of PCR products was 23bp longer than RNA probes, for instance GAPDH = 440bp; β-actin = 143bp; LSP = 253bp; BSP1 = 331bp.

This is a PCR-based technique for the preparation of RNA-probes. T7 RNA polymerase promoters were introduced at the 5'-end of gene-specific oligonucleotide primers enabling direct *in vitro* transcription of purified PCR-fragments. The amount of the DIG-labelled transcripts generated from PCR-templates was equivalent to those derived from a linearized plasmid. Selection of interesting clones can be dramatically accelerated by avoiding cloning and plasmid preparation steps using the PCR-approach, avoiding the uncertain promoter problem from TA-cloning vectors. However, the minimal length of the PCR-fragment should be at least 300bp as shorter probes are less sensitive (David and Wedlich, 2001). Due to time limitation, this Northern blotting assay was not continued and the cloning of AKAP1, -4 and -10 was started.

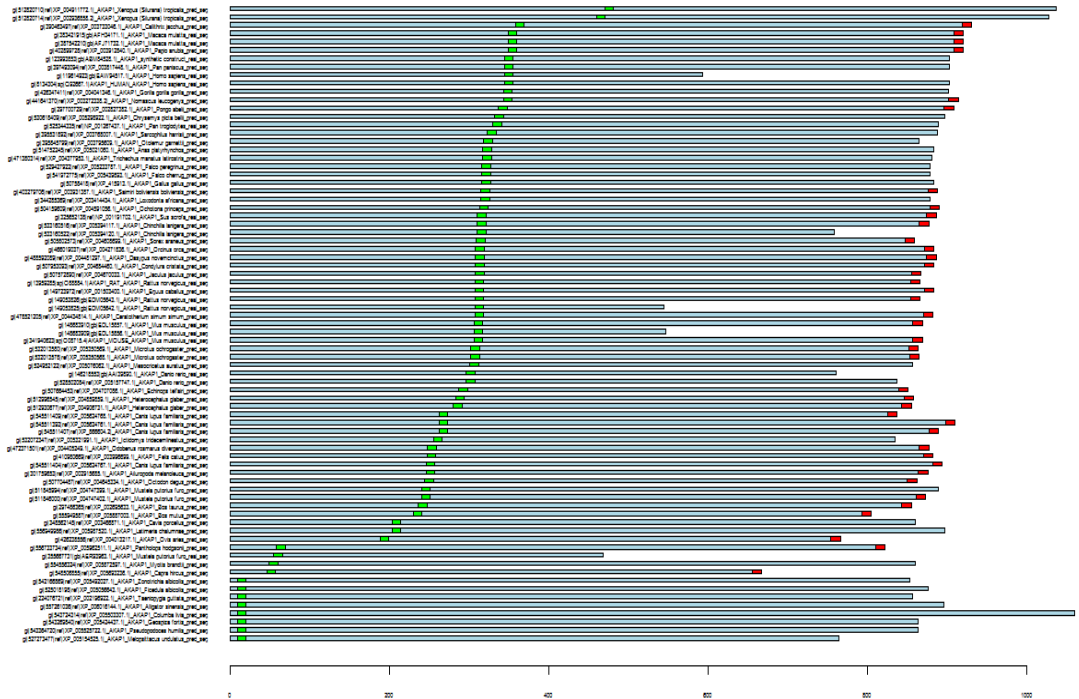
4.6 Basal analysis and over expression of AKAP1, AKAP4, AKAP10 in TM4 cells

The last 3 amino acids of AKAP1, AKAP4 and AKAP10 suggested they may contain PTS1 signals (Figure 17). Therefore, the following were carried out: 1) the tissue distribution and differences in expression of the mRNAs for these AKAPs; 2) cloning of the AKAPs in mammalian expression vectors; 3) to overexpress different myc-tag versions of the AKAPs in TM4 cells; and 4) analysis of the subcellular localization of the AKAPs and subsequent effect on peroxisome and mitochondria. Due to the unavailability of reliable antibodies for the detection of these AKAPs, the N- and C-terminals myc-tag versions of these AKAPs were used for the overexpression experiments.

4.6.1 Basic analysis of AKAP1, AKAP4, AKAP10

The putative C-terminal PTS1 “SKL-variant”-tripeptide of mouse AKAP1 is “ASL”, whereas “ANL” and “TKL” were found in mouse AKAP4 and AKAP10, respectively. However, it was reported that a PTS1 is not solely consisting of the C-terminal tripeptide (Brocard and Hartig, 2006). From this research group, an on-line PTS1 predictor was made available for public use^①. Therefore, an analysis could be done by computer programming (see Supplemental data S1) to show the possible “trend” for a putative PTS1 signal throughout the 3 AKAP family members.

^① <http://mendel.imp.ac.at/mendeljsp/sat/pts1/PTS1predictor.jsp>



The PTS1 predictor

PTS1 query prediction

Submitted sequence:
NRSLVERGLAQWVDSYYASL

Using general prediction function

Name	mAKAP1[O08715.4]_20aa
C-terminus	LAQWVDSYYASL
Score	0.169
Profile	5.506
<i>S_{ppt}</i> (non-accessibility)	-2.931
<i>S_{ppt}</i> (accessibility)	-2.406
<i>P</i> (false positive)	0.60%
Prediction classification	Targeted

The PTS1 predictor

PTS1 query prediction

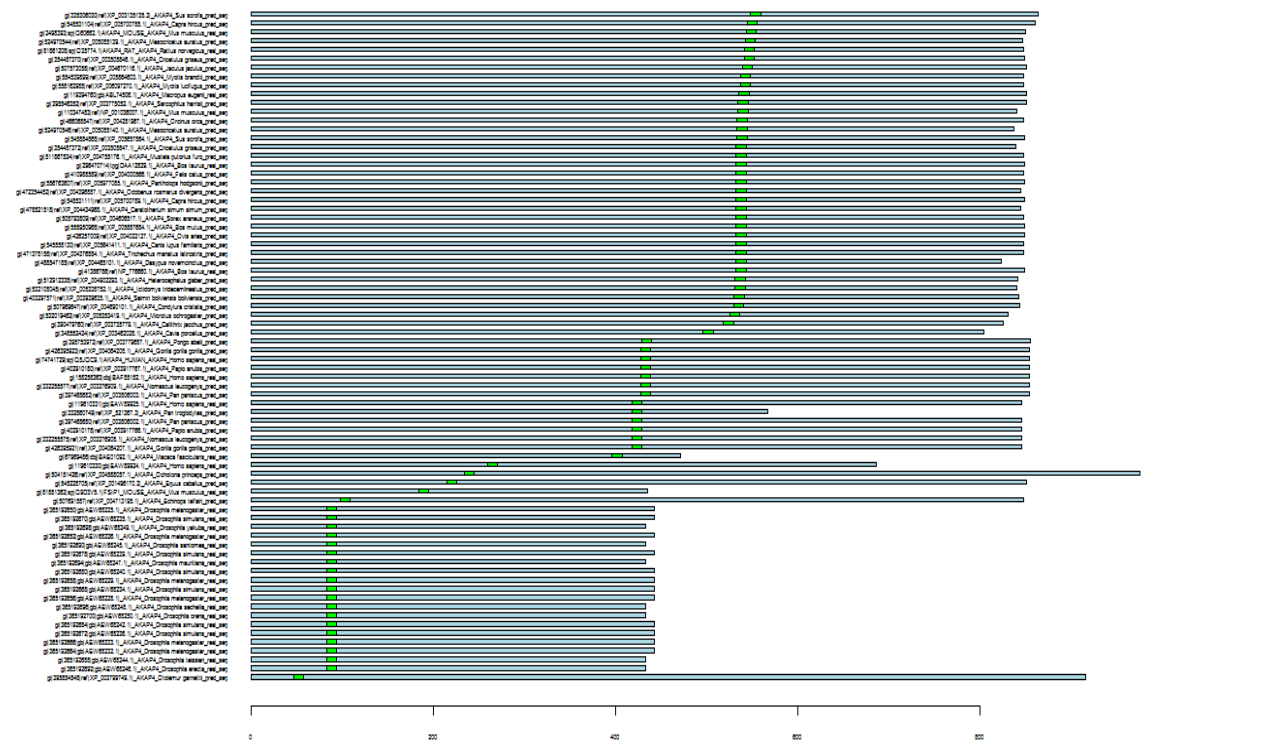
Submitted sequence:

MAIQLRSLFPLALPGMLALLGWWWFFSRKKDRLSSSDKQVETLKVGPALKDRRLSEACPGVLVSVAPTVT
 QPPGREEQRCVDKPTSTFLALPRTQVRRSESSGNLPSVADTRSPQPCRDLEAKVELSLMGDKAKSIP
 LGCPILLPKDASFPYEAVERCKQESALGKTPGRGWPSPYAASGEKARETGGETGDAVLGENVSEGLLS
 QECVSEVEKSEFPILAPGGGGEEVSHGPPQVAELLKKEEYTVGKLPSFVPEVHSEPVKDEDALQVVK
 GSSNTSDRLAGELDKDETVPENDQIKQAQFLISQVILEATEFRATTVGKTVQVHPTSATQPKGKEE
 SCVPASQETSLGQDTSPDASTRTGATASPSAALPPKTYVCLSSPLSGPTKDKQPKNSAHHSILAPCPP
 PVTQRQSLLEGASNPRGDDNFVACMANNSQSVLSVSSLGQCQSDPVSSTGLSDCTETISSSGDKAMTPPL
 PVSTQPFNSGNVLKBEESDLGTEGWTMDTEADHSGGSDGNSMDSVDSOGLTRPDSPQSVQAGSNPKKVD
 LIWIEIEVPKHLVGRIGKQGRYVSLKQTSQAKIYISTLPYTQNIQICHIEGSQHHVDKALNLIGKKFK
 ELNLINYPPLPSLALPSLMTWMLLPDGTITVEVTVVQVQVNAHGLFVQHTHTPTTHALRSLDQQMYLC
 YSQPGIPLTPTVEITVICAAPGADGAWWRAQVVASYEETNEVEIRYVDYGGYKRVKVDVLRQIRSDFTV
 FQGAEVLLDSVPLSDDDFHFSPEADAAMSEMTGNTALLAQVTSYSATGLPLQLWSVVGDEVVLNRS LVERGLAQWVDSYYASL

Using metazoa-specific prediction function

Name	AKAP1-mouse[O08715.4]
C-terminus	LAQWVDSYYASL
Score	-11.538
Profile	1.249
<i>S_{ppt}</i> (non-accessibility)	-10.442
<i>S_{ppt}</i> (accessibility)	-2.345
<i>P</i> (false positive)	2.01%
Prediction classification	Not targeted

Figure 38 PTS1 prediction of all AKAP1 family members present in different species (For a larger figure, see Supplemental data S5, color page 156). Light blue bars --- the length of AKAP1 proteins; green block --- position of PKA-binding domain; red block --- position of predicted PTS1 signal.



The PTS1 predictor

PTS1 query prediction

Submitted sequence:

DEAVGNMARKQLLDWLLANL

Using general prediction function

Name **mAkap4[Q60662.1]_20aa**
 C-terminus **RKQLLDWLLANL**
 Score **3.617**
 Profile 8.222
S_{ppt} (non-accessibility) -7.142
S_{ppt} (accessibility) -4.697
P(false positive) 1.28%
 Prediction classification **Twilight zone**

The PTS1 predictor

PTS1 query prediction

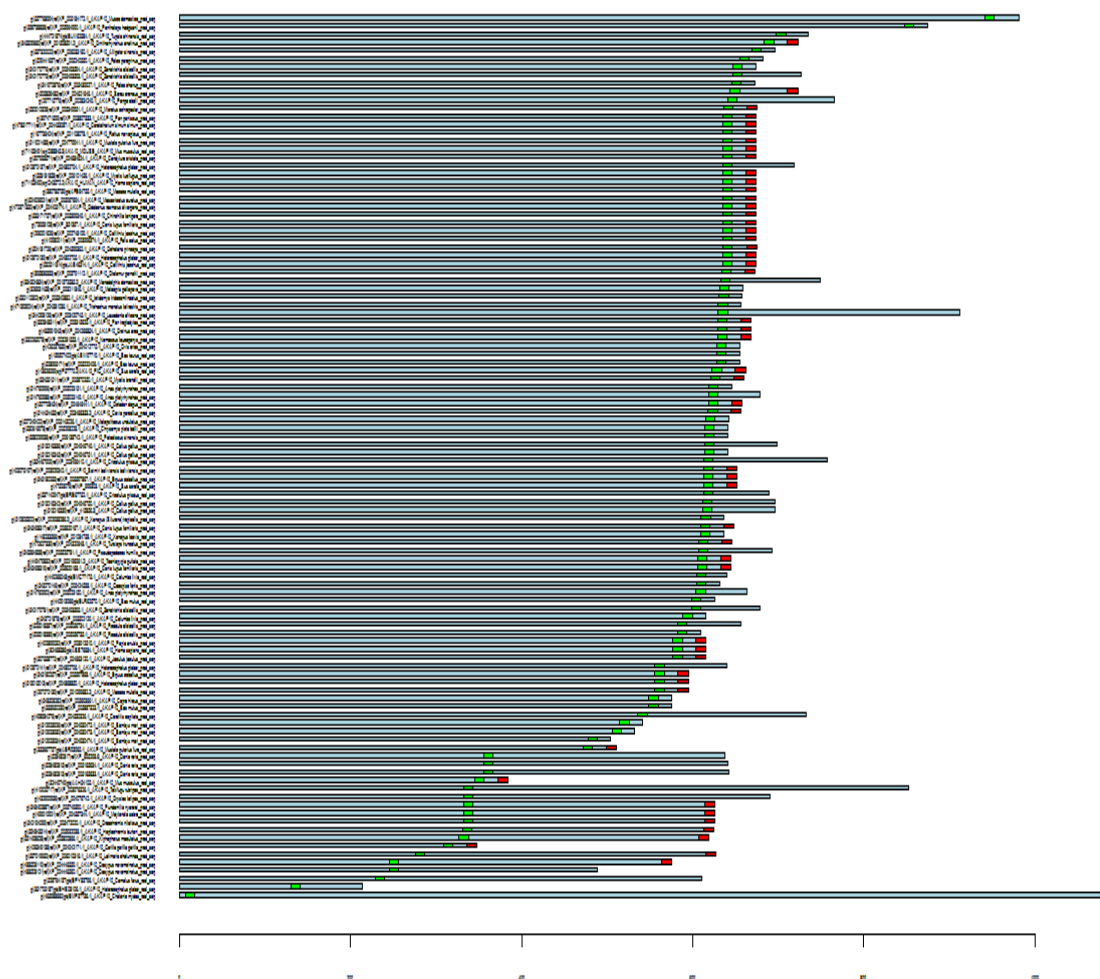
Submitted sequence:

MIA YCGTTTMSDDIDWLHSRRGVCKVDLYSPK GQQDQDRKVICFVDVSTLNVEDKDSK GAA GSRSEGLN
 LETLEEKETIVIKDTEK QDQSKTEGVSCLFK QAPSDPISVLNWLNDLQK YALGFQHALSPSASSCKHKV
 GDLEGDYKIPSENCYSVYADQVNFEDYLNK GPQNLRLLEMAASKNTNNNQSPSPNATKSPSNQRSVATPEG
 ECSMDLDSFYVNRLLSLLVIQMARKEIKDKLEGGSK CLHHSMYTS GDK GKTSPRS AVSKIASEMAHEAVEL
 TSSEMRGNGEDCRDGRKTFLYSEMCKNKNK CGEKGQMC PKDSKEFADSISK GLMVYANQVASDMMVSVMTK
 LKVHSCGKPIPA CVVLRKRVLLKHTKEIVSDLIDSCMKNLHNTGVLMTDSDFVSAVKRNLFNHGKQNAAD
 IMEAMLRKRLVSA LLGEKKETKSQSLAYATLKAGTNDPKCKNQSLFSAMKAEMK GKDKCKSKADPCCCKSL
 TSAERVSEHILKESLTMWNQKQGNQGVVTKNVCCTSKDEKREKISPTDSLAKDLIVSALMLLIQYHLTQ
 QAKGKDPCEBECGSSMGYMSQSAQYKCGGGQSSKSLSMKHFETRGA PGSTCMKENQLESQKMDMSNM
 VLSLIQKLLSESPFCDELTESDNRKCCDPRSSKAAPMAKRPEEQCQDNALDFISGMKQMNRFIDQLV
 ESMVKLCLIMAKYSNNGAALAELEEQAALVGSGRSGRDAAMMSQNYSETPGPEVIVNNQCSSTTNLQKQLQ
 LQWIAASQFNVPMLYFMGDDDGQLEKLFVSAKAAEK GYSVGDLLQEVMMKFAKERQL**DEAVGNMARKQLLDWLLANL**

Using metazoa-specific prediction function

Name **AKAP4-mouse[Q60662.1]**
 C-terminus **RKQLLDWLLANL**
 Score **-3.842**
 Profile 8.462
S_{ppt} (non-accessibility) -6.378
S_{ppt} (accessibility) -5.925
P(false positive) 0.54%
 Prediction classification **Twilight zone**

Figure 39 PTS1 prediction of all AKAP4 family members present in different species (For a larger figure, see Supplemental data S5, color page 157). Light blue bars --- the length of AKAP4 proteins; green block --- position of PKA-binding domain; red block --- position of predicted PTS1 signal.



The PTS1 predictor

PTS1 query prediction

Submitted sequence:
VSDVMQQAHHDDQPLEKSTKL

Using general prediction function

Name	mAKAP10[O88845.3]_20aa
C-terminus	HHDDQPLEKSTKL
Score	0.017
Profile	0.653
<i>S_{ppt}</i> (non-accessibility)	-0.415
<i>S_{ppt}</i> (accessibility)	-0.222
<i>P</i> (false positive)	0.62%
Prediction classification	Targeted

The PTS1 predictor

PTS1 query prediction

Submitted sequence:
 MRGAGPSPRHSRALRPDPGPAMSFRRKVKGRQEKTLVDVKSTKASVAVHSPQRSTKNHALLAAGPSH
 VAINAISANMDSFSSRTATLKKQPSHMEAAHFGLGRSCLDYQTQETKSSSKLTLEQVLRDVTVLPYFL
 QFMELRRMEHLVKFWLEAESFHTTWSRIRAHSLNTVKQSSLAEPVSPSKRHETPASSVTEALDRRLGDS
 SSAPLLVTQSEGTDLSSRTQNPQNHLLSQEGHSARSLHREAVARTGSHQIPTDSQDSSRLAVGSRNSCS
 SPLRELSEKLMK.SIEQDAVNITFKYISPDAAKPIPTTEAMRNDIAKICGEDGQVDPNCFVLAQAVVFS
 MEQEHFSEFLRSHHFCKYQIEVLTSQVYLAADILFCESALFYFSEYMEKEDAVNQLQFWLAADNFQSOLA
 AKKGGQYDQGEAQNDAMLIDYKQYSLQATHPLGFDVVRLEIESNICREGGPLNCFPTPLRQAWTTMEKV
 FLPGFLSSNLYKYLNDLIHVSVEGDEFLGNGVSLAAHGSVCLPEESHSGGSGSTAQSSVKKASIKILKN
 FDEAIVDAASLDPESLYQRTYAGKMSFGVRSDLGQFIRESEPEPDVKKSKGFMFSQAMKKWVQGNTEA QEELAWKIARM**VSDVMQQAHHDDQPLEKSTKL**

Using metazoa-specific prediction function

Name	AKAP10-mouse[O88845.3]
C-terminus	HHDDQPLEKSTKL
Score	-12.464
Profile	-10.949
<i>S_{ppt}</i> (non-accessibility)	-1.410
<i>S_{ppt}</i> (accessibility)	-0.104
<i>P</i> (false positive)	2.29%
Prediction classification	Not targeted

Figure 40 PTS1 prediction of all AKAP10 family members present in different species (For a larger figure, see Supplemental data S5, color page 158). Light blue bars --- the length of AKAP10 proteins; green block --- position of PKA-binding domain; red block --- position of predicted PTS1 signal.

For the prediction, the both verified- and predicted AKAP protein sequences were included. Because minimal 12 residues of the C-terminus was required as the query sequence by the online tool, the last 20 amino acids of AKAP protein members were used for the PTS1 prediction. Indeed, 52% members of AKAP1 and 48% members of AKAP10 were predicted to be peroxisomal. The prediction for the last 20 amino acids of mouse AKAP1 [O08715.4] with a putative PTS1 end “-ASL” as well as the mouse AKAP10 [O88845.3] with “-TKL” were also to be targeted to peroxisomes, but not their full sequences. Although none of AKAP4 was predicted to be a peroxisomal protein, the mouse AKAP4 [Q60662.1] with a known PTS1 end “-ANL” was predicted to be in “twilight zone”.

Based on the prediction result, it appears as the 3 mouse AKAPs (AKAP1, AKAP4 and AKAP10) may have a chance to target to peroxisomes. Moreover, the data from EST sources in NCBI showed that mouse AKAP1, AKAP4 and AKAP10 were the highly expressed endogenous proteins in testis (Figure 41).

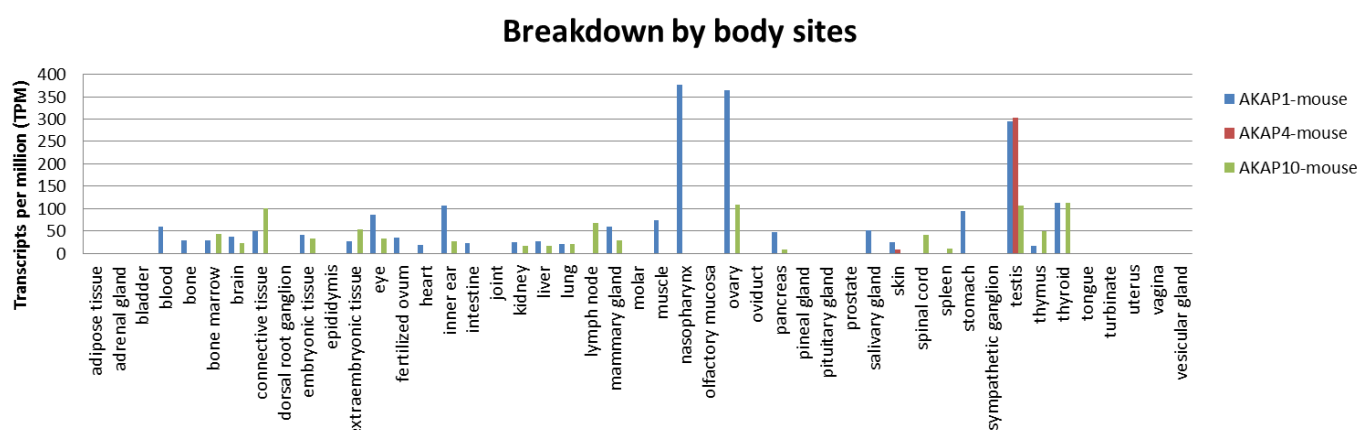


Figure 41 *Akap1*, *Akap4* and *Akap10* distribution profile (approximate expression pattern inferred from EST sources in NCBI) ^①

From Figure 41 based on mouse, *Akap1* transcripts are highly expressed in ovary and testis, which reflects its potential role in reproduction. *Akap4* mRNA is expressed

^① AKAP1: <http://www.ncbi.nlm.nih.gov/UniGene/ESTProfileViewer.cgi?uglist=Mm.2969>,
AKAP4: <http://www.ncbi.nlm.nih.gov/UniGene/ESTProfileViewer.cgi?uglist=Mm.1498>,
AKAP10: <http://www.ncbi.nlm.nih.gov/UniGene/ESTProfileViewer.cgi?uglist=Mm.274404>

only in testis, which suggested its specific function in spermatogenesis. *Akap10* mRNA is mainly expressed in connective tissue, ovary, testis and thyroid.

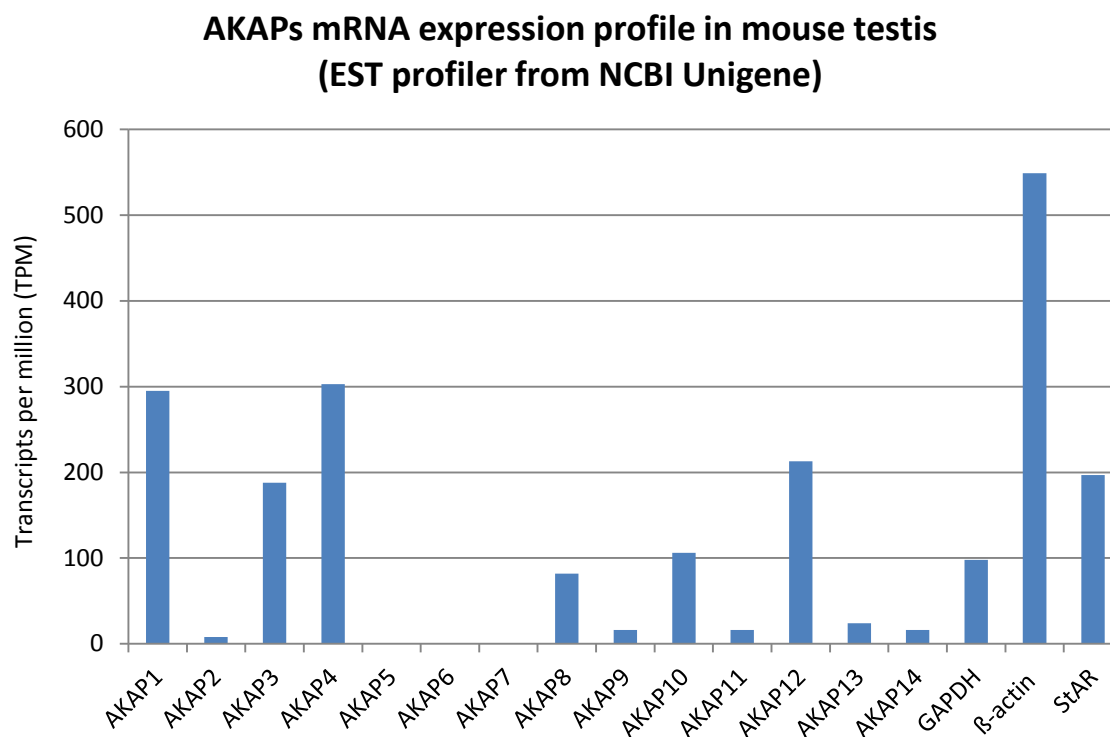


Figure 42 *Akap1*, *Akap4* and *Akap10* mRNA are high expressed in testis.

Among all *Akaps* mRNA profile in mouse testis, the highest expressed AKAP-candidates were AKAP1, -4 and -10, suggesting their possible roles in male fertility (Figure 42). In order to experimentally confirm the results from the EST database searching, pairs of primers were designed to check the expression level of endogenous *Akap1*, *Akap4* and *Akap10* in mouse testis (Figure 43).

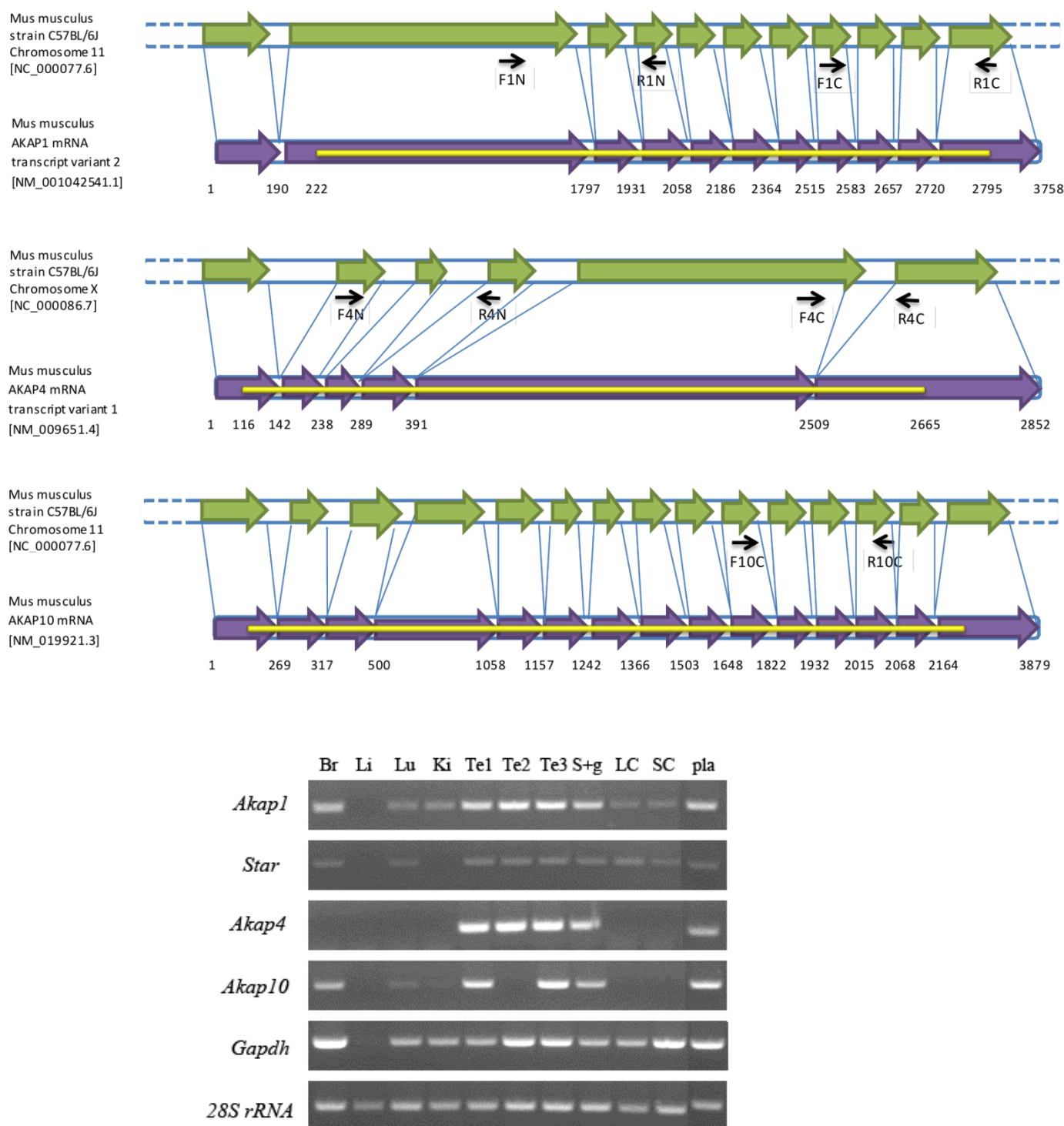


Figure 43 Test of designed primers for *Akap1*, *Akap4*, *Akap10*, and their expression level in different mouse organs. Br: Brain; Li: Liver; Lu: Lung; Ki: Kidney; Te1: Testis from mouse1; Te2: Testis from mouse2; Te3: Testis from mouse3; S+g: Sertoli cell + germ cell mixture; LC: Leydig cell line MLTC-1; SC: Sertoli cell line TM4; pla: the constructed plasmid with required gene fragment, used as positive template control.

The results showed that *Akap1*, *Akap4*, *Akap10* mRNA were highly transcribed in mouse testis, and AKAP1 was also highly expressed in brain in agreement with

previous reports (Dagda et al., 2011; Dyson et al., 2008; Hu et al., 2009; Webb et al., 2008). It was also observed that *Akap1* as well as *Star* mRNA were highly abundant in mouse seminiferous tubules (mixture of Sertoli cell + germ cells) and the TM4 Sertoli cell line. This was unexpected since AKAP1 has only been found in Leydig cells in the male where AKAP1 regulated StAR protein activity in mitochondria (Dyson et al., 2008). This observation raised several questions such as: What is AKAP1 function in Sertoli cells? Is it also localized at the mitochondria surface with *Star* mRNA and protein? What happens if the protein is mistargeted?

Akap4 and *Akap10* mRNAs were apparently only expressed in germ cells in testis, but not in the TM4 Sertoli cell line or in MLTC-1 Leydig tumor cells. Whether these AKAPs are expressed at low levels in Sertoli cells or Leydig cells has to be verified in the future by using isolated primary cells from the testis and higher amounts of cDNA as input template.

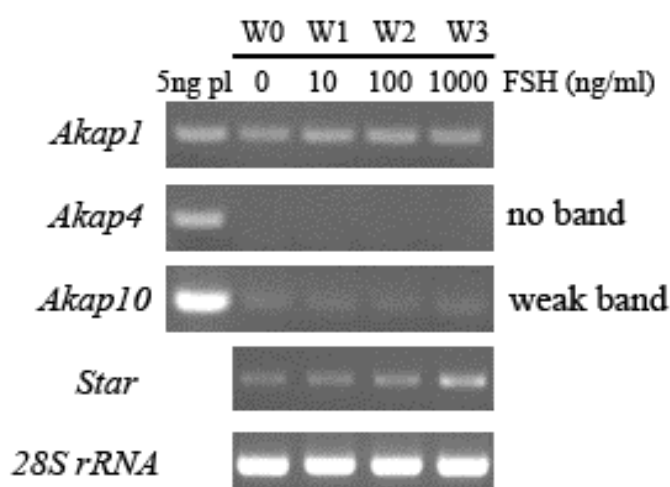


Figure 44 Test expression of *Akap1*, *Akap4*, *Akap10* in TM4 Sertoli cell line under the gradient FSH dose treatment (see Figure 18). Lane1: 5ng corresponding plasmids were used as positive template control for PCR detection. All the PCRs were run 35 cycles.

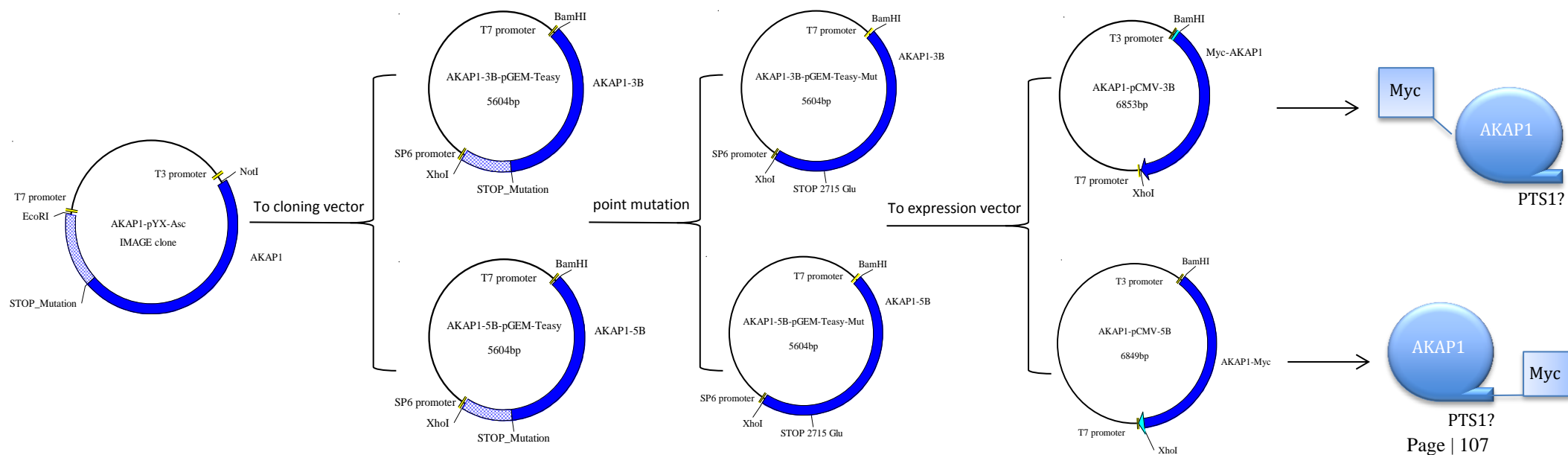
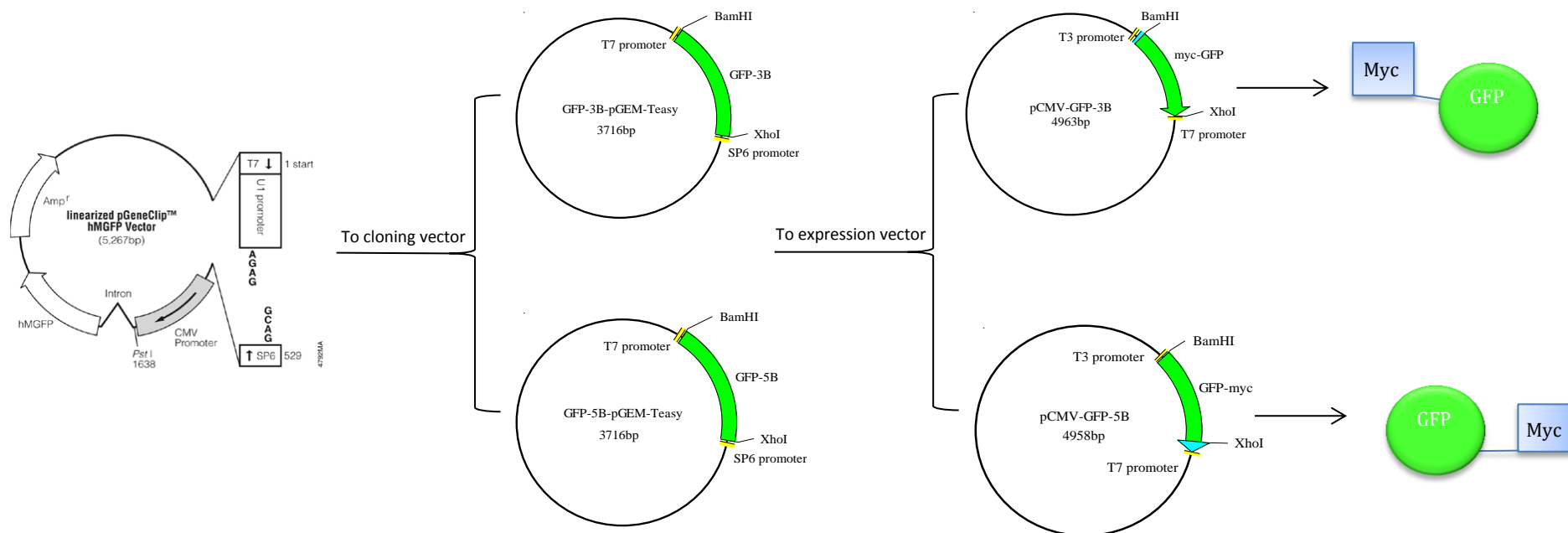
As described in the introduction (see subsection 1.2.3), the phosphorylation signal pathway in Sertoli cell is strongly influenced by FSH induction. But the three *Akaps* which control the PKA-dependent phosphorylation cascade in TM4 cell line showed almost no effect by FSH stimulation. *Akap4* and *Akap10* were hardly detectable in TM4 cell. Although *Akap1* was expressed quite strongly in TM4 cells, its function and regulation still remains a mystery. Whether the PKA substrate *Star* and StAR

protein in Sertoli cells are regulated in the same way as in Leydig cells is also a question.

4.6.2 Cloning and immunolocalization of myc-tagged AKAPs

The myc tag is a 10-amino acid polypeptide tag ($\text{NH}_2\text{-EQKLISEEDL-COOH}$) derived from the c-myc protein and it is frequently used for the localization of recombinant proteins. The myc-tag system is widely used to facilitate the detection or purification of fusion proteins. Mouse anti-myc antibodies are also well developed for immunochemistry. Two different types of vectors were used to monitor recombinant proteins expression with the myc-tag attached to the target protein at either the N- or C-terminus (pCMV-3B, pCMV-5B) (Terpe, 2003). Because the PTS1 signal is at C-terminus of the protein, two kinds of expression vectors were used for immunodetection to confirm whether a possible PTS1 signal is really functional. In contrast, mitochondrial targeting signals are frequently localized at the N-terminus of a protein and cleaved during the import into the mitochondria^① (Emanuelsson et al., 2001).

^① <http://www.fastbleep.com/biology-notes/31/172/978>



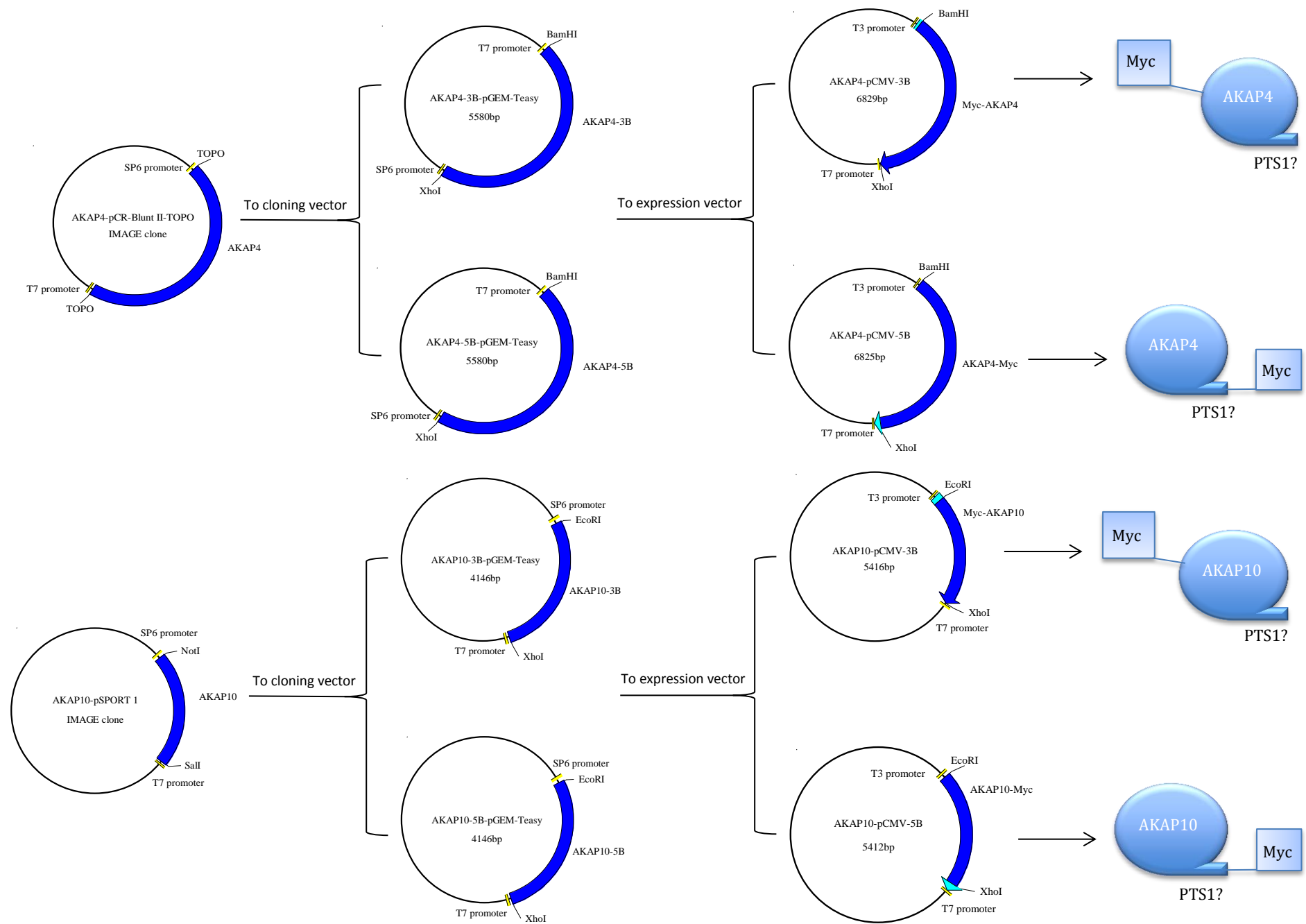


Figure 45 The instruction of myc-tag recombined plasmids generation (inserts are: GFP, AKAP1, AKAP4 and AKAP10)

The procedure for subcloning of myc-tagged GFP- and AKAP-fusion proteins had been described in detail in the methods (section 3.8). To check the localization of fusion protein *in vivo*, the critical point is the specific binding of the antibody against the tag in fusion protein. Two positive control plasmids, pCMV-GFP-3B and pCMV-GFP-5B, were constructed to test the functionality of the vectors to express the desired protein in TM4 cells. The myc-tag was fused to the N-terminus and C-terminus of the GFP, respectively.

GFP (green fluorescent protein) is a 238-residues green fluorescent protein with an emission peak at 509 nm, and it is widely used as a reporter of expression (Tsien, 1998). GFP was previously thought to have non- or low toxicity and exhibit no interference with any biological processes (Olivares-Fuster et al., 2002; Welsh and Kay, 1997). Therefore, many engineering GFP variants were generated for biological monitoring (Hoffman, 2008; Murphy et al., 2011). However, recently, some side effects of GFP were reported from *in vitro* and *in vivo* studies, such as cytotoxicity and apoptosis induction (Koike et al., 2013). Thus, in this thesis the myc-tag, which exhibited small size (only 10 amino acids) and no side effect, was used instead of GFP to track the fused AKAP proteins.

GFP is a cytoplasm protein with no targeting signal at any terminus, hence the attached myc-tag should not interfere with its cytoplasmic localization. This arrangement will also allow the co-localization of GFP and the myc-tag in the both two constructs, which was confirmed in Figure 46 (myc-GFP and GFP-myc). These two GFP fusion constructs were also used to optimize the transfection conditions and the staining conditions for the anti-myc tag antibody labelling.

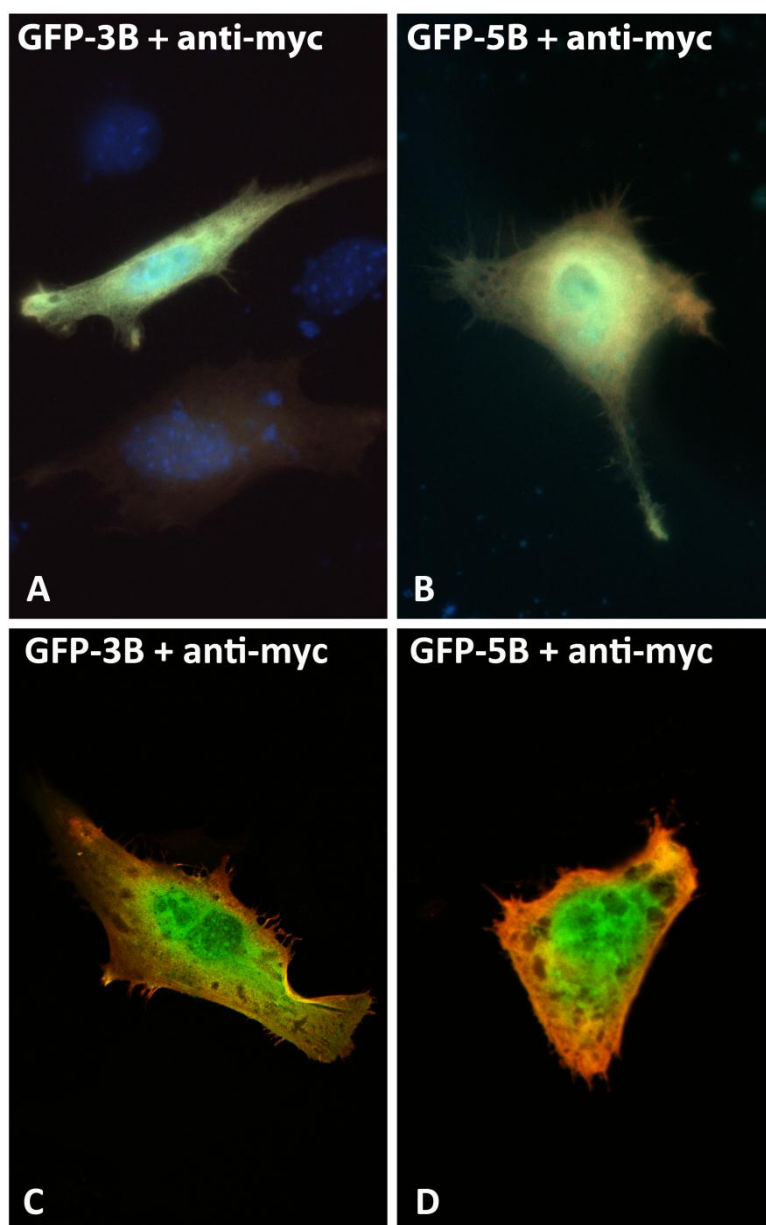


Figure 46 Co-localization test for the myc-tagged GFP-fusion proteins as positive controls, N-terminal myc-labelled GFP (GFP-3B) plasmid and C-terminal myc-labelled GFP (GFP-5B) plasmid. A and B were taken with a 63 × objective of the conventional fluorescence microscopy (Leica DMR). C and D were taken with a 63× objective of the confocal laser scanning microscopy (CLSM) (Leica TCS SP2).

N-myc-GFP (GFP-3B) and GFP-C-myc (GFP-5B) were both expressed in the cytoplasm and also nucleus, whilst the anti-myc antibodies only mainly stained the cytoplasm. These results can be explained in two ways. First, the binding of the antibodies to the

outer region will make the penetration to the interior of the cells and nucleus more difficult for next sets of antibodies. The second possibility is that the permeabilization of the nuclear pores after fixation of the cells during the immunofluorescence staining caused the poor penetration of antibodies into the nucleus, whereas the GFP-myc recombinant protein was transported in the living cell during the cell culture into the nucleus prior to the fixation already. The general entry permeabilization conditions for primary and secondary antibodies into mitochondria with a double membrane (outer and inner mitochondrial membrane, see Figure 48D-F. SOD2 in the mitochondrial matrix) and also into peroxisomes with a single limiting membrane (see Figure 48A-C. catalase staining in the peroxisomal matrix) gave excellent results.

It was suspected that the AKAP1, -4, -10 contain a putative PTS1 targeting signal at the C-terminus, and AKAP1 and AKAP10 have been suggested to contain a mitochondrial targeting motif in the N-terminus, it was necessary to visualize peroxisomes and mitochondria in the TM4 cell line under ordinary growth conditions (Figure 47 and Figure 48). Peroxisomes are numerous in TM4 cells (Figure 47A-D) can be well labelled with PEX14p (Figure 47C-D), a protein marker for peroxisomes that was strongly labelling in Sertoli cells in the testis (Grant et al., 2013; Nenicu et al., 2007).

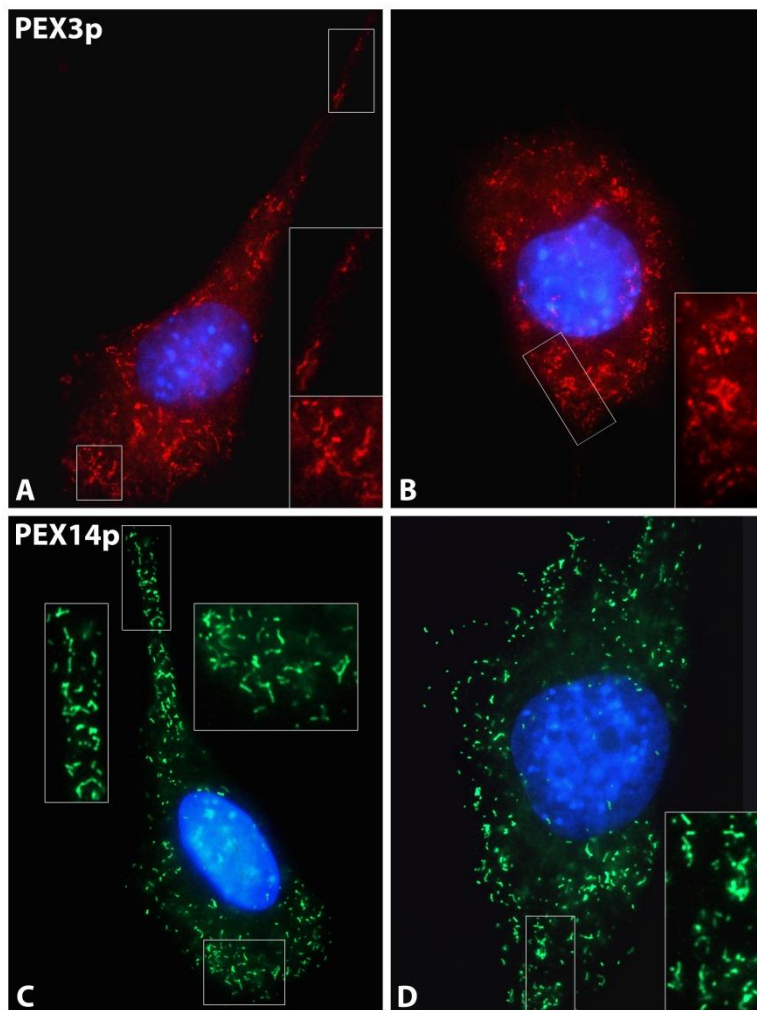


Figure 47 Immunofluorescence images showing peroxisomal membrane staining (A-D) in untreated TM4 cells. Micrographs were taken with a 63 × objective of the conventional fluorescence microscopy (Leica DMR).

PEX3p was less expressed and peroxisomal staining was only possible with high antibody concentrations, leading to more background (Figure 47A-B). TM4 cell peroxisomes are a mixture of round, rod-shaped and elongated, tubular

organelles that are distributed around the nucleus and sometimes form clusters or small network-like structures. In the TM4 cell processes, peroxisomes showed a heterogeneous pattern, with some processes exhibiting many peroxisomes until the end of the cellular extension (Figure 47C) and others exhibiting only few stretched organelles (Figure 47A), suggestive of a transport via microtubules in this region.

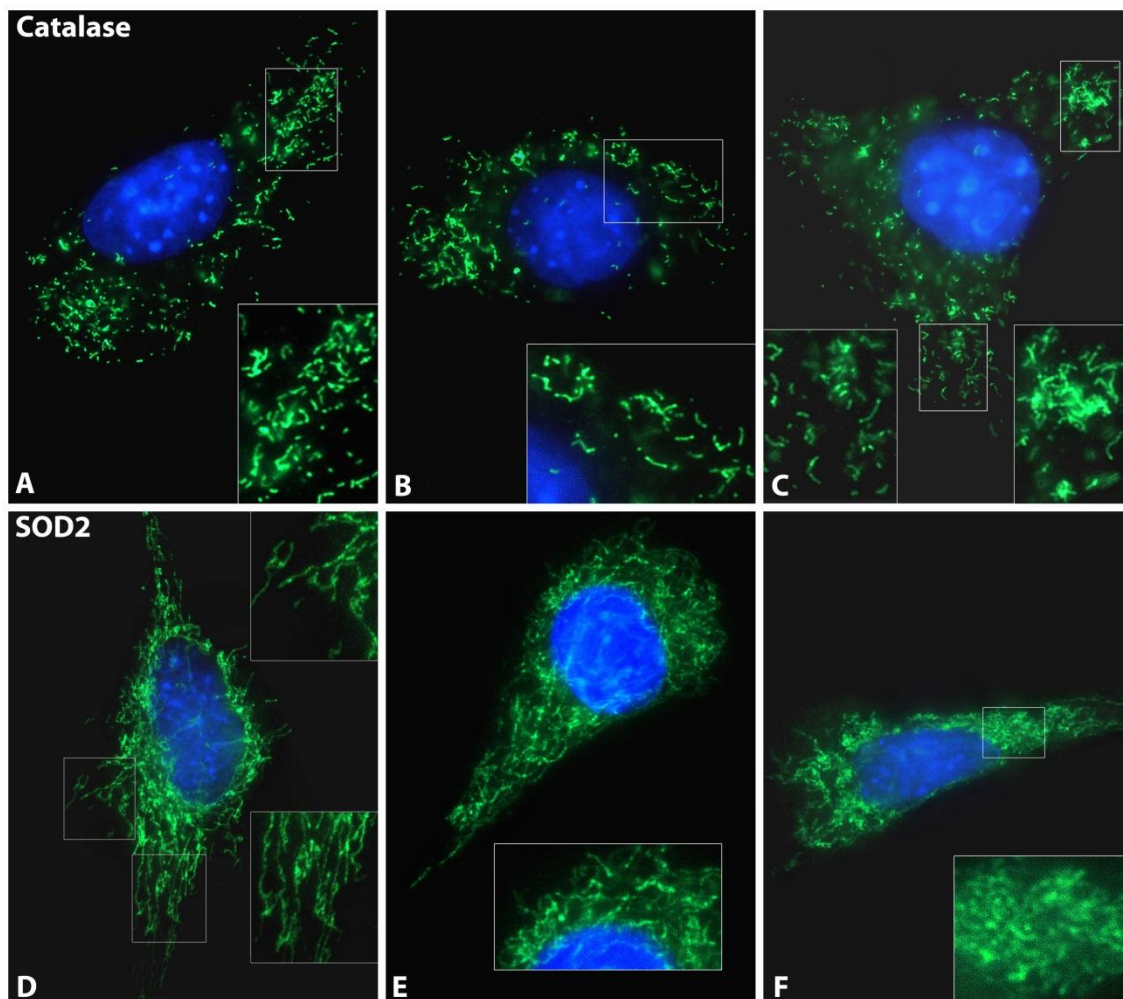


Figure 48 Immunofluorescence images showing peroxisomal (A-C) and mitochondrial (D-F) matrix staining in untreated TM4 cells. Micrographs were taken with a 63× objective of the conventional fluorescence microscopy (Leica DMR).

Staining for catalase provided a similar pattern in TM4 cells as for PEX14p (Figure 47C-D). Catalase was sometimes more enriched in the large, round and peripheral part of tubular peroxisomes (bright end) whereas less staining of the tubules in between was noted, which could even be better identified in less intensively stained peroxisomes (Figure 48B-C). Large clusters and network-like structures were also visible with the catalase staining (Figure 48A and C). Mitochondria were well stained with the anti-SOD2 antibody in TM4 cells (Figure 48D-F). Large differences were observed between the different TM4 cells in the same culture, with some cells exhibiting very long mitochondria in the cell periphery, which seem to extend from a perinuclear mitochondrial reticulum. Similar to catalase also SOD2 seems to be enriched in some matrix parts in the very long mitochondria (Figure 48D). In other TM4 cells (Figure 48E), mitochondria are arranged in a complete network up to the leading lamella of the cell (insert in Figure 48E: perinuclear mitochondrial network). In the

backward pole with an elongated extension, single long mitochondria were stretched underneath the plasma membrane and seemed to be transported along microtubules. Some TM4 cells contained a very dense mitochondrial network with rather small distances and high levels of SOD2 (Figure 48F).

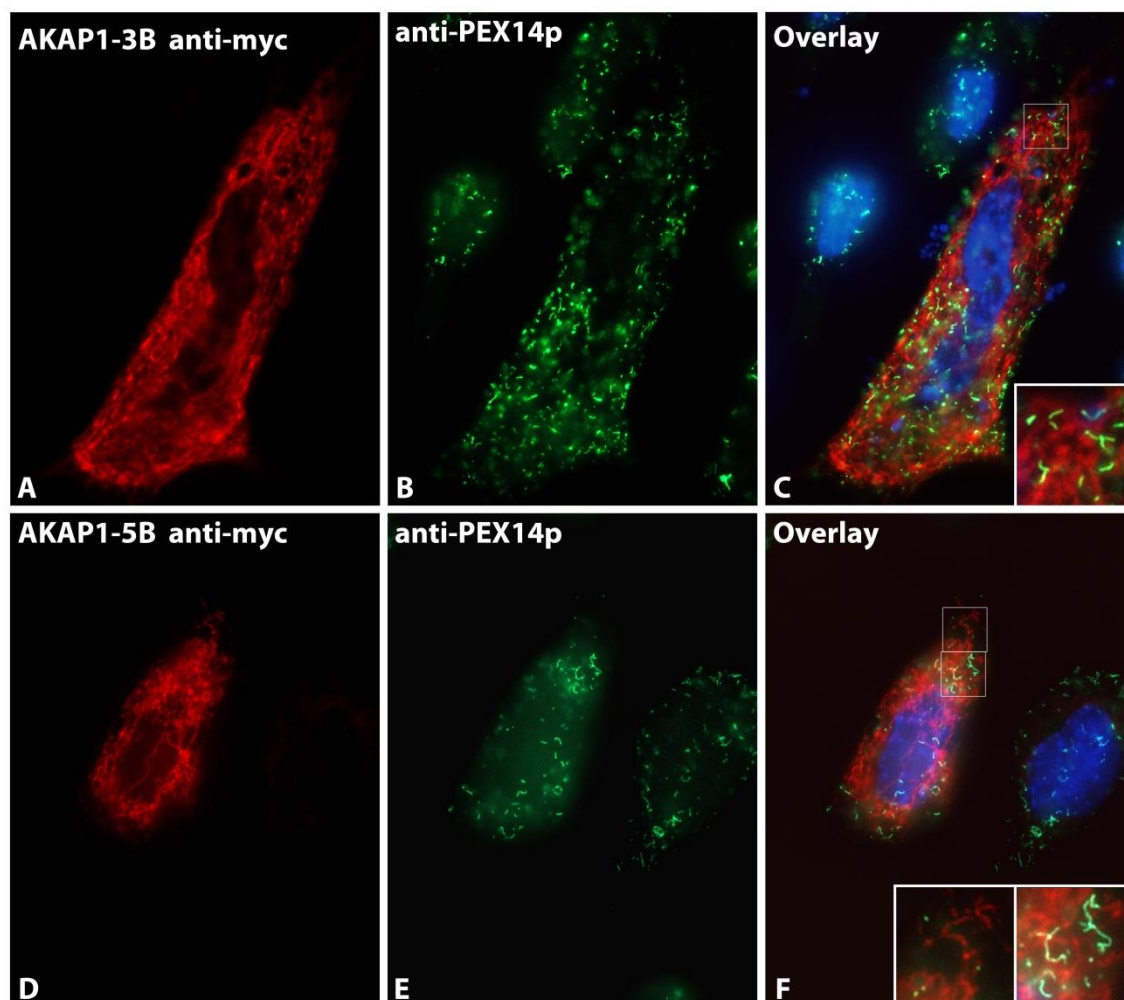


Figure 49 Double-immunofluorescence images of the myc-tag and PEX14p, revealing that both myc-tagged AKAP1 fusion proteins did not co-localize with peroxisomes. Micrographs were taken with a 63× objective of the conventional fluorescence microscopy (Leica DMR).

Inhibition of the mitochondrial targeting with the N-terminal myc-tag did not promote the targeting of the recombinant AKAP1 protein to peroxisomes (Figure 49A-C). In some cases, larger and nicely extended cells were observed in the cell cultures. These cells did not exhibit a high overexpression of the recombinant N-myc-AKAP1 protein. N-myc-AKAP1 was observed in a network-associated pattern without an association with peroxisomes (see Figure 49C), although peroxisomes were always

located at the areas of weakly labeling N-myc-AKAP1. Since some parts of the nuclear membrane seemed to be positively labelled with the anti-myc antibody (Figure 49C), the association of N-myc AKAP1 with the cytoplasmic face of the endoplasmic reticulum could be possible, but this has to be proven in the future with anti-ER-marker antibodies. In cells overexpressing AKAP1-C-myc, a typical mitochondrial pattern was observed. With the C-terminal myc-tag, a putative peroxisomal targeting would be blocked, since the PTS1 must be a “free” tripeptide signal at the extreme C-terminus to ensure the targeting of proteins into the peroxisomal matrix. In these cells, however, some peroxisomes exhibited very extended elongated structures with a size and appearance similar to mitochondria (see Figure 49F).

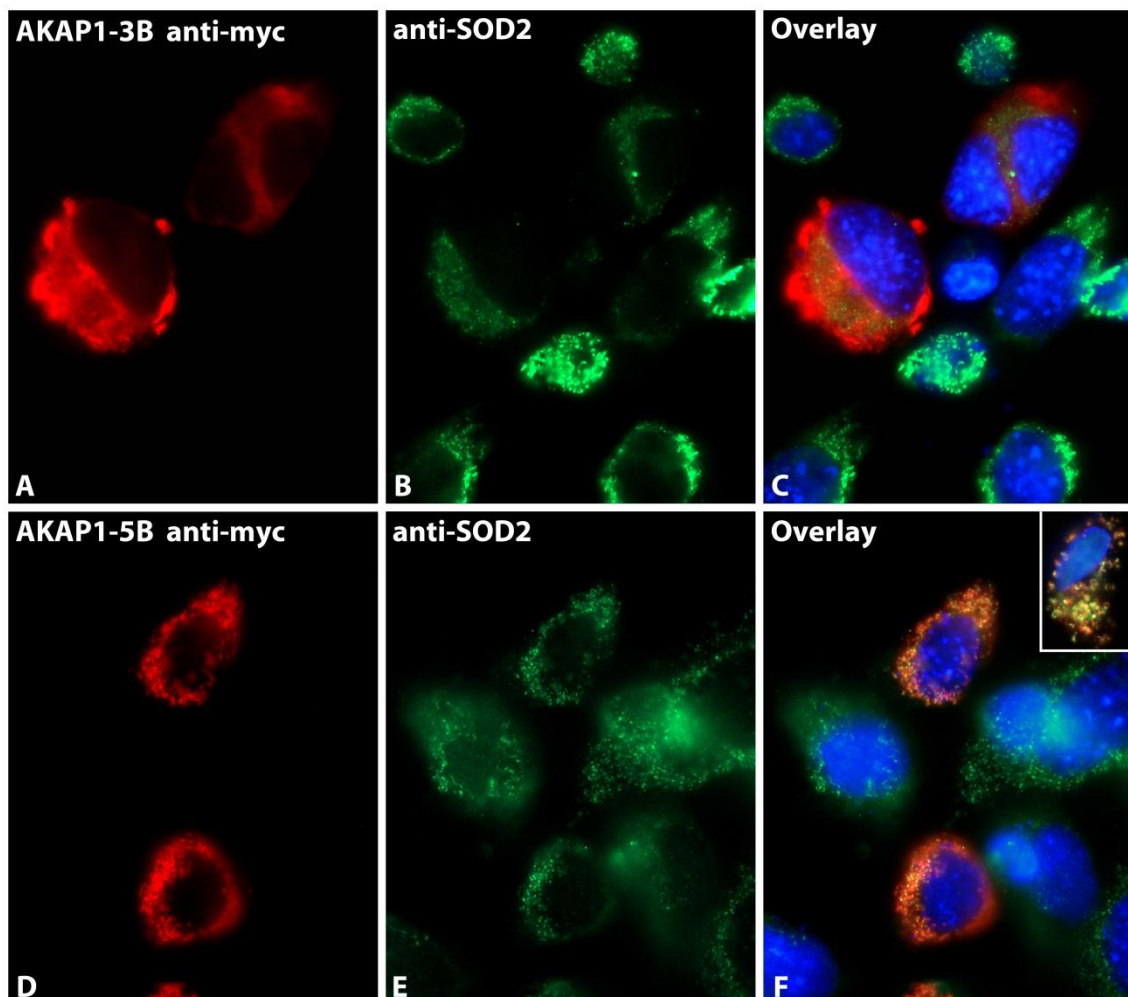


Figure 50 Double-immunofluorescence showing that N-terminal myc-tagged AKAP1 (AKAP1-3B) did not co-localize with mitochondria (Figure 50A-C), but C-terminal myc-tagged AKAP1 (AKAP1-5B) co-localized with mitochondria (Figure 50D-F). Micrographs were taken with a 63× objective of the conventional fluorescence microscopy (Leica DMR).

Also, in the co-localization staining for mitochondria, the recombinant AKAP1 protein with a myc-tag at the N-terminus (N-myc-AKAP1) exhibited a cytoplasmic localization with enrichment in some areas of the periphery, whereas the AKAP1 protein with a C-terminal myc-tag (AKAP1-C-myc) was targeted to mitochondria, as shown by the overlapping of myc and SOD2 stains. In cultures with overexpressed N-myc-AKAP1, a clear downregulation of SOD2 was noted in transfected cells, whereas some untransfected cells exhibited a much stronger SOD2 labelling, suggesting a difference in the reaction to oxidative stress between transfected and non-transfected cells. AKAP1-C-myc targeted to all mitochondria in a similar level, whereas the SOD2 was clearly localized only in some parts of these mitochondria. The insert in Figure 50F depicts a TM4 cell with ring-shaped mitochondria, in which the SOD2 was also heterogeneously localized. The overall heterogeneity of SOD2 localization in the mitochondria of “lipofected” TM4 cells seemed to be much higher than in regular control cells without any transfection (compare to Figure 48D-F). At higher magnifications, the punctate mitochondrial pattern could be identified in some cases as longer organelles, only labelled strongly at some parts with SOD2, forming “beads on a string”-like patterns inside the cells. The mitochondrial network in cells with high overexpression of AKAP1-C-myc was very dense and exhibited small organelles.

CLSM examinations of the immunofluorescence preparations revealed similar results as obtained by conventional fluorescence microscopy, therefore only the overlays of different examples of transfected cells are presented.

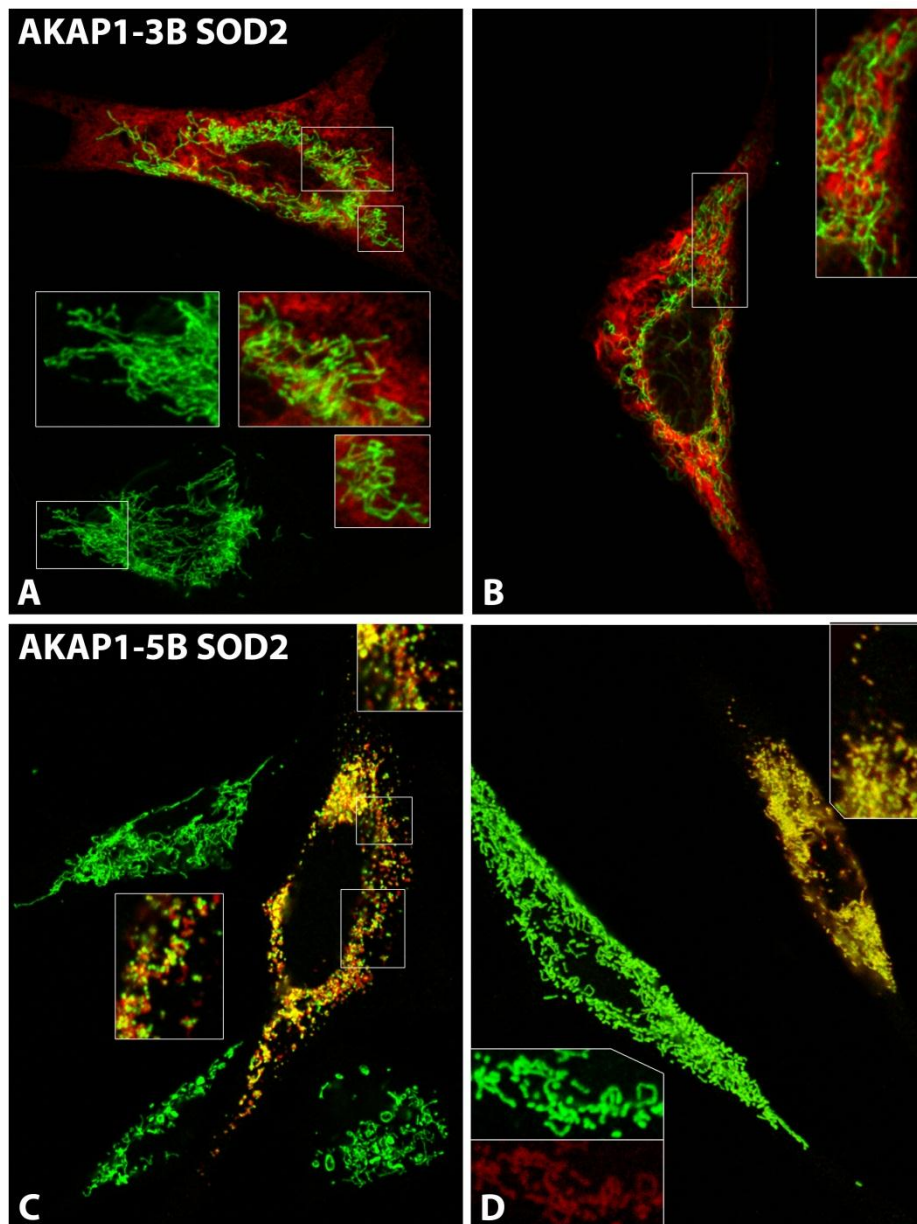


Figure 51 CLSM images of double-immunofluorescence for myc and SOD2, showing that N-terminal myc-tagged AKAP1 (AKAP1-3B) did not co-localize with mitochondria (Figure 51A-B), unlike the C-terminal myc-tagged AKAP1 (AKAP1-5B) (Figure 51C-D). Micrographs were taken with a 63× objective of the confocal laser scanning microscopy (Leica TCS SP2).

The overexpressed recombinant N-myc-AKAP1 protein clearly localized to special parts of the cytoplasm and network-like structures (Figure 51A), partially covering the nucleus (Figure 51B), suggesting that certain parts of the ER-system could be labelled. The mitochondrial network in N-myc AKAP1 overexpressing cells seemed to be slightly less extended to the periphery and more centrally localized in the perinuclear area. Moreover, the long mitochondria observed in the cytoplasmic region underneath of the nuclear region of non-transfected neighboring cells (Figure 51A) were

less frequently observed in transfected cells. Mitochondria were localized in N-myc-AKAP1 free areas, sometimes closely covered by N-myc-AKAP1 positive structures (Figure 51A & B). In strong AKAP1-C-myc overexpressing cells, AKAP1 was targeted to the complete mitochondrial population, whereas SOD2 was heterogeneously distributed, therefore in addition to the yellow color indicative of the overlapped stains, red and green colored mitochondria were clearly visible at higher magnifications (Figure 51C). In very strong AKAP1-C-myc overexpressing cells, mitochondria were rounded up and single organelles or packaged in a very dense network. Cells with lower expression of AKAP1-C-myc exhibited already proliferated mitochondria and a denser network than non-transfected TM4 cells. In addition, they exhibited a strong SOD2 staining of the entire mitochondrial network, therefore they appeared green even though a weak red staining of the low expressed AKAP1-C-myc in mitochondria was present (Figure 51D).

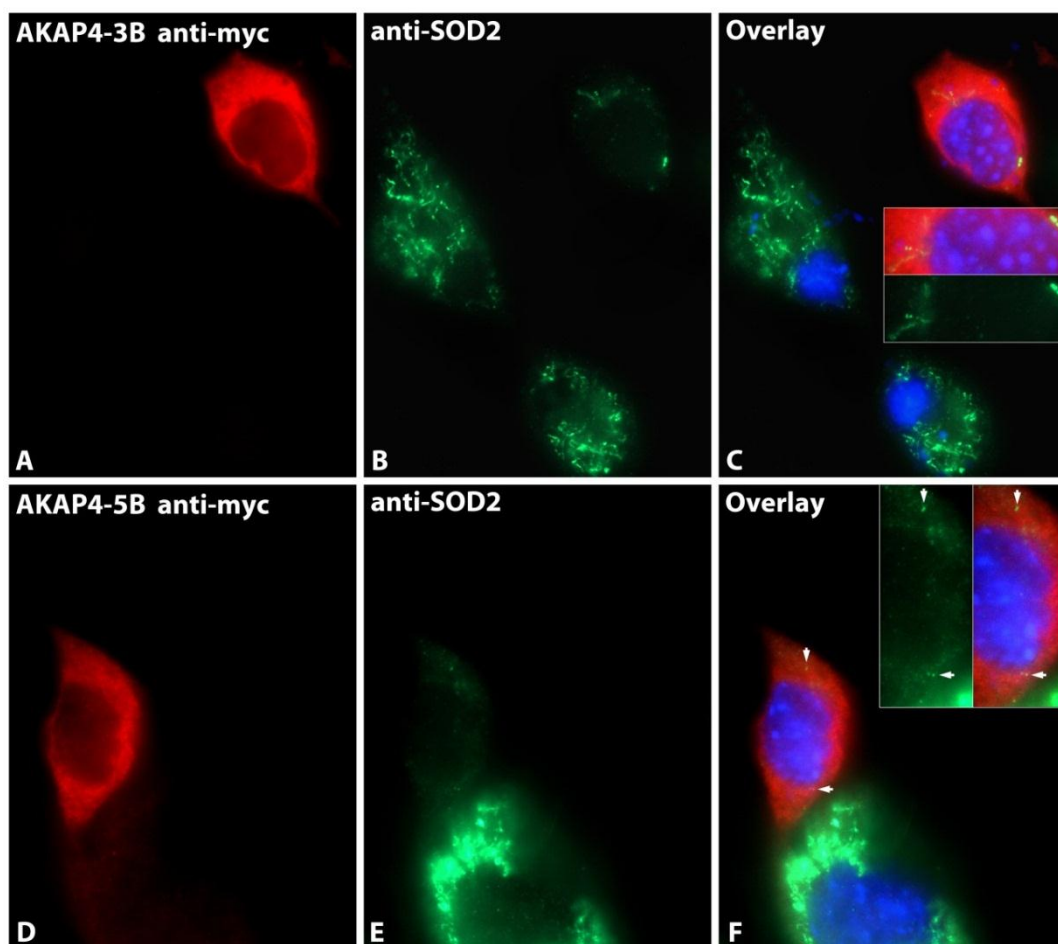


Figure 52 Double-immunofluorescence preparations for myc and SOD2, showing that the two types of myc-tagged AKAP4 were both expressed in the cytoplasm and did not co-localize with mitochondria in TM4 cell line. Micrographs were taken with a 63 × objective of the conventional fluorescence microscopy (Leica DMR).

Both overexpressed recombinant AKAP4 proteins were localized in the cytoplasm and reduced the abundance of mitochondrial SOD2 in transfected cells. In addition, the level of SOD2 was high in the mitochondria of neighboring TM4 cells that were not transfected with the AKAP4-C-myc protein.

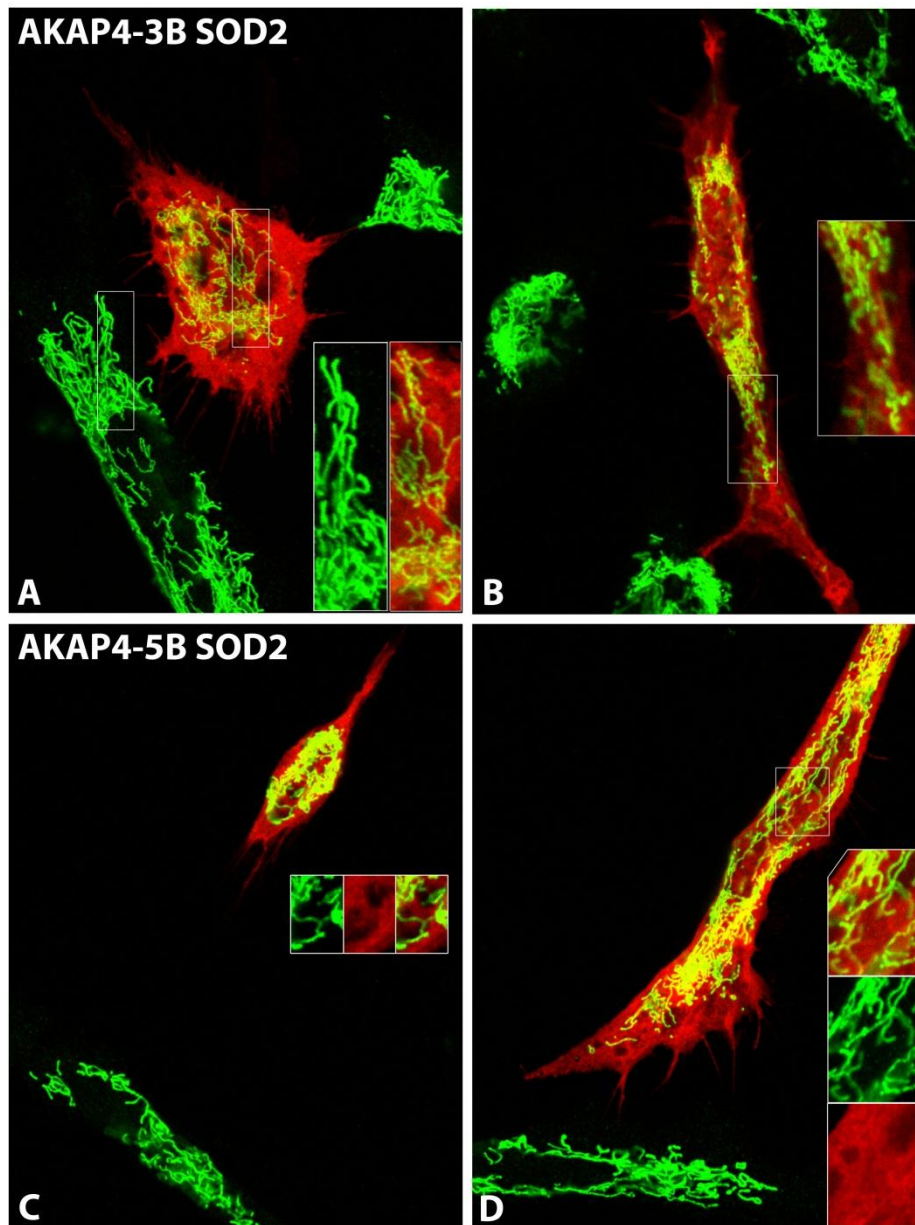


Figure 53 CLSM images of double immunofluorescence preparations for myc and SOD2, showing that the both types of myc-tagged AKAP4 fusion proteins localized within the cytoplasm but not to mitochondria in TM4 cell line. Micrographs were taken with a 63× objective of the confocal laser scanning microscopy (Leica TCS SP2).

Cells expressing intermediate levels of AKAP4 in the cytoplasm contained a more centrally localized mitochondrial network with lower levels of SOD2, especially when the N-myc AKAP4 was overexpressed. Only two positive cells were found overexpressing AKAP4-C-myc. The first one exhibited a collapsed perinuclear

mitochondrial network with only very few mitochondria extrusion (Figure 53C). The second cell appeared more normal, however, exhibited lower SOD2 levels than the neighboring non-transfected cells.

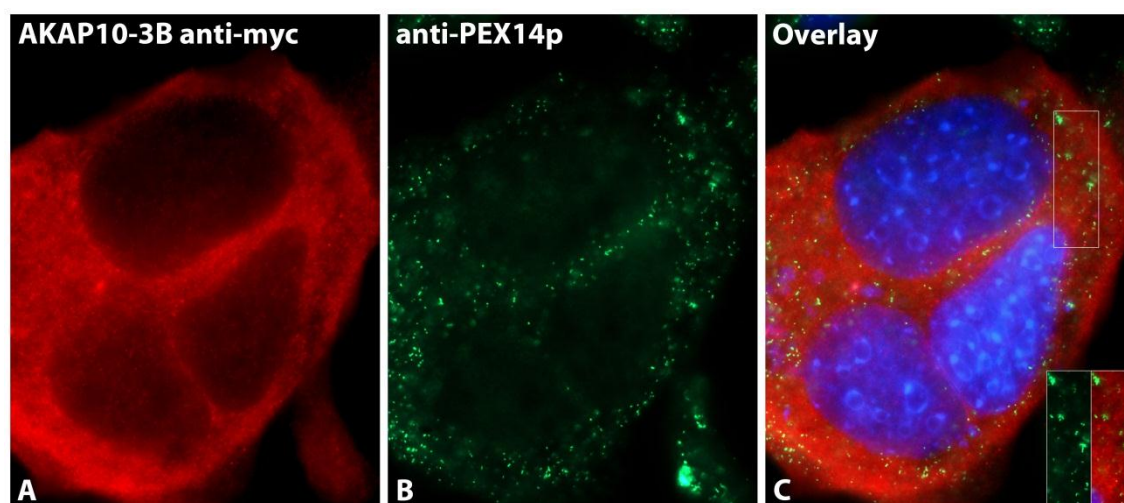


Figure 54 Double-immunofluorescence preparation for myc and PEX14p, showing that N-terminal myc-tagged AKAP10 (AKAP10-3B) did not co-localize with peroxisomes. Micrographs were taken with a 63× objective of the conventional fluorescence microscopy (Leica DMR).

In the N-myc AKAP10 overexpression experiments some giant cells were present. All cells exhibited a mainly cytoplasmic N-myc-AKAP10 staining, with some positive small and round organelles (Figure 54C). These dots did not colocalized with peroxisomes that were labelled for PEX14p (Figure 54C). The overall peroxisomal appearance and distribution pattern in these cells was also not altered. Most of the cells exhibited round to rod-shaped peroxisomes and less tubules.

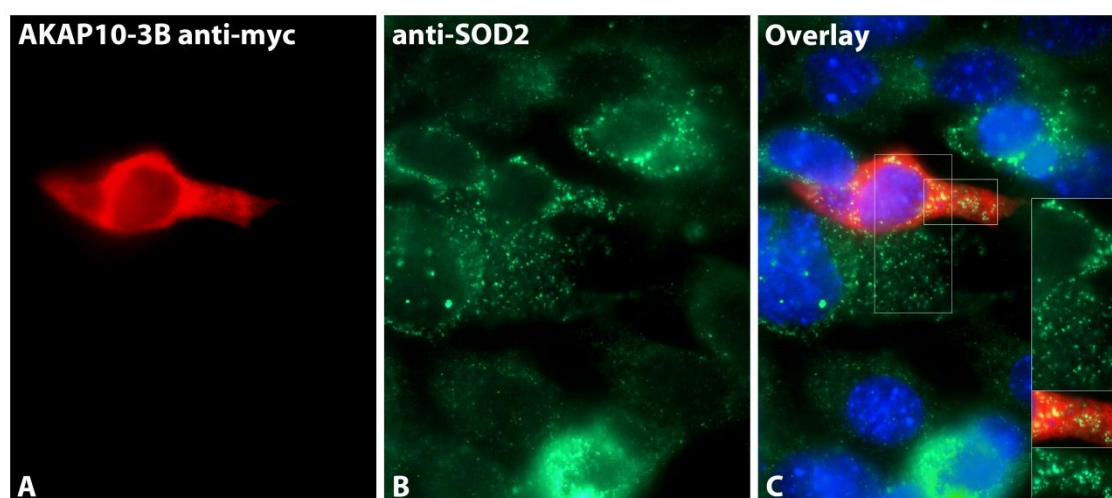


Figure 55 Double-immunofluorescence preparation for myc and SOD2, showing that the N-terminal myc-tagged AKAP10 (AKAP10-3B) did not co-localize with mitochondria. Micrographs were taken with a 63× objective of the conventional fluorescence microscopy (Leica DMR).

N-myc-AKAP10 was also localized in the cytoplasm, but did not lead to the reduction of mitochondrial number or the reduction of SOD2. AKAP10-C-myc overexpression seemed to be toxic since no positive transfected cells within 24 hours. The transfected cells probably died due to apoptosis, which might have been induced by altered mitochondrial function. To determine whether N-AKAP10 would have an effect on mitochondria and apoptosis induction, therefore earlier time-points after the transfection have to be used in future experiments.

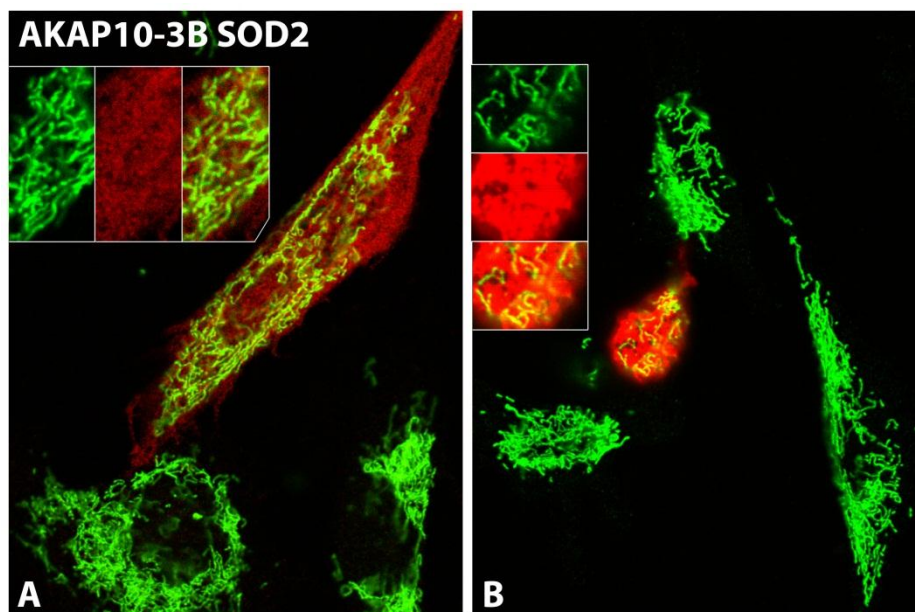


Figure 56 CLSM images of a double immunofluorescence preparation for myc and SOD2, showing that the N-terminal myc-tagged AKAP10 (AKAP10-3B) did not co-localize with mitochondria. Micrographs were taken with a 63× objective of the confocal laser scanning microscopy (Leica TCS SP2).

In comparison to neighboring non-transfected cells, cells with low N-myc-AKAP10 expression in the cytoplasm exhibited a less dense mitochondria network and a lower SOD2 labelling. The contrast of the AKAP10 and SOD2 staining was enhanced to aid better visualization of the mitochondrial network in the insets (Figure 56A). Cells with high N-myc-AKAP10 expression most probably went into apoptosis (round cell in Figure 56B with only few mitochondria).

5 Discussion

5.1 AKAP220 (-CRL) is probably an artifact

The A-kinase anchoring proteins (AKAPs) constitute a protein family that tether PKA and other enzymes to various specific subcellular locations, and play a critical role in the regulation of the cellular physiological metabolism. In 1996, a rat isoform of AKAP11 which was previously called rat AKAP220 [Q62924.1] due to its molecular mass, was reported to be localized in peroxisomes through a PTS1 signal (“-CRL”) and supposed to take part in testicular peroxisomal functions and phosphorylation events by Prof. Scott’s group, an AKAP research pioneer (Lester et al., 1996). As a peroxisome research group, this particular “peroxisomal” AKAP was interesting for us. However, during this thesis we revealed that this putative peroxisomal rat AKAP11 [Q62924.1] is an artifact, that was mistakenly identified in the literature.

First, a functional structure of a protein should be evolutionary conserved throughout the entire family of the protein (Nasir et al., 2014). It is unlikely that just one member possesses some functional domain not present in any other members of related species. From the information obtained from the literature and the screening of all AKAPs (Figure 17), we found that the reported sequence of rat AKAP11 [Q62924.1] is the only one with a distinct C-terminal end containing a putative PTS1 signal in the entire AKAP11 family, and clusters into a separate protein subfamily in the evolutionary tree.

Second, the result of the mRNA BLAST showed that the mRNA [U48288.1] of rat AKAP11 [Q62924.1] is not derived from a single chromosome, but combines three non-related gene fragments from three distinct chromosomes by two *EcoRI* linkers (Figure 27-28). In the 1990’s, *EcoRI* linker was frequently used for self-made cDNA library constructions, which could have been the source of the contamination. Although, “trans-splicing” events exist in nature that mRNA might be not 100% derived following exons order in genome (Caudevilla et al., 1998; Flouriot et al., 2002; Yang and Walsh, 2005). However, one mRNA from 3 separate chromosomes (2, 12 and 15) is very unlikely (Figure 27). Moreover, in the right exon from chromosome 15, an artificial frame shift (position: 8864-9726) in the cDNA clone caused an upper STOP codon, leading to the “-CRL” PTS1 signal.

Third, the antibody against AKAP220 used in Scott's paper was produced by the cloned artificial recombinant partial AKAP220 plasmid. Using this antibody, a double immunofluorescence staining showed the peroxisomal localization of AKAP220. Moreover, the antibody used in the Scott's paper is polyclonal, meaning that this antibody was composed of an antibody mixture targeted to different epitopes on rat AKAP220. This mixture most likely also contained antibody that recognized the tripeptide ("CRL") in the C-terminus of rat AKAP220. Antibodies against the C-terminal PTS1 signal, such as "-SKL", are frequently used to stain peroxisomal protein efficiently and will clearly label many proteins in the peroxisomal compartment (Stelzig et al., 2013). The "CRL" could also be potentially found at the C-terminus of other peroxisomal proteins which could be then detected by this antibody. Therefore, during the bioinformatics work for this thesis, the complete protein database of the rat was searched for a "CRL-STOP codon". Indeed, with the advice from the Swiss Institute of Bioinformatics, a rat peroxisomal protein Acot4 [D3ZIQ1] (421aa, 46kDa) was found with a "CRL" tripeptide at the C-terminal end. This could be an explanation for the detected peroxisomal staining for rat AKAP220 presented in Scott's paper.

We therefore suggest that the rat AKAP220 [Q62924.1] which was described to be a peroxisomal protein because of its "CRL" putative PTS1 signal, is an artifact, resulting from a non-accurate self-made cDNA library construction. This hypothesis is practically proved by our findings of the *EcoRI* linker at two different positions inside of the rat AKAP11 recombinant cDNA clone (Figure 28). Similar mistake was common in that period, due to technical limitations and the lack of the shared database information that we are able to access nowadays. For example, a shorter cloned mouse *AKAP10* gene was generated also due to an artificial cDNA library or false sequencing, causing a frame shift and a wrong STOP codon (Wang et al., 2001).

5.2 PTS1 prediction is useful for searching novel peroxisomal proteins

The peroxisomal enzyme composition in distinct organs and cell types is heterogeneous and varies strongly (Grant et al., 2013). Due to the limitation in pure peroxisome isolation from different cell types, the peroxisome proteome research still depends on the computational prediction to identify low abundance peroxisomal proteins. The C-terminal PTS1 tripeptides ("-SKL" variants) are the most important part

of the PTS1 signal and widely used as the first strategy to screen for potential new peroxisomal matrix proteins (Hayashi et al., 1997; Ma and Reumann, 2008).

However, the larger the database tested or the bigger the PTS1 tripeptides pattern matrix applied, the more candidates would be generated as well as the more false positive hits obtained. Because this screening algorithm excludes the analysis of other critical factors on the individual candidate, such as 1) upstream amino acid residues close to the PTS1 tripeptides, 2) other possible organelle targeting signals ahead or overlapping the PTS1 signal, and 3) the unpredictable C-terminal exposure efficiency. In 2008, a study applied a PTS1 tripeptides pattern matrix ([SAPC]-[KR]-[LMI]) to screen an *Arabidopsis* protein database and obtained 7 potential plant peroxisomal kinases from that screening. However, 4 candidates were verified with functional PTS1 only when they were partially expressed as oligopeptides, but not as full-length fusions which remained in the cytoplasm. The other 3 of the 7 sequences were incorrectly predicted through experimental validation (Ma and Reumann, 2008). Also a mammalian PTS1 motif was proposed ([SACKN]-[KRHQNS]-[LI]) (Amery et al., 2000). In this thesis, we applied a broad-ended PTS1 consensus ([ACHKNPQST]-[AHKNQRS]-[FILMV]) and a test database for AKAPs, and obtain 3 AKAP families with potential PTS1 signals which were highly expressed in the testis (Table 15 and Figure 17&41-42).

Furthermore, our second screening which included the upstream residues of the PTS1 terminus suggested a low possibility of peroxisomal proteins throughout these 3 AKAP families (Figure 38-40). Basic residues located close to PTS1 tripeptides play an enhancing role for the peroxisomal targeting, while acidic amino acids are functionally inhibitory instead, especially the critical residue at the 4th last position (Amery et al., 2000; Ma and Reumann, 2008). For example, a GFP construct derived from human 2-methylacyl-CoA racemase, which coded GFP-KVKASL, localized very well in peroxisomes. Amery and colleagues showed that a nonpolar side chain amino acid point mutant GFP-KVGASL displayed a cytoplasmic fluorescence (Amery et al., 2000).

In this respect, a closer look on the 3 individual mouse AKAPs was taken:

The mAKAP1 [O08715.4] contains the reported PTS1 variant “-ASL” (Amery et al., 2000), but without positive charged Lysine (Lys, K) at the 4th last position, on the contrary one negatively charged Aspartic acid (Asp, D) and 3 uncharged amino acids (Ser-Tyr-Tyr, SYT) upstream were found which might be inhibitory on the peroxisomal

targeting signal (Figure 38). In addition, mAKAP1 also contains a mitochondrial targeting signal in the N-terminal 30 residues, which maintains higher priority and is exposed first during translation.

Eventhough mAKAP4 [Q60662.1] also contains a prototypical PTS1 tripeptide “-ANL”, the presence of one Aspartic acid (Asp, D) and 3 hydrophobic amino acids (Trp-Leu-Leu, WLL) upstream might reduce the peroxisome targeting ability (Figure 39).

The C-terminal end “-TKL” in mAKAP10 [O88845.3], considered as a putative PTS1 signal here (Figure 40), has been suggested to act as typical class I PDZ-binding motif (“-STKL”) conserved among species (Tingley et al., 2007). PDZ domains are abundant and diverse and mediate protein-protein interactions. More than 200 types of structures are present to recognize the C-terminus of binding proteins, such as the C-terminal end of Shaker-type K⁺ channels (Kv11.4) and *N*-methyl-D-aspartate receptor 2B (NMDA) (Lee and Zheng, 2010; Saras and Heldin, 1996). The PDZ-binding motif can serve as signal peptide to target proteins to membrane receptor complexes (Hamuro et al., 2002). Moreover, AKAP10 was shown to localize at a highly specialized region of the plasma membrane in mouse kidney proximal tubular cells. This PDZ-binding motif in AKAP10 could be recognized by PDZ domain-containing proteins, which might influence phosphorylation of PKA substrates located in close proximity to the plasma membrane. For example, PDZK1, a protein with multiple PDZ domains, connects plasma membrane proteins and acts as an anchoring site for AKAP10 via its PDZ-binding motif (Gisler et al., 2003a; Gisler et al., 2003b). Thus, the putative PTS1 signals of these 3 AKAPs can hardly be functional under non-pathological conditions.

The on-line PTS1 predictor in the second round revealed that the mouse AKAP1, 4, 10 are probably not the targeted to peroxisomes (Figure 38-40), which was also confirmed by overexpression of AKAP1-pCMV-3B, AKAP4-pCMV-3B and AKAP10-pCMV-3B in this study (Figure 49-56). Thus, this web tool seems to be relatively reliable to predict the targeting possibility. In addition, a combined computer programming code (see Supplemental data S1) was developed for large amount sequence screenings. The programming languages named Python and R were used, both of which are easy to learn for beginners and are open-source free software for worldwide users (Prechelt, 2000; Tippmann, 2015). In this study, Python was used for screening PKA binding domain and PTS1 signals throughout the whole AKAP1, 4, and

10 family members in the protein database, and R was used for transferring results into pictures to be easily read. The code (Supplemental data S1) is free offered for any user, who has interest to have a predicted overview of sequence feature before executing experiments.

5.3 Exceptions to the rules of PTS1 prediction: alternative targeting of peroxisomal matrix proteins

Not all the sequences indicated by the PTS1 predictor are peroxisomal protein. Also, some peroxisomal proteins did not follow the general algorithm of defined PTS1 prediction, such as the proteins that contain “hidden” PTS1 signals, which are only appended by translational readthrough extension. For instance, lactate dehydrogenase, a cytoplasmic enzyme, was described in peroxisomes in 1996 (Baumgart et al., 1996a), however, nobody knew its targeting mechanism to the organelles. Last year, it was described that lactate dehydrogenase B (LDHB) contains a PTS1 signal at the C-terminal end that cannot be recognized by any available PTS1 prediction programs, because it is located after the STOP codon. Only when translational read-through occurs, it will be functional and will target LDHB to peroxisomes (Baumgart et al., 1996a; Schueren et al., 2014).

Some proteins don't contain a PTS1 signal, but are also transported into peroxisomes by binding a partner which contains a PTS1. For example, Cu/Zn superoxide dismutase 1 (SOD1) is an enzyme without any targeting signal, while its binding partner, the “copper chaperone of SOD1” (CCS), contains a weak PTS1 (“-AHL”). Therefore, SOD1 is co-imported by CCS into peroxisomes via a “piggyback” import-mechanism. When expressed together, SOD1 will be shuttled into peroxisomes by interacting with CCS. When a defect in the SOD1-CCS association occurs, for example by a mutation in the PTS1 end of CCS or in the peroxisomal import receptor PEX5p, both SOD1 and CCS remain in the cytoplasm (Islinger et al., 2009).

Some proteins can display dual localization under different situations. In rat, L-alanine: glyoxylate aminotransferase 1 (AGT1) is in mitochondria, and its N-terminal 22 residues were considered to be a putative mitochondrial targeting signal. In human, AGT1 lost these 22 amino acids during evolution and is targeted to peroxisomes. However, in primary hyperoxaluria type I patients, the AGT1 is transferred again back to mitochondria, caused by a point mutation in the initiation codon ATG to ATA

(Takada et al., 1990). A protein with real dual subcellular localization is human 2-methylacyl-CoA racemase, which is a protein containing both mitochondrial and peroxisomal targeting signals (Amery et al., 2000).

5.4 AKAP1 and mitochondrial fragmentation

It was reported in the literature that in many cell types (neurons, cardiomyocyte, etc.) the overexpression of AKAP1 could promote phosphorylation and inhibition of the pro-apoptotic BAD protein (Affaitati et al., 2003; Merrill and Strack, 2014). PKA phosphorylates BAD at Ser¹⁵⁵, which blocks BAD binding of Bcl-2 and inhibits apoptosis. Mitochondrial dysfunction is associated with apoptosis, indicating that mitochondrial-anchoring of PKA is critical for cell survival (Carlucci et al., 2008). Moreover, overexpression of AKAP1 and Ser⁶³⁷-phosphorylation of Drp1 was neuroprotective, promoting mitochondrial elongation by fusion (Cribbs and Strack, 2007; Merrill et al., 2011). In conclusion, high cellular AKAP1 levels were suggested to promote mitochondrial elongation or aggregation, and to reduce fragmentation or apoptosis (Kim et al., 2011).

Although it was shown that AKAP1 overexpression is good for the mitochondrial morphology and cell survival, in our case the extra myc-tag might hinder it. In this thesis, when AKAP1-pCMV-5B (C-term myc-tagged AKAP1) was overexpressed in TM4 cells, some cells displayed more fragmented mitochondria (Figure 51C-D). It was reported that AKAP1 with a defect in the KH domain induced changes in the mitochondrial morphology that appeared collapsed and rounded up rather than the normal elongated rod-like shape (Rogne et al., 2009). When the KH domain is phosphorylated by PKA, it is active to bind and stabilize RNA or ssDNA, such as *Star*, *Sod2* and ATP synthase *F0-f* mRNAs. A KH domain mutant is associated with some diseases, such as fragile X mental retardation syndrome and paraneoplastic opsoclonus-myoclonus-ataxia (POMA) neurodegenerative syndrome (Rogne et al., 2009). It is suggested that the C-terminal myc tag of recombinant AKAP1 may spatially hinder the KH domain phosphorylation or its mRNA association, possibly reducing mitochondrial protein content and inducing mitochondrial fragmentation.

Moreover, mislocalized AKAP1 reduced oxidative ATP synthesis and mitochondrial membrane potential ($\Delta\Psi_m$) and increased oxidative stress resulting in cell death, and the AKAP1 knockdown induced mitochondrial fragmentation and

apoptosis (Perrino et al., 2010). Thus, AKAP1 was suggested to play an important role in restoration of mitochondrial respiratory function, reduction of mitochondrial ROS and reduction of mitochondrial fission. However, in this study when AKAP1-pCMV-3B (N-term myc tagged AKAP1) was over-expressed in TM4 cells, the cells displayed normal elongated tubular mitochondria (Figure 51A-B). Additionally, the peroxisomal morphology remained unaffected regardless of the AKAP that was transfected.

5.5 Mitochondrial fusion and fission mechanisms

The mitochondria fusion and fission machinery is tightly controlled by protein phosphorylation. Mitochondrial fusion is controlled by three GTPase: Mitofusion1 (Mfn1), Mitofusion2 (Mfn2) and optic atrophy 1 (OPA1). Mfn1 and Mfn2 are anchored in the mitochondrial outer membrane (MOM), and OPA1 is localized to the intermembrane space and involved in the control of the cristae structure. The mitochondrial fission process is regulated by a cytosolic GTPase dynamin-related protein 1 (Drp1) and a small outer mitochondrial membrane binding protein Fis1. Fis1 is also responsible for peroxisomal division, which is discussed in following section 5.6.

As mentioned in section 5.4, Drp1 is inactivated by PKA phosphorylation at Ser⁶³⁷, which inhibits its GTPase activity. Inactivated Drp1 promotes elongation of mitochondria and enhances cellular resistance to pro-apoptotic stimuli. Dephosphorylation of Drp1 phospho-Ser⁶³⁷ by CaN (also called PP2B), an AKAP1 binding partner, induces mitochondrial fragmentation and cell death. When active, dephosphorylated Drp1 rapidly cycle between cytosol and mitochondria, suppressing mitochondria fusion into the cell protective reticulum (Merrill et al., 2011). AKAP1 at the mitochondrial membrane provides docking sites for the C-terminus of Drp1, as well as the central domain of PKA holoenzyme, which are indispensable for regulating mitochondrial morphology (Kim et al., 2011). Thus, it could be another possible explanation for the transfected AKAP1-myc induced mitochondria fragmentation. The C-terminal myc-tag might block the Drp1 docking site in AKAP1, wherefore, active Drp1 remain in the cytosol, a process inhibiting mitochondrial fusion and maintaining a punctate mitochondrial pattern.

5.6 Connection between peroxisomes and mitochondria

Distinct sets of enzymes are present in peroxisomes and mitochondria for lipid β -oxidation in animals, the fatty acid degradation still needs the cooperation of both organelles, because shortened fatty acids from peroxisomes are broken down in mitochondria (Colasante et al., 2015). For example, the peroxisomal acyl-CoA oxidases and the mitochondrial acyl-CoA dehydrogenases originated from a common ancestor gene (Baumgart et al., 1996b).

The division processes of peroxisomes and mitochondria also influence each other by shared fission proteins, such as PMD1 (Peroxisomal and Mitochondrial Division Factor 1), dynamin GTPases DLP1, Fis1 (Fission factor 1) and Mff (Mitochondrial fission factor). Fis1 promotes both mitochondrial and peroxisomal division, targets to peroxisomes by a PEX19p shuttle and contacts with PEX11 α and PEX11 β (Schrader et al., 2011). Mitochondria and peroxisomes also cooperate in anti-viral signaling and defense (Islinger et al., 2012). For example, mitochondrial antiviral signaling adaptor (MAVS) is also a dual-localized protein. When HIV-RNA attached on MAVS sites, the MAVS localized at peroxisomes (Berg et al., 2012). When peroxisome biogenesis is defective, the mitochondria also exhibit a dysfunction (Baumgart et al., 2001). For this reason, when defect AKAP1 causes mitochondrial dysfunction, repercussions might also affect peroxisomes.

Peroxisome proliferator-activated receptors (PPARs) are ligand-activated transcription factors. PPARs and their heterodimeric partner (retinoid X receptor, RXR) regulate target gene expression by binding the peroxisome proliferator responsive elements (PPREs) present in its promoter. Lipid metabolism is under the control of PPARs and PGC-1 α (PPAR γ coactivator-1 α) in both peroxisomes and mitochondria (Colasante et al., 2015; Finck, 2007). For example, PPARs regulated the transcripts level of the acyl-CoA oxidase 1 (ACOX1) in peroxisomal β -oxidation and carnitine-palmitoyltransferase (CPT1), acyl-CoA dehydrogenase (ACDH) and 3-ketoacyl-coenzyme A thiolase (THIO) in mitochondrial β -oxidation (Colasante et al., 2015). PPARs also play an important role in β -oxidation of fatty acids in testis, which associated with testicular functions (steroids synthesis). This subfamily consists of 3 isotypes: PPAR α , - β and - γ . PPAR α was known to be upregulated by FSH in the testis. However, PPAR γ /RXR γ complex is dominantly expressed in mature Sertoli cells (Thomas et al., 2010). In addition, PPAR γ regulates the lipolytic response by

influencing the mRNA level of PKAcata, *Akap1*, lipase gene *Pnplaz* (ATGL) and *Lipe* (HSL). It was showed that PKAcata and *Akap1* mRNA were downregulated in adipose tissues of humans. Moreover, a luciferase assay confirmed this PPAR γ regulation mechanism by identifying PPRE motifs at -600bp in the PKAcata promoter (5'-CGACCCTTGACCC-3') and at >7kb in the *Akap1* promotor (5'-AGGGAAGAGGTCA-3') (Rodriguez-Cuenca et al., 2012). In the testis, lipids are not only acting as energy source, but also as composition of spermatozoa membrane, such as long-chain fatty acids. Therefore, it is important to study male fertility by making a further clarification on the role of PPAR γ -AKAP1 in lipid metabolism between mitochondria and peroxisome in the Sertoli cell.

5.7 The role of AKAP1-StAR interaction in Sertoli cells

It is known that AKAP1 anchors PKA to the mitochondrial outer membrane to phosphorylate the StAR protein. Phosphorylated StAR transports cholesterol from the outer to the inner mitochondrial membrane, thereafter the cholesterol is converted by P450_{scc} (cholesterol side-chain cleavage enzyme, also called CYP11A1) to pregnenolone, which is the rate-limiting step in steroidogenesis (Castillo et al., 2014). This bioprocess occurs under the stimulation of LH in the theca of interstitial ovary cells in the female and Leydig cells of the testis in the male (Figure 57 upper portion). However, there are limited studies on the FSH and StAR expression in Sertoli cells. One study in 1998 reported that the regulation of FSH to StAR was not associated with cholesterol delivery and pregnenolone production but was rather associated with free fatty acid import into mitochondria (Gregory and DePhilip, 1998). Here we showed that the *Akap1* and *Star* mRNAs are expressed in the TM4 Sertoli cell line and that the overexpressed AKAP1 protein is localized in mitochondria in these cells under standard cell culture conditions for TM4 cells. We were also able to confirm that FSH stimulation resulted in elevated StAR protein amounts in TM4 Sertoli cells (Figure 43-44&51). To get a better understanding on steroidogenesis regulation, it would be interesting to explore further questions, such as: a) the role of AKAP1 and StAR in mitochondria in Sertoli cells, b) whether AKAP1 and StAR are also expressed in granulosa cell in the ovary of female (Figure 57 lower portion). Due to time restrictions, we were not able to test out any other experimental conditions, such as lipid treatment, hypoxia or other conditions that might provoke an additional targeting of AKAP1 to peroxisomes.

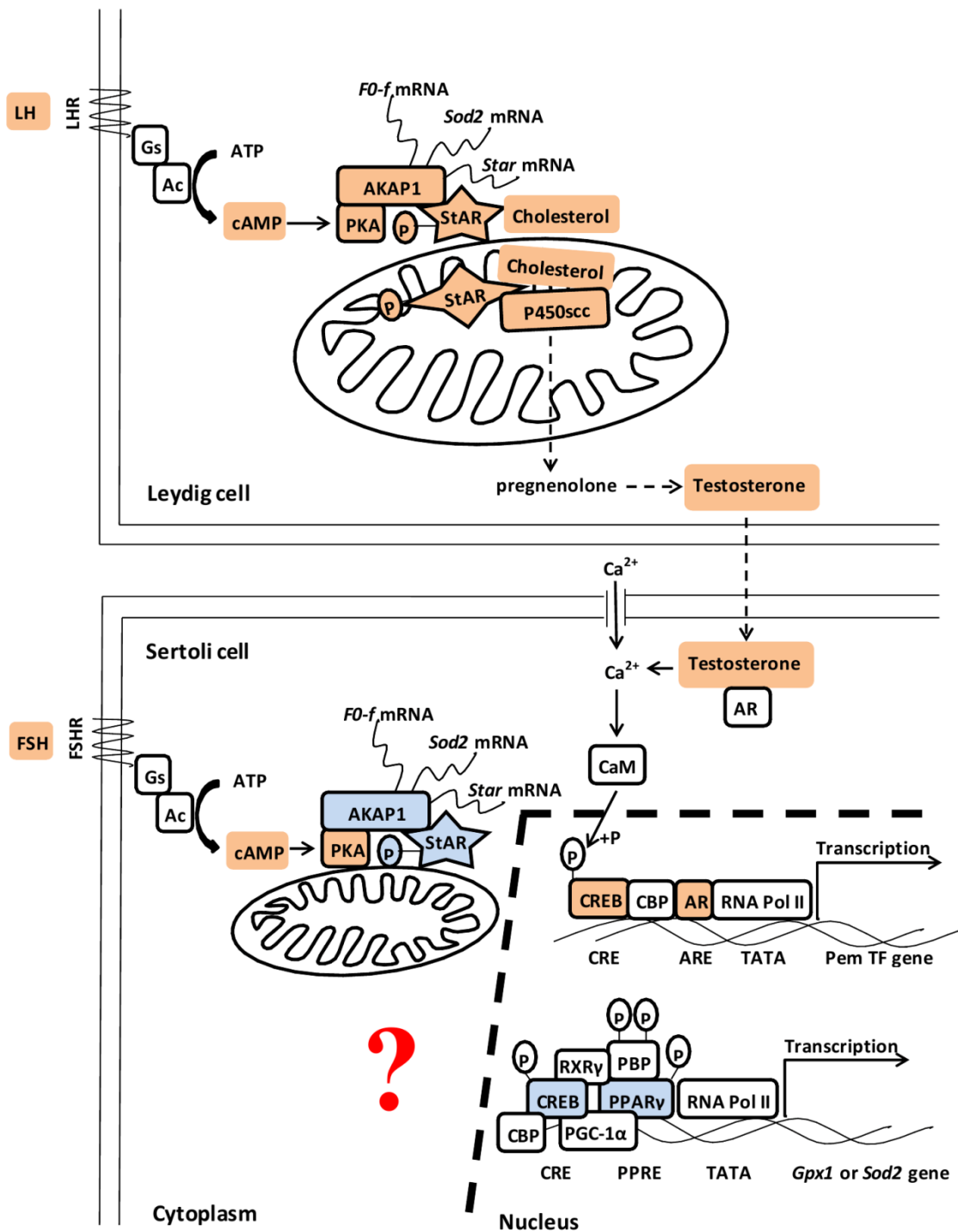


Figure 57 Testis steroidogenesis pathway cooperated between Leydig cell and Sertoli cells. This schematic representative picture includes the integrated information from literatures (Misra et al., 2002; Wahli et al., 1995; Walker and Cheng, 2005), KEGG Pathway Database^① and findings and hypothesis from this thesis.

^① http://www.kegg.jp/kegg-bin/highlight_pathway?scale=1.0&map=map04913&keyword=FSH%20LH%20StAR

5.8 AKAP4 detection and *in vitro* localization

AKAP4 plays a conserved role in spermatogenesis throughout mammalian evolution. A study on *Akap4* gene characterization in a marsupial showed that, *Akap4* was not observed in any stage of the juvenile developing testis, and could only be detected in adult testis but not in any other adult tissue. The *AKAP4* 2.9kb mRNA was present in the cytoplasm of round and elongated spermatids. After the cleavage of the precursor pro-AKAP4, the mature AKAP4 protein was then transferred and targeted to the principal piece of the flagellum in the sperm tail, confirming the same observation by Nipper in 2006 (Hu et al., 2009; Nipper et al., 2006).

Unfortunately, a good model system of germ cell lines to study spermatogenesis up to spermatozoa development is not available (Lüers et al., 2006). Only GC2 cell is an available spermatocyte cell line, however the cells died early after transfection experiments (non-published data of our group). Also other groups experienced this problem and had used somatic cell lines (NIH3T3 and HEK293) for overexpression studies of an AKAP4-GFP fusion protein. A series of AKAP4-GFP fusion constructions were expressed. The presence of the pro-domain, the GFP-pro-AKAP4 fusion protein displayed a diffuse cytoplasmic localization. The mature GFP-AKAP4 fusion protein showed a punctate cytoplasmic pattern instead. It was shown that the pattern of fusion protein localization was dependent on neither the type of cell line, nor the position of GFP (N- or C-termini) (Nipper et al., 2006). So the AKAP4 targeting signal sequence is probably not located in N- or C-terminus, but was suggested to be localized in the middle piece (Hu et al., 2009).

Consistent with these observations, *Akap4* mRNA was solely detected in mouse testis tissue in this study (Figure 43), but not in any other organs or TM4 cell line which was derived from immature mouse Sertoli cells (Figure 44). The expression of either N-term or C-term myc-tagged full length AKAP4 in TM4 cells proved to be extremely difficult and seemed to interfere with their viability. We were able to detect only one or two transfected cells which displayed a cytoplasmic staining in TM4 cells (Figure 52-53). In comparison to NIH3T3 and HEK293, transfections of full-length AKAP4 in TM4 cells seemed to be detrimental for the cell survival.

6 Outlook (future plan)

Many different external stimulations could initiate the cAMP generation and PKA activation. To get an appropriate downstream response it is critical to maintain a healthy and balanced cellular state. AKAPs enhance the efficiency of cAMP signal-transducing pathways by tethering PKA near sites of cAMP generation or PKA targets, and rigidly control the downstream response through specific spatial and temporal expression (McConnachie et al., 2006). Further research on the precise functional residues of AKAP complex and its tertiary and quaternary structure, could be a solution for gene cure application in medicine. For example, we supposed that the myc-tag in the C-terminus hindered the spatial structure of the AKAP1 KH domain. Further studies using overexpression of the recombinant AKAP1 without the KH domain or replaced with a junk sequence could verify whether it exerts an influence on its localization and the observed low SOD2 levels in mitochondria. A series of point mutation assays could provide answers concerning the critical binding residues.

AKAPs form signal transduction units, “transduceosomes”, which include not only protein kinases and phosphatases, but also adenylate cyclase (AC), PDE and mRNA. For example, AKAP1 and other binding partners form a “transduceosome” complex at the OMM that organizes different signaling enzymes, receptors, adaptor molecules and mRNAs. The “transduceosome” focuses and functionally integrates distinct transduction pathways, placing the enzymes into specific sub-cellular contexts and optimizing signaling events on co-localized effectors. This type of regulation, based on protein modification, can rapidly adapt mitochondrial activity to changes in metabolic demands and nutrients availability (Carlucci et al., 2008). At present, 3 recombinant AKAPs plasmids have been constructed with both N- and C-terminal myc tag (Figure 45). Further co-immunoprecipitation assays and construction of deletion mutants could be used for “transduceosome” research of AKAP1, 4 and 10, in order to reveal their binding partners and signaling pathway cross-talks.

Taken together, the data on AKAP1, 4 and 10 suggests their important role on precise regulation of cellular phosphorylation events. Future studies will focus on AKAPs sequence feature and metabolic pathway regulation mechanism.

7 Summary

Sertoli cells in the testis regulate spermatogenesis and are involved in the molecular pathogenesis of male infertility, an increasing problem worldwide. They are controlled by testosterone and FSH signaling, which increases the intracellular cAMP-levels, leading to the activation of protein kinase A (PKA) and downstream phosphorylation events. Compartmentalization of PKA-dependent phosphorylation is controlled by a variety of distinct A-kinase anchoring proteins (AKAPs), tethering PKA by high affinity binding to a particular subcellular location. In this respect, it is of interest that rat AKAP220, partially homologous to the AKAP11 family, was described in peroxisomes of rat Sertoli cells, essential organelles for maintenance of normal lipid homeostasis and spermatogenesis regulation in this cell type.

Therefore, the aims of this thesis were to analyze the effects of FSH treatment on peroxisomal gene expression, to characterize the effect of PKA-AKAP220 signaling on peroxisomes and to eventually discover new AKAP family members localized in this cell organelle or in mitochondria in Sertoli cells. Mouse TM4 Sertoli cells were used as cell culture model system to study the effects of FSH signaling on the peroxisomal and mitochondrial compartment. Since it is well established in the literature that the mitochondrial steroidogenic acute regulatory protein (StAR) is stimulated by LH-receptor/PKA-AKAP-signaling in testicular Leydig cells, the *Star* mRNA expression was assessed in TM4 Sertoli cells. Indeed, the *Star* gene was expressed in TM4 Sertoli cells and its expression level was also FSH-regulated. With optimized cell culture and FSH-treatment conditions, the gene expression for a variety of peroxisomal biogenesis and metabolic proteins was analyzed. FSH-treatment induced the expression of *Pex11a*, *Pex13*, *Cat*, *Acox2*, and *Abcd2* mRNAs, encoding proteins involved in proliferation, matrix protein import, ROS and lipid metabolism in peroxisomes, demonstrating that the organelle is influenced by FSH signaling. To verify the peroxisomal localization of AKAP220 (=AKAP11) and to study its effects on FSH-PKA-mediated spermatogenesis regulation, this protein was localized with a commercial antibody in different subcellular fractions and highly purified peroxisomes of TM4 cells. However, our follow-up experiments with Western blots, bioinformatic evolutionary tree analysis for conserved PTS1 signals in AKAPs, and sequence alignments between *Akap11* cDNA and genome sequences revealed that the reported cloned rat *Akap220* cDNA as well as the subsequent results of AKAP220 subcellular localization were artifacts.

Furthermore, during the series of experiments on rat *Akap11* mRNAs in our laboratory, total RNA from a variety of rat tissues was isolated and the tissue-specific *Akap11* gene expression was analyzed with specific sets of primer pairs, which revealed the highest *Akap11* mRNA levels in the testis, pituitary, total brain and spleen and intermediate levels in liver, lung, heart and skeletal muscle. The same primers were used for subcloning parts of *Akap11* in plasmid vectors for *in vitro* transcription of DIG-labelled cRNA-probes for *Akap11* as well as corresponding mRNA controls. A non-radioactive Northern blot method was established, which can be used for future experiments on alternative splicing of *Akap* mRNAs.

During the intensive bioinformatics screenings with partially program developed from Python and R in this study, new AKAP proteins (AKAP1, AKAP4 and AKAP10) were identified with a putative peroxisomal targeting signal 1 (PTS1), which were also highly expressed in testis as shown by RT-PCR analysis. Thereafter, series of subcellular localization experiments were performed to confirm the PTS1 prediction results. For this purpose, the complete open reading frames of mouse *Akap1*, *Akap4* and *Akap10* cDNAs were cloned into two different myc-tag vectors for expression of N- or C-terminal myc-tagged fusion proteins in TM4 Sertoli cells. As controls, myc-tagged GFP constructs were made in the same plasmid vectors, which were used for optimization of TM4 cells transfection and detection of the expressed fusion proteins by immunofluorescence with an anti-myc antibody. The expressed N- or C-terminal myc-tagged fusion proteins of all AKAPs (AKAP1, AKAP4 and AKAP10) were detected and tried to colocalize with mitochondria or peroxisomes by using double-immunofluorescence with antibodies against myc/SOD2 or myc/PEX14p, followed by analysis with conventional fluorescence microscopy or confocal laser scanning microscopy (CLSM). Only AKAP1-C-myc exhibited a typical mitochondrial distribution pattern and colocalization with SOD2 and exerted strong effects on the appearance of the mitochondrial network, whereas all other constructs exhibited a cytoplasmic localization pattern. Effects on SOD2 regulation in mitochondria were also noted. There was no co-localization of any of the fusion proteins with peroxisomes, suggesting that the putative C-terminal PTS1 in the AKAPs is not functional. In N-myc-AKAP10 preparations, the peroxisomes exhibited a more rod-shaped and less tubular pattern and giant cells were present. The absence of a single cell with AKAP10-C-myc expression indicates induction of cell death with yet unknown mechanism.

In conclusion, this thesis established the basic methods and the necessary recombinant tools were established to analyze the functions of several AKAPs in a Sertoli cell model system. AKAPs with putative C-terminal targeting signals (AKAP1, AKAP4, AKAP10) were not targeted to peroxisomes, but exerted strong effects on mitochondria or cell survival. How these proteins exert these effects on a molecular basis and whether other AKAP families are involved in the control of peroxisomal metabolism remains to be elucidated in the future.

8 Zusammenfassung

Sertoli-Zellen im Hoden regulieren die Spermatogenese und wirken an der molekularen Pathogenese männlicher Infertilität mit, einem zunehmenden medizinischen Problem weltweit. Sie werden durch Testosteron und den FSH-Signalweg kontrolliert, der den Anstieg von intrazellulärem cAMP induziert, zur Aktivierung der Proteinkinase A (PKA) führt und nachfolgende Phosphorylierungsreaktionen auslöst. Die subzelluläre Lokalisierung PKA-abhängiger Phosphorylierungsprozesse wird durch verschiedene „A-kinase anchoring“-Proteine durchgeführt, die PKA durch hochaffine Bindung in spezifischen zellulären Kompartimenten verankern. Hierbei ist von Interesse, dass AKAP220 (=AKAP11) in Sertoli-Zellen der Ratte in Peroxisomen beschrieben wurde, essentiellen Zellorganellen in diesem Zelltyp zur Aufrechterhaltung der Homöostase des Lipidstoffwechsels und der Regulierung der Spermatogenese.

Deshalb waren die Ziele dieser Dissertation, die Auswirkung von FSH auf die peroxisomale Genexpression sowie die Auswirkungen der PKA-AKAP220-Signalkaskade auf Peroxisomen aufzudecken und eventuell neue AKAP-Familienmitglieder in dieser Zellorganelle oder in Mitochondrien zu charakterisieren. Maus TM4 Sertoli-Zellen wurden als Zellkulturmodell zum Studium der FSH-Effekte auf das peroxisomale und mitochondriale Kompartiment etabliert. Weil aus der Literatur bekannt ist, dass das „steroidogene akut regulatorische Protein“ (StAR) durch den LH-receptor/PKA-AKAP-Signalweg in testikulären Leydig-Zellen stimuliert wird, wurde die *Star* mRNA-Expression in TM4-Sertoli-Zellen untersucht. Tatsächlich, war die *Star*-Gen-Expression in TM4 Sertoli-Zellen vorhanden und auch die FSH-vermittelte Regulierung des *Star*-mRNA-Spiegels konnte nachgewiesen werden. Nach Optimierung der Zellkulturbedingungen und der FSH-Konzentrationen, wurde die Expression einer großen Anzahl von Genen für Biogenese- und metabolische Proteine der Peroxisomen analysiert. FSH-Behandlung führte zur erhöhten Expression von *Pex11a*-, *Pex13*-, *Cat*-, *Acox2*- und *Abcd2*-mRNAs, die Proteine für Proliferation, Matrixproteinimport, ROS-und Lipid-Stoffwechsel in Peroxisomen kodieren, was die Beeinflussung dieser Zellorganelle durch den FSH-Signalweg demonstriert. Um die peroxisomale Lokalisation von AKAP220 nachzuweisen und dessen Effekt auf die FSH-/PKA-vermittelte Spermatogeneseregulierung auszutesten, wurde versucht, dieses

Protein mittels eines gekauften Antikörpers in unterschiedlichen subzellulären Fraktionen und hochgereinigten Peroxisomenfraktionen nachzuweisen. Jedoch erbrachten alle Folgeexperimente mit Western blots, bioinformatischer Evolutionsanalyse von AKAP-Proteinen mit konservierten PTS1-Signalen sowie Sequenzvergleiche zwischen *Akap11*-cDNA und -Genomsequenzen, dass die beschriebene, klonierte Ratte *Akap220*-cDNA sowie auch alle nachfolgenden Resultate über die subzelluläre Lokalisation des AKAP220-Proteins, Artefakte in der publizierten Literatur darstellten.

Innerhalb der Serie von Experimenten zur *Akap11*-mRNA-Expression in unserem Labor, wurden eine große Anzahl von Gesamt-RNA-Proben aus verschiedenen Rattenorganen isoliert und die gewebsspezifische Expressionsanalyse der *Akap11*-mRNA unter Verwendung spezifischer Primerpaare analysiert, welche die höchsten *Akap11*-mRNA-Spiegel in Gesamt-RNA aus Hoden, Hypophyse, Gehirn (gesamt) und Milz erbrachte, gefolgt von mittelhohen Mengen in Leber, Lunge, Herz und Skelettmuskel. Mithilfe der gleichen Primerpaare wurde die Subklonierung von verschiedenen *Akap11*-Anteilen in Plasmidvektoren zur Herstellung von DIG-markierten cRNA-Proben für *Akap11* durchgeführt, entsprechende Vektoren für interne Kontrollen kloniert und eine nichtradioaktive Northern Blot-Methode etabliert, mit deren Hilfe in zukünftigen Experimenten alternative Spleißformen von *Akap*-mRNAs nachgewiesen werden können.

Während der intensiven bioinformatischen Analysen mit teilweise selbst geschriebenen Softwareprogrammen, wurden neue AKAP-Proteine (AKAP1, AKAP4, AKAP10) mit potentiellen peroxisomalen Zielerkennungssignalen (PTS1, „peroxisomal targeting signal 1“) identifiziert, die auch in hoher Menge im Hoden vorkommen, wie durch RT-PCR-Analyse gezeigt wurde. Um die bioinformatische PTS1-Vorhersage zu verifizieren, wurden im Folgenden Serien von Experimenten zur subzellulären Lokalisation dieser Proteine durchgeführt. Für diesen Zweck wurden jeweils die proteinkodierenden Regionen PCR-amplifizierter *Akap1*-, *Akap4*- und *Akap10*-cDNAs der Maus in zwei unterschiedliche myc-Tag-Vektoren zur Expression N- und C-terminaler myc-Fusionsproteine in TM4 Sertoli-Zellen kloniert. Als Kontrollvektoren wurden myc-Tag-GFP-Konstrukte der gleichen Vektoren hergestellt, die die Optimierung der TM4 Sertoli-Zell-Transfektion und der Detektion der myc-Fusionsproteine durch Immunfluoreszenz mittels eines anti-myc-Antikörpers

ermöglichten. Die exprimierten N- und C-terminalen myc-Fusionsproteine aller AKAPs (AKAP1, AKAP4, AKAP10) wurden durch Doppelimmunfluoreszenz mit Antikörpern gegen myc/SOD2 oder myc/PEX14p detektiert und versucht, mit Mitochondrien oder Peroxisomen zu kolokalisieren. Alle Doppelimmunfluoreszenz-Präparate wurden mittels konventioneller Fluoreszenzmikroskopie und konfokaler Laserscanning-Mikroskopie (CLSM) ausgewertet. Nur das exprimierte AKAP1-C-myc-Protein zeigte ein typisch mitochondriales Verteilungsmuster, kolokalisierte mit SOD2 und induzierte starke Veränderungen des mitochondrialen Netzwerks, während alle anderen exprimierten Fusionsproteine eine cytoplasmatische Lokalisation aufwiesen. Kolokalisation der exprimierten Fusionsproteine mit Peroxisomen wurde nicht gefunden, was für die fehlende Funktionalität der putativen PTS1-Sequenz am C-terminalen Ende der AKAPs für den Import in Peroxisomen spricht. Jedoch wies das morphologische Organellenmuster der Peroxisomen in N-myc-AKAP10-exprimierenden Zellen vermehrt runde und weniger tubuläre Formen auf. Interessanterweise wurde in parallelen Experimenten keine einzige Zelle mit AKAP10-C-myc-Expression nachgewiesen, was für die Induktion von Zelltod durch dieses Fusionsprotein mittels eines bisher unbekannten Mechanismus spricht.

Zusammenfassend lässt sich feststellen, dass in dieser Dissertation die grundlegende Methodik und die notwendigen rekombinanten Werkzeuge zur Analyse der Funktionen verschiedener AKAPs in einem in einem Sertoli-Zellkultur-Modell etabliert wurden. AKAPs mit putativen PTS1-Sequenzen (AKAP1, AKAP4, AKAP10) wurden nicht in Peroxisomen importiert, lösten jedoch starke Effekte in dem mitochondrialen Netzwerk und auf das Zellüberleben aus. Wie diese Proteine diese Effekte auf molekularer Ebene auslösen und ob andere AKAP-Familien in die Kontrolle des peroxisomalen Metabolismus eingeschaltet sind, soll in der Zukunft aufgeklärt werden.

9 List of abbreviations

ABC	ATP-binding cassette
ABP	Androgen-binding protein
AC	Adenylyl cyclase
ACDH	Acyl-CoA dehydrogenase
ACOX1	Acyl-CoA oxidase 1
ADAPS	Alkyl dihydroxyacetonephosphate synthase
AKAP	A-kinase anchoring protein
Ago2	Argonaute 2
AGT1	Glyoxylate aminotransferase 1
ALD/AMN disease	Adrenoleukodystrophy/Adrenomyeloneuropathy disease
Amp	Ampicillin
AR	Androgen receptor
ARE	Androgen response elements
ARTs	Assisted reproductive techniques
AQP2	Aquaporin 2
AVP	Arginine vasopressin
BTB	Blood-testis barrier
BSA	Bovine Serum Albumin Acetylated
Ca ²⁺	Calcium
CaM	Calmodulin
cAMP	Cyclic adenosine monophosphate
CaN (PP2B)	Calcium-activated Ser/Thr phosphatase calcineurin
CCS	Copper chaperone of SOD1
CLSM	Confocal laser scanning microscopy
CNG (cNGC)	Cyclic nucleotide gated ion channel
COX	Cytochrome c oxidase
CPT1	Carnitine-palmitoyltransferase
CREB	cAMP response element binding protein
CT	Cholera toxin
DAPAT	Dihydroxyacetonephosphate acyltransferase
D/D domain	Dimerization/docking domain
DEPC	Diethyl pyrocarbonate
Drp1	Dynamin related protein 1

DIG	Digoxigenin
eSpt	elongated spermatids
Siah2	E3 ubiquitin-protein ligase 7 in absentia homolog 2
SOD1	Cu/Zn superoxide dismutase 1
EDAs	Endocrine disrupting agents
EGF	Epidermal growth factor
Epac	Exchange proteins directly activated by cAMP (cAMP-activated GTP-exchange factors)
EST	Expressed sequence tag
F0-f	ATP synthase F0 complex
FGF	Fibroblast growth factor
Fis1	Fission factor 1
FSH	Follicle-stimulating hormone
FSHR	Follicle-stimulating hormone receptor
FSIP1	Fibrous Sheath Interacting Proteins 1
FSK	Forskolin
GNPAT	Glyceronephosphate O-acyltransferase
GPCR	G protein-coupled receptor
GSK-3 β	Glycogen synthase kinase 3 β
GV stage	Germinal vesicle stage
HGNC	Human genome organization nomenclature committee
HIF-1 α	Hypoxia induced factor 1 α
HIV-1 RT	HIV-1 reverse transcriptase
IBMX	3-Isobutyl-1-methylxanthine
IGF-1	Insulin-like growth factor-1
IMAGE	Intergrated Molecular Analysis of Gonomes and their Expression
IQGAP1	IQ domain GTPase-activating protein 1
IVF	<i>in vitro</i> fertilization
KH domain	K homology domain
LDHA	Lactate dehydrogenase A
LDHB	Lactate dehydrogenase B
LPL	Lipoprotein lipase
LH	Luteinizing hormone
LHR	Luteinizing hormone receptor
MAVS	Mitochondrial antiviral signaling adaptor
Mff	Mitochondrial fission factor
Mfn1	Mitofusion1

MFP-2 (HSD17B4)	Multifunctional protein-2
MIS	Mullerian-inhibiting substance
MnSOD (SOD2)	Manganese superoxide dismutase
MOM	Mitochondrial outer membrane
MVBs	Multivesicular bodies
MYCBP (AMY-1)	c-myc binding protein
NMDA	<i>N</i> -methyl-D-aspartate receptor 2B
NMJ	Neuromuscular junction
ODFs	Outer dense fibers
OPA1	Optic atrophy 1
OPLs	Oral premalignant lesions
P450 _{scc} (CYP11A1)	cytochrome P450 side-chain cleavage enzyme
PBS	Phosphate-buffered saline
PC	Prostate cancer
PCR	Polymerase-chain reaction
PDE	Phosphodiesterase
PGC-1 α	PPAR γ coactivator -1 α
PKA	Protein kinase A
PMD1	Peroxisomal and Mitochondrial Division Factor 1
POMA	Paraneoplastic opsoclonus-myoclonus-ataxia
PP1	Protein phosphatase 1
PPAR γ	Peroxisome proliferator-activated receptor γ
PPRE	Peroxisome proliferator responsive element
PTC	Peritubular cells
PTPD1	Protein tyrosine phosphatase D1
PTS1	Peroxisomal targeting signal 1
PTSP	Peroxisomal Target Signal Predictor
PUFA	Polyunsaturated fatty acids
PVDF	Polyvinylidene fluoride
RIAD	RI-anchoring disruptor
RIIBD	RII-binding domain
RB protein	Retinoblastoma protein
rSpt	round spermatids
RXR	Retinoid X receptor
SC	Sertoli cells

SCD	Sudden cardiac death
SDS-PAGE	Sodium dodecyl sulfate-polyacrylamide gel electrophoresis
Siah2	Seven in absentia homolog
Spc	Spermatocytes
Spg	Spermatogonia
StAR	Steroidogenic acute regulatory protein
TDS	Testicular Dysgenesis Syndrome
THIO	3-ketoacyl-coenzyme A thiolase
TSHR	Thyroid-stimulating hormone receptor
TGF	Transforming growth factor
TSHR	Thyroid-stimulating hormone receptor
3'-UTR	3' untranslated region
V ₂ R	Vasopressin type 2 receptor
VLCFA	Very long chain fatty acids
WHO	world health organization

10 Figure index

Figure 1 Schematic illustration of testis structure (Figure 1A) and the hypothalamic-pituitary-testicular axis (Figure 1B).	9
Figure 2 FSH stimulated cAMP-PKA signaling pathway (Figure 2A) and localization of PKA C α in different cell types of a seminiferous tubule in the testis of a 120d-old wild-type mouse (Figure 2B ₁) and in TM4 Sertoli cells (Figure 2B ₂ -2B ₃).	11
Figure 3 AKAPs assemble the key enzymes and factors	15
Figure 4 Alignment of the PKA RII-binding regions of the indicated AKAPs and artificial disruptor peptides derived.....	16
Figure 5 Crystal structure (PDB ID: 2HWN).....	17
Figure 6 Schematic diagram of hAKAP220.....	19
Figure 7 Schematic diagram of AKAP220 complex leading function in cell migration	21
Figure 8 Schematic diagram of mouse AKAP1 (AKAP121).....	23
Figure 9 Structure of a KH domain (PDB ID: 2ANR).....	23
Figure 10 A model illustrating post-transcriptional and post-translational regulation of StAR.	25
Figure 11 A model illustrating of AKAP1 scaffold complex on the mitochondrial outer membrane	27
Figure 12 Normal sperm structure.....	28
Figure 13 Brief overview of major metabolic pathways and peroxins (in number) in peroxisomes of the mammalian testis. This picture is adapted from (Colasante et al., 2015; Fahimi and Baumgart, 1999).....	33
Figure 14 Schematic illustration of peroxisome purification by OptiPrep™ (keep all solutions and carry out all operations at 4 °C).	57
Figure 15 An example of RNA-Chip results to check the quality of isolated RNAs.....	60
Figure 16 workflow of Northern blot	61
Figure 17 Phylogenetic tree of AKAPs with putative PTS1	75
Figure 18 Conventional RT-PCR of internal control and positive control	78

Figure 19 Conventional RT-PCR results of alterations of mRNA levels of peroxins on peroxisome proliferation	78
Figure 20 Conventional RT-PCR results of alterations of mRNA levels of peroxins on peroxisomal matrix protein import.....	78
Figure 21 Conventional RT-PCR results of alterations of mRNA levels of antioxidative enzymes	79
Figure 22 Conventional RT-PCR results of alterations of mRNA levels of Acyl-CoA oxidases	79
Figure 23 Conventional RT-PCR results of alterations of mRNA levels of fatty acid transporters	80
Figure 24 Conventional RT-PCR results of PPAR transcription factors	80
Figure 25 Peroxisome marker PEX14p	82
Figure 26 Western blot of AKAP220.....	82
Figure 27 BLAST Results of <i>Akap11</i> mRNAs from Genome Database	85
Figure 28 The sequence in the orange frame shows two potential <i>EcoRI</i> linkers in mRNA [U48288.1].....	87
Figure 29 Schematic illustration of the alignment and position of <i>Akap11</i> rat mRNA .	89
Figure 30 Constructed plasmids maps, including <i>Akap11</i> rat mRNA specific hybridization probes LSP (230bp), BSP1 (308bp), BSP2 (893bp) and BSP3 (608bp) and housekeeping gene probes, such as GAPDH (417bp), β -actin (120bp), 28S rRNA (254bp), and StAR (292bp).....	90
Figure 31 Plasmids linearization for <i>in vitro</i> transcription.....	91
Figure 32 Sensitivity of DIG-labeled antisense RNA probes were verified by dot blot assay (40s exposure).....	91
Figure 33 Test of 9 different types of washing buffer with 2 distinct dilutions of anti-DIG concentration (40s exposure)	92
Figure 34 Rat tissue total RNA dot blot hybridization with 4 probes	94
Figure 35 Total RNA separation by electrophoresis	95
Figure 36 Distribution profile of <i>Akap11</i> mRNA in different rat organs.....	96

Figure 37 PCR product with T7 promotor	97
Figure 38 PTS1 prediction of all AKAP1 family members in different species.....	99
Figure 39 PTS1 prediction of all AKAP4 family members in different species,.....	100
Figure 40 PTS1 prediction of all AKAP10 family members in different species,.....	101
Figure 41 <i>Akap1</i> , <i>Akap4</i> and <i>Akap10</i> distribution profile	102
Figure 42 <i>Akap1</i> , <i>Akap4</i> and <i>Akap10</i> mRNA are high expressed in testis.	103
Figure 43 Test of designed primers for <i>Akap1</i> , <i>Akap4</i> , <i>Akap10</i> , and their expression level in different mouse organs	104
Figure 44 Test expression of <i>Akap1</i> , <i>Akap4</i> , <i>Akap10</i> in TM4 Sertoli cell line	105
Figure 45 The instruction of myc-tag recombined plasmids generation (inserts are: GFP, AKAP1, AKAP4 and AKAP10).....	108
Figure 46 Co-localization test for the myc-tagged GFP-fusion proteins as positive controls, N-terminal myc-labelled GFP (GFP-3B) plasmid and C-terminal myc- labelled GFP (GFP-5B) plasmid.	110
Figure 47 Immunofluorescence images showing peroxisomal membrane staining (A-D) in untreated TM4 cells.....	111
Figure 48 Immunofluorescence images showing peroxisomal (A-C) and mitochondrial (D-F) matrix staining in untreated TM4 cells..	112
Figure 49 Double-immunofluorescence showing for the myc-tag and PEX14p, revealing that both myc-tagged AKAP1 fusion proteins did not co-localize with peroxisomes.....	113
Figure 50 Double-immunofluorescence showing that N-terminal myc-tagged AKAP1 (AKAP1-3B) was not co-localized with mitochondria (Figure 50A-C), but C- terminal myc-tagged AKAP1 (AKAP1-5B) was (Figure 50D-F)..	114
Figure 51 CLSM images of double-immunofluorescence for myc and SOD2, showing that N-terminal myc-tagged AKAP1 (AKAP1-3B) was not co-localized with mitochondria (Figure 51A-B), but C-terminal myc-tagged AKAP1 (AKAP1-5B) was (Figure 51C-D).....	116

Figure 52 Double-immunofluorescence preparations for myc and SOD2, showing two types of myc-tagged AKAP4 were both expressed in the cytoplasm and did not co-localize with mitochondria in TM4 cell line..	117
Figure 53 CLSM images of double immunofluorescence preparations for myc and SOD2, showing two types of myc-tagged AKAP4 fusion proteins which were both localized with cytoplasm and did not target to mitochondria in TM4 cell line..	118
Figure 54 Double-immunofluorescence preparation for myc and PEX14p, showing that N-terminal myc-tagged AKAP10 (AKAP10-3B) did not co-localize with peroxisomes.....	119
Figure 55 Double-immunofluorescence preparation for myc and SOD2, showing that the N-terminal myc-tagged AKAP10 (AKAP10-3B) did not co-localize with mitochondria.....	119
Figure 56 CLSM images of a double immunofluorescence preparation for myc and SOD2, showing that the N-terminal myc-tagged AKAP10 (AKAP10-3B) did not co-localize with mitochondria.....	120
Figure 57 Testis steroidogenesis pathway cooperated between Leydig cell and Sertoli cells.....	130

11 Tabel index

Table 1 Cell line and medium (information from ATCC search and Health Protection Agency cell line data sheet 50004291)	36
Table 2 Routine reagents list	36
Table 3 Buffer recipes	39
Table 4 Commercial plasmids information	41
Table 5 List of primers designed and used in this study	42
Table 6 Antibody dilution list.....	47
Table 7 Properties and preparation of Iodixanol-sucrose solution	55
Table 8 <i>Taq</i> -PCR reaction	65
Table 9 <i>Pfu</i> -PCR reaction.....	65
Table 10 Restriction enzyme digestion of GFP and 3 AKAPs (4h incubation at 37 °C) 67	
Table 11 Ligation reaction (overnight incubation at 4 °C).....	68
Table 12 Chemical structure of common used antibiotics.....	70
Table 13 AKAP1-Mutation-PCR reagent.....	70
Table 14 AKAP1-Mutation-PCR <i>Dpn</i> I digestion (4h incubation at 37 °C).....	71
Table 15 Summarized PTS1 tripeptides derived from the “Peroxisomal Target Signal Predictor (PTSP)”	74
Table 16 Optimization of cell density to obtain a monolayer of TM4 cells on Day 4-677	
Table 17 Total RNA was isolated using combined methods, and the RNA quality was checked by RNA-Chip analysis	87
Table 18 Total RNA precipitation	97

12 Supplemental data

S 1 Python codes used in this study (see subsection 3.1.3)

seq_num_len_des_read-code.py:

```
from Bio import SeqIO
AKAP_file = 'All AKAP1 protein from NCBI-143 seq.fasta'
Read_file = 'seq_num_len_des_read.txt'
Handle = open(Read_file,'w')
Handle.write("seq_index\t" + "seq_length\t" + "seq_description\n")
num = 0
for seq_record in SeqIO.parse(AKAP_file,'fasta'):
    num = num + 1
    seq_len = str(len(seq_record.seq))
    seq_des = str(seq_record.description)
    Handle.write(str(num) + '\t' + seq_len + 'aa\t' + seq_des + '\n')
Handle.close()
```

Remove_duplicate_seq-code.py:

```
from Bio import SeqIO
from Bio.Seq import Seq
from Bio.SeqRecord import SeqRecord

seq_map_des = { }
AKAP_file = 'All AKAP1 protein from NCBI-143 seq.fasta'
Handle_out = open("seq_without_duplicate.txt", "w")
Handle_id = open("id_order.txt", "w")

for seq_record in SeqIO.parse(AKAP_file, "fasta"):

    seq_str = str(seq_record.seq)
    seq_des = str(seq_record.description)
    if seq_str not in seq_map_des:

        seq_map_des[seq_str] = [seq_des]
    else:

        if len(seq_des) > len(seq_map_des[seq_str][0]):
            seq_map_des[seq_str].insert(0,seq_des)
        else:

            seq_map_des[seq_str].append(seq_des)

num = 0
for map_seq in seq_map_des:
    Handle_out.write(">" + seq_map_des[map_seq][0] + "\n" + map_seq + "\n")
    num = num + 1
    Handle_id.write(str(num) + ":\t" + str(len(map_seq)) + "aa\t" + ''.join(seq_map_des[map_seq]) + '\n')
Handle_out.close()
Handle_id.close()
```

AKAP_domain_selection-code.py:

```
from Bio import SeqIO
import re
AKAP_file = 'seq_without_duplicate.txt'
True_file = 'AKAP_true_protein.txt'
False_file = 'AKAP_false_protein.txt'
True_file_info = 'AKAP_true_protein_info.txt'
```



```

Handle_info = open(True_file_info, 'w')
Handle_info.write('Seq_num' + '\t' + 'Seq_ID' + '\t' + 'Length_aa' + '\t' + 'AKAP_domain' + '\t' +
'AKAP_Start' + '\t' + 'AKAP_End' + '\n')

Handle_False = open(False_file, 'w')
Handle_True = open(True_file, 'w')

num = 0
for seq_record in SeqIO.parse(AKAP_file, 'fasta'):
    seq_id = seq_record.id
    seq_des = seq_record.description
    seq_len = str(len(seq_record))
    seq_str = str(seq_record.seq)

    pattern = '[AVLISE]..[AVLIF][AVLI]..[AVLI][AVLIF]..[AVLISE]'
    find_pattern = re.search(pattern, str(seq_record.seq))
    if find_pattern:
        num = num + 1
        start_site = str(find_pattern.start() + 1)
        end_site = str(find_pattern.end())
        Handle_info.write(str(num) + '\t' + seq_id + '\t' + seq_len + '\t' + find_pattern.group() + '\t' +
start_site + '\t' + end_site + '\n')
        Handle_True.write('>' + seq_des + '\n' + seq_str + '\n')
    else:
        Handle_False.write('>' + seq_des + '\n' + seq_str + '\n')

Handle_info.close()
Handle_True.close()
Handle_False.close()

```

PTS1_predictor_filter-code.py:

```

import urllib
from Bio import SeqIO
import re

handle_file = open("PTS1_pred_score.txt", "w")
handle_file.write("Seq_num" + "\t" + "Seq_name" + "\t" + "C-terminus_12seq" + "\t" + "Pred_Score"
+" \t" + "Classification" + "\n")

url = 'http://mendel.imp.ac.at/jspcgi/cgi-bin/pts1/pts1.cgi'
num = 0
for seq_record in SeqIO.parse('AKAP_true_protein.txt', 'fasta'):
    num = num + 1
    speices_pattern = re.compile("[(.+)\]")
    name_data = "AKAP1_" + speices_pattern.findall(seq_record.description)[0]
    pred_in = re.search("PREDICTED", seq_record.description)
    if pred_in:
        name_data = name_data + "_pred_seq"
    else:
        name_data = name_data + "_real_seq"
    seq_data = str(seq_record.seq)[-20:] + '\n'
    query_data = {"function": "3", "name": name_data, "sequence": seq_data}
    result_info = urllib.urlopen(url, urllib.urlencode(query_data))
    result = result_info.read()

    C_ter_pattern = re.compile('<tr><td>C-terminus</td><td>(.+)</td></tr>')
    score_pattern = re.compile("<tr><td><b>Score</b><td><b>(.+)</b></td></tr>")
    pred_clas_pattern = re.compile("<tr><td><i>Prediction classification</i></td><td>(.+)</td></tr>")

```

```

C_terminus = C_ter_pattern.findall(result)[0]
score = score_pattern.findall(result)[0]
pred_clas = pred_clas_pattern.findall(result)[0]

  handle_file.write(str(num) + "\t" + seq_record.id + "_" + name_data + "\t" + C_terminus + "\t" + score
+ "\t" + pred_clas + "\n")

handle_file.close()

```

Barplot_AKAP1.R:

```

Rdata <- read.table("AKAP_PTS1_for_R.txt", sep = "\t", header = TRUE)
domain_start <- Rdata$AKAP_Start
domain_end <- Rdata$AKAP_End
seq_length <- Rdata$Length_aa
seq_name <- as.matrix(Rdata$Seq_name)
PTS1_Pred <- as.matrix(Rdata$Classification)
c_terminus <- as.matrix(Rdata$C.terminus_12seq)

barplot_data = NULL
for(i in 1:length(domain_start))
{
  if(PTS1_Pred[i] == "Targeted")
  {
    barplot_data <- cbind(barplot_data, c(domain_start[i] - 0, domain_end[i] - domain_start[i],
seq_length[i] - domain_end[i], 12))
  }
  else
  {
    barplot_data <- cbind(barplot_data, c(domain_start[i] - 0, domain_end[i] - domain_start[i],
seq_length[i] - domain_end[i], 0))
  }
}
colnames(barplot_data) = seq_name

png(filename = "AKAP1_domain_feature.png", width = 1200, height = 600, pointsize = 12)

par(mar=c(2, 18, 1, 1),bg = grey(1), ps= 6.5,cex =1)

b <- barplot(barplot_data, horiz = TRUE, col = c("light blue", "green", "light blue", "red"),space = 0.95,
las=1, xlim = c(0, max(seq_length) + 500))

text(x = seq_length + 90, y = b, labels = c_terminus)

dev.off()

pdf(file = "AKAP1_domain_feature.pdf", paper = "a4", width = 12, height = 12)

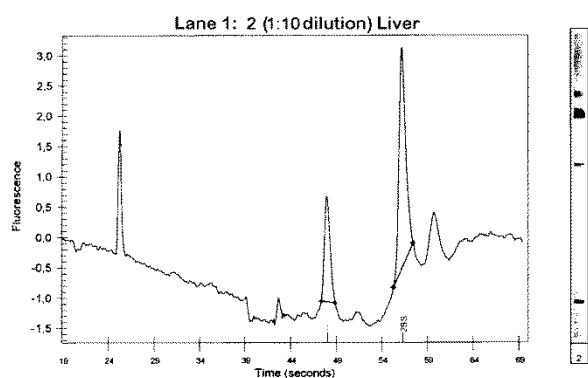
par(mar=c(2, 18, 1, 1),bg = grey(1), ps= 6.5,cex =1)
b <- barplot(barplot_data, horiz = TRUE, col = c("light blue", "green", "light blue", "red"),space = 0.95,
las=1, xlim = c(0, max(seq_length) + 500))

text(x = seq_length + 180, y = b, labels = c_terminus)

dev.off()

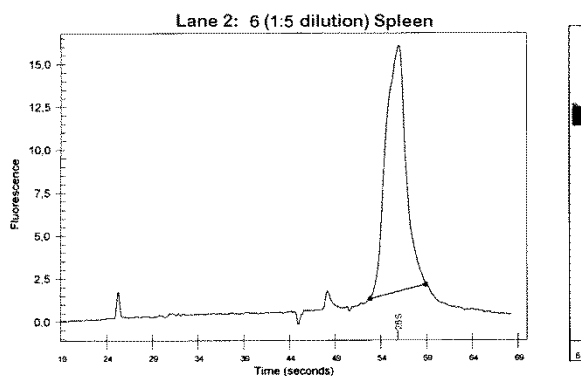
```

S 2 RNA Chip result to show the quality of total RNA isolated from rat tissues (see subsection 4.5.3)



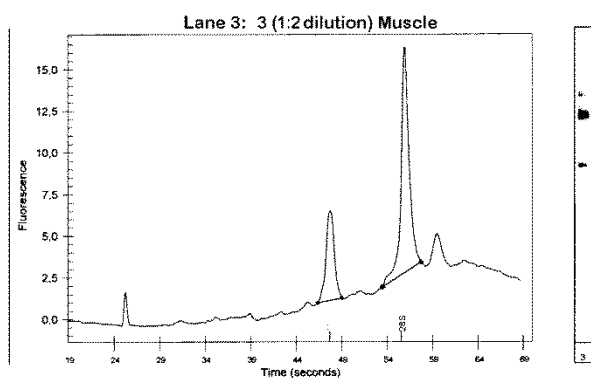
Corrected RNA Area: 5.47
RNA Concentration: 24.70 ng/ul
rRNA Ratio [28S / 18S]: 2.18

#	Name	Start Time (s)	End Time (s)	Corr.Area	% of total Area
1	18S	47.35	48.65	2.55	46.58
2	28S	55.25	57.40	5.56	101.69



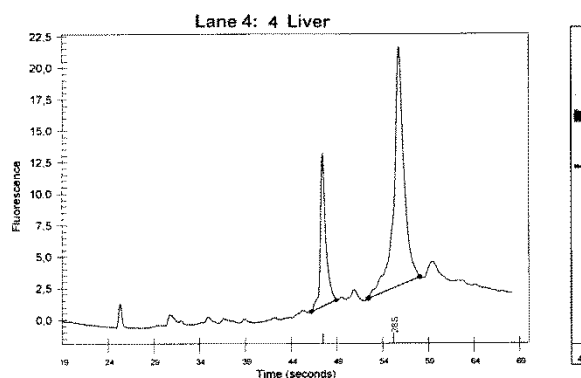
Corrected RNA Area: 110.61
RNA Concentration: 499.36 ng/ul
rRNA Ratio [28S / 18S]: 0.00

#	Name	Start Time (s)	End Time (s)	Corr.Area	% of total Area
1	28S	52.85	58.90	66.04	59.70



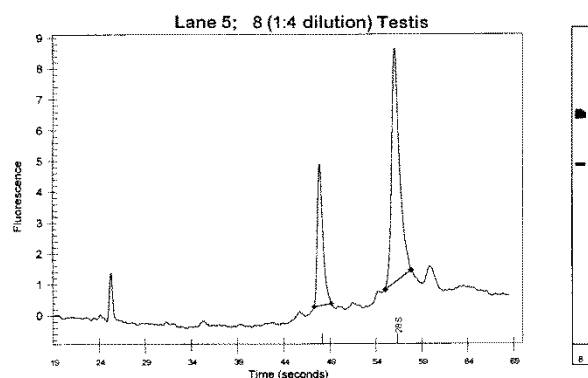
Corrected RNA Area: 59.71
RNA Concentration: 269.58 ng/ul
rRNA Ratio [28S / 18S]: 2.12

#	Name	Start Time (s)	End Time (s)	Corr.Area	% of total Area
1	18S	48.40	49.05	11.76	19.70
2	28S	53.50	57.70	24.89	41.69



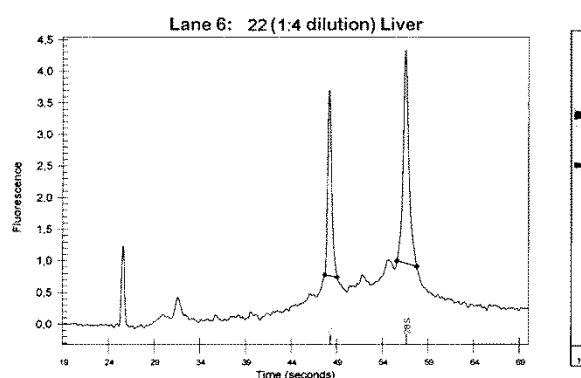
Corrected RNA Area: 88.54
RNA Concentration: 399.72 ng/ul
rRNA Ratio [28S / 18S]: 2.55

#	Name	Start Time (s)	End Time (s)	Corr.Area	% of total Area
1	18S	46.15	48.65	17.27	19.51
2	28S	52.40	58.05	44.06	49.76



Corrected RNA Area: 28.83
RNA Concentration: 130.14 ng/ul
rRNA Ratio [28S / 18S]: 2.06

#	Name	Start Time (s)	End Time (s)	Corr.Area	% of total Area
1	18S	47.25	49.15	6.50	22.55
2	28S	55.00	57.80	13.38	46.40



Corrected RNA Area: 26.17
RNA Concentration: 62.15 ng/ul
rRNA Ratio [28S / 18S]: 1.42

#	Name	Start Time (s)	End Time (s)	Corr.Area	% of total Area
1	18S	47.70	49.05	3.05	11.67
2	28S	55.60	57.75	4.34	16.57

S 3 The 531 types of C-terminal tripeptides of all known AKAPs retrieved from “UniProt” database (the orange marked are hits by the Combination Matrix from Table 15)

No.											
1	AAA	DEA	ENS	GQE	KEK	LGQ	NIR	PSS	RRR	TES	VLC
2	AAE	DED	ENT	GRD	KER	LIE	NKK	PST	RSR	TEY	VNL
3	ACQ	DEG	EPE	GSR	KGS	LIK	NLF	PTE	RTP	TFD	VQI
4	AEH	DEN	EPL	GTK	KIH	LIL	NLI	PTG	RVK	TFS	VRG
5	AES	DEV	EPT	GVA	KIT	LKF	NLT	PVH	RVL	TGS	VRR
6	AFI	DFS	EPV	HDT	KIV	LKK	NLY	PWN	RVV	THA	VSK
7	AFL	DGF	EQE	HFD	KKA	LKR	NNE	QAC	SAS	THH	VSP
8	AFW	DGK	EQN	HFY	KKI	LKV	NNS	QAD	SCH	TKG	VTE
9	AGP	DGS	ERG	HGK	KKK	LKW	NPG	QAL	SCL	TKI	VTV
10	AGS	DGT	ERH	HLG	KKR	LLH	NPR	QAQ	SDS	TKL	VVE
11	AHQ	DHS	ETL	HLL	KLA	LLK	NPS	QAV	SEA	TKR	VVM
12	AIE	DKK	EVI	HLS	KLC	LLQ	NPY	QDN	SEE	TKV	VYE
13	AIQ	DLI	EVV	HTA	KLL	LLS	NRK	QDY	SEI	TLN	VYS
14	AKG	DMY	FEC	HTE	KLS	LMY	NRR	QEV	SEN	TLT	WEA
15	AKL	DNE	FEM	HTG	KLV	LNA	NRV	QLE	SET	TLV	WLE
16	AKP	DNV	FGT	ICL	KMC	LNF	NSE	QLK	SFL	TMR	WNR
17	AKS	DNY	FHF	IDF	KMF	LQA	NTI	QMF	SFS	TMT	WSG
18	AKV	DQL	FIK	IDL	KMR	LQR	NVE	QNL	SGA	TNL	WSR
19	ALA	DRI	FKK	IEK	KNI	LRR	NVN	QRA	SGC	TPE	WSS
20	ALK	DSF	FLF	IFA	KPE	LRS	NVT	QRR	SGR	TQR	WTA
21	ALP	DSL	FLI	IFC	KPP	LSC	NYK	QRT	SIC	TRR	YAG
22	ALW	DSY	FNL	IFD	KQA	LSE	NYR	QRY	SIS	TSL	YAL
23	ANL	DTQ	FNN	IGA	KQD	LSI	PAC	QSC	SKK	TTC	YAP
24	ARK	DVE	FPE	IGE	KQI	LSK	PAE	QSF	SLE	TTI	YDP
25	ASE	EAE	FSL	IGK	KQN	LSM	PAV	QSG	SLG	TTL	YDT
26	ASG	EAP	FTL	IGR	KQP	LSR	PDP	QSP	SLS	TTV	YGS
27	ASL	EDA	FVK	IIC	KQS	LSV	PDT	QSQ	SNI	TTY	YIW
28	ASP	EDC	FYD	IIL	KRE	LSY	PEE	QTD	SPM	TVM	YKQ
29	ATE	EDN	GAP	IKE	KRL	LTK	PER	QTE	SPR	TVS	YMG
30	ATP	EDS	GCG	ILK	KRN	LTS	PES	QTG	SPS	TVV	YRN
31	ATV	EEE	GDE	IME	KSK	LVL	PFE	QVD	SRA	TYD	YSC
32	AVL	EEG	GEG	INF	KSN	LVQ	PGC	QVL	SRG	TYI	
33	AVQ	EEL	GEP	INR	KSP	LVS	PGE	RAA	SRS	TYK	
34	AWC	EEN	GET	INT	KTE	MAQ	PGG	RAE	SRV	VAA	
35	AYG	EEV	GGA	IPF	KVI	MEE	PGH	RAT	SSG	VAH	
36	CCP	EGF	GGG	IPS	KVL	MEQ	PGQ	RGF	SSL	VAP	
37	CDI	EGK	GGP	IQE	KVR	MFI	PGS	RGL	SSS	VDS	
38	CGK	EGT	GGS	IRR	KVV	MHR	PGW	RGR	SST	VEK	
39	CLF	EHA	GIS	ISK	KYL	MHS	PHK	RHL	STE	VER	
40	CLI	EIA	GKS	ISN	LDM	MIK	PIL	RKF	STI	VES	
41	CMK	EKD	GLG	ITF	LDQ	MKL	PKE	RKI	STK	VEV	
42	CPF	EKI	GLH	ITL	LEC	MKQ	PKN	RKY	STL	VFV	
43	CRL	EKK	GLP	IYE	LEE	MLE	PLN	RLA	STV	VGH	

44	CSK	EKT	GLS	KAL	LEF	MLV	PLP	RLC	SVL	VHA
45	CSQ	ELE	GME	KCY	LEK	MRR	PLQ	RLE	SVS	VHR
46	CTE	ELG	GNA	KDQ	LET	MVV	PLS	RLQ	TAS	VHV
47	DAS	ELT	GNE	KDS	LFF	NCK	PNV	RMA	TCE	VIV
48	DDD	ENA	GNG	KEA	LFL	NDN	PPE	RPV	TEE	VKL
49	DDE	ENI	GNL	KEE	LFQ	NEN	PPS	RQM	TEL	VKT
50	DDQ	ENP	GPA	KEF	L GK	NFS	PRE	RRD	TEM	VLA

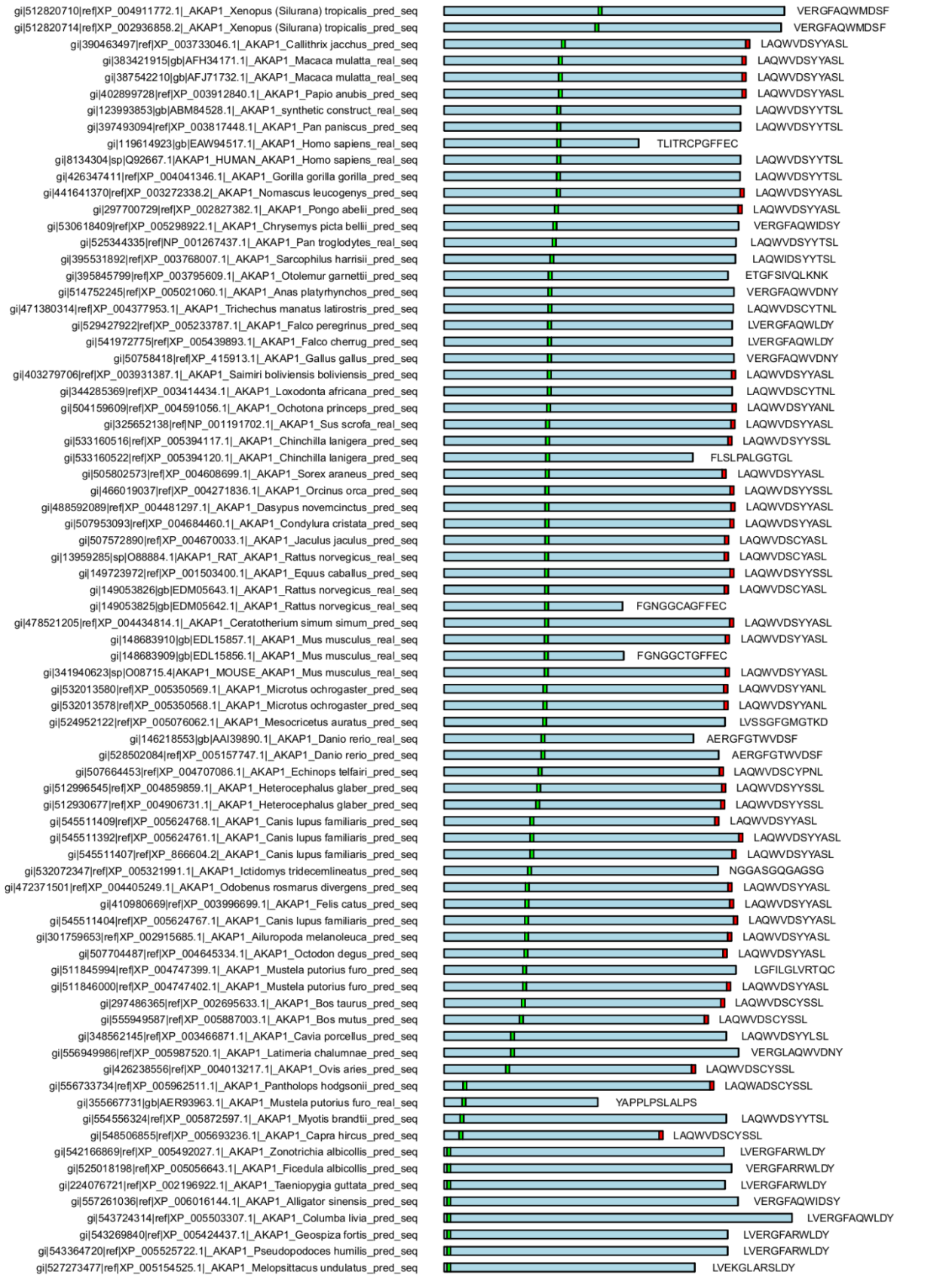
S 4 All known PTS1 binding sites downloaded from PTS1 BLOCK (http://216.92.14.62/diy_PTS1.html) at the “PeroxisomalDB Home” website

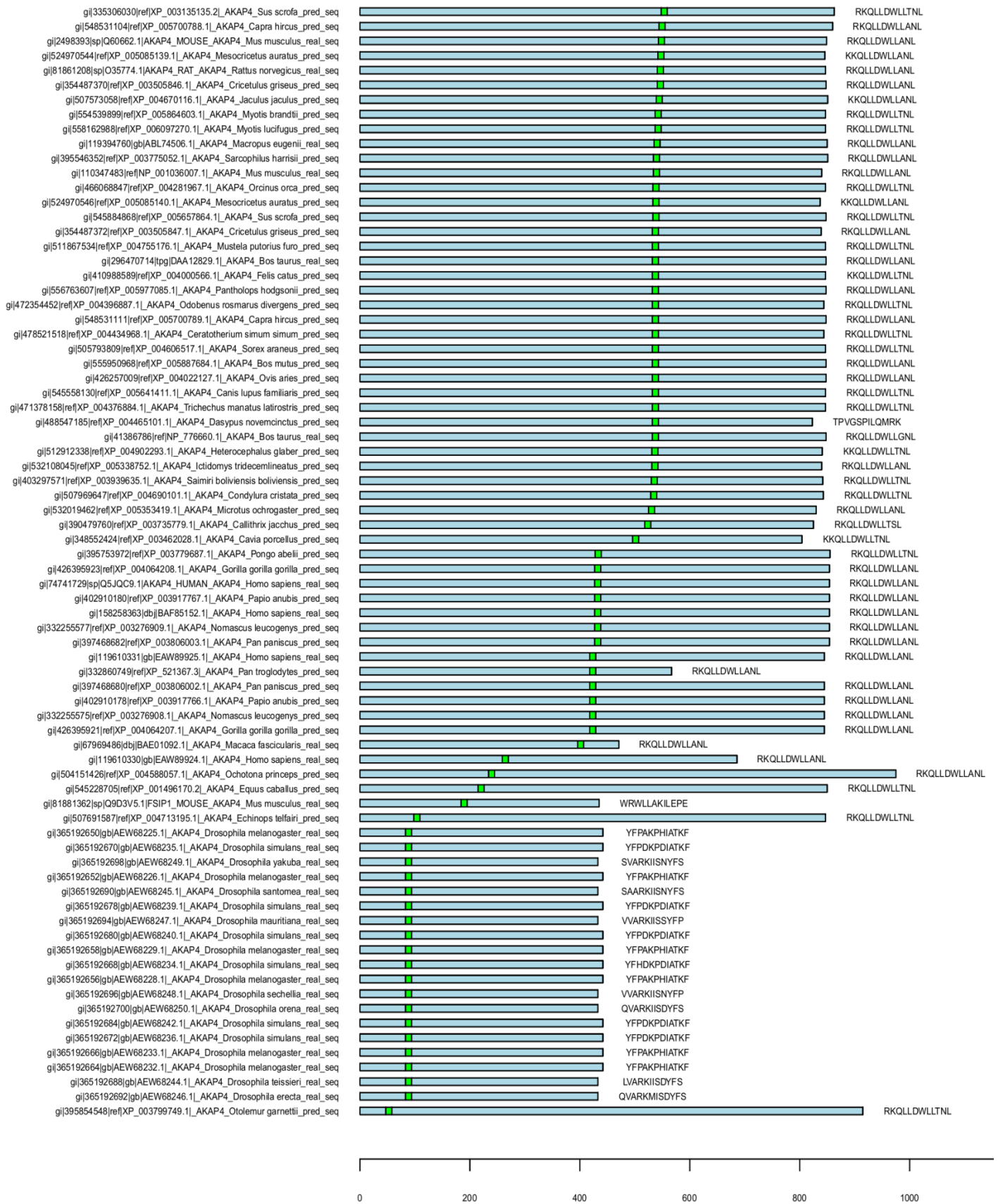
No.	Peroxisomal proteins	Their last 12-aa residues	Their last 3-aa residues
1	GOX1	TEWDTPRPSARL	ARL
2	GGT1	TQYDNNFGYSKM	SKM
3	EHHADH	WQSLAGSPSSKL	SKL
4	mmSerhl	LQGLQRMTSARL	ARL
5	mmCrot	HDMIQLMNTAHL	AHL
6	AAT2	EVVRFYTIEAKL	AKL
7	AT5G18100.1	IIGLQSSADAKL	AKL
8	mmEphx2	TEVQNPSVTSKI	SKI
9	OPR3	TDYPFLAPFSRL	SRL
10	mmEhhadh	WQSLAGPHSSKL	SKL
11	CIT2	YKELVKNIESKL	SKL
12	DHRS4	TVVVGGGTPSRL	SRL
13	LYS4	KGGLEGWVKSQL	SQL
14	AOAT2	SQYADNFGYSRM	SRM
15	mmCrat	RTLLQNHPRAKL	AKL
16	mmMlycd	SLVAQFQNN SKL	SKL
17	HMGCL	TSSKVAQATCKL	CKL
18	NUDT19	NYIVNKRYTAHL	AHL
19	MLS	IVAHYPINVSRL	SRL
20	mmAgxt	REALQHCPKNKL	NKL
21	PTE2b	LGGTQKTAVPKL	PKL
22	PTE2	LGGHEGTIPSKV	SKV
23	BAAT	RKHLIPDVTSQL	SQL
24	GNPAT	KTPIGKPATAKL	AKL
25	DAMOX	EKKLSRMPPSHL	SHL
26	mmPte2a	LDGKKKTIPAKL	AKL
27	mmGnpat	KKPIGKPATAKL	AKL
28	SPS19	PEALIKSMTSKL	SKL
29	PAOX	WAPQVQQPRPRL	PRL
30	EPHX2	SDARNPPVVSKM	SKM
31	CRAT	RALLQSHPRAKL	AKL
32	GSTK1	MGPIPPAVNARL	ARL
33	PRDX5	TCSLAPNIISQL	SQL
34	ACH2	ARPPKPSGTSKL	SKL

35	IDE	VKPHINFMAAKL	AKL
36	PECI	AVVNFLSRKSKL	SKL
37	PTE1	IRVKPQVSESKL	SKL
38	ACOX2	IRPLLQSWRSKL	SKL
39	mmPaox	WDSQVEQSRPRL	PRL
40	MLYCD	SLVAQFQKNSKL	SKL
41	GOX2	TEWDTPRHLPRL	PRL
42	IDP3	SSNEDKKGMCKL	CKL
43	HAO2	EINRNLVQFSRL	SRL
44	AGT	LQHHIPLIPSRI	SRI
45	AT3G06860.1	LSAPVKQASSRL	SRL
46	mmDao1	EKKLSRLPPSHL	SHL
47	PDCR	GLPDFASFSAKL	AKL
48	AT5G63380.1	TKIAVDGNASKL	SKL
49	CHY1	RNNLPALGIAKL	AKL
50	MLS1	STKATPTDLSKL	SKL
51	mmHao3	EISPDLIQFSRL	SRL
52	IDH1	ENLKIKLAQAKL	AKL
53	PECR	KMKETFKEKAKL	AKL
54	CAT2	ALENENKRKAKL	AKL
55	DCI1	KQLQEGNRRHKL	HKL
56	mmAcox2	IRPLMQSWKPKL	PKL
57	ECH1	NKELKTVTFSKL	SKL
58	mmPecr	RIKESFKKKAKL	AKL
59	CROT	HDMIQLMNSTHL	THL
60	mmBC016076	LSGDKRPSPAKL	AKL
61	mmPte1	IRLKPQVSESKL	SKL
62	mmAcox1	YYKHLKPLQSKL	SKL
63	FOX2	AAVKLSQAQSKL	SKL
64	AT1G68010.1	NSKALGLPVSKL	SKL
65	AT3G51840.1	IASFKPATRSRL	SRL
66	mmUox	TGTVKRKLP SRL	SRL
67	PCS60	TFAKSSRNKSKL	SKL
68	DASOX	HALRTPIPKSNL	SNL
69	mmAmacr	RIVESDKLKANL	ANL
70	NPY1	YKNLRKTSSSHL	SHL
71	mmHsd17b4	KLQMILKDYAKL	AKL
72	HSD17B4	KLQMILKDYAKL	AKL
73	MDH3	KGKSFILDSSKL	SKL
74	AGXT	RAALQHCPKKKL	KKL
75	mmDecr2	QLLEFESFSAKL	AKL
76	AT2G35690.1	PLIKQRF RSAKL	AKL
77	mmPte2b	LGSTHSRASCRL	CRL
78	mmAcox3	NKSVADRLKSQL	SQL
79	ACOX3	NKSVADRLKSQL	SQL
80	TES1	VYGSE RDIRAKF	AKF

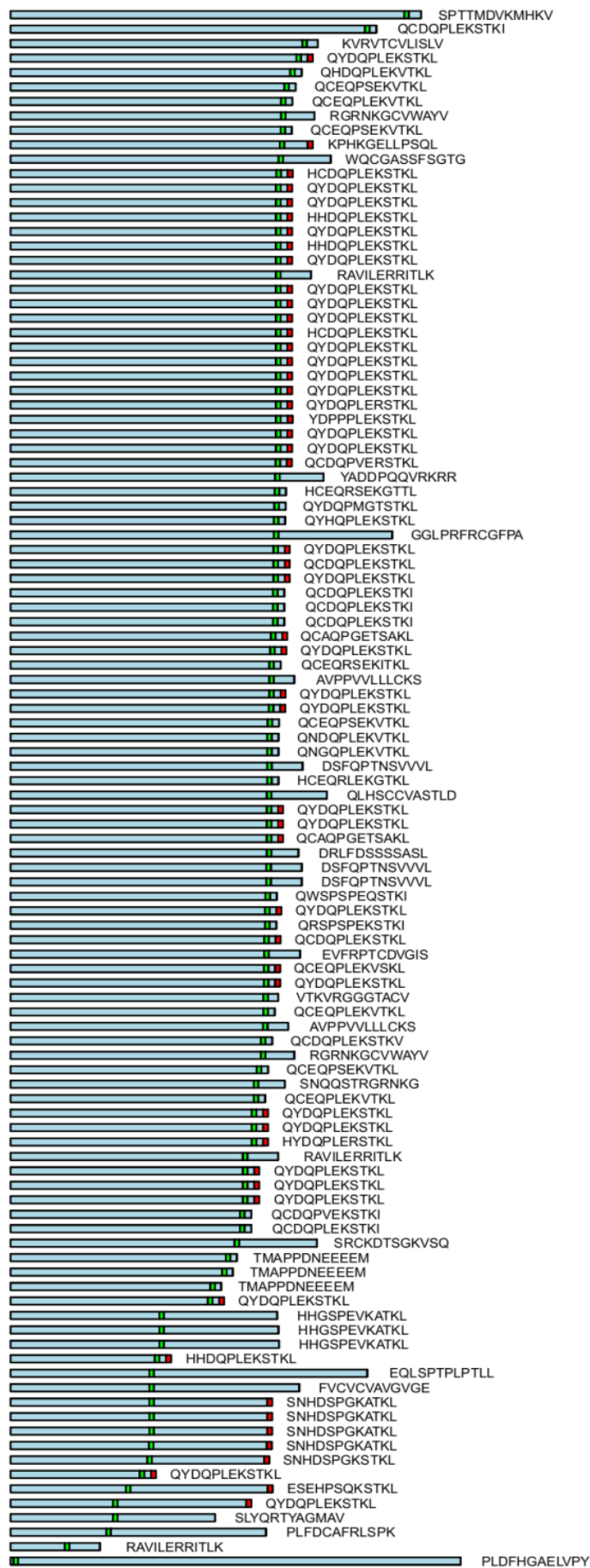
81	mmHao1	LVRKNPLAVSKI	SKI
82	ECI1	RQLGSKQRKHRL	HRL
83	HAO1	LVRKNPLAVSKI	SKI
84	ACOX1	SYKHLKSLQSKL	SKL
85	LONP	VKTRPGLLNSKL	SKL
86	mmEch1	KRDTKSITFSKL	SKL
87	mm5330420D20Rik	HTLRTPASLSKL	SKL
88	PIPOX	ISRFPSLGKAHL	AHL
89	mmNudt7	RTFLWRYLSKL	SKL
90	GPK1	NKDNDITTDKI	AKI
91	mmPeci	AIMSFVSRKPKL	PKL
92	GTO1	VPLGPKPDISRL	SRL
93	ACOX	FNWVEANAWSSL	SSL
94	AMACR	KIIESNKVKASL	ASL
95	LYS1	RHCARVKRSSRL	SRL
96	CAT	GSHLAAREKANL	ANL
97	mmIdi1	SPFVDHEKIHRL	HRL
98	mmCat	TGEPVELKTQAL	QAL

S 5 PTS1 prediction of AKAP1, -4, -10 family members





gi|557768994|ref|XP_005184172.1|_AKAP10_Musca domestica_pred_seq
 gi|556738838|ref|XP_005964990.1|_AKAP10_Pantholops hodgsonii_pred_seq
 gi|444721874|gb|ELW62584.1|_AKAP10_Tupaia chinensis_real_seq
 gi|345329660|ref|XP_001508501.2|_AKAP10_Ornithorhynchus anatinus_pred_seq
 gi|557320022|ref|XP_006033160.1|_AKAP10_Alligator sinensis_pred_seq
 gi|529441637|ref|XP_005240550.1|_AKAP10_Falco peregrinus_pred_seq
 gi|542170776|ref|XP_005493594.1|_AKAP10_Zonotrichia albicollis_pred_seq
 gi|542170773|ref|XP_005493593.1|_AKAP10_Zonotrichia albicollis_pred_seq
 gi|541972876|ref|XP_005439927.1|_AKAP10_Falco cherrug_pred_seq
 gi|505856485|ref|XP_004621646.1|_AKAP10_Sorex araneus_pred_seq
 gi|297715776|ref|XP_002834249.1|_AKAP10_Pongo abelii_pred_seq
 gi|532012328|ref|XP_005349951.1|_AKAP10_Microtus ochrogaster_pred_seq
 gi|397471509|ref|XP_003807333.1|_AKAP10_Pan paniscus_pred_seq
 gi|478517711|ref|XP_004433087.1|_AKAP10_Ceratotherium simum simum_pred_seq
 gi|167736404|ref|NP_001108078.1|_AKAP10_Rattus norvegicus_real_seq
 gi|511921488|ref|XP_004779941.1|_AKAP10_Mustela putorius furo_pred_seq
 gi|71153491|sp|O88845.3|AKA10_MOUSE_AKAP10_Mus musculus_real_seq
 gi|507953571|ref|XP_004684624.1|_AKAP10_Condylura cristata_pred_seq
 gi|512872137|ref|XP_004892704.1|_AKAP10_Heterocephalus glaber_pred_seq
 gi|558181858|ref|XP_006101456.1|_AKAP10_Myotis lucifugus_pred_seq
 gi|71153490|sp|O43572.2|AKA10_HUMAN_AKAP10_Homo sapiens_real_seq
 gi|380785759|gb|AFE64755.1|_AKAP10_Macaca mulatta_real_seq
 gi|524962921|ref|XP_005067694.1|_AKAP10_Mesocricetus auratus_pred_seq
 gi|472371350|ref|XP_004405174.1|_AKAP10_Odobenus rosmarus divergens_pred_seq
 gi|533171757|ref|XP_005399349.1|_AKAP10_Chinchilla lanigera_pred_seq
 gi|73956108|ref|XP_851367.1|_AKAP10_Canis lupus familiaris_pred_seq
 gi|296201626|ref|XP_002748109.1|_AKAP10_Callithrix jacchus_pred_seq
 gi|410980011|ref|XP_003996374.1|_AKAP10_Felis catus_pred_seq
 gi|504181726|ref|XP_004599362.1|_AKAP10_Ochotona princeps_pred_seq
 gi|512872139|ref|XP_004892705.1|_AKAP10_Heterocephalus glaber_pred_seq
 gi|532511814|gb|JAB463.14.1|_AKAP10_Callithrix jacchus_real_seq
 gi|395836333|ref|XP_003791112.1|_AKAP10_Otolemur garnettii_pred_seq
 gi|334324854|ref|XP_001372535.2|_AKAP10_Monodelphis domestica_pred_seq
 gi|326931458|ref|XP_003211846.1|_AKAP10_Meleagris gallopavo_pred_seq
 gi|532112392|ref|XP_005340882.1|_AKAP10_Ictidomys tridecemlineatus_pred_seq
 gi|471393924|ref|XP_004381036.1|_AKAP10_Trichechus manatus latirostris_pred_seq
 gi|344298126|ref|XP_003420745.1|_AKAP10_Loxodonta africana_pred_seq
 gi|332848311|ref|XP_003315625.1|_AKAP10_Pan troglodytes_pred_seq
 gi|465991945|ref|XP_004266854.1|_AKAP10_Orcinus orca_pred_seq
 gi|332265078|ref|XP_003281553.1|_AKAP10_Nomascus leucogenys_pred_seq
 gi|426237659|ref|XP_004012775.1|_AKAP10_Ovis aries_pred_seq
 gi|159507402|gb|ABW97719.1|_AKAP10_Pan troglodytes_real_seq
 gi|528995171|ref|XP_005220406.1|_AKAP10_Bos taurus_pred_seq
 gi|13626099|sp|P57770.2|AKA10_PIG_AKAP10_Sus scrofa_real_seq
 gi|554551511|ref|XP_005870250.1|_AKAP10_Myotis brandtii_pred_seq
 gi|514760996|ref|XP_005023151.1|_AKAP10_Anas platyrhynchos_pred_seq
 gi|514760988|ref|XP_005023149.1|_AKAP10_Anas platyrhynchos_pred_seq
 gi|507708454|ref|XP_004646441.1|_AKAP10_Octodon degus_pred_seq
 gi|514454455|ref|XP_003466353.2|_AKAP10_Cavia porcellus_pred_seq
 gi|527249422|ref|XP_005143026.1|_AKAP10_Melospittacus undulatus_pred_seq
 gi|530616978|ref|XP_005298228.1|_AKAP10_Chrysemys picta bellii_pred_seq
 gi|558229938|ref|XP_006138742.1|_AKAP10_Pelodiscus sinensis_pred_seq
 gi|513216336|ref|XP_004946749.1|_AKAP10_Gallus gallus_pred_seq
 gi|513216345|ref|XP_004946751.1|_AKAP10_Gallus gallus_pred_seq
 gi|354467909|ref|XP_003496410.1|_AKAP10_Cricetulus griseus_pred_seq
 gi|403275197|ref|XP_003929342.1|_AKAP10_Saimiri boliviensis boliviensis_pred_seq
 gi|545180255|ref|XP_005597867.1|_AKAP10_Equus caballus_pred_seq
 gi|47523076|ref|NP_999303.1|_AKAP10_Sus scrofa_real_seq
 gi|537140947|gb|ERE67752.1|_AKAP10_Cricetulus griseus_real_seq
 gi|513216342|ref|XP_004946750.1|_AKAP10_Gallus gallus_pred_seq
 gi|513216339|ref|XP_415856.3|_AKAP10_Gallus gallus_pred_seq
 gi|512825322|ref|XP_002938286.2|_AKAP10_Xenopus (Silurana) tropicalis_pred_seq
 gi|545498317|ref|XP_005620167.1|_AKAP10_Canis lupus familiaris_pred_seq
 gi|148233566|ref|NP_001084758.1|_AKAP10_Xenopus laevis_real_seq
 gi|470627339|ref|XP_004320648.1|_AKAP10_Tursiops truncatus_pred_seq
 gi|543364838|ref|XP_005525781.1|_AKAP10_Pseudopodoces humilis_pred_seq
 gi|449479832|ref|XP_002196061.2|_AKAP10-Taeniopygia guttata_pred_seq
 gi|545498319|ref|XP_005620168.1|_AKAP10_Canis lupus familiaris_pred_seq
 gi|449266048|gb|EMC77175.1|_AKAP10_Columba livia_real_seq
 gi|543270146|ref|XP_005424538.1|_AKAP10_Geospiza fortis_pred_seq
 gi|514760992|ref|XP_005023150.1|_AKAP10_Anas platyrhynchos_pred_seq
 gi|440913066|gb|ELR62570.1|_AKAP10_Bos mutus_real_seq
 gi|542170781|ref|XP_005493595.1|_AKAP10_Zonotrichia albicollis_pred_seq
 gi|543721878|ref|XP_005502129.1|_AKAP10_Columba livia_pred_seq
 gi|525018387|ref|XP_005056734.1|_AKAP10_Ficedula albicollis_pred_seq
 gi|525018389|ref|XP_005056735.1|_AKAP10_Ficedula albicollis_pred_seq
 gi|402899032|ref|XP_003912510.1|_AKAP10_Papio anubis_pred_seq
 gi|82468586|gb|ABB76684.1|_AKAP10_Homo sapiens_real_seq
 gi|507558772|ref|XP_004663120.1|_AKAP10_Jaculus jaculus_pred_seq
 gi|512872141|ref|XP_004892706.1|_AKAP10_Heterocephalus glaber_pred_seq
 gi|545180257|ref|XP_005597868.1|_AKAP10_Equus caballus_pred_seq
 gi|513015013|ref|XP_004868850.1|_AKAP10_Heterocephalus glaber_pred_seq
 gi|297272139|ref|XP_001099682.2|_AKAP10_Macaca mulatta_pred_seq
 gi|548508282|ref|XP_005693661.1|_AKAP10_Capra hircus_pred_seq
 gi|555950239|ref|XP_005887323.1|_AKAP10_Bos mutus_pred_seq
 gi|498984276|ref|XP_004530326.1|_AKAP10_Ceratitis capitata_pred_seq
 gi|512923926|ref|XP_004930472.1|_AKAP10_Bombyx mori_pred_seq
 gi|512923930|ref|XP_004930473.1|_AKAP10_Bombyx mori_pred_seq
 gi|512923934|ref|XP_004930474.1|_AKAP10_Bombyx mori_pred_seq
 gi|355667737|gb|AER93965.1|_AKAP10_Mustela putorius furo_real_seq
 gi|528480817|ref|XP_695298.6|_AKAP10_Danio rerio_pred_seq
 gi|528480815|ref|XP_005165634.1|_AKAP10_Danio rerio_pred_seq
 gi|528480813|ref|XP_005165633.1|_AKAP10_Danio rerio_pred_seq
 gi|32449749|gb|AAH54105.1|_AKAP10_Mus musculus_real_seq
 gi|410925717|ref|XP_003976326.1|_AKAP10_Takifugu rubripes_pred_seq
 gi|432900956|ref|XP_004076742.1|_AKAP10_Oryzias latipes_pred_seq
 gi|548492887|ref|XP_005749590.1|_AKAP10_Pundamilia nyererei_pred_seq
 gi|499010921|ref|XP_004557344.1|_AKAP10_Maylandia zebra_pred_seq
 gi|542194099|ref|XP_005472020.1|_AKAP10_Oreochromis niloticus_pred_seq
 gi|554843314|ref|XP_005932038.1|_AKAP10_Haplochromis burtoni_pred_seq
 gi|551498628|ref|XP_005800866.1|_AKAP10_Xiphophorus maculatus_pred_seq
 gi|426349138|ref|XP_004042171.1|_AKAP10_Gorilla gorilla gorilla_pred_seq
 gi|557019952|ref|XP_006010316.1|_AKAP10_Latimeria chalumnae_pred_seq
 gi|488508119|ref|XP_004446559.1|_AKAP10_Dasyptus novemcinctus_pred_seq
 gi|488508121|ref|XP_004446560.1|_AKAP10_Dasyptus novemcinctus_pred_seq
 gi|528764137|gb|EPY83796.1|_AKAP10_Camelus ferus_real_seq
 gi|351705187|gb|EH808106.1|_AKAP10_Heterocephalus glaber_real_seq
 gi|465986660|gb|EMP37756.1|_AKAP10_Chelonia mydas_real_seq



13 Acknowledgements

At first, I am really thankful to Professor Eveline Baumgart-Vogt and the China Scholarship Council (CSC) committee to give me the opportunity to broad my horizons in scientific knowledge and international culture.

Since 2011 autumn, I have studied in Justus-Liebig-University Giessen for 4 years. During these 4 years, I have attended lots of seminars and workshops from International Giessen Graduate Centre for the Life Sciences (GGL), enjoying the fantastic research from experts and developing more skills. Thanks to the work and offer from GGL committee, I have chance to participate the DAAD (Deutscher Akademischer Austauschdienst) granted teaching assistantships (STIBET) and to share my bioinformatics skills with other PhD students in life science. These 4 years are my most valuable experience, so I tried my best to learn and to contribute my effort.

I would like to thank my Prof. Baumgart-Vogt very much for allowing me to take this important step in my scientific career as a part of her team. I am thankful for her help, her patience in all our discussions and for her advice during those past 4 years, especially during my thesis correction period. She spent huge time and patience on my English writing and experimental photos, gave me plenty of suggestions to improve its quality, and checked each point in detail to make sure all the information is correct. She is a very responsible, reliable and sincere “Doktormutter”!

I am also thankful to Dr. Colasante. She has not only helped me a lot in my experiments, such as the RNA isolation and precipitation, Northern blot “sandwiches” set, washing buffer recipes, the principle of expression primer design and so on, but also spent lots of time to guide and correct my thesis as well as the last proofreading. Heartfelt thanks to Dr. Barbara Ahlemeyer for helping me to take photos from laser scan confocal microscope. Thank sincerely my friend Francisca Alagboso for her great help on the English correction of my whole thesis.

I am grateful for the friendly atmosphere in our team and lab and want to thank my colleagues and technicians for the nice moments we could share in and besides work. They are all nice and friendly and always the first one whom I share my joy and tear with. Thanks to them, whenever I had trouble in my work or life, I could always get suggestions and encouragement; thanks to them, I didn’t feel lonely in every birthday

and Christmas and lunch time; thanks to them, my album is full of smiling eyes and sunny faces. Special thanks go to Frau Andrea Toxtor, who not only was a trusting partner for my work, but also a great help for improving my German language. And thank the technicians to help me in the cell culture and immunofluorescence, who also lent German books to me for reading.

I also want to thank the Chinese government, because it would have been impossible for me to complete my PhD studies in Germany without their scholarship.

Further I especially want to thank my mother, who always supported and encouraged me to follow my interest and studies with her greatest love. I am also grateful for all the support and patience I received from my family and friends, especially my boyfriend who always encouraged me whenever needed and gave me strength for the final steps in getting PhD.

Now it is almost the end of PhD study, however, it is also a new start to face further chance and challenge. I believe I can be more brave and prepared to welcome future. Because I know the concern and support is always surrounding closely.

14 Curriculum vitae

The curriculum vitae was removed from the electronic version of the paper.

15 Reference

- Affaitati, A., L. Cardone, T. de Cristofaro, A. Carlucci, M.D. Ginsberg, S. Varrone, M.E. Gottesman, E.V. Avvedimento, and A. Feliciello. 2003. Essential role of A-kinase anchor protein 121 for cAMP signaling to mitochondria. *Journal of Biological Chemistry*. 278:4286-4294.
- Alam, I., Q. Sun, D.L. Koller, L. Liu, Y. Liu, H.J. Edenberg, T. Foroud, and C.H. Turner. 2010. Genes influencing spinal bone mineral density in inbred F344, LEW, COP, and DA rats. *Functional & integrative genomics*. 10:63-72.
- Amery, L., M. Fransen, K. De Nys, G.P. Mannaerts, and P.P. Van Veldhoven. 2000. Mitochondrial and peroxisomal targeting of 2-methylacyl-CoA racemase in humans. *Journal of lipid research*. 41:1752-1759.
- Anway, M.D., J. Folmer, W.W. Wright, and B.R. Zirkin. 2003. Isolation of Sertoli cells from adult rat testes: an approach to ex vivo studies of Sertoli cell function. *Biology of Reproduction*. 68:996-1002.
- Asirvatham, A.L., S.G. Galligan, R.V. Schillace, M.P. Davey, V. Vasta, J.A. Beavo, and D.W. Carr. 2004. A-kinase anchoring proteins interact with phosphodiesterases in T lymphocyte cell lines. *The Journal of Immunology*. 173:4806-4814.
- Baumgart, E. 1997. Application of in situ hybridization, cytochemical and immunocytochemical techniques for the investigation of peroxisomes. *Histochemistry and cell biology*. 108:185-210.
- Baumgart, E., H.D. Fahimi, A. Stich, and A. Vökl. 1996a. L-Lactate Dehydrogenase A- and AB Isoforms Are Bona Fide Peroxisomal Enzymes in Rat Liver EVIDENCE FOR INVOLVEMENT IN INTRAPEROXISOMAL NADH REOXIDATION. *Journal of Biological Chemistry*. 271:3846-3855.
- Baumgart, E., J.C. Vanhooren, M. Fransen, P. Marynen, M. Puype, J. Vandekerckhove, J.A. Leunissen, H.D. Fahimi, G.P. Mannaerts, and P.P. Van Veldhoven. 1996b. Molecular characterization of the human peroxisomal branchedchain acyl-CoA oxidase: cDNA cloning, chromosomal assignment, tissue distribution, and evidence for the absence of the protein in Zellweger syndrome. *Proceedings of the National Academy of Sciences*. 93:13748-13753.
- Baumgart, E., I. Vanhorebeek, M. Grabenbauer, M. Borgers, P.E. Declercq, H.D. Fahimi, and M. Baes. 2001. Mitochondrial alterations caused by defective peroxisomal biogenesis in a mouse model for Zellweger syndrome (PEX5 knockout mouse). *The American journal of pathology*. 159:1477-1494.
- Beasley, E.M., S. Müller, and G. Schatz. 1993. The signal that sorts yeast cytochrome b2 to the mitochondrial intermembrane space contains three distinct functional regions. *The EMBO journal*. 12:2303.
- Berg, R.K., J. Melchjorsen, J. Rintahaka, E. Diget, S. Søbø, K.A. Horan, R.J. Gorelick, S. Matikainen, C.S. Larsen, and L. Ostergaard. 2012. Genomic HIV RNA induces innate immune responses through RIG-I-dependent sensing of secondary-structured RNA.
- Bridges, D., J.A. MacDonald, B. Wadzinski, and G.B. Moorhead. 2006. Identification and characterization of D-AKAP1 as a major adipocyte PKA and PP1 binding protein. *Biochemical and biophysical research communications*. 346:351-357.
- Brocard, C., and A. Hartig. 2006. Peroxisome targeting signal 1: is it really a simple tripeptide? *Biochimica et Biophysica Acta (BBA)-Molecular Cell Research*. 1763:1565-1573.

- Brown, P.R., K. Miki, D.B. Harper, and E.M. Eddy. 2003. A-kinase anchoring protein 4 binding proteins in the fibrous sheath of the sperm flagellum. *Biology of Reproduction*. 68:2241-2248.
- Cardone, L., T. de Cristofaro, A. Affaitati, C. Garbi, M.D. Ginsberg, M. Saviano, S. Varrone, C.S. Rubin, M.E. Gottesman, and E.V. Avvedimento. 2002. A-kinase anchor protein 84/121 are targeted to mitochondria and mitotic spindles by overlapping amino-terminal motifs. *Journal of molecular biology*. 320:663-675.
- Carlson, C.R., B. Lygren, T. Berge, N. Hoshi, W. Wong, K. Taskán, and J.D. Scott. 2006. Delineation of type I protein kinase A-selective signaling events using an RI anchoring disruptor. *Journal of Biological Chemistry*. 281:21535-21545.
- Carlucci, A., L. Lignitto, and A. Feliciello. 2008. Control of mitochondria dynamics and oxidative metabolism by cAMP, AKAPs and the proteasome. *Trends in cell biology*. 18:604-613.
- Carr, D.W., A. Fujita, C.L. Stentz, G.A. Liberty, G.E. Olson, and S. Narumiya. 2001. Identification of sperm-specific proteins that interact with A-kinase anchoring proteins in a manner similar to the type II regulatory subunit of PKA. *Journal of Biological Chemistry*. 276:17332-17338.
- Carr, D.W., R.E. Stofko-Hahn, I. Fraser, R.D. Cone, and J.D. Scott. 1992. Localization of the cAMP-dependent protein kinase to the postsynaptic densities by A-kinase anchoring proteins. Characterization of AKAP 79. *Journal of Biological Chemistry*. 267:16816-16823.
- Castillo, A.F., U. Orlando, K.E. Helfenberger, C. Poderoso, and E.J. Podesta. 2014. The role of mitochondrial fusion and StAR phosphorylation in the regulation of StAR activity and steroidogenesis. *Molecular and cellular endocrinology*.
- Caudevilla, C., D. Serra, A. Miliar, C. Codony, G. Asins, M. Bach, and F.G. Hegardt. 1998. Natural trans-splicing in carnitine octanoyltransferase pre-mRNAs in rat liver. *Proceedings of the National Academy of Sciences*. 95:12185-12190.
- Chen, Q., R.-Y. Lin, and C.S. Rubin. 1997. Organelle-specific Targeting of Protein Kinase AII (PKAII) MOLECULAR AND IN SITU CHARACTERIZATION OF MURINE A KINASE ANCHOR PROTEINS THAT RECRUIT REGULATORY SUBUNITS OF PKAII TO THE CYTOPLASMIC SURFACE OF MITOCHONDRIA. *Journal of Biological Chemistry*. 272:15247-15257.
- Chiriva - Internati, M., Y. Yu, L. Mirandola, N. D'Cunha, F. Hardwicke, M.J. Cannon, E. Cobos, and W.M. Kast. 2012. Identification of AKAP - 4 as a new cancer/testis antigen for detection and immunotherapy of prostate cancer. *The Prostate*. 72:12-23.
- Colasante, C., J. Chen, B. Ahlemeyer, and E. Baumgart-Vogt. 2015. Peroxisomes in cardiomyocytes and the peroxisome/peroxisome proliferator-activated receptor-loop. *Thromb Haemost*. 113:452-463.
- Cribbs, J.T., and S. Strack. 2007. Reversible phosphorylation of Drp1 by cyclic AMP - dependent protein kinase and calcineurin regulates mitochondrial fission and cell death. *EMBO reports*. 8:939-944.
- Dagda, R.K., A.M. Gusdon, I. Pien, S. Strack, S. Green, C. Li, B. Van Houten, S. Cherra, and C.T. Chu. 2011. Mitochondrially localized PKA reverses mitochondrial pathology and dysfunction in a cellular model of Parkinson's disease. *Cell Death & Differentiation*. 18:1914-1923.
- Dastig, S., A. Nenicu, D.M. Otte, A. Zimmer, J. Seitz, E. Baumgart-Vogt, and G.H. Lüers. 2011. Germ cells of male mice express genes for peroxisomal metabolic pathways implicated in the regulation of spermatogenesis and the protection against oxidative stress. *Histochemistry and cell biology*. 136:413-425.

- David, R., and D. Wedlich. 2001. PCR-based RNA probes: a quick and sensitive method to improve whole mount embryo in situ hybridizations. *Biotechniques*. 30:769-775.
- Day, M.E., G.M. Gaietta, M. Sastri, A. Koller, M.R. Mackey, J.D. Scott, G.A. Perkins, M.H. Ellisman, and S.S. Taylor. 2011. Isoform-specific targeting of PKA to multivesicular bodies. *The Journal of cell biology*. 193:347-363.
- De Capua, A., A. Del Gatto, L. Zaccaro, G. Saviano, A. Carlucci, A. Livigni, C. Gedressi, T. Tancredi, C. Pedone, and M. Saviano. 2004. A synthetic peptide reproducing the mitochondrial targeting motif of AKAP121: a conformational study. *Peptide Science*. 76:459-466.
- Dell'Acqua, M.L., and J.D. Scott. 1997. Protein kinase A anchoring. *Journal of Biological Chemistry*. 272:12881-12884.
- Diviani, D., L.K. Langeberg, S.J. Doxsey, and J.D. Scott. 2000. Pericentrin anchors protein kinase A at the centrosome through a newly identified RII-binding domain. *Current Biology*. 10:417-420.
- Dyson, M.T., J.K. Jones, M.P. Kowalewski, P.R. Manna, M. Alonso, M.E. Gottesman, and D.M. Stocco. 2008. Mitochondrial A-kinase anchoring protein 121 binds type II protein kinase A and enhances steroidogenic acute regulatory protein-mediated steroidogenesis in MA-10 mouse Leydig tumor cells. *Biology of Reproduction*. 78:267-277.
- Emanuelsson, O., G. von Heijne, and G. Schneider. 2001. Analysis and prediction of mitochondrial targeting peptides. *Methods in cell biology*:175-189.
- Fahimi, H.D., and E. Baumgart. 1999. Kleine Ursache - tragische Wirkung. *Forschungsmagazin der Universität Heidelberg*. 2:18-24.
- Fehr, J.E., G.W. Trotter, J.T. Oxford, and D.A. Hart. 2000. Comparison of Northern blot hybridization and a reverse transcriptase-polymerase chain reaction technique for measurement of mRNA expression of metalloproteinases and matrix components in articular cartilage and synovial membrane from horses with osteoarthritis. *American journal of veterinary research*. 61:900-905.
- Feliciello, A., C.S. Rubin, E.V. Avvedimento, and M.E. Gottesman. 1998. Expression of a kinase anchor protein 121 is regulated by hormones in thyroid and testicular germ cells. *Journal of Biological Chemistry*. 273:23361-23366.
- Ferdinandusse, S., G. Jimenez-Sanchez, J. Koster, S. Denis, C.W. Van Roermund, I. Silva-Zolezzi, A.B. Moser, W.F. Visser, M. Gulluoglu, and O. Durmaz. 2014. A novel bile acid biosynthesis defect due to a deficiency of peroxisomal ABCD3. *Human molecular genetics*:ddu448.
- Finck, B.N. 2007. The PPAR regulatory system in cardiac physiology and disease. *Cardiovascular research*. 73:269-277.
- Flouriot, G., H. Brand, B. Seraphin, and F. Gannon. 2002. Natural trans-spliced mRNAs are generated from the human estrogen receptor- α (hER α) gene. *Journal of Biological Chemistry*. 277:26244-26251.
- Furusawa, M., T. Ohnishi, T. Taira, S.M. Iguchi-Ariga, and H. Ariga. 2001. AMY-1, a c-Myc-binding protein, is localized in the mitochondria of sperm by association with S-AKAP84, an anchor protein of cAMP-dependent protein kinase. *Journal of Biological Chemistry*. 276:36647-36651.
- Gao, X., D. Chaturvedi, and T.B. Patel. 2010. p90 Ribosomal S6 Kinase 1 (RSK1) and the Catalytic Subunit of Protein Kinase A (PKA) Compete for Binding the Pseudosubstrate Region of PKAR1 α : role in the regulation of PKA and RSK1 activities. *Journal of Biological Chemistry*. 285:6970-6979.

- Garnis, C., M.P. Rosin, L. Zhang, and W.L. Lam. 2005. Alteration of AKAP220, an upstream component of the Rb pathway, in oral carcinogenesis. *International journal of cancer*. 116:813-819.
- Ginsberg, M.D., A. Feliciello, J.K. Jones, E.V. Avvedimento, and M.E. Gottesman. 2003. PKA-dependent binding of mRNA to the mitochondrial AKAP121 protein. *Journal of molecular biology*. 327:885-897.
- Gisler, S.M., C. Madjdpour, D. Bacic, S. Pribanic, S.S. Taylor, J. Biber, and H. Murer. 2003a. PDZK1: II. an anchoring site for the PKA-binding protein D-AKAP2 in renal proximal tubular cells. *Kidney international*. 64:1746-1754.
- Gisler, S.M., S. Pribanic, D. Bacic, P. Forrer, A. Gantenbein, L.A. Sabourin, A. Tsuji, Z.-S. Zhao, E. Manser, and J. Biber. 2003b. PDZK1: I. A major scaffold in brush borders of proximal tubular cells. *Kidney international*. 64:1733-1745.
- Gold, M.G., B. Lygren, P. Dokurno, N. Hoshi, G. McConnachie, K. Taskán, C.R. Carlson, J.D. Scott, and D. Barford. 2006. Molecular basis of AKAP specificity for PKA regulatory subunits. *Molecular cell*. 24:383-395.
- Gomez-Concha, C., O. Flores-Herrera, S. Olvera-Sanchez, M.T. Espinosa-Garcia, and F. Martinez. 2011. Progesterone synthesis by human placental mitochondria is sensitive to PKA inhibition by H89. *The International Journal of Biochemistry & Cell Biology*. 43:1402-1411.
- Gould, S., G.-A. Keller, and S. Subramani. 1987. Identification of a peroxisomal targeting signal at the carboxy terminus of firefly luciferase. *The Journal of cell biology*. 105:2923-2931.
- Gould, S.J., G.-A. Keller, N. Hosken, J. Wilkinson, and S. Subramani. 1989. A conserved tripeptide sorts proteins to peroxisomes. *The Journal of cell biology*. 108:1657-1664.
- Graham, J. 2002a. Purification of peroxisomes in a self-generated gradient. *The Scientific World Journal*. 2:1532-1535.
- Graham, J. 2002b. Purification of peroxisomes using a density barrier in a swinging-bucket rotor. *The Scientific World Journal*. 2:1400-1443.
- Grant, P., B. Ahlemeyer, S. Karnati, T. Berg, I. Stelzig, A. Nenicu, K. Kuchelmeister, D.I. Crane, and E. Baumgart-Vogt. 2013. The biogenesis protein PEX14 is an optimal marker for the identification and localization of peroxisomes in different cell types, tissues, and species in morphological studies. *Histochemistry and cell biology*. 140:423-442.
- Gregory, C.W., and R.M. DePhilip. 1998. Detection of steroidogenic acute regulatory protein (StAR) in mitochondria of cultured rat Sertoli cells incubated with follicle-stimulating hormone. *Biology of Reproduction*. 58:470-474.
- Griswold, M.D., C. Morales, and S.R. Sylvester. 1987. Molecular biology of the Sertoli cell. *Oxford reviews of reproductive biology*. 10:124-161.
- Grozdanov, P.N., and D.M. Stocco. 2012. Short RNA Molecules with High Binding Affinity to the KH Motif of A-Kinase Anchoring Protein 1 (AKAP1): Implications for the Regulation of Steroidogenesis. *Molecular Endocrinology*. 26:2104-2117.
- Guo, Y., Y. Hai, C. Yao, Z. Chen, J. Hou, Z. Li, and Z. He. 2015. Long-term culture and significant expansion of human Sertoli cells whilst maintaining stable global phenotype and AKT and SMAD1/5 activation. *Cell Communication and Signaling*. 13:20.
- Hafeez, S., R. Sharma, R. Huddart, D. Dearnaley, and A. Horwich. 2007. Challenges in treating patients with Down's syndrome and testicular cancer with chemotherapy

- and radiotherapy: The Royal Marsden experience. *Clinical Oncology*. 19:135-142.
- Hamuro, Y., L.L. Burns, J.M. Canaves, R.C. Hoffman, S.S. Taylor, and V.L. Woods. 2002. Domain organization of D-AKAP2 revealed by enhanced deuterium exchange-mass spectrometry (DXMS). *Journal of molecular biology*. 321:703-714.
- Harrison, C.A., P.G. Farnworth, K.L. Chan, P.G. Stanton, G.T. Ooi, J.K. Findlay, and D.M. Robertson. 2001. Identification of Specific Inhibin A-Binding Proteins on Mouse Leydig (TM3) and Sertoli (TM4) Cell Lines 1. *Endocrinology*. 142:1393-1402.
- Hayashi, M., M. Aoki, M. Kondo, and M. Nishimura. 1997. Changes in targeting efficiencies of proteins to plant microbodies caused by amino acid substitutions in the carboxy-terminal tripeptide. *Plant and cell physiology*. 38:759-768.
- Herberg, F.W., A. Maleszka, T. Eide, L. Vossebein, and K. Tasken. 2000. Analysis of A-kinase anchoring protein (AKAP) interaction with protein kinase A (PKA) regulatory subunits: PKA isoform specificity in AKAP binding. *Journal of molecular biology*. 298:329-339.
- Hoffman, R.M. 2008. Use of GFP for in vivo imaging: concepts and misconceptions. In Biomedical Optics (BiOS) 2008. International Society for Optics and Photonics. 68680E-68680E-68687.
- Howe, C. 2007. Gene cloning and manipulation. Cambridge University Press.
- Hu, Y., H. Yu, A.J. Pask, D.A. O'Brien, G. Shaw, and M.B. Renfree. 2009. A-kinase anchoring protein 4 has a conserved role in mammalian spermatogenesis. *Reproduction*. 137:645-653.
- Huang, L.J.-s., L. Wang, Y. Ma, K. Durick, G. Perkins, T.J. Deerinck, M.H. Ellisman, and S.S. Taylor. 1999. NH2-terminal targeting motifs direct dual specificity A-kinase-anchoring protein 1 (D-AKAP1) to either mitochondria or endoplasmic reticulum. *The Journal of cell biology*. 145:951-959.
- Hundsruker, C., P. Skroblin, F. Christian, H.-M. Zenn, V. Popara, M. Joshi, J. Eichhorst, B. Wiesner, F.W. Herberg, and B. Reif. 2010. Glycogen synthase kinase 3 β interaction protein functions as an A-kinase anchoring protein. *Journal of Biological Chemistry*. 285:5507-5521.
- Hunzicker-Dunn, M., and E.T. Maizels. 2006. FSH signaling pathways in immature granulosa cells that regulate target gene expression: branching out from protein kinase A. *Cellular signalling*. 18:1351-1359.
- Huyghe, S., H. Schmalbruch, K. De Gendt, G. Verhoeven, F. Guillou, P.P. Van Veldhoven, and M. Baes. 2006. Peroxisomal multifunctional protein 2 is essential for lipid homeostasis in Sertoli cells and male fertility in mice. *Endocrinology*. 147:2228-2236.
- Inhorn, M.C., and P. Patrizio. 2015. Infertility around the globe: new thinking on gender, reproductive technologies and global movements in the 21st century. *Human reproduction update*:dmv016.
- Islinger, M., S. Grille, H.D. Fahimi, and M. Schrader. 2012. The peroxisome: an update on mysteries. *Histochemistry and cell biology*. 137:547-574.
- Islinger, M., K.W. Li, J. Seitz, A. Vökl, and G.H. Liers. 2009. Hitchhiking of Cu/Zn superoxide dismutase to peroxisomes—evidence for a natural piggyback import mechanism in mammals. *Traffic*. 10:1711-1721.
- Jin, Y., L. Wang, M. Ruan, J. Liu, Y. Yang, C. Zhou, B. Xu, and Z. Fu. 2011. Cypermethrin exposure during puberty induces oxidative stress and endocrine disruption in male mice. *Chemosphere*. 84:124-130.

- Kaczmarek, K., E. Niedzialkowska, M. Studencka, Y. Schulz, and P. Grzmil. 2009. Ccdc33, Predominantly Testis-Expressed Gene, Encodes a Putative Peroxisomal Protein.
- Kim, H., M.C. Scimia, D. Wilkinson, R.D. Trelles, M.R. Wood, D. Bowtell, A. Dillin, M. Mercola, and Z.e.A. Ronai. 2011. Fine-tuning of Drp1/Fis1 availability by AKAP121/Siah2 regulates mitochondrial adaptation to hypoxia. *Molecular cell*. 44:532-544.
- Kim, J., L. Jia, M. Stallcup, and G. Coetzee. 2005. The role of protein kinase A pathway and cAMP responsive element-binding protein in androgen receptor-mediated transcription at the prostate-specific antigen locus. *Journal of molecular endocrinology*. 34:107-118.
- Kinderman, F.S., C. Kim, S. von Daake, Y. Ma, B.Q. Pham, G. Spraggon, N.-H. Xuong, P.A. Jennings, and S.S. Taylor. 2006. A dynamic mechanism for AKAP binding to RII isoforms of cAMP-dependent protein kinase. *Molecular cell*. 24:397-408.
- Koike, M., Y. Yutoku, and A. Koike. 2013. Ku80 attenuates cytotoxicity induced by green fluorescent protein transduction independently of non-homologous end joining. *FEBS open bio*. 3:46-50.
- Kota, B.P., T.H.W. Huang, and B.D. Roufogalis. 2005. An overview on biological mechanisms of PPARs. *Pharmacological Research*. 51:85-94.
- Lazennec, G., L. Canaple, D. Saugy, and W. Wahli. 2000. Activation of peroxisome proliferator-activated receptors (PPARs) by their ligands and protein kinase A activators. *Molecular Endocrinology*. 14:1962-1975.
- Leal, M., S. Becker-Silva, H. Chiarini-Garcia, and L. Frana. 2004. Sertoli cell efficiency and daily sperm production in goats (*Capra hircus*). *Anim. Reprod*. 1:122-128.
- Lee, B., R. Cao, Y.S. Choi, H.Y. Cho, A.D. Rhee, C.K. Hah, K.R. Hoyt, and K. Obrietan. 2009. The CREB/CRE transcriptional pathway: protection against oxidative stress - mediated neuronal cell death. *Journal of neurochemistry*. 108:1251-1265.
- Lee, H.-J., and J.J. Zheng. 2010. Review PDZ domains and their binding partners: structure, specificity, and modification. *Cell Communication and Signaling*. 8:18.
- Lemay, J., P. Maidou-Peindara, R. Cancio, E. Ennifar, G. Coadou, G. Maga, J.-C. Rain, R. Benarous, and L.X. Liu. 2008. AKAP149 binds to HIV-1 reverse transcriptase and is involved in the reverse transcription. *Journal of molecular biology*. 383:783-796.
- Lester, L.B., V.M. Coghlan, B. Nauert, and J.D. Scott. 1996. Cloning and characterization of a novel A-kinase anchoring protein. *Journal of Biological Chemistry*. 271:9460.
- Li, M., X. Wang, M.K. Meintzer, T. Laessig, M.J. Birnbaum, and K.A. Heidenreich. 2000. Cyclic AMP promotes neuronal survival by phosphorylation of glycogen synthase kinase 3 β . *Molecular and cellular biology*. 20:9356-9363.
- Lin, R.-Y., S.B. Moss, and C.S. Rubin. 1995. Characterization of S-AKAP84, a novel developmentally regulated A kinase anchor protein of male germ cells. *Journal of Biological Chemistry*. 270:27804-27811.
- Livigni, A., A. Scorziello, S. Agnese, A. Adornetto, A. Carlucci, C. Garbi, I. Castaldo, L. Annunziato, E.V. Avvedimento, and A. Feliciello. 2006. Mitochondrial AKAP121 links cAMP and src signaling to oxidative metabolism. *Molecular Biology of the Cell*. 17:263-271.

- Lodish, H., A. Berk, S.L. Zipursky, P. Matsudaira, D. Baltimore, and J. Darnell. 2000. Processing of rRNA and tRNA.
- Logel, J., D. Dill, and S. Leonard. 1992. Synthesis of cRNA probes from PCR-generated DNA. *Biotechniques*. 13:604-610.
- Logue, J.S., J.L. Whiting, B. Tunquist, L.K. Langeberg, and J.D. Scott. 2011a. Anchored protein kinase A recruitment of active Rac GTPase. *Journal of Biological Chemistry*. 286:22113-22121.
- Logue, J.S., J.L. Whiting, B. Tunquist, D.B. Sacks, L.K. Langeberg, L. Wordeman, and J.D. Scott. 2011b. AKAP220 protein organizes signaling elements that impact cell migration. *Journal of Biological Chemistry*. 286:39269-39281.
- Lüers, G.H., S. Thiele, A. Schad, A. Vökl, S. Yokota, and J. Seitz. 2006. Peroxisomes are present in murine spermatogonia and disappear during the course of spermatogenesis. *Histochemistry and cell biology*. 125:693-703.
- Ma, C., and S. Reumann. 2008. Improved prediction of peroxisomal PTS1 proteins from genome sequences based on experimental subcellular targeting analyses as exemplified for protein kinases from Arabidopsis. *Journal of experimental botany*. 59:3767-3779.
- Ma, Y., and S.S. Taylor. 2008. A Molecular Switch for Targeting between Endoplasmic Reticulum (ER) and Mitochondria CONVERSION OF A MITOCHONDRIA-TARGETING ELEMENT INTO AN ER-TARGETING SIGNAL IN DAKAP1. *Journal of Biological Chemistry*. 283:11743-11751.
- Manna, P.R., M.T. Dyson, and D.M. Stocco. 2009. Regulation of the steroidogenic acute regulatory protein gene expression: present and future perspectives. *Molecular human reproduction*. 15:321-333.
- Marques-Pinto, A., and D. Carvalho. 2013. Human infertility: are endocrine disruptors to blame? *Endocrine connections*. 2:R15-R29.
- McConnachie, G., L.K. Langeberg, and J.D. Scott. 2006. AKAP signaling complexes: getting to the heart of the matter. *Trends in molecular medicine*. 12:317-323.
- McGuinness, M.P., C.C. Linder, C.R. Morales, L.L. Heckert, J. Pikus, and M.D. Griswold. 1994. Relationship of a mouse Sertoli cell line (MSC-1) to normal Sertoli cells. *Biology of Reproduction*. 51:116-124.
- McLean, D.J., P.J. Friel, D. Pouchnik, and M.D. Griswold. 2002. Oligonucleotide microarray analysis of gene expression in follicle-stimulating hormone-treated rat Sertoli cells. *Molecular Endocrinology*. 16:2780-2792.
- Mendis-Handagama, S., P.A. Watkins, S.J. Gelber, and T.J. Scallen. 1992. Leydig cell peroxisomes and sterol carrier protein-2 in luteinizing hormone-deprived rats. *Endocrinology*. 131:2839-2845.
- Merrill, R.A., R.K. Dagda, A.S. Dickey, J.T. Cribbs, S.H. Green, Y.M. Usachev, and S. Strack. 2011. Mechanism of neuroprotective mitochondrial remodeling by PKA/AKAP1. *PLoS biology*. 9:e1000612.
- Merrill, R.A., and S. Strack. 2014. Mitochondria: A kinase anchoring protein 1, a signaling platform for mitochondrial form and function. *The International Journal of Biochemistry & Cell Biology*. 48:92-96.
- Miller, W.L., and H.S. Bose. 2011. Early steps in steroidogenesis: intracellular cholesterol trafficking Thematic Review Series: Genetics of Human Lipid Diseases. *Journal of lipid research*. 52:2111-2135.
- Misra, P., E.D. Owuor, W. Li, S. Yu, C. Qi, K. Meyer, Y.-J. Zhu, M.S. Rao, A.-N.T. Kong, and J.K. Reddy. 2002. Phosphorylation of Transcriptional Coactivator Peroxisome Proliferator-activated Receptor (PPAR)-binding Protein (PBP) STIMULATION OF TRANSCRIPTIONAL REGULATION BY MITOGEN-

- ACTIVATED PROTEIN KINASE. *Journal of Biological Chemistry*. 277:48745-48754.
- Møller, N., K. Møller, R. Lammers, A. Kharitonov, I. Sures, and A. Ullrich. 1994. Src kinase associates with a member of a distinct subfamily of protein-tyrosine phosphatases containing an ezrin-like domain. *Proceedings of the National Academy of Sciences*. 91:7477-7481.
- Murphree, A.L., and W.F. Benedict. 1984. Retinoblastoma: clues to human oncogenesis. *Science*. 223:1028-1033.
- Murphy, M.P., A. Holmgren, N.-G. Larsson, B. Halliwell, C.J. Chang, B. Kalyanaraman, S.G. Rhee, P.J. Thornalley, L. Partridge, and D. Gems. 2011. Unraveling the biological roles of reactive oxygen species. *Cell metabolism*. 13:361-366.
- Nasir, A., K.M. Kim, and G. Caetano-Anollés. 2014. Global patterns of protein domain gain and loss in superkingdoms. *PLoS computational biology*. 10.
- Nenicu, A. 2010. Influence of peroxisomes on development, maturation and adult functions of the testis. Universitätsbibliothek Giessen.
- Nenicu, A., G.H. Lüers, W. Kovacs, M. Bergmann, and E. Baumgart-Vogt. 2007. Peroxisomes in human and mouse testis: differential expression of peroxisomal proteins in germ cells and distinct somatic cell types of the testis. *Biology of Reproduction*. 77:1060-1072.
- Nettersheim, D., K. Biermann, A.J. Gillis, K. Steger, L.H. Looijenga, and H. Schorle. 2011. NANOG promoter methylation and expression correlation during normal and malignant human germ cell development. *Epigenetics*. 6:114-122.
- Newhall, K.J., A.R. Criniti, C.S. Cheah, K.C. Smith, K.E. Kafer, A.D. Burkart, and G.S. McKnight. 2006. Dynamic anchoring of PKA is essential during oocyte maturation. *Current Biology*. 16:321-327.
- Nipper, R.W., B.H. Jones, G.L. Gerton, and S.B. Moss. 2006. Protein domains govern the intracellular distribution of mouse sperm AKAP4. *Biology of Reproduction*. 75:189-196.
- Okutsu, R., T. Rai, A. Kikuchi, M. Ohno, K. Uchida, S. Sasaki, and S. Uchida. 2008. AKAP220 colocalizes with AQP2 in the inner medullary collecting ducts. *Kidney international*. 74:1429-1433.
- Olivares-Fuster, O., L. Pena, N. Duran - Vila, and L. Navarro. 2002. Green fluorescent protein as a visual marker in somatic hybridization. *Annals of botany*. 89:491-497.
- Perkins, G.A., L. Wang, L.J. Huang, K. Humphries, V.J. Yao, M. Martone, T.J. Deerinck, D.M. Barraclough, J.D. Violin, and D. Smith. 2001. PKA, PKC, and AKAP localization in and around the neuromuscular junction. *BMC neuroscience*. 2:17.
- Perrino, C., A. Feliciello, G.G. Schiattarella, G. Esposito, R. Guerriero, L. Zaccaro, A. Del Gatto, M. Saviano, C. Garbi, and R. Carangi. 2010. AKAP121 downregulation impairs protective cAMP signals, promotes mitochondrial dysfunction, and increases oxidative stress. *Cardiovascular research*:cvq155.
- Plyte, S.E., K. Hughes, E. Nikolakaki, B.J. Pulverer, and J.R. Woodgett. 1992. Glycogen synthase kinase-3: functions in oncogenesis and development. *Biochimica et Biophysica Acta (BBA)-Reviews on Cancer*. 1114:147-162.
- Prechelt, L. 2000. An empirical comparison of C, C++, Java, Perl, Python, Rexx and Tcl. *IEEE Computer*. 33:23-29.
- Rebourcet, D., P.J. O'Shaughnessy, A. Monteiro, L. Milne, L. Cruickshanks, N. Jeffrey, F. Guillou, T.C. Freeman, R.T. Mitchell, and L.B. Smith. 2014. Sertoli cells

- maintain Leydig cell number and peritubular myoid cell activity in the adult mouse testis.
- Reijo, R., R.K. Alagappan, D. Page, and P. Patrizio. 1996. Severe oligozoospermia resulting from deletions of azoospermia factor gene on Y chromosome. *The Lancet*. 347:1290-1293.
- Reinton, N., P. Collas, T.B. Haugen, B.S. Skålhegg, V. Hansson, T. Jahnsen, and K. Taskiran. 2000. Localization of a novel human A-kinase-anchoring protein, hAKAP220, during spermatogenesis. *Developmental biology*. 223:194-204.
- Rodemer, C., T.-P. Thai, B. Brugger, T. Kaercher, H. Werner, K.-A. Nave, F. Wieland, K. Gorgas, and W.W. Just. 2003. Inactivation of ether lipid biosynthesis causes male infertility, defects in eye development and optic nerve hypoplasia in mice. *Human molecular genetics*. 12:1881-1895.
- Rodriguez-Cuenca, S., S. Carobbio, V.R. Velagapudi, N. Barbarroja, J.M. Moreno-Navarrete, F.J. Tinahones, J.M. Fernandez-Real, M. Orešič, and A. Vidal-Puig. 2012. Peroxisome proliferator-activated receptor γ -dependent regulation of lipolytic nodes and metabolic flexibility. *Molecular and cellular biology*. 32:1555-1565.
- Rogne, M., H.B. Landsverk, A. Van Eynde, M. Beullens, M. Bollen, P. Collas, and T. K ntziger. 2006. The KH-Tudor domain of a-kinase anchoring protein 149 mediates RNA-dependent self-association. *Biochemistry*. 45:14980-14989.
- Rogne, M., A.J. Stokka, K. Taskiran, P. Collas, and T. K ntziger. 2009. Mutually exclusive binding of PP1 and RNA to AKAP149 affects the mitochondrial network. *Human molecular genetics*. 18:978-987.
- Saras, J., and C.-H. Heldin. 1996. PDZ domains bind carboxy-terminal sequences of target proteins. *Trends in biochemical sciences*. 21:455-458.
- Schillace, R.V., and J.D. Scott. 1999. Association of the type 1 protein phosphatase PP1 with the A-kinase anchoring protein AKAP220. *Current Biology*. 9:321-324.
- Schillace, R.V., J.W. Voltz, A.T.R. Sim, S. Shenolikar, and J.D. Scott. 2001. Multiple interactions within the AKAP220 signaling complex contribute to protein phosphatase 1 regulation. *Journal of Biological Chemistry*. 276:12128-12134.
- Schrader, M., N. Bonekamp, and M. Islinger. 2011. Fission and proliferation of peroxisomes. *Biochimica et Biophysica Acta (BBA)-Molecular Basis of Disease*.
- Schrader, M., and H.D. Fahimi. 2008. The peroxisome: still a mysterious organelle. *Histochemistry and cell biology*. 129:421-440.
- Schueren, F., T. Lingner, R. George, J. Hofhuis, C. Dickel, J. G rtner, and S. Thoms. 2014. Peroxisomal lactate dehydrogenase is generated by translational readthrough in mammals. *Elife*. 3:e03640.
- Scientific, T. 2013. Assessment of nucleic acid purity. *T042-Technical Bulletin Nano Drop Spectrophotometers, nanodrop. com/Library/T042-NanoDrop-Spectrophotometer-Nucleic-Acid-Purity-Ratios. pdf*. Accessed 20th November.
- Scobey, M.J., S. Bertera, J.P. Somers, S.C. Watkins, A.J. Zeleznik, and W.H. Walker. 2001. Delivery of a Cyclic Adenosine 3' , 5' -Monophosphate Response Element-Binding Protein (CREB) Mutant to Seminiferous Tubules Results in Impaired Spermatogenesis 1. *Endocrinology*. 142:948-954.
- Sharpe, R.M., C. McKinnell, C. Kivlin, and J.S. Fisher. 2003. Proliferation and functional maturation of Sertoli cells, and their relevance to disorders of testis function in adulthood. *Reproduction*. 125:769-784.
- Skinner, M.K., and M.D. Griswold. 2004. Sertoli cell biology. Academic press.

- Skroblin, P., S. Grossmann, G. Schäfer, W. Rosenthal, and E. Klusmann. 2010. Chapter Five-Mechanisms of Protein Kinase A Anchoring. *International review of cell and molecular biology*. 283:235-330.
- Smith, F.D., L.K. Langeberg, and J.D. Scott. 2006. The where's and when's of kinase anchoring. *Trends in biochemical sciences*. 31:316-323.
- Stelzig, I., S. Karnati, K.P. Valerius, and E. Baumgart-Vogt. 2013. Peroxisomes in dental tissues of the mouse. *Histochemistry and cell biology*. 140:443-462.
- Streit, S., C.W. Michalski, M. Erkan, J. Kleeff, and H. Friess. 2008. Northern blot analysis for detection and quantification of RNA in pancreatic cancer cells and tissues. *Nature protocols*. 4:37-43.
- Takada, Y., N. Kaneko, H. Esumi, P. Purdue, and C. Danpure. 1990. Human peroxisomal L-alanine: glyoxylate aminotransferase. Evolutionary loss of a mitochondrial targeting signal by point mutation of the initiation codon. *Biochem. J.* 268:517-520.
- Tanji, C., H. Yamamoto, N. Yorioka, N. Kohno, K. Kikuchi, and A. Kikuchi. 2002. A-kinase anchoring protein AKAP220 binds to glycogen synthase kinase-3 β (GSK-3 β) and mediates protein kinase A-dependent inhibition of GSK-3 β . *Journal of Biological Chemistry*. 277:36955-36961.
- Tasken, K., and E.M. Aandahl. 2004. Localized effects of cAMP mediated by distinct routes of protein kinase A. *Physiological reviews*. 84:137-167.
- Terpe, K. 2003. Overview of tag protein fusions: from molecular and biochemical fundamentals to commercial systems. *Applied microbiology and biotechnology*. 60:523-533.
- Thomas, K., D. Sung, X. Chen, W. Thompson, Y. Chen, J. McCarrey, W. Walker, and M. Griswold. 2010. Developmental patterns of PPAR and RXR gene expression during spermatogenesis. *Frontiers in bioscience (Elite edition)*. 3:1209-1220.
- Tingley, W.G., L. Pawlikowska, J.G. Zaroff, T. Kim, T. Nguyen, S.G. Young, K. Vranizan, P.-Y. Kwok, M.A. Whooley, and B.R. Conklin. 2007. Gene-trapped mouse embryonic stem cell-derived cardiac myocytes and human genetics implicate AKAP10 in heart rhythm regulation. *Proceedings of the National Academy of Sciences*. 104:8461-8466.
- Tippmann, S. 2015. Programming tools: Adventures with R. *Nature*. 517:109-110.
- Tsien, R.Y. 1998. The green fluorescent protein. *Annual review of biochemistry*. 67:509-544.
- Turner, R.M., L.R. Johnson, L. Haig-Ladewig, G.L. Gerton, and S.B. Moss. 1998. An X-linked Gene Encodes a Major Human Sperm Fibrous Sheath Protein, hAKAP82 GENOMIC ORGANIZATION, PROTEIN KINASE A-RII BINDING, AND DISTRIBUTION OF THE PRECURSOR IN THE SPERM TAIL. *Journal of Biological Chemistry*. 273:32135-32141.
- Tvrda, E., A. Agarwal, and N. Alkuhaimi. 2015. Male Reproductive Cancers and Infertility: A Mutual Relationship. *International journal of molecular sciences*. 16:7230-7260.
- Uawithya, P., T. Pisitkun, B.E. Ruttenberg, and M.A. Knepper. 2008. Transcriptional profiling of native inner medullary collecting duct cells from rat kidney. *Physiological genomics*. 32:229-253.
- van Roermund, C.W., L. IJlst, T. Wagemans, R.J. Wanders, and H.R. Waterham. 2014. A role for the human peroxisomal half-transporter ABCD3 in the oxidation of dicarboxylic acids. *Biochimica et Biophysica Acta (BBA)-Molecular and Cell Biology of Lipids*. 1841:563-568.

- van Roermund, C.W., W.F. Visser, L. IJlst, H.R. Waterham, and R.J. Wanders. 2011. Differential substrate specificities of human ABCD1 and ABCD2 in peroxisomal fatty acid β -oxidation. *Biochimica et Biophysica Acta (BBA)-Molecular and Cell Biology of Lipids*. 1811:148-152.
- Van Veldhoven, P.P., E. Baumgart, and G.P. Mannaerts. 1996. Iodixanol (Optiprep), an improved density gradient medium for the iso-osmotic isolation of rat liver peroxisomes. *Analytical biochemistry*. 237:17-23.
- Wahli, W., O. Braissant, and B. Desvergne. 1995. Peroxisome proliferator activated receptors: transcriptional regulators of adipogenesis, lipid metabolism and more.... *Chemistry & Biology*. 2:261-266.
- Walker, W.H., and J. Cheng. 2005. FSH and testosterone signaling in Sertoli cells. *Reproduction*. 130:15-28.
- Wang, L., R.K. Sunahara, A. Krumins, G. Perkins, M.L. Crochiere, M. Mackey, S. Bell, M.H. Ellisman, and S.S. Taylor. 2001. Cloning and mitochondrial localization of full-length D-AKAP2, a protein kinase A anchoring protein. *Proceedings of the National Academy of Sciences*. 98:3220-3225.
- Warren, K., D. Warrilow, L. Meredith, and D. Harrich. 2009. Reverse transcriptase and cellular factors: regulators of HIV-1 reverse transcription. *Viruses*. 1:873-894.
- Webb, R.J., L. Tinworth, G.M. Thomas, M. Zaccolo, and J. Carroll. 2008. Developmentally acquired PKA localisation in mouse oocytes and embryos. *Developmental biology*. 317:36-45.
- Welch, E.J., B.W. Jones, and J.D. Scott. 2010. Networking with AKAPs: context-dependent regulation of anchored enzymes. *Molecular Interventions*. 10:86.
- Welsh, S., and S.A. Kay. 1997. Reporter gene expression for monitoring gene transfer. *Current opinion in biotechnology*. 8:617-622.
- Wong, W., and J.D. Scott. 2004. AKAP signalling complexes: focal points in space and time. *Nature Reviews Molecular Cell Biology*. 5:959-970.
- Yang, Y., and C.E. Walsh. 2005. Spliceosome-mediated RNA trans-splicing. *Molecular Therapy*. 12:1006-1012.
- Yoo, H., H.J. Cha, J. Lee, E.-O. Yu, S. Bae, J.H. Jung, I. Sohn, S.-J. Lee, K.-H. Yang, and S.-H. Woo. 2008. Specific proteolysis of the A-kinase-anchoring protein 149 at the Asp582 residue by caspases during apoptosis. *Oncology reports*. 19:1577-1582.
- Zimmerman, S.G., N.C. Peters, A.E. Altaras, and C.A. Berg. 2013. Optimized RNA ISH, RNA FISH and protein-RNA double labeling (IF/FISH) in *Drosophila* ovaries. *Nature protocols*. 8:2158-2179.
- Zirkin, B.R., R. Santulli, C.A. Awoniyi, and L.L. Ewing. 1989. Maintenance of Advanced Spermatogenic Cells in the Adult Rat Testis: Quantitative Relationship to Testosterone Concentration within the Testis*. *Endocrinology*. 124:3043-3049.